Degradation and deactivation of bacterial antibiotic resistance genes during exposure to (waste)water treatment and health-care disinfectants

Huan He

A dissertation

submitted in partial fulfillment of the

requirements for the degree of

Doctor of Philosophy

University of Washington

2020

Reading Committee:

Michael C. Dodd, Chair

Yunho Lee

Marilyn C. Roberts

John S. Meschke

Program Authorized to Offer Degree:

Civil and Environmental Engineering

University of Washington

Abstract

Degradation and deactivation of bacterial antibiotic resistance genes during exposure to (waste)water treatment and health-care disinfectants

Huan He

Chair of the Supervisory Committee:
Professor Michael C. Dodd
Department of Civil and Environmental Engineering

Conventional disinfectants applied in (waste)water treatment and healthcare practice can potentially provide important barriers to antibiotic resistance dissemination through inactivation of antibiotic resistant bacteria (ARB). However, limited information is available on whether and how these disinfection processes could effectively eliminate ARGs and their biological activities in disseminating resistance traits to non-resistant bacterial populations via horizontal gene transfer processes such as natural transformation. In this context, this work was undertaken to investigate the degradation (i.e., chemical modification as measured by qPCR) and/or deactivation (i.e., biological activity loss as measured by culture-based natural transformation assays) of various extra/intra-cellular ARGs, including *blt*, *mec*A, *van*A, *tet*(A), *amp*C, bla_{NDM}, and/or bla_{KPC} (harbored by *Bacillus subtilis*, *Staphylococcus aureus*, *Enterococcus faecium*,

Escherichia coli, *Pseudomonas aeruginosa*, and *Klebsiella pneumoniae*, respectively) during treatment of commonly-used (waste)water disinfectants/oxidants, including free available chlorine (FAC), monochloramine (NH_2Cl), ozone (O_3), chlorine dioxide (ClO_2), ultraviolet (UV) light, and hydroxyl radical ($^{\bullet}OH$), as well as healthcare disinfectants/antiseptics, including glutaraldehyde, chlorhexidine, ethanol, povidone-iodine, benzalkonium chloride, phenol, sodium hypochlorite, and hydrogen peroxide (H_2O_2).

Kinetics results of (waste)water disinfections highlighted a wide range of ARG susceptibilities toward different chemical disinfectants, with reactivities declining in the order $HO^{\bullet}$ >> O3 > FAC >> ClO_2 > NH_2Cl. For a given disinfectant, second-order or fluence-based first-order rate constants determined for various ARG or 16S rRNA gene amplicons (ranging from 143–1509 bp) increased linearly with contents of AT+GC base pairs (for FAC, NH_2Cl, O_3) or intrastrand doublets of 5'-TT-3' (for UV) or 5'-GG-3' (for ClO_2) per amplicon. For FAC, NH_2Cl, O_3, ClO_2, and UV, *blt* gene *deactivation* paralleled *degradation* of amplicons approximating a ~800-1000 bp *acfA*-flanking sequence required for natural transformation in *B. subtilis*, whereas *deactivation* outpaced *degradation* for $^{\bullet}OH$, due to its distinctive mechanism of DNA fragmentation rather than nucleobase alteration.

These results enabled the development of a modeling approach for predicting degradation/deactivation rate constant and kinetics of a given DNA segment, based on its DNA sequence length or nucleotide content and elementary reactions toward each of the above disinfectants (except $^{\bullet}OH$). This kinetics-based modeling framework has been validated and utilized to predict degradation/deactivation profiles of a broad array of ARGs and 16S rRNA gene segments during bench-scale disinfections in clean buffer and/or wastewater matrixes, as well as their removal efficiencies in selected full-scale processes. At practical exposure ranges,

extra- and intracellular ARGs/16S rRNA gene were 1-3 log_{10} degraded/deactivated by FAC, O_3, and UV, but recalcitrant to NH_2Cl and ClO_2, which can be adequately predicted by the kinetics-based model under certain circumstances. Intracellular ARG degradation/deactivation always lagged behind host ARB inactivation. Bench-scale experimental and modeling results supported observations at local wastewater treatment plants (WWTPs) that UV provided ~1 log_{10} ARG elimination, while chlorination of high-ammonia (non-nitrified) wastewater yielded no significant ARG removal, due to rapid conversion of FAC into NH_2Cl (non-reactive toward DNA) in excess ammonia.

Last, this work was extended to healthcare disinfections by treating the model *blt* gene (primarily in its intracellular form) with each healthcare disinfectant on inanimate surface or in aqueous phase. Surface disinfection results demonstrated that typical healthcare conditions provided non-significant or minimal (< 1-log_{10}) elimination of *blt* gene copy numbers on hard surfaces, although 2–5-log_{10} ARB inactivation was achieved by each disinfectant (except H_2O_2). Results of H_2O_2 treatment in aqueous phase elucidated that intracellular ARG deactivation in the presence of H_2O_2, also lagging behind ARB inactivation, is likely due to H_2O_2 decomposition to form $^{\bullet}OH$ catalyzed by intracellular iron, leading to DNA strand fragmentation without base alteration. Findings of this work have provided systematic understanding of ARG fate during exposures of various disinfectants, and highlighted that ARGs could persist after effective ARB inactivation, potentially leading to resistance dissemination into downstream environments. Outcomes of this work provided significant implications on how to select, design, and improve disinfection practices in (waste)water treatment and clinical facilities.

TABLE OF CONTENTS

LIST OF FIGURES

LIST OF TABLES

ACKNOWLEDGEMENTS

First and foremost, I would like to express the deepest thanks to my advisor Prof. Michael Dodd, for his guidance throughout my doctorial study and life, with constant encouragement, tremendous support, insightful ideas, and profound thoughts.

I would like to convey my grateful thanks to my committee members, Profs. Yunho Lee, Marilyn Roberts, and J. Scott Meschke, for their valuable input and precious advices in completion of this dissertation. I would like to say thanks to Prof. Yunho for his consistent and in-depth collaboration though in a remote way, and to Profs. Marilyn and Scott, for sharing their microbiology knowledge and offering technical support in South Campus or Roosevelt.

I would like to give great thanks to my wonderful colleagues in Dodd Group. First, I want to say many thanks to Peiran Zhou and Kyle K. Shimabuku, who built solid foundation of this project and trained me from zero; I want to express special thanks to Tessora (Tess) Young, who is a great labmate and friend of mine I cannot feel luckier to have for the past five years; Huge thanks also go to Sin-Yi Liu, Younggun Yoon, Yegyun Choi, Minju Lee, Shuangyang Zhao, and Chaoqun Tan, who have supported me in or out of the lab in many different aspects. Acknowledgments also go to all the undergraduate students (in order of their joint time) who worked with me for their valuable participation in this work: Xuzhi (Mark) Fang, Annika K. Anderson, Tyler Oshiro, Joel Corlew, and Sean J. Wu.

I would like to express great thanks and appreciation to other professors, including Profs. Gregory Korshin, Mark Benjamin, David Stahl, Mari Winkler, and Beth Traxler, who have mentored and advised me in class and/or on research. I would also like to give thanks to the scientists, staffs, and graduate students in CEE or Public Health, who helped me in

accomplishment of this work: to J. Sean Yeung and Songlin Wang, for always being available and supportive in equipment troubleshooting; to Nicola Beck, Christine Fagnant, Kelley Meinhardt, and David No, for their assistance on access of instrumentation and bacterial strains; to my friends and colleagues in CEE, Nicolette Zhou, Siamak Modarresi, Khaled Salam, Bao Nguyen Quoc, Stephany Wei, Kathryn Cogert, Wei Qin, Hongguang Guo, Zhengyu Tian, and Haoqi (Nina) Zhao, for their unselfish help and fruitful discussion with me. I also want to thank all the undergraduate students in CEE 354 class I have served as TA, who brought me big fun and motivation in teaching and mentoring.

I want to broaden my thanks to people outside my study at UW. Specially, I want to recognize my previous supervisor in Tongji University, Prof. Bingzhi Dong, for always being a beacon in my career voyage (and for sharing your playlist of classical music in your old iPod). I know I would not be able to pursue PhD without his encouragement and support. I would also like to thank all my friends I met in Seattle, who have created a lot of fantastic memories with me to be cherished like pearls. Specially, to Yang (Vera) Lu and Lei (Elaine) Zhao, who gave me huge help and care in initiating my adventure in Seattle. I would also like to deeply thank my old friends, many of whom started friendship with me since high school or college, and are now spreading around the world in Chongqing, Shanghai, Guangzhou, Trondheim, Darmstadt, München, San Francisco, New Haven, and other cities. Thanks for your sincere regards across oceans and continents and through years (many as postcards), and your help to me on finding my default mode and exploring as many variants of myself as possible.

My last and greatest thanks go to my family, who live in Chongqing, China, for their unconditional love through my growth and distantly strong support during my stay in Seattle.

Chapter 1. Introduction

1.1 OVERVIEW

1.1.1 *Emergence of antibiotic resistance*

The term of antibiotic resistance is used to describe the ability of bacteria to survive, and even thrive, in the presence of antibiotics.[1] Bacteria possessing resistance to antibiotics are called antibiotic resistant bacteria (ARB), and the segments of DNA (located on either chromosome or plasmid) encoding such resistance are identified as antibiotic resistance genes (ARGs). Primarily, ARGs empower bacteria to fight against antibiotics through three major routes: (1) enzymatic destruction or modification of the antibiotic; (2) export of antibiotics out of the bacterial cytoplasm by efflux pumps; (3) replacement or modification of the cellular antibiotic target with an insensitive form.[2]

ARB and their associated ARGs originate from commensal bacterial populations of human or animals, as well as within natural environmental systems.[3, 4] Under the pressure to adapt or die, bacteria attacked by antibiotics can develop self-defense mechanisms through genetic mutation on their own (i.e., intrinsic resistance), or attain resistance from innately-resistant antibiotic producers via horizontal gene transfer (HGT) (i.e., acquired resistance).[2] The evolutionary rate of bacteria is so fast that antibiotic resistance generally would emerge in clinical settings within a decade or less after deployment of a new antibiotic, based on observations shown in Table 1.1.[1, 5] Once obtaining resistance, a major challenge occurs during antibiotic therapy that ARB populations have selective growth advantage to become dominant.[6] That is to say, clinical treatment using antibiotics (especially at low dosage) selects for and enriches resistant strains.

Since the first discovery and deployment in the early 20th century, antibiotics have been overused and abused on human, veterinary medicine, and agriculture over the past 70 years. As a

consequence, antibiotic resistance has been found to develop and spread among bacterial populations in both phenotypes and genotypes. Within the past few decades, numerous studies in epidemiology have reported significant increases in the proportions of antibiotic-resistant infection (ARI), either community-associated or hospital-acquired. Some famous (and threatful) examples of resistant human pathogens include methicillin-resistant *Staphylococcus aureus* (MRSA),[7] penicillin- and cephalosporin-resistant *Streptococcus pneumoniae*,[8] carbapenem-resistant *Acinetobacter spp.*,[9] clarithromycin-resistant *Helicobacter pylori*,[10], and fluoroquinolone- and macrolide- resistant *Campylobacter* spp.[11]

Table 1.1. Evolution of resistance to antibiotics.[1, 5]

Antibiotic	Year	
	deployment	Resistance observed
Sulfonamides	1930s	1940s
Penicillin	1943	1946
Streptomycin	1943	1959
Chloramphenicol	1947	1959
Tetracycline	1948	1953
Erythromycin	1952	1988
Vancomycin	1956	1988
Methicillin	1960	1961
Ampicillin	1961	1973

The increasing cases of ARI leads to not only decreasing effectiveness of antibiotics but also huge social economy loss.[3] Statistics show that each year in the United States, more than 2.8 million people get infected by antibiotic resistant bacteria (ARB), accounting for ~13.5% of total patients, and causing 35,000 deaths with a mortality higher than 1.15%,[12] which results in an additional direct cost (i.e., medical treatment) of $20 billion and an extra indirect cost (i.e., loss of productivity) of $30 billion according to estimation.[13] Furthermore, due to high difficulties, low profits and unpredictable risks in antibiotic development and manufacture, human discovery of new drugs has a slower rate than bacterial evolution of antibiotic resistance, which means we

are facing growing scarcity of effective antibiotics and possibility of a post-antibiotic era with no useful treatment against bacterial infections.[14]

1.1.2 *Horizontal gene transfer of antibiotic resistance*

Another of the biggest challenges in the issue of antibiotic resistance is that ARGs, either chromosomally-encoded or plasmid-borne, may be transmitted over successive bacterial generations and persist across a wide range of hosts (ascribed to the spirit of sharing among different bacteria species), even in the absence of selective pressure.[15, 16] That is to say, the antibiotic resistance traits are able to disseminate amongst bacterial populations not only by vertical transfer (i.e., cell division), but also by various processes of HGT, including conjugation (i.e., bacterial mating), transduction (i.e., viral mediated), and natural transformation (i.e., uptake of extracellular DNA from dead cells).[1, 17] Major characteristics of each HGT mechanism are illustrated in Figure 1.1. Briefly, during conjugation, gene exchange happens between mated donor-recipient pairs of bacterial cells, both of which require to be metabolically active; In contrast, gene transfer during transduction or natural transformation is a single-participant process: the donor cell doesn't need to be metabolically alive, but only the recipient cell needs to be active to incorporate an external DNA segment derived from the donor cell into its own genome via homologous recombination or as its own plasmid or other autonomously replicating element.[18] The external DNA segment can either be phage-borne in the case of transduction, or free by itself for natural transformation. Ascribed to the modularity and mobility of genetic units, HGT processes occur massively between bacteria populations (and also commonly within archaea or unicellular eukarya species), which greatly accelerate the pace of genome evolution.

During natural transformation, the free DNA captured by competent recipient bacteria can be incorporated into the recipient cell's genome via homologous recombination, homology-

facilitated illegitimate recombination, or by forming an autonomously replicating element (such as plasmid),[18] while in the processes of conjugation and transduction, mobile genetic elements (e.g., plasmids, bacteriophages, transposons, insertion sequence elements, integrons, gene cassettes, genomic islands, etc.) play important roles as gene transfer vehicles (or called vectors).[19]

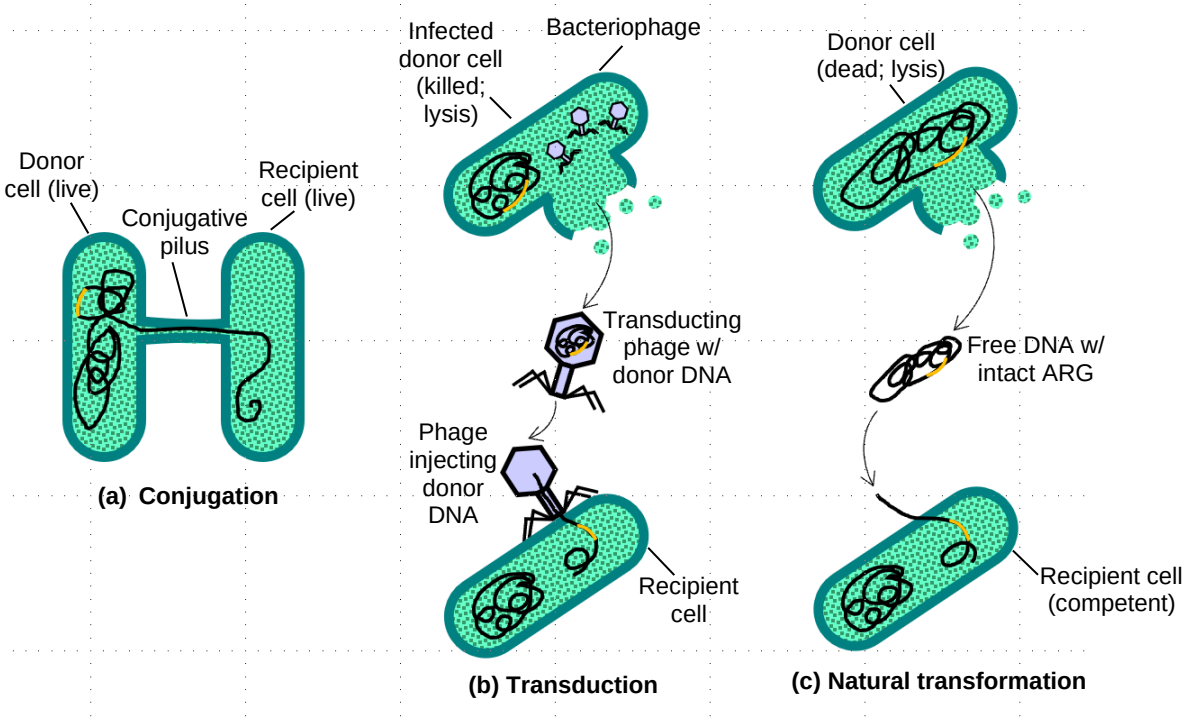

Figure 1.1. Illustrations of major mechanisms of horizontal gene transfer including (a) conjugation, (b) transduction, and (c) natural transformation.

Since the only requirement (becides live recepient cells) for natural transformation is biologically-active free DNA originated from dead donor cells, it is the most conservative way to evaluate dissemination capability of ARGs (and other genetic traits). Therefore nowadays, direct measurement of changes in biological activity via culture-based transformation assay still represents a "gold standard" approach for evaluating the impact of treatment processes on ARG dissemination risk.[20, 21] A wide variety of strains have been identified to be naturally

competent,[22, 23] including many clinically-important human pathogens, including *S. pneumoniae*, *N. gonorrhoeae*, *H. influenzae*, *H. pylori*, *Legionnaire pneumophila*, *Campylobacter jejuni*, and *Vibrio cholerae*, etc.[24] In addition, although natural transformation is typically most facile amongst the same species, interspecies transformation is also possible.[22, 25]

1.1.3 *Occurrence of antibiotic resistance in aquatic environments*

The existence of antibiotic resistance has been detected worldwide in natural and engineered aquatic environments, including municipal wastewaters,[26-32] reclaimed waters,[32-34] surface waters and sediments,[31, 32, 35, 36] drinking water treatment plants and distribution systems.[37, 38] In these systems listed above, ARB have often been detected at relatively high levels in proportion to total bacterial cell density, as well as ARGs and/or ARG abundance (i.e., normalization of ARG copy number to 16S rRNA gene copy number, a proxy for total bacterial concentration).[39-42] Major types of ARGs ever reported in various aquatic environments are categorized according to their target antibiotic and function mechanism in Table 1.2, and more details about their biological sources (e.g., chromosomal or plasmid-borne, host strain range) and environmental harbours can be found in the review by Zhang et al. (2009).[43] It is noteworthy that the resistance of certain antibiotic may be associated with different ARGs based on more than one mechanism, while one certain ARG often coexists with other resistance determinants (ARGs or heavy metal resistance genes) on the same mobile genetic element (like plasmid), which increases the possibility of multidrug resistance in environmental bacterial populations. It should also be noticed that sometimes the ARG names might be incorrectly presented in publications, since authors often name a newly identified gene using a term already approved for other genetically distinct genes, or assign new names to resistance determinants previously designated. Therefore, it is necessary to correct and harmonize the nomenclature of ARGs.[44]

Table 1.2. Types of ARGs reported in water environments [a]

Antibiotics	ARG	Function
Tetracycline/ oxytetracycline	*tet*(A), *tet*(B), *tet*(C), *tet*(D), *tet*(E), *tet*(G), *tet*(H), *tet*(J), *tet*(Y), *tet*(Z), *tet*33, *tet*39; *otr*B	Tetracycline efflux protein
	tet(M), *tet*(O), *tet*(Q), *tet*(S), *tet*(T), *tet*(W); *otr*A	Ribosomal protection protein
Aminoglycoside	*aac*A4, *aac*A29b, *aac*C1, *aac*C2, *aac*C3, *aac*C4; *aac*(6')-Ib [b]; *sat*1, *sat*2	Aminoglycoside acetyltransferases
	*aph*A1, *aph*A2, *aph*D, *aph*(3″)-Ic; *npt*II; *str*A, *str*B	Aminoglycoside phosphotransferases
	*aad*A1, *aad*A2, *aad*A5, *aad*A13, *aad*B	Aminoglycoside adenylyltransferase
Macrolide–lincosamide–streptogramin (MLS)	*erm*A, *erm*B, *erm*C, *erm*E, *erm*F, *erm*T, *erm*V, *erm*X	Ribosomal RNA (rRNA) methylases (to prevent binding with ribosomal protein)
	*mph*A	Macrolide-2'-phosphotransferase
Chloramphenicol/ florfenicol	*cat*B2, *cat*B3, *cat*I, *cat*II, *cat*III, *cat*IV	Chloramphenicol acetyltransferases
	*cml*A1 and *cml*A5; flo_R	Chloramphenicol/florfenicol efflux protein
Vancomycin	*van*A, *van*B, *van*C[45]	Vancomycin resistance protein
Sulphonamide and trimethoprim	*dfr*A1, *dfr*A5, *dfr*A7, *dfr*A12, *dfr*A15, *dfr*A17, *dfr*18	Modification of dihydrofolate reductase
	*sul*I, *sul*II, *sul*III, and *sul*A	Modification of dihydropteroate synthase
β-Lactams	*amp*C; bla_{OXA}, bla_{CTX}, bla_{PSE}, bla_{NDM}, bla_{KPC}[31, 32, 46, 47]	β-lactamases
	*mec*A; *pen*A	Penicillin-binding protein
Quinolones	*qnr*A, *qnr*B, *qnr*C, *qnr*D, *qnr*S[48]	Protection of DNA gyrase and topoisomerase IV from quinolone inhibition by Qnr proteins
	*qep*A, *oqx*A, *oqx*B[48]	Quinolone efflux pump

[a] All the contents in Table 1.2 were modified from Zhang et al. (2009)[43] unless otherwise specified; [b] The *aac*(6')-Ib-cr gene (variant of *aac*(6')-Ib) confers resistance to expanded substrate spectrum including quinolones.[49]

A growing body of evidence has been found that clinical resistance is intimately linked with antibiotic resistance genes (ARGs) and associated ARB in natural environmental systems. Over the past decades, the growing level of various ARGs in sediment samples shows consistency with the increasing proportion of ARB in clinical isolates.[50] One of the more specific examples is that the *vanHAX* gene clusters, which emerged on clinical strains of *Enterococci* and

Staphylococci in the late 1980s and confer resistance to the "last-resort" antibiotic, vancomycin, have been found to be likely acquired from environmental bacteria (e.g., *Streptomycetes*).[51] Recent studies have highlighted that water environments can serve as recipients, reservoirs, and sources of ARGs of clinical concern, and at the same time, water environments also receive inputs of antibiotics from wastewater treatment plants (WWTPs), livestock operations, aquaculture, and industry, which contribute to selection pressure for elevation of resistance level in native bacteria.[52-55]

1.1.4 *Dissemination of antibiotic resistance through aquatic environments*

Considering that drinking water supplies, municipal wastewater systems, clinical facilities, and agricultural/aquacultural sites are interconnected via water cycling, it is obvious that ARB and ARGs may be disseminated amongst bacterial populations by various pathways in these aquatic systems, even when the involved bacterial populations are separated temporally and/or spatially. Here the term of dissemination includes the aspects of both transportation (physically through water cycling) and spreading (biologically by vertical and/or horizontal gene transfer). As illustrated in Figure 1.2, municipal wastewater treatment facilities may discharge considerable amounts of ARB and ARGs into downstream receiving waters, especially when the disinfection processes are not sufficiently effective. Agricultural soils and lagoons may become another significant source of ARB and ARGs, if they are impacted by animal manure and wastes originated from confined animal feed operations, where antibiotics are usually applied in a large scale.[39-42] Storm events could initiate surface and ground runoffs in agricultural soils, as well as overflows out of lagoon, thus release large quantities of untreated animal waste and manure carrying antibiotics and corresponding ARB/ARGs into nearby receiving waters.[54, 56, 57]

After entry into natural aquatic systems, surface waters and associated sediments often serve as reservoirs for ARB propagation and ARG amplification. Interestingly, seasonal variations of ARG and 16S rRNA levels have been observed in surface waters, suggesting that high-flow conditions (i.e., summer time, with higher temperature, higher nutrient availability and lower antibiotics concentration) could be conducive to faster microbial growth than low-flow periods.[36] In addition, migration of ARGs (free or in association with resistant bacteria) occurs between surface waters and sediments, which might be driven by dynamic equilibrium of ARGs between these two compartments.[58] Furthermore, it has been frequently found that the relative abundance of certain types of ARGs in river sediments are significantly correlated to specific transposons and integrons, which might explain the transmission mechanisms of these ARGs through natural environmental systems.[36, 59]

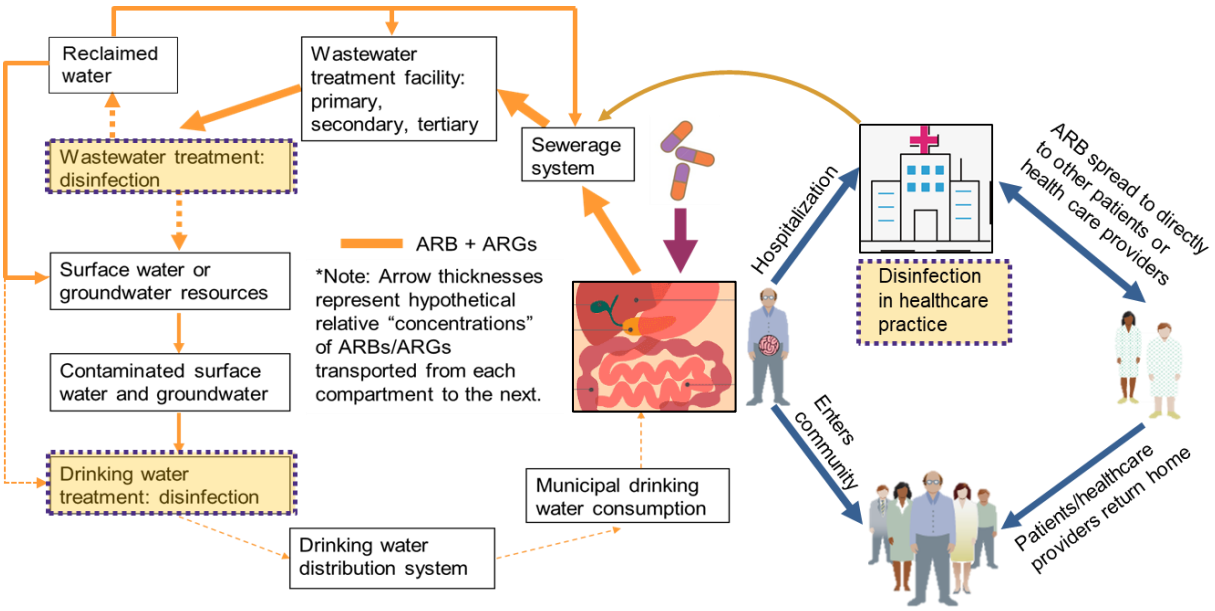

Figure 1.2. Identified and predicted dissemination pathways of antibiotic resistance in aquatic environments and healthcare facilities (Source: Shimabuku et al. (2014)[60])

ARB and ARGs in surface water or groundwater could potentially return to human populations, if these water bodies serve as drinking water resources for downstream

communities. Following water intakes, drinking water treatment may fail to fully eliminate ARB or ARGs and perhaps even selectively enrich ARG abundance.[38, 61, 62] Afterwards in drinking water distribution systems, the biofilms accumulated within aged pipelines could potentially become a hot spot for ARB proliferation and ARG amplification. Therefore, it is reasonable to conceive that ARB and ARGs could be ingested via drinking by human populations. Beside drinking water supplies, reclaimed waters (e.g., spray irrigation sites or reused water in WWTP) are also indicated to be exposure sources of ARB and ARGs, which have recently raised high attention of the public.[33, 34]

In the cycles of natural and engineered aquatic systems above, wastewaters and WWTPs deserve further discussion because they may represent a critical node for controlling spread of antibiotic resistance.[29] Particular concerns should be paid to special wastewaters from hospitals and other healthcare facilities, where ARB/ARGs could be frequently transmitted amongst patients and healthcare providers, inside or across facilities, as well as from healthcare facilities into communities, leading to increasing cases of antibiotic resistant infection.[63] Healthcare settings constantly generate wastewaters, which may contain high levels of residual antibiotics as well as a variety of ARB/ARGs either excreted by patients or dumped down the drain.[64-66] These wastewaters, sometimes feeding into sewerage without pretreatment, may play the role of potential hotbeds for antibiotic resistance prevalence.[67]

Massive numbers of studies over the past decade have investigated occurrences of ARB/ARGs in different compartments of WWTPs by applying cultivation-based approaches and/or molecular tools such as (quantitative) polymerase chain reaction ((q)PCR) and metagenomic analyses,[68-71] which have demonstrated that WWTPs make significant contributions to promoting antibiotic resistance dissemination. Although the overall numbers of

bacterial cells can be effectively reduced prior to discharge, considerable numbers of ARB cells, which harbor active ARGs, are often found to be still present in treated effluents.[72-74] In addition, the proportion of certain ARB/ARGs over total bacterial cells actually increase after wastewater treatment processes, which indicate some treatment steps processes may result in selective enrichment of resistant determinants.[75-77] For example, in a conventional WWTP system, biological treatment processes such as activated sludge are commonly designed to reach conditions of high growth rates and high microbial densities to remove organic matters, and nutrients.[78] However, such conditions may contribute to boosting the frequency of HGTs (especially conjugation, which requires cell-cell interaction) and facilitate multi-drug resistance among bacteria. Compared to aerobic reactors, biological treatment under anaerobic conditions may accomplish better ARG removal, possibly by stimulating bacteria to lose ARGs to conserve metabolism and shifting microbial community profile to a narrower host range.[28, 79]

1.1.5 *(Potential) impacts of (waste)water and healthcare disinfection practices on antibiotic resistance dissemination*

Disinfection processes in drinking water and wastewater treatment could potentially prevent and mitigate antibiotic resistance dissemination by providing effective inactivation of microorganisms including ARB. However, recent findings indicate that ARGs might persist even after effective ARB inactivation by disinfection processes, and be released to surface waters through effluent discharge or transported into drinking water distribution systems, potentially resulting in HGT events (e.g., natural transformation) in those environments.[21, 80]

Therefore, attention has been increasingly paid to the fate of ARGs (or bacterial DNA) during common (waste)water disinfection processes. Some earlier studies provided relatively qualitative evaluations showing common (waste)water disinfectants exhibited wide range of

efficiencies in destroying ARGs (and their biological activities). For example, it has been demonstrated that exposure to ozone (O_3) resulted in the linearization and loss of transforming activity of pAT153 plasmid DNA containing an ampicillin resistance gene (unfortunately transferred O_3 dose was not determined).[81] Similarly, free available chlorine (FAC), was found to yield deactivation of chromosomal ARGs in DNA isolated from a multi-drug resistant strain of *H. influenzae* (FAC dosing conditions were not reported).[82] In contrast, DNA contained within streptomycin-resistant *H. influenzae* cells treated with chlorine dioxide (ClO_2) retained nearly all of its transforming activity even after 6-log inactivation of the cells themselves, at CT values ranging from 1-2 mg/L·min (pH 8, 20° C).[83] Ultraviolet (UV) irradiation was able to suppress conjugation frequency of plasmid hosted by a multidrug-resistant *E. coli* strain, whereas low-dosage chlorination of wastewaters (governed by monochloramine, NH_2Cl) promote its conjugation by enhancing cell permeability while retaining cell viability.[84] Many other studies have also reported conflicting results on the effectiveness of chlorination in eliminating ARGs (and their biological activities) in wastewater matrixes,[46, 84-88] which requires further investigation and fundamental explanation.

More recent studies have started to focus on quantifying ARG or DNA segment degradation/deactivation kinetics during bench-scale (waste)water disinfection processes or derived fundamental kinetics parameters (e.g., rate constants, disinfectant exposures), mainly for disinfectants of FAC,[89, 90] ozone (O_3),[90, 91] and UV irradiation.[20, 92-94] Several of these studies have highlighted that elimination rate of DNA segments by UV might depend on its sequence length or some specific nucleotide content (such as number of potential dimer formation sites),[20, 92-94] which implies a promising possibility to establish universal modeling approach for predicting reactivity of DNA segment toward UV and potentially other chemical disinfectants.

Likewise, considering similar action mode of healthcare disinfectants as wastewater disinfectants/oxidants, it is also of great prudence to investigate the capabilities of surface disinfectants/antiseptics commonly used in healthcare practice to eliminate the ARGs that may remain following ARB cell death. Although very limited information is available in this field, one can still speculate potential efficacies of common healthcare disinfectants in degrading/deactivating ARGs, according to their interaction mode with various biomolecules comprising bacterial cells, as summarized below in Table 1.3.

Table 1.3. Characteristics of common healthcare disinfectants and antiseptics[95-98]

Reagents	Usage in healthcare practice	Primary mechanisms of bacterial inactivation (target sites and interactions)	Expected ARG degradation/ deactivation
Glutaraldehyde	Disinfectant	Cell envelope damage (alkylation of amino groups in protein and DNA; crosslinking of macromolecules)	Likely
Chlorhexidine	Antiseptic	Membrane disruption; cytoplasm coagulation	No
Ethanol	Disinfectant /Antiseptic	Membrane disruption (denaturation or precipitation of cytoplasmic and membrane proteins)	No
Povidone-Iodine	Antiseptic	Enzyme degradation (oxidation of thio groups; halogenation of amino acids)	Likely
Benzalkonium chloride	Disinfectant /Antiseptic	Membrane disruption (binding to lipids in cell membranes)	No
Phenol	Disinfectant /Antiseptic	Membrane disruption (denaturation or precipitation of cytoplasmic and membrane proteins)	No
Free chlorine (NaOCl)	Disinfectant	Enzyme degradation; DNA damage; DNA synthesis inhibition (oxidation of thio groups; halogenation of amino acids)	Likely
H_2O_2	Disinfectant /Antiseptic	Cell envelope damage; enzyme degradation; DNA damage (thiol groups in proteins; formation of hydroxyl free radicals)	Likely

For part of the common disinfectants/antiseptics (e.g., chlorhexidine, ethanol, benzalkonium chloride, and phenol), they have cellular inactivation mechanisms of membrane

permeabilization or enzyme degradation, not corresponding to DNA modification. Therefore, it is anticipated that minimal degradation/deactivation of intracellular ARGs could be achieved by treatment with these disinfectants. Even for those that interact with DNA molecules (e.g., glutaraldehyde, povidone-Iodine, and free chlorine), the disinfectant must first penetrate the cell envelope and other intracellular components before reaching ARG-containing DNA.[99] Accordingly, ARG degradation/deactivation may not have the same pace with bacterial viability loss, and the extent of "lagging" may depend strongly on the relative reactivities of disinfectants toward important cell constituents, including amino acids, lipids, saccharides, and nucleic acids (i.e., DNA and RNA).[99]

1.2 DISSERTATION LAYOUT

In light of the above, this work is undertaken to provide a comprehensive investigation of commonly-applied (waste)water and healthcare disinfectants on their reaction kinetics, mechanisms, and capabilities in degrading and deactivating bacterial ARGs. The work presented in this dissertation is formatted as a compilation of published peer-reviewed articles and manuscripts prepared for submission to peer-reviewed journals. The content of each chapter is briefly summarized below.

Chapter 1. Introduction: An overview of background and motivation of this study, including brief review of antibiotic resistance in environmental and clinical contexts, and potential impacts of disinfection processes in (waste)water treatment and healthcare practice on controlling antibiotic resistance dissemination.

Chapter 2. Degradation and deactivation of bacterial antibiotic resistance genes during exposure to free chlorine, monochloramine, chlorine dioxide, ozone, ultraviolet light, and hydroxyl radical: A fundamental study on determining kinetic parameters and

mechanisms governing ARG *degradation* (chemical modification captured by qPCR) and *deactivation* (transforming activity loss) by common (waste)water disinfectants/oxidants (as listed in the title), and developing a modeling framework in predicting ARG degradation and deactivation kinetics during disinfectant treatment according to its DNA sequence.

Chapter 3. Validation and application of a kinetics-based modeling approach to predict antibiotic resistance gene degradation during UV- and chlorine-based wastewater disinfection processes: from bench-scale to full-scale. A study on improvement and validation of the kinetics-based model proposed in Chapter 2, and application of the improved model to a broader array of ARGs/16S rRNA gene segments in selected bench/full-scale wastewater disinfection processes using chlorine and UV as disinfectants.

Chapter 4. Efficacy of healthcare disinfectants glutaraldehyde, chlorhexidine, ethanol, povidone-iodine, benzalkonium chloride, phenol, free chlorine, and hydrogen peroxide in eliminating antibiotic resistance gene on inanimate surface or in aqueous phase. A screening investigation on assessing the efficacies of common healthcare disinfectants/antiseptics (as listed in the title) in degrading and/or deactivating ARGs primarily in intracellular forms, at typical clinically-relevant treatment conditions.

Chapter 5. General conclusion. Important results of the present dissertation, as well as environmental significance, practical implications, future works are summarized in this chapter.

REFERENCE

1. Pruden, A., Balancing water sustainability and public health goals in the face of growing concerns about antibiotic resistance. *Environmental science & technology* **2013,** *48*, (1), 5-14.
2. Walsh, C., *Antibiotics: actions, origins, resistance*. American Society for Microbiology (ASM): 2003.

3. Davies, J.; Davies, D., Origins and Evolution of Antibiotic Resistance. *Microbiol. Mol. Biol. Rev.* **2010,** *74*, (3), 417-433.
4. Aminov, R. I.; Mackie, R. I., Evolution and ecology of antibiotic resistance genes. *FEMS microbiology letters* **2007,** *271*, (2), 147-161.
5. Palumbi, S. R., Humans as the world's greatest evolutionary force. *Science* **2001,** *293*, (5536), 1786-1790.
6. Levy, S. B.; Marshall, B., Antibacterial resistance worldwide: causes, challenges and responses. *Nature medicine* **2004,** *10*, S122-S129.
7. McDougal, L. K.; Steward, C. D.; Killgore, G. E.; Chaitram, J. M.; McAllister, S. K.; Tenover, F. C., Pulsed-field gel electrophoresis typing of oxacillin-resistant Staphylococcus aureus isolates from the United States: establishing a national database. *Journal of clinical microbiology* **2003,** *41*, (11), 5113-5120.
8. Coffey, T. J.; Daniels, M.; McDougal, L. K.; Dowson, C. G.; Tenover, F. C.; Spratt, B. G. J. A. a.; chemotherapy, Genetic analysis of clinical isolates of Streptococcus pneumoniae with high-level resistance to expanded-spectrum cephalosporins. **1995,** *39*, (6), 1306-1313.
9. *Antibiotic Resistance Theats in the United States, 2013*; U.S. Department of Health and Human Services Centers for Disease Control and Prevention: 2013.
10. Megraud, F., H pylori antibiotic resistance: prevalence, importance, and advances in testing. *Gut* **2004,** *53*, (9), 1374-1384.
11. Luangtongkum, T.; Jeon, B.; Han, J.; Plummer, P.; Logue, C. M.; Zhang, Q., Antibiotic resistance in Campylobacter: emergence, transmission and persistence. **2009**.
12. Control, C. f. D.; Prevention In *Antibiotic resistance threats in the United States*, 2013; CDC Atlanta: 2013.
13. Van Hoek, A. H.; Mevius, D.; Guerra, B.; Mullany, P.; Roberts, A. P.; Aarts, H. J., Acquired antibiotic resistance genes: an overview. *Front. Microbiol.* **2011,** *2*, 203.
14. Carlet, J.; Jarlier, V.; Harbarth, S.; Voss, A.; Goossens, H.; Pittet, D.; Forum, t. P. o. t. r. W. H.-A. I., Ready for a world without antibiotics? The Pensieres Antibiotic Resistance Call to Action. *Antimicrobial Resistance and Infection Control* **2012,** *1*, (1), 11.
15. Heinemann, J. A.; Ankenbauer, R. G.; Amábile-Cuevas, C. F., Do antibiotics maintain antibiotic resistance? *Drug discovery today* **2000,** *5*, (5), 195-204.
16. Schrag, S. J.; Perrot, V.; Levin, B. R., Adaptation to the fitness costs of antibiotic resistance in Escherichia coli. *Proceedings of the Royal Society of London. Series B: Biological Sciences* **1997,** *264*, (1386), 1287-1291.
17. Lorenz, M. G.; Wackernagel, W., Bacterial gene transfer by natural genetic transformation in the environment. *Microbiological reviews* **1994,** *58*, (3), 563.
18. de Vries, J.; Heine, M.; Harms, K.; Wackernagel, W., Spread of recombinant DNA by roots and pollen of transgenic potato plants, identified by highly specific biomonitoring using natural transformation of an Acinetobacter sp. *Applied and environmental microbiology* **2003,** *69*, (8), 4455-4462.
19. Heuer, H.; Smalla, K., Horizontal gene transfer between bacteria. *Environmental biosafety research* **2007,** *6*, (1-2), 3-13.
20. Chang, P. H.; Juhrend, B.; Olson, T. M.; Marrs, C. F.; Wigginton, K. R., Degradation of extracellular antibiotic resistance genes with UV254 treatment. *Environ. Sci. Technol.* **2017,** *51*, (11), 6185-6192.
21. Vikesland, P. J.; Pruden, A.; Alvarez, P. J.; Aga, D.; Bürgmann, H.; Li, X.-d.; Manaia, C. M.; Nambi, I.; Wigginton, K.; Zhang, T., Toward a Comprehensive Strategy to Mitigate

Dissemination of Environmental Sources of Antibiotic Resistance. *Environ. Sci. Technol.* **2017,** *51*, (22), 13061-13069.
22. Lorenz, M. G.; Wackernagel, W., Bacterial Gene Transfer by Natural Genetic Transformation in the Environment. *Microbiol. Rev.* **1994,** *58*, (3), 563-602.
23. Johnsborg, O.; Eldholm, V.; Havarstein, L. S., Natural genetic transformation: prevalence, mechanisms and function. *Res. Microbiol.* **2007,** *158*, (10), 767-778.
24. Canada, P. H. A. o. Pathogen Safety Data Sheets and Risk Assessment. http://www.phac-aspc.gc.ca/lab-bio/res/psds-ftss/index-eng.php#e
25. Domingues, S.; Harms, K.; Fricke, W. F.; Johnsen, P. J.; da Silva, G. J.; Nielsen, K. M., Natural Transformation Facilitates Transfer of Transposons, Integrons and Gene Cassettes between Bacterial Species. *PLOS Pathog.* **2012**.
26. Auerbach, E. A.; Seyfried, E. E.; McMahon, K. D., Tetracycline resistance genes in activated sludge wastewater treatment plants. *Water research* **2007,** *41*, (5), 1143-1151.
27. Zhang, T.; Zhang, M.; Zhang, X.; Fang, H. H., Tetracycline resistance genes and tetracycline resistant lactose-fermenting Enterobacteriaceae in activated sludge of sewage treatment plants. *Environmental science & technology* **2009,** *43*, (10), 3455-3460.
28. Ma, Y.; Wilson, C. A.; Novak, J. T.; Riffat, R.; Aynur, S.; Murthy, S.; Pruden, A., Effect of various sludge digestion conditions on sulfonamide, macrolide, and tetracycline resistance genes and class I integrons. *Environmental science & technology* **2011,** *45*, (18), 7855-7861.
29. Szczepanowski, R.; Linke, B.; Krahn, I.; Gartemann, K.-H.; Gützkow, T.; Eichler, W.; Pühler, A.; Schlüter, A., Detection of 140 clinically relevant antibiotic-resistance genes in the plasmid metagenome of wastewater treatment plant bacteria showing reduced susceptibility to selected antibiotics. *Microbiology* **2009,** *155*, (7), 2306-2319.
30. Luo, Y.; Yang, F.; Mathieu, J.; Mao, D.; Wang, Q.; Alvarez, P., Proliferation of multidrug-resistant New Delhi metallo-β-lactamase genes in municipal wastewater treatment plants in northern China. *Environmental Science & Technology Letters* **2013,** *1*, (1), 26-30.
31. Mathys, D. A.; Mollenkopf, D. F.; Feicht, S. M.; Adams, R. J.; Albers, A. L.; Stuever, D. M.; Grooters, S. V.; Ballash, G. A.; Daniels, J. B.; Wittum, T. E., Carbapenemase-producing Enterobacteriaceae and Aeromonas spp. present in wastewater treatment plant effluent and nearby surface waters in the US. *PloS one* **2019,** *14*, (6), e0218650.
32. Zhang, A.; Call, D. R.; Besser, T. E.; Liu, J.; Jones, L.; Wang, H.; Davis, M. A., β-lactam resistance genes in bacteriophage and bacterial DNA from wastewater, river water, and irrigation water in Washington State. *Water Res.* **2019**.
33. Goldstein, R. E. R.; Micallef, S. A.; Gibbs, S. G.; George, A.; Claye, E.; Sapkota, A.; Joseph, S. W.; Sapkota, A. R., Detection of vancomycin-resistant enterococci (VRE) at four US wastewater treatment plants that provide effluent for reuse. *Science of the total environment* **2014,** *466*, 404-411.
34. Goldstein, R. E. R.; Micallef, S. A.; Gibbs, S. G.; He, X.; George, A.; Sapkota, A.; Joseph, S. W.; Sapkota, A. R., Occupational exposure to Staphylococcus aureus and Enterococcus spp. among spray irrigation workers using reclaimed water. *International journal of environmental research and public health* **2014,** *11*, (4), 4340-4355.
35. Mao, D.; Luo, Y.; Mathieu, J.; Wang, Q.; Feng, L.; Mu, Q.; Feng, C.; Alvarez, P., Persistence of extracellular DNA in river sediment facilitates antibiotic resistance gene propagation. *Environmental science & technology* **2013,** *48*, (1), 71-78.

36. Luo, Y.; Mao, D.; Rysz, M.; Zhou, Q.; Zhang, H.; Xu, L.; JJ Alvarez, P., Trends in antibiotic resistance genes occurrence in the Haihe River, China. *Environmental science & technology* **2010,** *44*, (19), 7220-7225.
37. Xi, C.; Zhang, Y.; Marrs, C. F.; Ye, W.; Simon, C.; Foxman, B.; Nriagu, J., Prevalence of antibiotic resistance in drinking water treatment and distribution systems. *Applied and environmental microbiology* **2009,** *75*, (17), 5714-5718.
38. Guo, X.; Li, J.; Yang, F.; Yang, J.; Yin, D., Prevalence of sulfonamide and tetracycline resistance genes in drinking water treatment plants in the Yangtze River Delta, China. *Science of the Total Environment* **2014,** *493*, 626-631.
39. McKinney, C. W.; Loftin, K. A.; Meyer, M. T.; Davis, J. G.; Pruden, A., Tet and sul antibiotic resistance genes in livestock lagoons of various operation type, configuration, and antibiotic occurrence. *Environmental science & technology* **2010,** *44*, (16), 6102-6109.
40. Chee-Sanford, J. C.; Aminov, R. I.; Krapac, I.; Garrigues-Jeanjean, N.; Mackie, R. I., Occurrence and diversity of tetracycline resistance genes in lagoons and groundwater underlying two swine production facilities. *Applied and environmental microbiology* **2001,** *67*, (4), 1494-1502.
41. Koike, S.; Aminov, R. I.; Yannarell, A. C.; Gans, H. D.; Krapac, I. G.; Chee-Sanford, J. C.; Mackie, R. I., Molecular ecology of macrolide–lincosamide–streptogramin B methylases in waste lagoons and subsurface waters associated with swine production. *Microbial ecology* **2010,** *59*, (3), 487-498.
42. Sengeløv, G.; Agersø, Y.; Halling-Sørensen, B.; Baloda, S. B.; Andersen, J. S.; Jensen, L. B., Bacterial antibiotic resistance levels in Danish farmland as a result of treatment with pig manure slurry. *Environment international* **2003,** *28*, (7), 587-595.
43. Zhang, X.-X.; Zhang, T.; Fang, H. H., Antibiotic resistance genes in water environment. *Applied microbiology and biotechnology* **2009,** *82*, (3), 397-414.
44. Roberts, M. C.; Schwarz, S.; Aarts, H. J., Erratum: Acquired antibiotic resistance genes: an overview. *Frontiers in microbiology* **2012,** *3*, 384.
45. Nishiyama, M.; Iguchi, A.; Suzuki, Y., Identification of Enterococcus faecium and Enterococcus faecalis as vanC-type vancomycin-resistant enterococci (VRE) from sewage and river water in the provincial city of Miyazaki, Japan. *Journal of Environmental Science and Health, Part A* **2015,** *50*, (1), 16-25.
46. Luo, Y.; Yang, F.; Mathieu, J.; Mao, D.; Wang, Q.; Alvarez, P. J. J., Proliferation of Multidrug-Resistant New Delhi Metallo-β-lactamase Genes in Municipal Wastewater Treatment Plants in Northern China. *Environ. Sci. Technol. Lett* **2013,** *1*, (1), 26-30.
47. Yang, F.; Huang, L.; Li, L.; Yang, Y.; Mao, D.; Luo, Y., Discharge of KPC-2 genes from the WWTPs contributed to their enriched abundance in the receiving river. *Science of the Total Environment* **2017,** *581*, 136-143.
48. Yan, L.; Liu, D.; Wang, X.-H.; Wang, Y.; Zhang, B.; Wang, M.; Xu, H., Bacterial plasmid-mediated quinolone resistance genes in aquatic environments in China. *Scientific reports* **2017,** *7*, (1), 1-12.
49. Ramirez, M. S.; Nikolaidis, N.; Tolmasky, M., Rise and dissemination of aminoglycoside resistance: the aac (6′)-Ib paradigm. *Front. Microbiol.* **2013,** *4*, 121.
50. Knapp, C. W.; Dolfing, J.; Ehlert, P. A.; Graham, D. W., Evidence of increasing antibiotic resistance gene abundances in archived soils since 1940. *Environmental science & technology* **2009,** *44*, (2), 580-587.

51. Wright, G. D., *Antibiotic resistome: A framework linking the clinic and the environment*. John Wiley & Sons, Inc., Hoboken, New Jersey: 2012.
52. Martinez, J. L., The role of natural environments in the evolution of resistance traits in pathogenic bacteria. *Proceedings of the Royal Society of London B: Biological Sciences* **2009,** *276*, (1667), 2521-2530.
53. Wright, G. D., Antibiotic resistance in the environment: a link to the clinic? *Curr. Opin. Microbiol.* **2010,** *13*, (5), 589-594.
54. Chee-Sanford, J. C.; Mackie, R. I.; Koike, S.; Krapac, I. G.; Lin, Y.-F.; Yannarell, A. C.; Maxwell, S.; Aminov, R. I., Fate and transport of antibiotic residues and antibiotic resistance genes following land application of manure waste. *Journal of environmental quality* **2009,** *38*, (3), 1086-1108.
55. Pruden, A.; Larsson, D. J.; Amézquita, A.; Collignon, P.; Brandt, K. K.; Graham, D. W.; Lazorchak, J. M.; Suzuki, S.; Silley, P.; Snape, J. R., Management options for reducing the release of antibiotics and antibiotic resistance genes to the environment. *Environmental Health Perspectives (Online)* **2013,** *121*, (8), 878.
56. Pei, R.; Kim, S.-C.; Carlson, K. H.; Pruden, A., Effect of river landscape on the sediment concentrations of antibiotics and corresponding antibiotic resistance genes (ARG). *Water research* **2006,** *40*, (12), 2427-2435.
57. Storteboom, H.; Arabi, M.; Davis, J.; Crimi, B.; Pruden, A., Identification of antibiotic-resistance-gene molecular signatures suitable as tracers of pristine river, urban, and agricultural sources. *Environmental science & technology* **2010,** *44*, (6), 1947-1953.
58. Engemann, C. A.; Keen, P. L.; Knapp, C. W.; Hall, K. J.; Graham, D. W., Fate of tetracycline resistance genes in aquatic systems: migration from the water column to peripheral biofilms. *Environmental science & technology* **2008,** *42*, (14), 5131-5136.
59. Enne, V. I.; King, A.; Livermore, D. M.; Hall, L. M., Sulfonamide resistance in Haemophilus influenzae mediated by acquisition of sul2 or a short insertion in chromosomal folP. *Antimicrobial agents and chemotherapy* **2002,** *46*, (6), 1934-1939.
60. Shimabuku, K. K.; Zhou, P.; Dodd, M. C. In *Deactivation of antibiotic resistance genes with ozone and hydrogen peroxide*, Abstracts of Papers of the Amarican Chemical Society, 2014; AMER CHEMICAL SOC 1155 16TH ST, NW, WASHINGTON, DC 20036 USA: 2014.
61. Armstrong, J. L.; Calomiris, J. J.; Seidler, R. J., Selection of antibiotic-resistant standard plate count bacteria during water treatment. *Applied and environmental microbiology* **1982,** *44*, (2), 308-316.
62. Calomiris, J.; Armstrong, J. L.; Seidler, R. J., Association of metal tolerance with multiple antibiotic resistance of bacteria isolated from drinking water. *Applied and environmental microbiology* **1984,** *47*, (6), 1238-1242.
63. Mulvey, M. R.; Simor, A. E., Antimicrobial resistance in hospitals: how concerned should we be? *Cmaj* **2009,** *180*, (4), 408-415.
64. Bäumlisberger, M.; Youssar, L.; Schilhabel, M. B.; Jonas, D., Influence of a non-hospital medical care facility on antimicrobial resistance in wastewater. *PloS one* **2015,** *10*, (3).
65. Wang, Q.; Wang, P.; Yang, Q., Occurrence and diversity of antibiotic resistance in untreated hospital wastewater. *Science of the Total Environment* **2018,** *621*, 990-999.
66. Rodriguez-Mozaz, S.; Chamorro, S.; Marti, E.; Huerta, B.; Gros, M.; Sànchez-Melsió, A.; Borrego, C. M.; Barceló, D.; Balcázar, J. L., Occurrence of antibiotics and antibiotic resistance genes in hospital and urban wastewaters and their impact on the receiving river. *Water Res.* **2015,** *69*, 234-242.

67. Michael, I.; Rizzo, L.; McArdell, C.; Manaia, C.; Merlin, C.; Schwartz, T.; Dagot, C.; Fatta-Kassinos, D., Urban wastewater treatment plants as hotspots for the release of antibiotics in the environment: a review. *Water research* **2013,** *47*, (3), 957-995.
68. Szczepanowski, R.; Linke, B.; Krahn, I.; Gartemann, K.-H.; Guetzkow, T.; Eichler, W.; Pühler, A.; Schlueter, A., Detection of 140 clinically relevant antibiotic-resistance genes in the plasmid metagenome of wastewater treatment plant bacteria showing reduced susceptibility to selected antibiotics. *Microbiology* **2009,** *155*, (7), 2306-2319.
69. Czekalski, N.; Berthold, T.; Caucci, S.; Egli, A.; Buergmann, H., Increased levels of multiresistant bacteria and resistance genes after wastewater treatment and their dissemination into Lake Geneva, Switzerland. *Front. Microbiol.* **2012**.
70. Zhang, Y.; Li, A.; Dai, T.; Li, F.; Xie, H.; Chen, L.; Wen, D., Cell-free DNA: a neglected source for antibiotic resistance genes spreading from WWTPs. *Environ. Sci. Technol.* **2018,** *52*, (1), 248-257.
71. Ju, F.; Beck, K.; Yin, X.; Maccagnan, A.; McArdell, C. S.; Singer, H. P.; Johnson, D. R.; Zhang, T.; Bürgmann, H., Wastewater treatment plant resistomes are shaped by bacterial composition, genetic exchange, and upregulated expression in the effluent microbiomes. *The ISME journal* **2019,** *13*, (2), 346.
72. Pruden, A.; Pei, R.; Storteboom, H.; Carlson, K. H., Antibiotic resistance genes as emerging contaminants: studies in northern Colorado. *Environmental science & technology* **2006,** *40*, (23), 7445-7450.
73. Guardabassi, L.; Wong, D. M. L. F.; Dalsgaard, A., The effects of tertiary wastewater treatment on the prevalence of antimicrobial resistant bacteria. *Water research* **2002,** *36*, (8), 1955-1964.
74. Schwartz, T.; Kohnen, W.; Jansen, B.; Obst, U., Detection of antibiotic-resistant bacteria and their resistance genes in wastewater, surface water, and drinking water biofilms. *FEMS microbiology ecology* **2003,** *43*, (3), 325-335.
75. Czekalski, N.; Berthold, T.; Caucci, S.; Egli, A.; Bürgmann, H., Increased levels of multiresistant bacteria and resistance genes after wastewater treatment and their dissemination into Lake Geneva, Switzerland. *Frontiers in microbiology* **2012,** *3*.
76. Zhang, Y.; Marrs, C. F.; Simon, C.; Xi, C., Wastewater treatment contributes to selective increase of antibiotic resistance among Acinetobacter spp. *Science of the Total Environment* **2009,** *407*, (12), 3702-3706.
77. Kim, S.; Park, H.; Chandran, K., Propensity of activated sludge to amplify or attenuate tetracycline resistance genes and tetracycline resistant bacteria: a mathematical modeling approach. *Chemosphere* **2010,** *78*, (9), 1071-1077.
78. Jelic, A.; Gros, M.; Ginebreda, A.; Cespedes-Sánchez, R.; Ventura, F.; Petrovic, M.; Barcelo, D., Occurrence, partition and removal of pharmaceuticals in sewage water and sludge during wastewater treatment. *Water research* **2011,** *45*, (3), 1165-1176.
79. Ghosh, S.; Ramsden, S. J.; LaPara, T. M., The role of anaerobic digestion in controlling the release of tetracycline resistance genes and class 1 integrons from municipal wastewater treatment plants. *Applied microbiology and biotechnology* **2009,** *84*, (4), 791-796.
80. Pruden, A., Balancing water sustainability and public health goals in the face of growing concerns about antibiotic resistance. *Environ. Sci. Technol.* **2014,** *48*, (1), 5-14.
81. Hamelin, C., Production of Single- and Double-strand Breaks in Plasmid DNA by Ozone. *Int. J. Radiat. Oncol. Biol. Phys.* **1985,** *11*, (2), 253-257.

82. Hsu, Y. C., Resistance of infectious RNA and transforming DNA to iodine which inactivates f_2 phage and cells. *Nature* **1964,** *203*, (494), 152-153.
83. Roller, S. D.; Olivieri, V. P.; Kawata, K., Mode of bacterial inactivation by chlorine dioxide. *Water Res.* **1980,** *14*, (6), 635-641.
84. Guo, M.-T.; Yuan, Q.-B.; Yang, J., Distinguishing effects of ultraviolet exposure and chlorination on the horizontal transfer of antibiotic resistance genes in municipal wastewater. *Environ. Sci. Technol.* **2015,** *49*, (9), 5771-5778.
85. Huang, J.-J.; Hu, H.-Y.; Tang, F.; Li, Y.; Lu, S.-Q.; Lu, Y., Inactivation and reactivation of antibiotic-resistant bacteria by chlorination in secondary effluents of a municipal wastewater treatment plant. *Water Res.* **2011,** *45*, (9), 2775-2781.
86. Zhang, Y.; Zhuang, Y.; Geng, J.; Ren, H.; Zhang, Y.; Ding, L.; Xu, K., Inactivation of antibiotic resistance genes in municipal wastewater effluent by chlorination and sequential UV/chlorination disinfection. *Science of the Total Environment* **2015,** *512*, 125-132.
87. Munir, M.; Wong, K.; Xagoraraki, I., Release of antibiotic resistant bacteria and genes in the effluent and biosolids of five wastewater utilities in Michigan. *Water Res.* **2011,** *45*, (2), 681-693.
88. Shi, P.; Jia, S.; Zhang, X.-X.; Zhang, T.; Cheng, S.; Li, A., Metagenomic insights into chlorination effects on microbial antibiotic resistance in drinking water. *Water Res.* **2013,** *47*, (1), 111-120.
89. Yoon, Y.; Chung, H. J.; Di, D. Y. W.; Dodd, M. C.; Hur, H.-G.; Lee, Y., Inactivation efficiency of plasmid-encoded antibiotic resistance genes during water treatment with chlorine, UV, and UV/H2O2. *Water Res.* **2017,** *123*, 783-793.
90. Pak, G.; Salcedo, D. E.; Lee, H.; Oh, J.; Maeng, S. K.; Song, K. G.; Hong, S. W.; Kim, H.-C.; Chandran, K.; Kim, S. J. E. S.; Technology, Comparison of antibiotic resistance removal efficiencies using ozone disinfection under different pH and suspended solids and humic substance concentrations. **2016,** *50*, (14), 7590-7600.
91. Czekalski, N.; Imminger, S.; Salhi, E.; Veljkovic, M.; Kleffel, K.; Drissner, D.; Hammes, F.; Bürgmann, H.; Von Gunten, U., Inactivation of antibiotic resistant bacteria and resistance genes by ozone: from laboratory experiments to full-scale wastewater treatment. *Environ. Sci. Technol.* **2016,** *50*, (21), 11862-11871.
92. Yoon, Y.; Dodd, M. C.; Lee, Y., Elimination of transforming activity and gene degradation during UV and UV/H2O2 treatment of plasmid-encoded antibiotic resistance genes. *Environ. Sci.: Wat. Res. Technol.* **2018,** *4*, 1239-1251.
93. McKinney, C. W.; Pruden, A., Ultraviolet disinfection of antibiotic resistant bacteria and their antibiotic resistance genes in water and wastewater. *Environ. Sci. Technol.* **2012,** *46*, (24), 13393-13400.
94. Süß, J.; Volz, S.; Obst, U.; Schwartz, T., Application of a molecular biology concept for the detection of DNA damage and repair during UV disinfection. *Water Res.* **2009,** *43*, (15), 3705-3716.
95. Rutala, W. A.; Weber, D. J., Guideline for disinfection and sterilization in healthcare facilities, 2008. **2008**.
96. Block, S. S., *Disinfection, sterilization, and preservation*. Lippincott Williams & Wilkins: 2001.
97. Fraise, A. P.; Lambert, P. A.; Maillard, J.-Y., *Russell, Hugo & Ayliffe's principles and practice of disinfection, preservation and sterilization*. John Wiley & Sons: 2008.

98. Wendt, C.; Frei, R.; Widmer, A. F., Decontamination, Disinfection, and Sterilization. In *Manual of Clinical Microbiology, Eleventh Edition,* American Society of Microbiology: 2015; pp 183-216.
99. Dodd, M. C., Potential impacts of disinfection processes on elimination and deactivation of antibiotic resistance genes during water and wastewater treatment. *J. Environ. Monit.* **2012,** *14*, 1754–1771.

Chapter 2. Degradation and Deactivation of Bacterial Antibiotic Resistance Genes during Exposure to Free Chlorine, Monochloramine, Chlorine Dioxide, Ozone, Ultraviolet Light, and Hydroxyl Radical

ABSTRACT

This work investigated *degradation* (measured by qPCR) and biological *deactivation* (measured by culture-based natural transformation) of extra- and intracellular antibiotic resistance genes (eARGs and iARGs) by free available chlorine (FAC), NH_2Cl, O_3, ClO_2, UV and $^{\bullet}OH$, using a chromosomal ARG (*blt*) of multidrug-resistant *Bacillus subtilis* 1A189. Rate constants for *degradation* of four 266-1017 bp amplicons adjacent to or encompassing the *acfA* mutation enabling *blt* overexpression increased in proportion to #AT+GC bps/amplicon, or #5'-GG-3' or 5'-TT-3' doublets/amplicon, with respective values ranging from 0.59-2.3($\times 10^{11}$ $M^{-1}s^{-1}$) for $^{\bullet}OH$, 1.8-6.9($\times 10^{4}$ $M^{-1}s^{-1}$) for O_3, 3.9-9.2($\times 10^{3}$ $M^{-1}s^{-1}$) for FAC, 0.35-1.2($\times 10^{1}$ $M^{-1}s^{-1}$) for ClO_2, and 2.0-8.8($\times 10^{-2}$ cm^2/mJ) for UV at pH 7, and 1.7-4.4 $M^{-1}s^{-1}$ for NH_2Cl at pH 8. For FAC, NH_2Cl, O_3, ClO_2, and UV, ARG *deactivation* paralleled *degradation* of amplicons approximating a ~800-1000 bp *acfA*-flanking sequence required for natural transformation in *B. subtilis*, whereas *deactivation* outpaced *degradation* for $^{\bullet}OH$. At practical disinfectant exposures, eARGs and iARGs were ≥90% degraded/deactivated by FAC, O_3, and UV, but recalcitrant to NH_2Cl and ClO_2. iARG *degradation*/*deactivation* always lagged cell inactivation. These findings provide a quantitative framework for evaluating ARG fate during disinfection/oxidation, and support using qPCR as a proxy for tracking ARG *deactivation* under carefully selected circumstances.

2.1 INTRODUCTION

The proliferation of antibiotic resistance since the early 20th century has decreased the therapeutic effectiveness of antibiotics,[1] leading to associated increasing mortality, morbidity, and economic losses worldwide.[2, 3] Antibiotic resistant bacteria and resistance genes (ARB and ARGs) are now known to be widespread in aquatic environments. For example, ARBs and ARGs have been found in liquid animal wastes and manure derived from confined animal feed operations,[4, 5] municipal wastewaters,[4, 6-8] surface waters and associated sediments,[4, 6, 9] and drinking water treatment and distribution systems.[4, 10, 11]

In this context, (waste)water treatment could potentially provide an important barrier to ARB/ARG dissemination. (Waste)water disinfection processes may play a particularly critical role by inactivating ARB. However, even if ARB are fully inactivated during disinfection, intact DNA remnants within the resulting cell debris could possibly confer resistance to downstream bacterial populations via horizontal gene transfer (HGT). For example, through natural transformation, ARGs carried on extracellular plasmid or genomic DNA originating from a donor cell can be taken up by a "competent" non-resistant recipient cell, incorporated into the latter's genome, and expressed by the transformed recipient cell.[12, 13] A wide variety of naturally competent strains have been identified,[13, 14] including many important human pathogens.[15] In addition, while natural transformation is typically most facile amongst the same species, interspecies transformation is also possible.[13, 16] Because extracellular DNA molecules may persist within aquatic systems over extended periods via adsorption onto or complexation with cellular debris, clay, sand, or humic constituents,[13, 17, 18] natural transformation could also mediate ARG transfer to bacterial populations temporally or spatially distant from donor cells.[13]

Previous studies have demonstrated that ARGs are degraded with widely varying efficiencies by disinfectants/oxidants including free available chlorine (FAC),[19] monochloramine (NH_2Cl),[20, 21] chlorine dioxide (ClO_2),[22] ozone (O_3),[23, 24] ultraviolet (UV) light[19, 21, 25-29] and hydroxyl radical ($^{\bullet}OH$).[19] However, few have elucidated the fundamental kinetic parameters governing ARG *degradation*,[19, 24, 27] making it difficult to compare prior results obtained under different experimental conditions. In addition, relatively few have investigated the impacts of disinfection processes on ARG biological activities,[27] in turn hindering assessment of the environmental/biological implications of ARG degradation during these processes. Furthermore, recent attention has focused primarily on reactions of disinfectants/oxidants with plasmid-borne ARGs[19, 24, 27] rather than chromosomal ARGs, even though natural transformation with chromosomal DNA is generally far more efficient than with plasmid DNA.[13]

This work was therefore undertaken to provide a comprehensive investigation of the fundamental kinetic parameters and mechanisms governing ARG *degradation* and *deactivation* by common (waste)water disinfectants/oxidants, including FAC, NH_2Cl, ClO_2, O_3, UV light, and $^{\bullet}OH$, using a model chromosomal ARG (*blt*) harbored by multidrug-resistant *Bacillus subtilis* strain 1A189. *blt* is a widely studied member of the major facilitator superfamily of multidrug transporters with broad substrate specificity, and a close homolog of the clinically-relevant *norA* gene conferring fluoroquinolone resistance in *Staphylococcus aureus*.[30-32] *B. subtilis* was selected as a model bacterium on account of its ease of culturing and natural competence, widely available gene sequence data, and the relevance of it and related *Bacilli* – including pathogenic strains of *Streptococcus*, *Enterococcus*, and *Staphylococcus* spp., with which *B. subtilis* may exchange ARGs – as important members of soil, water, and human gastrointestinal microflora.[33]

The ability of each disinfectant to *degrade* and *deactivate* extracellular and intracellular ARGs was assessed by subjecting purified DNA and intact *B. subtilis* 1A189 cells to increasing disinfectant exposures representative of (waste)water practice. A combination of culture-based and molecular microbiological techniques was used in parallel to monitor ARG *degradation* (i.e., decreases in ARG copy numbers measured by qPCR), ARG *deactivatio*n (i.e., elimination of ARG transforming activities), and donor ARB cell inactivation. *Degradation* kinetics were quantified for each disinfectant using a set of four 266-1017bp *blt* amplicons with different nucleotide contents located adjacent to or encompassing the *acfA* mutation that enables *blt* over-expression in *B. subtilis* 1A189. Observed rate constants for the four amplicons were compared to their specific nucleotide contents to enable determination of fundamental *sequence-independent* rate constants for DNA reaction with each disinfectant. These fundamental kinetics parameters were in turn applied to predict the kinetics with which the DNA region responsible for *blt* transformation was *degraded* and *deactivated* during extra- and intracellular treatment by each disinfectant.

2.2 MATERIALS AND METHODS

2.2.1 *Chemicals and Materials.*

All chemicals and growth media were purchased from commercial suppliers, certified-nuclease free, and of at least reagent-grade purity. Molecular biology grade water (Corning, NY) was utilized in DNA standard preparations, transformation assays and qPCR analyses. Milli-Q grade (≥18.2 MΩ cm) water was otherwise used to prepare chemical reagents and growth media, which (except disinfectants) were then autoclaved or filter-sterilized prior to use. Preparations of

aqueous stocks of FAC, NH_2Cl, ClO_2, O_3 and hydrogen peroxide (H_2O_2), as well as other reagents and culture media, are described in Supporting Information, Text S2.1.

2.2.2 *Bacterial Strains.*

B. subtilis strains 1A1 (non-resistant) and 1A189 (multidrug-resistant) were obtained from the Bacillus Genetic Stock Center (BGSC; Ohio State University), revived, and cultured according to BGSC instructions. Genomic DNA of *B. subtilis* 1A189 exhibits a point mutation (*acfA* – an A-T base-pair deletion) in the promoter region of the 1203-bp wild-type *blt* gene, which is part of the *bltR-blt-bltD* genome segment characteristic of *B. subtilis*, as illustrated in Scheme 2.1. The mutant genome segment encodes constitutional efflux-mediated resistance to a wide variety of antibiotics (including fluoroquinolones, chloramphenicol, doxorubicin, and acriflavine), whereas the wild-type segment does not.[34]

2.2.3 *DNA Extraction.*

High molecular weight DNA was isolated from *B. subtilis* 1A189 cells by phenol-chloroform-isoamyl alcohol extraction,[35] with additional purification steps. Detailed extraction procedures and recovery yields are provided in Text S2.2.

2.2.4 *Natural transformation assay.*

Transforming activity of *B. subtilis* 1A189 DNA was quantified by natural transformation, using *B. subtilis* 1A1 as the recipient,[36, 37] with key steps depicted in Scheme 2.1 and detailed protocols provided in Text S2.3. Transformation *frequency* was calculated as transformant cell density (CFU/mL) measured on selective media (with 4-mg/L acriflavine) over total recipient cell density (CFU/mL) on non-selective media (Text S2.4).

2.2.5 *Quantitative polymerase chain reaction (qPCR).*

qPCR assays were performed using an Eppendorf RealPlex^4 Mastercycler (Hauppauge, NY) with SsoFast™ EvaGreen® Supermix[29] (Bio-Rad, Hercules, CA) to quantify gene copy numbers of 266-1017 bp *blt* amplicons. Primers were designed based on the *B. subtilis* 168 *bltR-blt-bltD* gene sequence (GenBank accession number: AL009126.3), and purchased from Eurofins (Huntsville, AL). The 266 and 832 bp amplicons target the *blt* gene, whereas the 870 and 1017 bp amplicons encompass the *acfA* mutation and span the *blt* promoter between the *bltR* and *blt* genes (Scheme 2.1). Locations and sequences of the amplicons with corresponding primers are shown in Text S2.5. Their nucleotide contents, including numbers of interstrand AT, GC, and AT+GC base pairs (bps), and numbers of intrastrand 5'-GG-3', and 5'-TT-3'doublets per amplicon, are summarized in Table S2.1. qPCR assay protocols (including amplification efficiencies, limits of detection and quantification (LODs & LOQs), etc.) are provided in Text S2.6.

2.2.6 *Other DNA analyses.*

DNA fragment sizes were analyzed by pulsed-field gel electrophoresis (PFGE) (Text S2.7). Double-stranded DNA (dsDNA) and monomeric deoxyribonucleoside 5'-monophosphate (dNMP, or nucleotide) concentrations were measured by (i) Hoechst 33258 fluorescence assay with a DNA Quantitation Kit (Bio-Rad) and (ii) nuclease P1 (Sigma) digestion followed by high performance liquid chromatography,[38] respectively.

2.2.7 *Treatment of extracellular ARGs (eARGs).*

B. subtilis 1A189 DNA was diluted and exposed to each disinfectant in autoclaved 10-mM phosphate buffer (PB) at pH 7 for FAC, ClO_2, O_3, UV and $^{\bullet}OH$, and pH 8 for NH_2Cl to

minimize NH_2Cl self-decomposition (see Text S2.8 for discussion of limited NH_2Cl experiments at pH 7), with FAC, NH_2Cl, ClO_2, and O_3 at ≥ 10-fold molar excess of DNA (as [dNMPs]). For FAC, NH_2Cl, and ClO_2, disinfection was performed in continuously stirred batch reactors by adding disinfectant stocks to 1-mg/L DNA solutions (3.2×10^{-6} M as total dNMPs). At pre-defined time intervals, reaction solutions were sampled and quenched with sodium thiosulfate ($Na_2S_2O_3$) (≥ 20-fold molar excess of [disinfectant]). For O_3, reactions were undertaken with 1-mg/L DNA solutions in the presence of 50-mM *tert*-butanol (*t*-BuOH) using a continuous-flow, quenched-reaction system (Text S2.8).[39] For UV, 1-mg/L DNA solutions contained in quartz tubes were irradiated with a low-pressure Hg lamp in a "merry-go-round" photoreactor apparatus, and sampled at pre-defined times (Text S2.8). For $^{\bullet}OH$, 10-mg/L DNA solutions containing 10-mM H_2O_2 and 1-μM *para*-chlorobenzoic acid (*p*CBA, a $^{\bullet}OH$ probe) were irradiated with near-UV wavelengths (290-400 nm) to preclude DNA damage by direct photolysis. At pre-defined times, samples were collected and quenched with bovine liver catalase (Sigma; ≥10-units/μmole H_2O_2).

Residual disinfectant concentrations were monitored colorimetrically using DPD for FAC and NH_2Cl,[40] ABTS for ClO_2,[41] and indigo trisulfonate for O_3.[42] Fluence rates (*I*, in mW/cm^2) for UV irradiation experiments were quantified using atrazine,[43] iodide/iodate,[44] and/or ferrioxalate[44] actinometry. Pathlength was determined according to Zepp (1978),[45] using ferrioxalate actinometry.[44] Cumulative integrated exposures (or *CT* values) for chemical disinfectants were calculated as $\int_0^t [\text{Disinfectant}]\,dt$ (in mg/L•min), while fluences (or *IT* values) for UV were calculated as $I \times t$ (in mJ/cm^2). $^{\bullet}OH$ exposures were determined by monitoring *p*CBA *degradation* in near-UV/H_2O_2 experiments.[46] Details of reactor configurations, additional experiments, and disinfectant exposure measurements are provided in Text S2.8.

2.2.8 *Treatment of intracellular ARGs (iARGs).*

Vegetative cells of *B. subtilis* 1A189 were dosed into autoclaved 10-mM PB solutions and exposed to each disinfectant at the same pH as in eARG treatment (*B. subtilis* intracellular pH has been reported to be ~7.4 with an extracellular pH maintained at 6-8).[47] Disinfectant stocks were dosed to 1-L, 10^6-CFU/mL cell suspensions in batch reactors under stirring to yield 2 mg/L of FAC, NH_2Cl, or ClO_2, and 1 mg/L of O_3. O_3 experiments were performed with and without 50-mM *t*-BuOH (•OH scavenger) to evaluate potential contributions of •OH to iARG *degradation/deactivation* during ozonation. At pre-defined times, each 1-L reaction suspension was quenched with $Na_2S_2O_3$. For UV, 100-mL, 10^6-CFU/mL cell suspensions were equally split into four quartz tubes, irradiated for pre-defined times, and combined for subsequent analyses. Disinfectant exposures were determined as described above.

Treated cell viabilities were determined by direct spread-plating or spot-titering[48] of sample aliquots on selective media, with LODs permitting measurement of ~5.5- and ~5.1-$\log_{10}$ inactivation, respectively. Treated cells were recovered by vacuum filtration of full sample volumes through 0.2 μm track-etched polycarbonate membranes (Whatman, NJ) and processed for DNA extraction as described in Text S2.2. Intracellular DNA recovery was determined by measuring dsDNA concentration or dNMP concentrations if the former was below the fluorescence assay LOQ.

Scheme S2.1 provides an overview of the above experimental procedures. All experiments were performed in at least duplicate at 25±1 °C (UV) or 20±1 °C (other disinfectants). ARG transforming activities, ARG copy numbers, and DNA fragment sizes of collected DNA samples were analyzed as specified above. Normalized gene copy numbers (N/N_0) or normalized transformation frequencies (f/f_0) were calculated as gene copy number or

transformation frequency of a given sample divided by that of a corresponding untreated control, respectively.

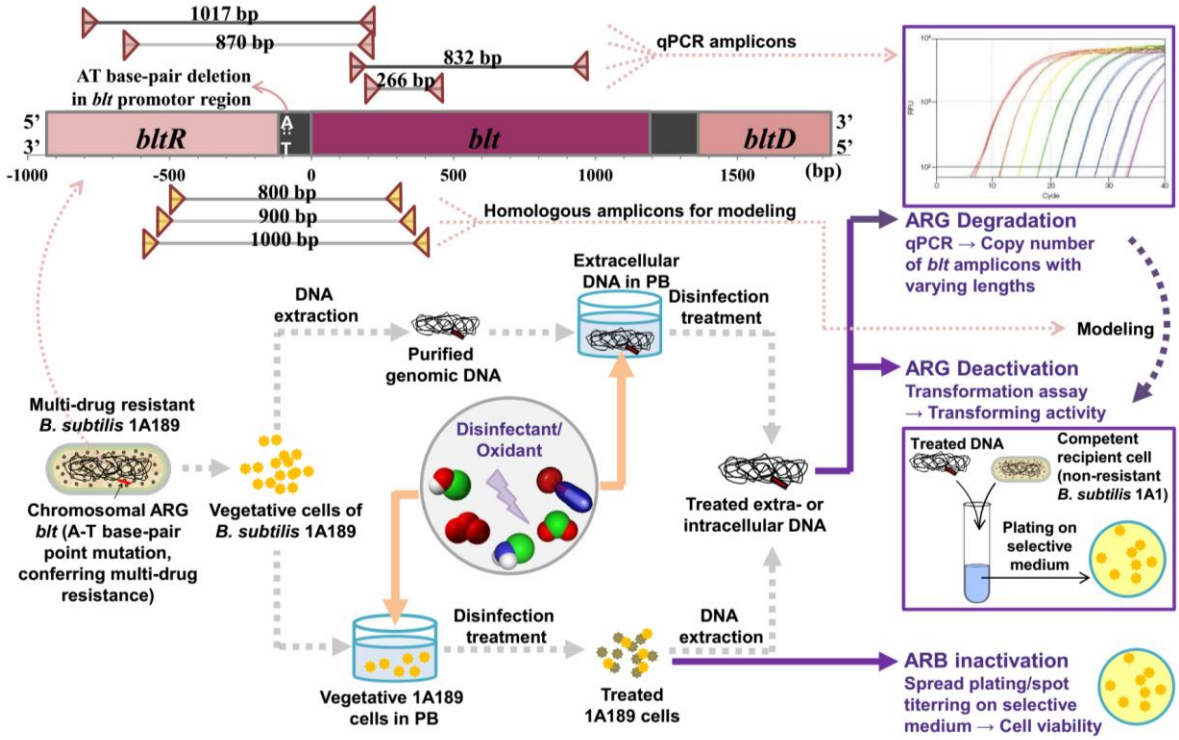

Scheme 2.1. Procedures for treatment of eARGs and iARGs and subsequent analyses including qPCR, transformation assay, and spread plating or spot titering – to track ARG degradation, ARG deactivation and ARB inactivation, respectively.

2.2.9 *Statistical analysis.*

Data from independent replicate experiments were pooled in order to perform least-square linear regressions (using SigmaPlot 12.0) or non-linear regressions (using Microsoft Excel SOLVER; Text S2.9) for determining first- or second-order rate constants (and associated uncertainties) of each *blt* amplicon in its reaction with each disinfectant. The method of weighted linear regression was applied to perform uncertainty-weighted regression analyses of first-order rate constants for each amplicon versus disinfectant concentrations, or for amplicon-specific second-order rate constants versus amplicon nucleotide contents, since the rate constants derived in each of these cases carry associated standard errors (since they are themselves obtained by

linear regressions of measured data).[49] Here, for an *n*-number dataset with *y*-direction standard errors (x_i, $y_i \pm e_i$), the individual weights (w_i) were defined as,

$$w_i = \frac{e_i^{-2}}{\sum_i e_i^{-2}/n} \tag{2.1}$$

The slope and intercept of the weighted regression line, their associated standard errors, in addition to the coefficient of determination (R^2), were calculated as below,

$$\text{Slope} = \frac{\sum_i w_i x_i y_i - n\bar{x}_w \bar{y}_w}{\sum_i w_i x_i^2 - n\bar{x}_w^2} \tag{2.2}$$

$$\text{Intercept} = \bar{y}_w - \text{Slope} \cdot \bar{x}_w \tag{2.3}$$

$$\text{Slope\_error} = \frac{\sqrt{\sum_i w_i (y_i - y_{i,p})^2/(n-2)}}{\sqrt{\sum_i w_i (x_i - \bar{x}_w)^2}} \tag{2.4}$$

$$\text{Intercept\_error} = \sqrt{\frac{\sum_i w_i (y_i - y_{i,p})^2}{n-2}} \cdot \sqrt{\frac{\sum_i w_i x_i^2}{n\sum_i w_i (x_i - \bar{x}_w)^2}} \tag{2.5}$$

$$R^2 = \frac{\left[\sum_i w_i (x_i - \bar{x}_w)(y_i - \bar{y}_w)\right]^2}{\left[\sum_i w_i (x_i - \bar{x}_w)^2\right] \cdot \left[\sum_i w_i (y_i - \bar{y}_w)^2\right]} \tag{2.6}$$

where $\bar{x}_w$ and $\bar{y}_w$ are the weighted mean values of x_i and y_i, which equal to $\sum_i w_i x_i / n$ and $\sum_i w_i y_i / n$, respectively; and $y_{i,p}$ is predicted from the weighted regression line as $\text{Slope} \cdot x_i + \text{Intecept}$. In this work, the weighted linear regressions were undertaken using either Minitab® 18, or by manually establishing eqs 1-6 in Microsoft Excel spreadsheet, which have each been confirmed to yield consistent results.

Slopes of linear regressions obtained for datasets from selected UV experiments were compared using two-tailed *t*-tests with statistical significance defined as $p < 0.05$, and null

hypothesis as no significant difference existing between slopes from the two datasets. Statistical analyses pertaining to determination of LODs & LOQs for qPCR assays are provided in Text S2.6.

2.3 RESULTS AND DISCUSSION

2.3.1 *ARG amplicon degradation: Reaction kinetics and rate constants.*

Degradation rates of 266-1017 bp *blt* amplicons were monitored by qPCR during eARG treatment by each disinfectant to quantify damage to DNA sequences in the vicinity of the *acfA* point mutation responsible for *B. subtilis* 1A189 multidrug-resistance. Previous work has confirmed that various types of DNA lesions – e.g., 5'-TT-3' cyclobutane pyrimidine dimers (TT-CPDs, the primary UV-induced lesions), 8-oxo-7,8-dihydro-2'-deoxyadenosine (8-oxoG), and abasic sites – can block or greatly hinder *Taq* polymerase (utilized in the qPCR assays here) from reading along a stretch of dsDNA.[50, 51] Although it has been reported that certain lesions (e.g., a single 8-oxoG) can be bypassed by the *Taq* polymerase, and are thus effectively non-detectable by qPCR,[51] such lesions would most likely also be bypassed or even repaired by *B. subtilis* polymerases.[52] Thus, detectable losses in qPCR signal were tentatively taken to correspond to the introduction of one or more biologically-relevant lesions, which would also block native *B. subtilis* polymerases, in the population of targeted amplicons within a given sample. Plots of $\ln(N/N_0)$ of the four amplicons versus *CT* or *IT* (to normalize for differences in disinfectant/oxidant concentrations and experimental timeframes) are presented for each disinfectant in Figure 2.1.

For FAC and NH_2Cl, amplicon *degradation* rates were observed to accelerate with increasing *CT* values for all four amplicons (Figure 2.1a, b). To explain these trends, it is hypothesized that FAC/NH_2Cl reacts with DNA in a sequential reaction pathway, with two steps,

each following second-order kinetics: (i) initial N-chlorination at an amino group of a nucleotide (reversible by $Na_2S_2O_3$, and hence, not directly detectable by qPCR) – characterized by the rate constant $k_{FAC/NH_2Cl,Amp}$, and leading to organochloramine formation, H-bond disruption, and exposure of the nucleotide and its pairing partner toward subsequent attack by FAC/NH_2Cl, followed by (ii) irreversible C-chlorination at a carbon of one of the non-H-bonded nucleotides of an N-chlorinated nucleotide base pair (N-Cl bp) – characterized by $k_{FAC/NH_2Cl,N\text{-}Cl\ bp}$, and leading to formation of stable halogenated products (with 5-chloro- and 8-chloro-derivatives likely prevailing for pyrimidines and purines, respectively),[53, 54] and blockage of amplification as captured by qPCR. Further discussion on the complex kinetics of FAC and NH_2Cl, as well as determination of $k_{FAC/NH_2Cl,Amp}$ and $k_{FAC/NH_2Cl,N\text{-}Cl\ bp}$, are provided in Text S2.9 and Figures S2.3-S2.11.

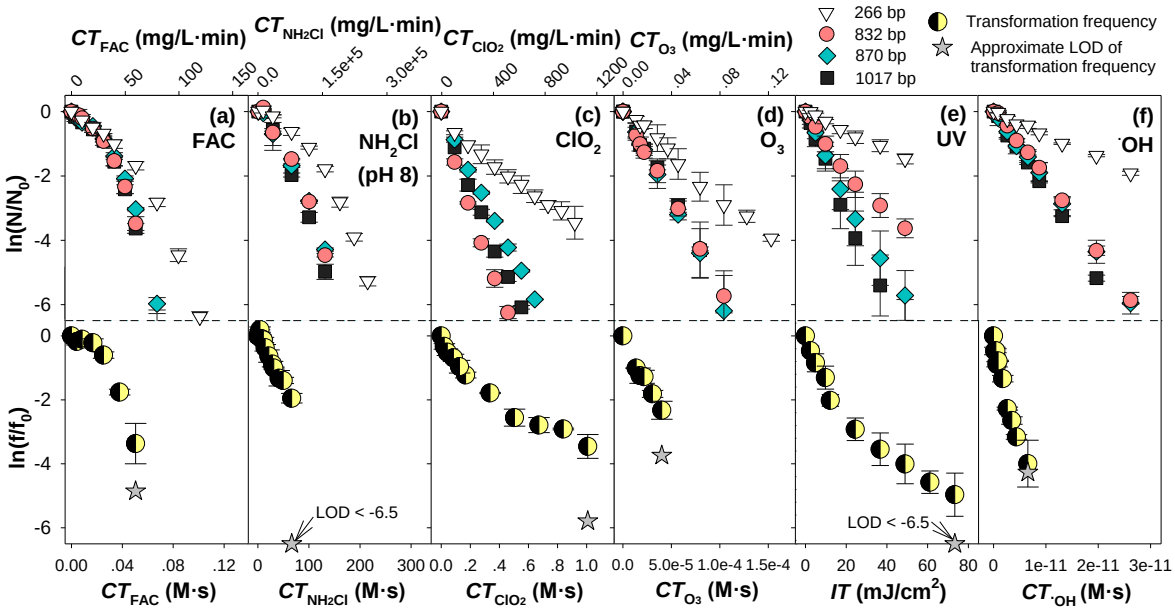

Figure 2.1. Normalized (natural log-scale) qPCR amplicon copy numbers (upper) and *blt* transformation frequency (lower) versus *CT* values for (a) FAC, (b) NH_2Cl, (c) ClO_2, (d) O_3, and (f) $^{\bullet}OH$; and *IT* values for (e) UV. All data were obtained by treatment of extracellular *B. subtilis* 1A189 DNA in 10-mM phosphate buffer at pH 7 (FAC, ClO_2, O_3, $^{\bullet}OH$, and UV) or 8 (NH_2Cl only). LODs of normalized qPCR amplicon copy numbers were all below the lower y-axis limits (i.e., < -6.5 natural log-loss, and are thus not shown), while LODs of normalized transformation frequencies are shown with star symbols for each disinfectant. Error bars represent standard deviations obtained from at least duplicate experiments conducted independently.

$\ln(N/N_0)$ was linearly related to *CT* or *IT* for the four amplicons during treatment with ClO_2, O_3, $^{\bullet}OH$, and UV (Figure 2.1c-f), indicating that amplicon *degradation* by these disinfectants followed second-order or fluence-based first-order kinetics, according to eqs 7 or 8, respectively.

$$\ln(N/N_0) = -k_{\text{Disinfectant,Amp}} \int_0^t [\text{disinfectant}]\, dt = -k_{\text{Disinfectant,Amp}} CT \quad (2.7)$$

$$\ln(N/N_0) = -k_{\text{Disinfectant,Amp}} (I \times t) = -k_{\text{Disinfectant,Amp}} IT \quad (2.8)$$

Determinations of the rate constants $k_{\text{Disinfectant,Amp}}$ for ClO_2, O_3, UV and $^{\bullet}OH$ from linear regression of the data are presented in Figures S12, S13, S14 and S15, respectively. Note that linear regressions for UV data were performed only up to 45 mJ/cm^2 to exclude moderate tailing in the data at higher *IT*s (potentially due to CPD photoreversal,[55] as discussed later).

The measured values of $k_{\text{Disinfectant,Amp}}$ for *degradation* of the four amplicons by each disinfectant are summarized in Table 2.1, and compared with available literature values in Table S2.3. For a given amplicon, the DNA reactivity toward the chemical disinfectants declines in the order $^{\bullet}OH$ >> O_3 > FAC >> ClO_2 > NH_2Cl. The measurements of $k_{\text{O}_3\text{,Amp}}$ and $k_{\text{UV,Amp}}$ both agree well with literature values,[19, 24, 27] while the measured $k_{\text{FAC,Amp}}$ values (for initial N-chlorination by FAC) are >10× higher than those reported by Yoon et el. for 806-850 bp amplicons on the pUC4K plasmid.[19] This may be due to inherent differences in plasmid and genomic DNA reactivities, though it is worth noting that the prior values were determined according to an assumption of pseudo-first-order kinetics rather than the sequential-reaction model here. The $k_{^{\bullet}\text{OH,Amp}}$ values determined here are ~10× higher than measurements by Yoon et al.[19] for plasmid-borne ARGs, but agree well with estimates of theoretical diffusion-controlled rate constants for polymeric (linear or supercoiled) DNA (Text S2.10).

Table 2.1. Summary of kinetics parameters (as mean ± standard error) for ARG *degradation* measured in this study

$k_{Disinfectant,Amp}$ [a]	266 bp	832 bp	870 bp	1017 bp	$k_{Disinfectant,Specific}$ [d]	$k_{Disinfectant,0}$ [d]
$k_{FAC,Amp}$ [b] ($M^{-1}s^{-1}$)	$3.9(\pm0.3)\times10^{3}$	$8.5(\pm0.5)\times10^{3}$	$8.1(\pm0.5)\times10^{3}$	$9.2(\pm0.5)\times10^{3}$	$7.2(\pm0.5)$ $(M\ AT+GC)^{-1}s^{-1}$	$2.1(\pm0.4)\times10^{3}$ $M^{-1}s^{-1}$
$k_{FAC,N\text{-}Cl\ bp}$ [c] ($M^{-1}s^{-1}$)	$3.9(\pm0.2)\times10^{-1}$				N.A.	N.A.
$k_{NH_2Cl,Amp}$ [b] ($M^{-1}s^{-1}$)	$1.7(\pm0.1)$	$3.6(\pm0.1)$	$3.8(\pm0.2)$	$4.4(\pm0.2)$	$3.6(\pm0.1)\times10^{-3}$ $(M\ AT+GC)^{-1}s^{-1}$	$6.9(\pm0.6)\times10^{-1}$ $M^{-1}s^{-1}$
$k_{NH_2Cl,N\text{-}Cl\ bp}$ [c] ($M^{-1}s^{-1}$)	$1.6(\pm0.1)\times10^{-4}$				N.A.	N.A.
$k_{ClO_2,Amp}$ ($M^{-1}s^{-1}$)	$3.5(\pm0.3)$	$1.2(\pm0.2)\times10^{1}$	$8.9(\pm0.2)$	$1.2(\pm0.2)\times10^{1}$	$2.6(\pm0.1)\times10^{-1}$ $(M\ 5'\text{-}GG\text{-}3')^{-1}s^{-1}$	$-8.1(\pm1.8)\times10^{-1}$ $M^{-1}s^{-1}$
$k_{O_3,Amp}$ ($M^{-1}s^{-1}$)	$1.8(\pm0.5)\times10^{4}$	$6.1(\pm1.2)\times10^{4}$	$5.3(\pm0.8)\times10^{4}$	$6.9(\pm0.8)\times10^{4}$	$6.5(\pm0.7)\times10^{1}$ $(M\ AT+GC)^{-1}s^{-1}$	$0.5(\pm4.5)\times10^{3}$ $M^{-1}s^{-1}$
$k_{UV,Amp}$ (cm^2/mJ)	$2.0(\pm0.1)\times10^{-2}$	$5.2(\pm0.2)\times10^{-2}$	$7.8(\pm0.4)\times10^{-2}$	$8.8(\pm0.4)\times10^{-2}$	$2.8(\pm0.3)\times10^{-4}$ $(M\ 5'\text{-}TT\text{-}3'/M\ amplicon)^{-1}$ (cm^2/mJ)	$5.0(\pm3.3)\times10^{-3}$ cm^2/mJ
$k_{\cdot OH,Amp}$ ($M^{-1}s^{-1}$)	$5.9(\pm0.8)\times10^{10}$	$1.9(\pm0.2)\times10^{11}$	$2.0(\pm0.2)\times10^{11}$	$2.3(\pm0.3)\times10^{11}$	$2.3(\pm0.1)\times10^{8}$ $(M\ AT+GC)^{-1}s^{-1}$	$-1.4(\pm2.2)\times10^{9}$ $M^{-1}s^{-1}$

[a] All data were obtained by treatment of extracellular *B. subtilis* 1A189 DNA in 10-mM phosphate buffer at pH 7 (FAC, ClO_2, O_3, $^{\bullet}OH$, and UV) or 8 (NH_2Cl only). Significands of standard errors of $k_{Disinfectant,Amp}$ were rounded up to 0.1 if below 0.1. [b] Rate constant for the first step in the sequential reaction, i.e., reversible N-chlorination of amplicons (see eqs S2.1 and S2.6 for FAC and NH_2Cl, respectively). [c] Rate constant for the second step in the sequential reaction, i.e., irreversible C-chlorination of N-chlorinated amplicons – assumed to represent an "average" value for N-chlorinated bps, and to be the same for all four amplicons. (see eqs S2.4 and S2.8 for FAC and NH_2Cl, respectively); [d] For each disinfectant, $k_{Disinfectant,Specific}$ and $k_{Disinfectant,0}$ are, respectively, the slope and intercept of the strongest correlations obtained by linear regression of the rate constants, $k_{Disinfectant,Amp}$, for the four amplicons versus corresponding specific nucleotide contents (Figure 2.2). $k_{Disinfectant,Specific}$ represents the *sequence-independent*, bp- or doublet-specific rate constant for each disinfectant, and $k_{Disinfectant,0}$ is attributed to factors influencing DNA reactivity (e.g., secondary targets, specific sequence elements) that are not fully accounted for by eq S2.9 (see further discussion in Text S2.11). Significands of standard errors of $k_{Disinfectant,Specific}$ were rounded up to 0.1 if below 0.1.

Several prior investigators have also reported rate constants for reactions of DNA with FAC, O_3, and $^{\bullet}OH$ in terms of [dNMPs]; namely, ~10 (M dNMP)$^{-1}$s^{-1} for FAC (an estimated value specifically for dsDNA *denaturation* by FAC),[56] 410 (M dNMP)$^{-1}$s^{-1} for O_3,[57] and 1.1-4.6(×10^8) (M dNMP)$^{-1}$s^{-1} for $^{\bullet}OH$.[57-59] If the values of $k_{\mathrm{FAC,Amp}}$, $k_{\mathrm{O_3,Amp}}$, and $k_{\bullet\mathrm{OH,Amp}}$ measured here are each normalized to [dNMPs] (i.e., by dividing $k_{\mathrm{Disinfectant,Amp}}$ by the total number of dNMPs – or twice of the number of AT+GC bps – in each amplicon), they yield values ranging from 4.5-7.4 (M dNMP)$^{-1}$s^{-1}, 30-36 (M dNMP)$^{-1}$s^{-1}, and 1.1-1.2(×10^8) (M dNMP)$^{-1}$s^{-1}, respectively. While the dNMP-normalized values for FAC and $^{\bullet}OH$ agree well with the prior measurements, the reason for the differences for O_3 is uncertain. Several possibilities are that the presence of impurities within or partial denaturation of the calf thymus DNA utilized within the prior work (which was conducted under pseudo-first-order conditions, with DNA in excess of O_3) could have resulted in adventitious acceleration of O_3 decomposition (and overestimation of $k_{\mathrm{O_3}}$), or that the qPCR analyses utilized here did not capture all DNA lesions generated by reaction with O_3 (e.g., 8-oxoG). Investigation of these possibilities is recommended for future work.

With respect to the FAC rate constants determined here (Table 2.1), it is important to note that under various conditions, the kinetics of FAC reactions with organic molecules can be driven in part by chlorine species other than HOCl and OCl^-, namely Cl_2 and Cl_2O, where Cl_2 becomes more important at higher [Cl^-] and lower pH, while Cl_2O becomes more important especially at higher [HOCl].[60, 61] In cases for which Cl_2O contributions to observed reaction kinetics are important, deviations from first-order dependencies on [FAC] can be expected, on account of the second-order dependence of Cl_2O formation on [HOCl].[60, 61] As the FAC kinetics measurements obtained here indicated a clear first-order dependence on [FAC] (Text S2.9,

Figure S2.9), it seems unlikely that Cl_2O contributed significantly to the observed rates of qPCR amplicon degradation. With regard to possible Cl_2 contributions – under the conditions used here, [Cl^-] levels should not have exceeded 1-2 mM (due primarily to background Cl^- from the saline citrate used in preparing DNA stock solutions). Prior work suggests that under similar conditions (pH 7, 1 mM Cl^-), Cl_2 is unlikely to contribute to more than ~10% of the observed degradation of aromatic compounds with measured rate constants of greater than ~600 $M^{-1}s^{-1}$ during treatment.[61] As values of $k_{FAC,Amp}$ were all in excess of 10^3 $M^{-1}s^{-1}$, it seems unlikely that Cl_2 could have contributed significantly to the proposed initial step of DNA chlorination (N-chlorination and H-bond disruption). However, a contribution of Cl_2 to the proposed slower second step of DNA chlorination (irreversible nucleotide halogenation) cannot be ruled out on the basis of the available data. Although this does not alter any of the conclusions reached here, it is an important possibility that should be investigated in future work on DNA reactions with FAC.

2.3.2 *ARG amplicon degradation: Influence of amplicon length and nucleotide content.*

Variations in $k_{Disinfectant,Amp}$ with amplicon composition were investigated by comparing measured $k_{Disinfectant,Amp}$ values with the length and nucleotide content of each amplicon, in order to determine whether consistent, predictable dependences of the magnitudes of $k_{Disinfectant,Amp}$ values on DNA sequence content could be identified. For each disinfectant, $k_{Disinfectant,Amp}$ generally increased in proportion to amplicon length (AT+GC bps), indicating that a larger number of nucleotides per amplicon results in a higher probability of an amplicon sustaining damage that prevents qPCR amplification (Figure 2.2a-f). Weighted linear regressions showed strong linear relationships of $k_{Disinfectant,Amp}$ with numbers of AT+GC bps per amplicon ($R^2 \geq$

0.98) for FAC, NH_2Cl, O_3, and $^{\bullet}OH$ (Figure 2.2a,b,d,f), while weaker relationships ($R^2 \leq 0.95$) were observed for ClO_2 and UV (Figure 2.2c, e).

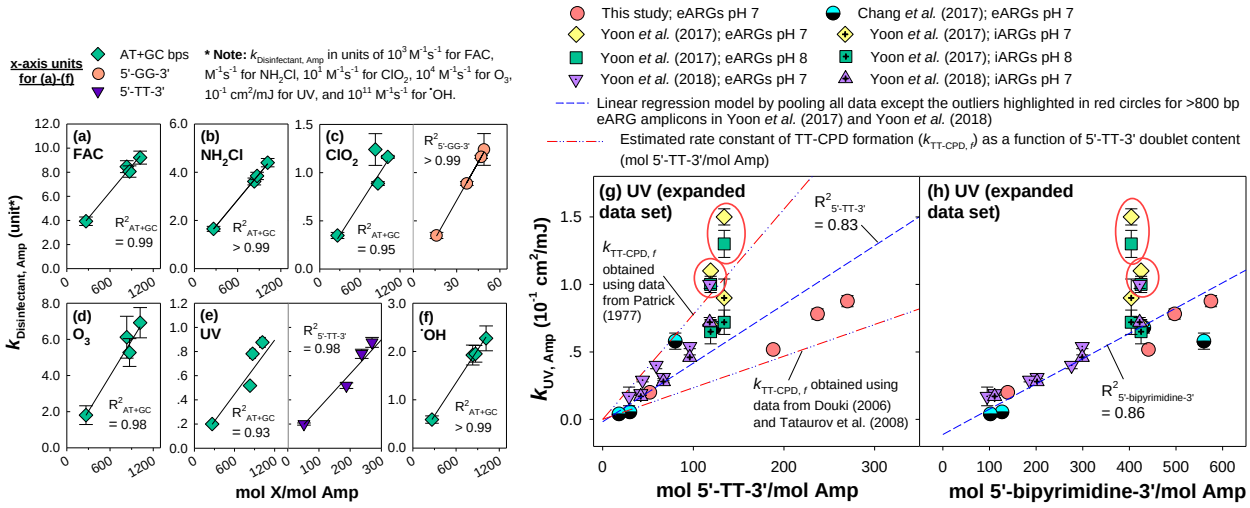

Figure 2.2. Second-order rate constants for (a) FAC, (b) NH_2Cl, (c) ClO_2, (d) O_3, and (f) $^{\bullet}OH$, and fluence-based first-order rate constant for (e) UV, plotted versus molar contents of nucleotide bps or specific doublets for 266 bp, 832 bp, 870 bp and 1017 bp amplicons. All data were obtained by treatment of extracellular *B. subtilis* 1A189 DNA in 10-mM phosphate buffer at pH 7 (FAC, ClO_2, O_3, $^{\bullet}OH$, and UV) or 8 (NH_2Cl only). Panels (g) and (h) depict linear regressions of UV data from this study, with data from prior studies by Chang et al. (2017),[27] Yoon et al. (2017),[19] and Yoon et al. (2018),[62] as well as the theoretical rate constant of TT-CPD formation as a function of mol 5'-TT-3'/mol Amp calculated using data either from Patrick (1977),[63] or from Douki (2006),[64] and Tataurov et al. (2008),[57] according to the method of Yoon et al. (2018) [62]. Regressions in (g) and (h) were performed without $k_{UV,Amp}$ measurements obtained for >800 bp eARG amplicons from the works by Yoon et al., as these latter measurements may have been influenced by incidental photochemical generation of radicals from trace transition metals remaining in DNA extracts.[62] Error bars represent standard errors of $k_{Disinfectant, Amp}$ determined in this work (Table 2.1) or reported by prior studies. Trendlines and R^2 in panels (a)-(h) were obtained by weighted linear regressions of $k_{Disinfectant, Amp}$ versus specific nucleotide contents.

The strengths of the regressions for FAC, NH_2Cl, O_3, and $^{\bullet}OH$ suggest that their reactivities toward a given amplicon depend on both the AT and GC bp content of the amplicon. While no prior measurements of NH_2Cl-nucleobase kinetics appear to be available for comparison, these trends are consistent with prior observations that FAC and O_3 react relatively rapidly ($k \sim 10^3$-10^4 $M^{-1}s^{-1}$) with both thymine and guanine nucleotides,[56, 57] and that $^{\bullet}OH$ exhibits very high, non-selective reactivity ($k \sim 10^9$-10^{10} $M^{-1}s^{-1}$) toward all nucleobases.[65, 66] The relatively weaker relationships of $k_{Disinfectant,Amp}$ with AT+GC bp content observed for ClO_2 and

UV suggest that their reactivities toward a given amplicon likely depend more specifically on either AT or GC bp contents, or on the content(s) of some other sequence element(s) (e.g., nucleotide doublets or triplets) not captured by more general correlations of $k_{\text{Disinfectant,Amp}}$ with amplicon length.

This latter possibility was evaluated by undertaking additional weighted linear regressions of $k_{\text{ClO}_2\text{,Amp}}$ and $k_{\text{UV, Amp}}$ versus numbers of interstrand AT bps, GC bps, and all possible intrastrand nucleotide doublet and triplet permutations within each amplicon. $k_{\text{ClO}_2\text{,Amp}}$ was indeed found to correlate much more strongly with intrastrand 5'-GG-3' doublet content ($R^2_{\text{5'-GG-3'}} > 0.99$) in each amplicon (Figure 2.2c). This observation is in agreement with prior findings that guanine is the most susceptible nucleobase in dsDNA toward one-electron oxidants such as ClO_2 ($k_{\text{ClO}_2\text{,5'-GMP}} = 4.5\times10^2\ M^{-1}s^{-1}$ at pH 7),[67] and that one-electron oxidation reactions preferentially lead to damage at the 5'-guanine of 5'-GG-3' doublets.[68] (Note that the counts of intrastrand 5'-GG-3' doublets used for correlations exclude those within 5'-GGG-3' or 5'-GGGG-3' sequences (Table S2.1), which have been reported to react by single-electron transfer ~5-9× slower than isolated 5'-GG-3' doublets at pH 7.0.[69])

$k_{\text{UV, Amp}}$ was likewise found to correlate much more strongly with intrastrand 5'-TT-3' doublet content ($R^2_{\text{5'-TT-3'}} = 0.98$) (Figure 2.2e). This result agrees with previous findings,[19, 27-29, 62] and can be explained by the tendency of UV to generate CPDs at intrastrand 5'-bipyrimidine-3' sites, with 5'-TT-3' more susceptible than 5'-TC-3', 5'-CT-3' and 5'-CC-3' ($R^2_{\text{5'-TC-3'}} = 0.96$, $R^2_{\text{5'-CT-3'}} = 0.95$, and $R^2_{\text{5'-CC-3'}} = 0.71$).[29, 64] Although DNA can also sustain damage at 5'-TC-3', 5'-CT-3', and 5'-CC-3', model predictions of the relative photoreactivities of each of these four 5'-bipyrimidine-3' doublets indicate that 5'-TT-3' CPDs are likely to account for the majority of UV-induced lesions in the 266-1017 bp amplicons under the conditions applied here (SI Text

S2.12). Consistent with this, $k_{UV, Amp}$ values measured for the 266-1016 bp amplicons are within the ranges of theoretical rate constants for TT-CPD formation in each amplicon ($k_{TT\text{-}CPD, f}$), calculated as described in SI Text S2.12 (Figure 2.2g, SI Table S2.3).

Values of $k_{UV, Amp}$ from three recent studies investigating various plasmid-borne ARGs[19, 27, 62] are also shown in Figure 2.2g for comparison with the values measured here. These data indicate that the $k_{UV, Amp}$ values from all four studies correlate with 5'-TT-3' content, though considerable spread is apparent in the trends, with the plasmid-borne amplicons from the prior studies appearing to exhibit higher photoreactivities per unit of molar 5'-TT-3' content than the chromosomal 266-1017 bp amplicons investigated here. While the possibility of inherent differences in chromosomal vs. plasmid-borne amplicon photoreactivities cannot be excluded, it should be noted that these differences may rather arise from wide variations in the amplicons' proportions of 5'-TT-3' doublets relative to total 5'-bipyrimidine-3'doublets ($f_{\frac{\text{5'-TT-3'}}{\text{5'-bipyrimidine-3'}}} = \frac{\text{\#5'-TT-3'}}{\text{\#5'-TT-3' + \#5'-TC-3' + \#5'-CT-3' + \#5'-CC-3'}}$). The amplicons from the previous three studies are more enriched in GC bps relative to AT bps, and are thus also more enriched in 5'-TC-3', 5'-CT-3', and 5'-CC-3' doublets relative to 5'-TT-3', with $f_{\frac{\text{5'-TT-3'}}{\text{5'-bipyrimidine-3'}}}$ varying from 0.14-0.29 for the Chang et al. (2017)[27] data set, 0.21-0.38 for the Yoon et al. (2017, 2018)[19, 62] data sets, and 0.37-0.48 for the 266-1017 bp amplicons investigated in this work. Consequently, the simple correlation of $k_{UV,Amp}$ with 5'-TT-3' – which works very well for the 266-1017 bp amplicons – may not fully account for the role of the 5'-TC-3', 5'-CT-3', and 5'-CC-3'doublets in governing photoreactivities of the amplicons from the prior works. This is supported by the stronger aggregate correlation of the $k_{UV,Amp}$ values from the four studies with overall 5'-bipyrimidine-3' content (Figure 2.2h). In accord with these observations, Figure S2.16 and the

discussion in Text S2.12 show that theoretical rate constants for TT-CPD formation, $k_{TT\text{-}CPD,\,f}$, cannot reconcile the differences in $k_{UV,Amp}$ values of the amplicons investigated across all four studies, whereas theoretical predictions of rate constants for *overall* bipyrimidine lesion formation, $k_{\text{all lesions},\,f}$ (based on data from Douki et al. (2006)[64] and Tataurov (2008)[70]), align well with the measured values of $k_{UV,Amp}$ across the whole set of amplicons (aside from the outliers noted from the Yoon et al. studies[19, 62]). This suggests that for ARGs that are significantly more enriched in GC bps than the *bltR-blt-bltD* genome segment investigated here, it may be important to account for the photoreactivities not only of 5'-TT-3', but also of 5'-TC-3', 5'-CT-3', and 5'-CC-3'.

Interestingly, correlations between $k_{Disinfectant,Amp}$ and various nucleotide bps, doublets, or triplets for FAC, NH_2Cl, O_3, and $^{\bullet}OH$ indicated that each of these oxidants may also exhibit preferential reactivities toward specific target sites within a given DNA sequence (e.g., FAC for GC bps and/or 5'-GT-3' doublets, NH_2Cl for AT bps and 5'-AG-3' doublets, O_3 for GC bps and 5'-GT-3' doublets, and $^{\bullet}OH$ for 5'-TG-3' doublets). Although more extensive evidence is needed to confirm the preferential occurrence of reactions at these sites (as has been demonstrated for attack of 5'-GG-3' and 5-TT-3' doublets by ClO_2 and UV),[64, 68, 69] these correlations may prove useful in guiding identification of reactive sites in future work.

The strong linear relationships of $k_{Disinfectant,Amp}$ with AT+GC bps for FAC, NH_2Cl, O_3, and $^{\bullet}OH$, 5'-GG-3' doublets for ClO_2, and 5'-TT-3' doublets for UV suggest that the reactivity of a given DNA segment toward each disinfectant can be predicted using a model such as eq 2.9,

$$k_{Disinfectant,Amp} = k_{Disinfectant,Specific} \cdot (\text{mol X/mol Amp}) + k_{Disinfecant,0} \quad (2.9)$$

where $k_{\text{Disinfectant,Specific}}$ and $k_{\text{Disinfectant,0}}$ are the respective slopes and intercepts of the corresponding regression lines in Figure 2.2a-f. $k_{\text{Disinfectant,Specific}}$ represents the rate constant for a given disinfectant normalized to nucleotide *bps* or *doublets* of type X (where X = AT+GC bps for FAC, NH_2Cl, O_3, and $^{\bullet}OH$; 5'-GG-3' doublets for ClO_2; and 5'-TT-3' doublets for UV), and $k_{\text{Disinfectant,0}}$ is attributed to factors influencing DNA reactivity (e.g., secondary targets, specific sequence elements) that are not fully accounted for in the relatively simple single-parameter model represented by eq 2.9 (see further discussion in Text S2.11). The resulting $k_{\text{Disinfectant,Specific}}$ and $k_{\text{Disinfectant,0}}$ values are summarized in Table 2.1.

2.3.3 *Relationship of ARG transforming activity to qPCR signals.*

While qPCR is a rapid, widely-accessible, and affordable analytical tool to quantify damage within a DNA segment, direct measurement of changes in biological activity via culture-based transformation assay represents a "gold standard" approach for evaluating the true impact of treatment processes on ARG dissemination risk.[27, 71] In order to ascertain whether one measurement can be directly related to the other, changes in qPCR measurements for each amplicon were compared with changes in measurements of residual transforming activities during exposure to each disinfectant. As shown in Figure 2.1a-e, for FAC, NH_2Cl, ClO_2, O_3, and UV, ARG *deactivation* kinetics were significantly faster than for 266 bp amplicon *degradation*, but generally close to 832 bp, 870 bp, and/or 1017 bp amplicon *degradation* kinetics over the monitored exposure ranges (except for ClO_2 at CT_{ClO_2} > ~0.2 M•s and UV at IT > ~45 mJ/cm^2). Figure 2.3 depicts measurements of residual transforming activity vs. amplicon copy number (each normalized to initial conditions). For FAC, NH_2Cl, ClO_2, O_3, and UV, Figure 2.3a-e clearly illustrates that the 266 bp amplicon underestimates damage as measured by the

transformation assay, while the 832-1017 bp amplicons generally capture damage at similar (~1:1) rates as the transformation assay (except at >70% or >90% *deactivation* by ClO_2 or UV, respectively). Results observed for NH_2Cl at pH 7 were consistent with those at pH 8 (Figure S2.17). In contrast, ARG *deactivation* by $^{\bullet}OH$ greatly outpaced *degradation* of all four amplicons (Figures 2.1f and 2.3f).

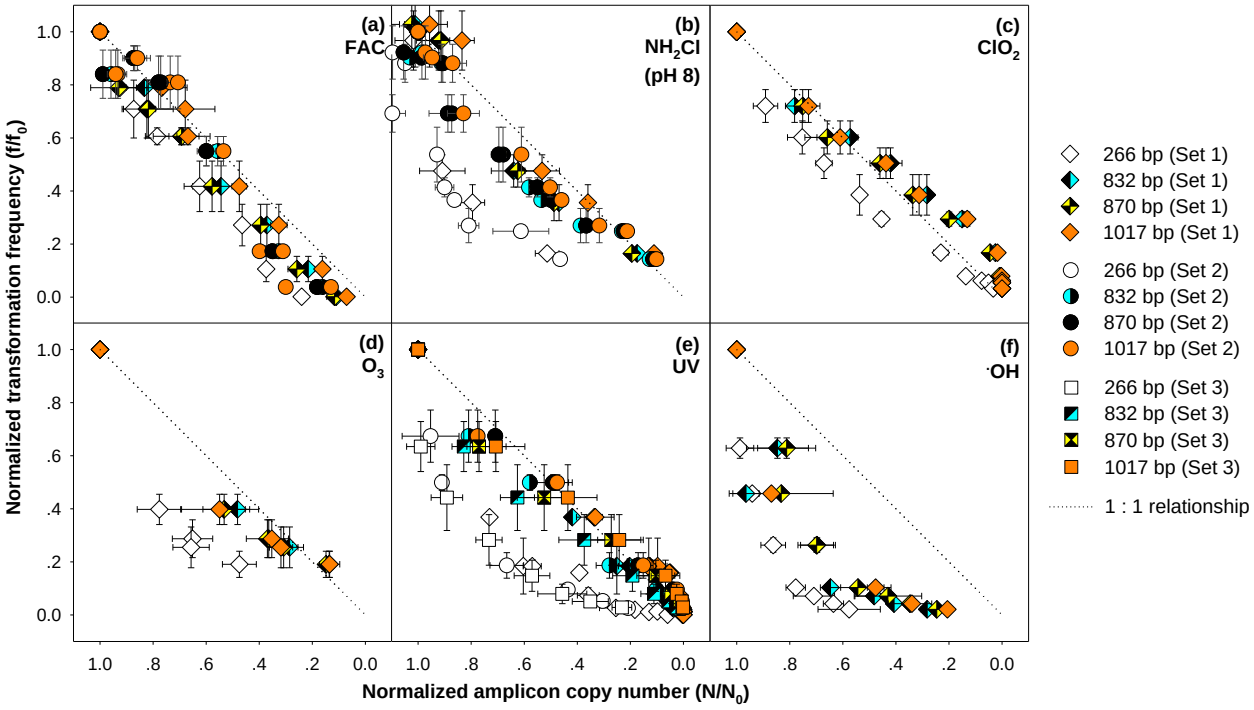

Figure 2.3. Normalized transformation frequency (f/f_0) plotted versus normalized copy number (N/N_0) of 266 bp, 832 bp, 870 bp and 1017 bp amplicons for eARG treatment with (a) FAC, (b) NH_2Cl, (c) ClO_2, (d) O_3, (e) UV and (f) $^{\bullet}OH$. All data were obtained by treatment of extracellular *B. subtilis* 1A189 DNA in 10-mM phosphate buffer at pH 7 (FAC, ClO_2, O_3, $^{\bullet}OH$, and UV) or 8 (NH_2Cl only). Different symbol shapes represent replicate data sets obtained at the same experimental condition. (Notes: The *CT*s used for NH_2Cl and ClO_2 were much greater than *CT*s typically applied in practice. The narrow range of O_3 data is attributable to the inability to collect samples at lower exposure ranges using the continuous flow, quenched-reaction method (Text S2.8) – on account of the very rapid kinetics of the O_3-DNA reaction. Sets 1, 2, and 3 represent experiments undertaken on different dates – each in at least duplicate), and error bars represent standard deviations obtained from at least duplicate experiments conducted independently on the same date. The dotted lines represent theoretical 1:1 relationships, as opposed to regression lines.

The above relationships between ARG *degradation* and *deactivation* can be understood in light of DNA integrity requirements for bacterial natural transformation driven by homologous

recombination. Prior studies have reported that a minimum length of homology (~400-500 bp) is required on each side of a non-homologous sequence (here a point mutation, *acfA*, so ~800-1,000 bp in total) for successful natural transformation in *B. subtilis*, in analogy with requirements observed for various other bacterial species.[72, 73] Damage within the requisite homologous flanking sequence would be anticipated to disable transformation. It has also been shown that a decrease in donor DNA size from several kbps down to the minimum required length causes a continual decrease in transformation frequency – potentially due to a decrease in attachment and/or donor-acceptor complexation efficiencies.[72, 74]

For FAC, NH_2Cl, ClO_2, O_3 and UV, which attack DNA primarily through selective nucleotide modification without impacting DNA strand size (as confirmed by PFGE; Figure S2.18a-e), ARG transforming activity would not be diminished unless lesions occur within the ~800-1,000 bp flanking region noted above. In an analogous manner, one or more lesions within the targeted amplicon would result in *detectable* loss of qPCR signals, while those outside would have no influence. If the monitored qPCR amplicon comprises either the homologous flanking region itself, or another region with similar nucleotide content at a different locus (even far from the flanking region), synchronization in the kinetics of amplicon *degradation* and ARG *deactivation* would therefore be expected. Here, the 832-1017 bp amplicons incur damage by FAC, NH_2Cl, ClO_2, O_3 and UV at similar rates as ARG *deactivation* (Figure 2.3a-e) because they have nucleotide contents similar to (but only partly overlapping with) the ~800-1,000 bp homologous flanking sequences centered on the *acfA* mutation (Text S2.5, Table S2.1, Scheme 2.1).

In contrast, $^{\bullet}OH$ damages DNA predominantly by strand fragmentation (via phosphate backbone cleavage), resulting in decreased DNA length and most likely diminished attachment

and/or donor-acceptor complexation efficiencies with increasing exposure (Figure S2.18f).[75] Consequently, even if •OH damages a DNA strand at a location outside of the requisite flanking region (or the region encompassed by the monitored amplicon), ARG transforming activity can be lowered due to a decrease in strand length, while monitored amplicons may remain undamaged, leading to consistently faster rates of ARG *deactivation* than amplicon *degradation* (Figures 2.1f and 2.3f).

The tailing in ARG *deactivation* by ClO_2 and UV (Figure 2.1c, e) and consequent deviation from 1:1 *degradation:deactivation* relationships (Figure 2.3c, e) may be partly due to dark-repair of ClO_2-[76] or UV-damaged[26, 77] DNA upon uptake by the *B. subtilis* 1A1 recipient cells during transformation assays. Photo-repair can be excluded since transformation assays were conducted with only brief exposures to indoor light (only during sample handling at room temperature, prior to/between incubations in the dark) and yielded results consistent with controls conducted fully in the dark (data not shown). For UV, the tailing effect (also observable to a lesser degree in qPCR results; Figure S2.14) may also be partly explained by CPD photoreversal at higher fluences.[55] Prior work has also demonstrated tailing in ARG *degradation*[27, 29] and *deactivation*[25] profiles during UV irradiation.

The correlations of qPCR analyses with genomic ARG transforming activity measurements observed here may extend to a number of other bacteria. In addition to *Bacillus*, many other naturally competent bacterial genera – including important pathogens (e.g., *Haemophilus*,[78] *Streptococcus*,[79] *Neiserria*,[80] *Acinetobacter*[81]) – exhibit minimum flanking homology requirements for natural transformation with genomic DNA, suggesting that *deactivation* of ARGs encoded within their genomes could likewise depend on damage to identifiable “critical sequences” of DNA. For cases involving plasmid transformation (not

generally driven by homologous recombination), ARG *deactivation* appears less likely to correlate directly with qPCR measurements of ARG *degradation*.[27, 62] In such cases, plasmids' origins of replication, which are critical to plasmid function, may represent an alternative target for tracking ARG activity loss.[62]

2.3.4 *iARG deactivation and ARB inactivation.*

Degradation and *deactivation* of iARGs by each disinfectant was also investigated as a comparison to eARG results, and to evaluate the possible influence of cell constituents on ARG *degradation/deactivation*. Direct exposure of iARGs to $^{\bullet}OH$ was not included, as $^{\bullet}OH$ has previously been shown to have negligible effect on iARGs, even under conditions typical of advanced oxidation processes (e.g., UV/H_2O_2).[19]

As shown in Figure 2.4, iARG *deactivation* lagged ARB inactivation for all of the five disinfectants investigated. Analogous results were observed for iARG *degradation* (Figure S2.19), clearly demonstrating that iARGs may "survive" disinfection processes even if the associated ARB cells are effectively inactivated. Similar results have been reported in previous studies of iARG *degradation* by various disinfectants,[19, 22, 24, 29] These findings can be explained by the fact that disinfectants often react preferentially with other vital cellular components (e.g., cell-envelope lipids or proteins, cellular enzymes, etc.) before reaching DNA within the cytoplasm, as for FAC, NH_2Cl, ClO_2, and O_3. In the case of UV, damage to the full bacterial genome that inhibits vital cellular functions accumulates much faster than damage to a much shorter ARG, leading to cell inactivation prior to measurable ARG damage.[82]

General consistency was found in the kinetics of iARG and eARG *deactivation* within investigated exposure ranges for each disinfectant, indicating that the cell envelope and other cellular biomolecules did not significantly hinder the ability of disinfectants to reach and react

with the ARB cells' DNA. Only a marginal difference was observed between iARG *deactivation* by O_3 with and without *t*-BuOH (Figure 2.4d), suggesting a minimal role of $^{\bullet}OH$ due to its rapid scavenging by other intracellular components.[19] For UV (Figure 2.4e), iARG *deactivation* exhibited tailing similar to that observed during eARG *deactivation* (presumably for similar reasons as discussed above).

Differences were observed between iARG and eARG *deactivation* curves for NH_2Cl at CT_{NH_2Cl} < 60 mg/L•min and O_3 at CT_{O_3} > 0.1 mg/L•min. For NH_2Cl (Figure 2.4b), iARG transforming activity initially exhibited a rapid drop followed by minimal subsequent loss, whereas the four qPCR amplicons remained largely intact throughout the investigated exposure range (Figure S2.20b). This is analogous to trends observed in reaction of $^{\bullet}OH$ with eARGs (Figure 2.2f), and may have resulted from DNA fragmentation due to $^{\bullet}OH$ or Fe(IV) generation by NH_2Cl reactions with intracellular reduced metal ions (e.g., Fe^{2+}).[56, 83] Although FAC is also known to be able to induce formation of such radicals under similar conditions,[83, 84] FAC's reaction with iARGs may have been fast enough to outweigh radical contributions (in contrast with the exceptionally slow kinetics of NH_2Cl). For O_3 (Figure 2.4d), the evident tailing in iARG deactivation at higher exposures may be attributable to accelerated direct consumption and/or radical chain decomposition of O_3 within the vicinity of the cell envelope and/or cytoplasm of the *B. subtilis* 1A189 cells, due to increased solubilization of reactive biomolecules (e.g., cell-envelope amino acids or unsaturated lipids) during cell lysis.[82, 85]

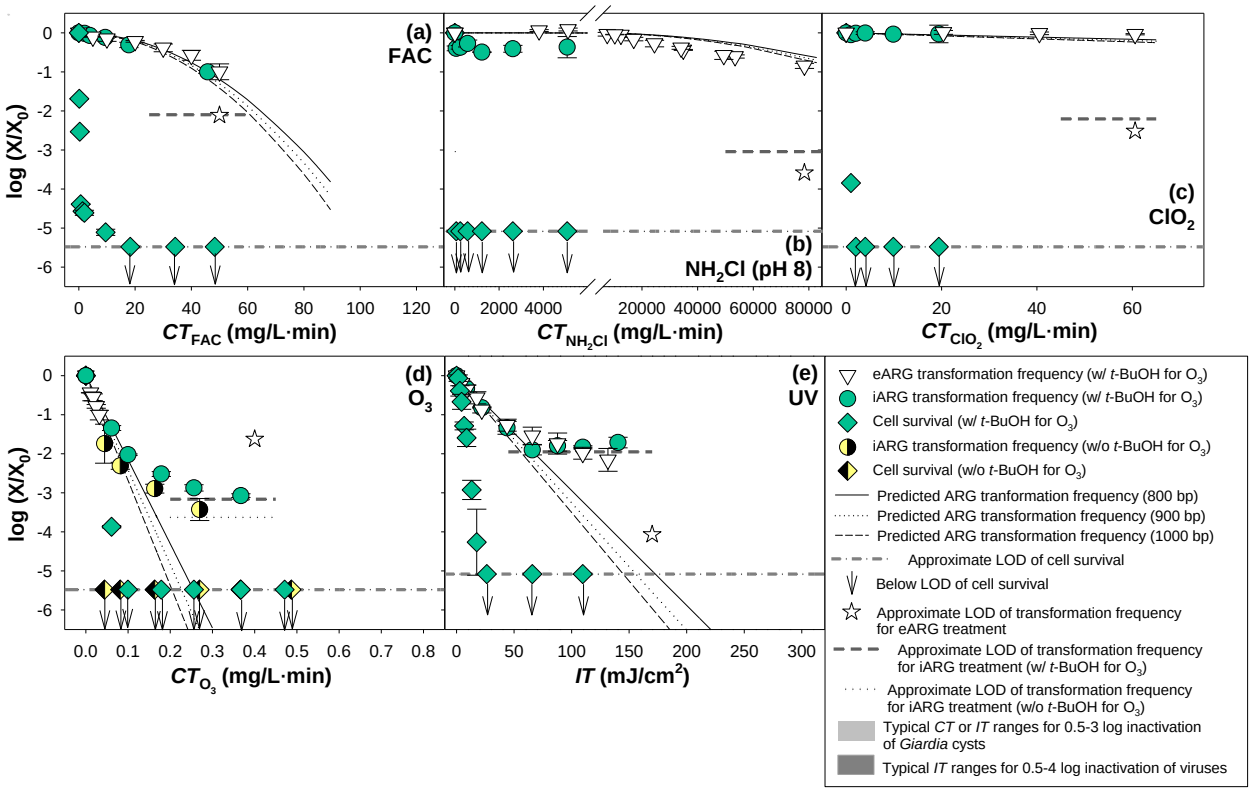

Figure 2.4. Normalized (log_{10}-scale) *measured* transformation frequency, cell survival, and *modeled* (predicted) transformation frequency (with the latter obtained using 800 bp, 900 bp, and 1000 bp homologous *acfA*-flanking sequences) versus disinfectant exposure for (a) FAC, (b) NH_2Cl, (c) ClO_2, (d) O_3, and (e) UV, during treatment of extracellular *B. subtilis* 1A189 DNA or intact *B. subtilis* 1A189 cells with each disinfectant in 10-mM phosphate buffer at pH 7 (FAC, ClO_2, O_3, and UV) or 8 (NH_2Cl only). Typical *CT* and *IT* ranges applied in drinking water practice when using each disinfectant to inactivate *Giardia* cysts[86] or viruses[87] are indicated by grey shaded and dotted areas, respectively. Kinetics-based predictions of transformation frequency losses were obtained using the model in SI Text S2.9 for FAC and NH_2Cl, eq 2.7 for ClO_2 and O_3, and eq 2.8 for UV, where theoretical degradation rate constants, $k_{\text{Disinfectant,Amp}}$, for the 800 bp, 900 bp and 1000 bp homologous *acfA*-flanking sequences (Table S2.1, Scheme 2.1) were calculated by means of eq 2.9, using the values of $k_{\text{Disinfectant,Specific}}$ and $k_{\text{Disinfectant,0}}$ provided in Table 2.1, and specific nucleotide contents of the homologous sequences (Table S2.1). The relatively high LOD for transformation frequency during UV treatment of iARGs is attributable to the lower total sample volume treated in UV experiments (100 mL) compared to other iARG experiments (1 L), which resulted in a lower sample pre-concentration factor during the workup for analyses in the UV experiments. Error bars (representing standard deviations) for transformation frequency and cell survival were obtained from duplicate experiments conducted independently, except that cell viabilities for (c) ClO_2 were only measured for one of the duplicate experiments (and are thus shown without error bars).

2.3.5 *Implications for (waste)water disinfection practice.*

To facilitate comparison of experimental conditions with practical scenarios, eARG and iARG *deactivation* data in Figure 2.4 are overlain with exposure ranges likely to be encountered

in (waste)water disinfection practice (conservatively based on drinking water disinfection requirements).[86, 87] Analogous comparisons for ARG *degradation* are provided in Figure S2.19. Gray-shaded areas in Figure 2.4a-e represent *CTs* or *ITs* required for 0.5-3-$\log_{10}$ inactivation of *Giardia* cysts at pH 7, 20 °C for each disinfectant.[86] The dotted area in Figure 2.4e represents *ITs* required for 0.5-4-$\log_{10}$ inactivation of viruses by UV.[87] The *CT* and *IT* requirements for 2-$\log_{10}$ *deactivation* of eARGs and iARGs, and 2-$\log_{10}$ *degradation* of the four eARG amplicons (based on Figures 2.1 and 2.4), are also summarized with available literature values for each disinfectant in Table S2.3.

These comparisons indicate that FAC should be capable of achieving up to ~2-$\log_{10}$ chromosomal ARG *deactivation* at practical CT_{FAC} ranges (Figure 2.4a), which is ~2.5× less efficient than previously reported for plasmid-borne ARGs[19] (possibly due to differences in plasmid and genomic DNA reactivities toward FAC, as noted above). For O_3, up to ~3-$\log_{10}$ ARG *deactivation* should be achievable at practical CT_{O_3} ranges (Figure 2.4d), consistent with previous findings.[24] UV light would be anticipated to yield <1-$\log_{10}$ ARG *deactivation* at the upper end of the *IT* range for *Giardia* cysts, and ~2-$\log_{10}$ *deactivation* within the *IT* range for viruses (Figure 2.4e). These observations are generally consistent with previous findings obtained under comparable conditions,[19, 27, 29, 62] although lower UV efficiencies have also been reported.[28]

In contrast to FAC, O_3, and UV, ClO_2 and NH_2Cl were found to yield minimal ARG *deactivation* even at their highest practical *CT* levels for (waste)water treatment. Previous studies have also shown that NH_2Cl[20] and ClO_2[22, 67, 88] exhibit marginal reactivity toward bacterial DNA. For instance, NH_2Cl treatment at 37 °C was found to yield <0.8-$\log_{10}$ *deactivation* of extracellular *B. subtilis* DNA at a CT_{NH_2Cl} up to ~4000 mg/L•min, and ~0.7-$\log_{10}$ *deactivation* for

its intracellular form at a CT_{NH_2Cl} of ~170 mg/L•min[20] (also consistent with the differences in levels of iARG and eARG *deactivation* observed here at lower NH_2Cl exposures). For ClO_2, *deactivation* of an eARG of *H. influenzae* DNA was moderately faster than observed here, but a CT_{ClO_2} of ~75 mg/L•min still only yielded <1-log_{10} *deactivation*.[22] These results highlight the wide variations in abilities of different disinfectants to degrade/deactivate ARGs at practical *CT* or *IT* ranges.

It also is important to note that applications of O_3 and UV may frequently be based on more or less conservative criteria than disinfection requirements. For example, O_3 exposures targeting micropollutant elimination have been shown to yield inefficient ARG *degradation*.[24] In contrast, UV fluences applied in UV/H_2O_2 processes – likely to be greater than even the highest *IT*s required for virus inactivation (Figure 2.4e),[89, 90] have been reported to yield ≥2-log_{10} ARG *degradation*.[19] Furthermore, application of FAC for achieving coliform inactivation during wastewater disinfection is likely ineffective for ARG *deactivation* under typical conditions, as FAC would be converted almost instantaneously to non-reactive NH_2Cl in non-nitrified wastewaters unless breakpoint chlorination is achieved.[91]

The influence of water quality parameters (e.g., the presence of dissolved organic matter, turbidity, pH) and susceptibilities of ARGs (plasmid-borne and genomic) from a wider variety of bacterial species should be evaluated further to more fully assess the practical performance of each disinfectant.

2.3.6 *qPCR and kinetics-based models for predicting elimination of ARG biological activity.*

The results depicted in Figures 2.3, 2.4, and S2.19 suggest that in addition to direct qPCR analyses of a "critical sequence" required for natural transformation of an ARG, qPCR analyses

of any other alternative sequence on the bacterial chromosome with a nucleotide content equivalent to the critical sequence, could be used to detect damage at a rate equivalent to ARG *deactivation*. It is also possible that qPCR analyses could be used to detect damage to other important chromosomally encoded genes (e.g., virulence factors) as an indication of their transforming activities. This concept has parallels in the use of qPCR to monitor losses of viral infectivity[92] and bacterial plasmid transforming activity during UV irradiation.[27] The potential to target such *alternative* sequence(s) presents an attractive option for qPCR assays, as it is sometimes difficult to reliably amplify a desired DNA region due to issues such as primer dimerization or non-specific amplification.

Furthermore, the clear dependence of qPCR amplicon *degradation* kinetics on contents of certain bps or doublets (Figure 2.2, Table 2.1, and associated discussion) also suggests that under certain circumstances, it may be possible to predict the kinetics of ARG *degradation* (and hence, ARG *deactivation*) by a disinfectant *a priori*, based on knowledge of the sequences of the ARG and its flanking regions (or other "critical sequence(s)"), coupled with appropriate *sequence-independent* rate constants (Table 2.1). As a demonstration of this, an envelope of theoretical ARG *deactivation* curves was modeled by predicting the *degradation* rate constants of the 800 bp, 900 bp and 1000 bp homologous flanking sequences centered on the *acfA* mutation in *B. subtilis* 1A189 DNA (Scheme 2.1), using their nucleotide contents (Table S2.1) and the sequence-independent rate constants $k_{\text{Disinfectant,Specific}}$ and $k_{\text{Disinfecant,0}}$ for FAC, NH_2Cl, ClO_2, O_3, or UV (Table 2.1). As shown in Figure 2.4, the resulting model predictions generally agreed well with measured results for *deactivation* of eARGs and iARGs up to exposures sufficient to yield roughly 1-2 $\log_{10}$ *deactivation*. The overall good predictions (Figure 2.4), along with the strong *degradation:deactivation* correlations in Figure 2.3, suggest that such models may prove useful

as a generally-applicable means for predicting ARG *degradation and deactivation* during treatment with these five disinfectants.

Based on the findings reported here and in previous work, it appears that qPCR analyses and kinetics-based model predictions have the potential to be employed as surrogates for ARG *deactivation* when "critical sequences" required for transformation of genomic or plasmid-borne ARGs can be identified. However, such approaches should be applied with caution. As discussed above, significant tailing in ARG *deactivation* curves was noted during treatment of iARGs and/or eARGs with ClO_2, O_3, and UV at high exposures (Figures 2.1c, 2.4d, 2.4e, respectively). In such cases, qPCR-based approximations or kinetics-based predictions of ARG *deactivation* could result in overestimation of actual *deactivation* levels. Furthermore, additional work will be required to determine how generally these findings apply to different ARGs and bacterial species.

ACKNOWLEDGEMENTS

This material is based upon work supported by the National Science Foundation under Grant Number CBET-1254929. Dr. Daniel R. Zeigler (BGSC), Dr. Heidi Gough, Dr. J. Scott Meschke, Dr. Nicolette Zhou, and statistics tutors at the UW Statistics Tutor & Study Center are greatly acknowledged for their technical support and advice. Three anonymous reviewers are gratefully acknowledged for their insightful and helpful comments, which have greatly strengthened this work.

REFERENCE

1. Davies, J.; Davies, D., Origins and Evolution of Antibiotic Resistance. *Microbiol. Mol. Biol. Rev.* **2010,** *74*, (3), 417-433.

2. *Antibiotic Resistance Theats in the United States, 2013*; U.S. Department of Health and Human Services Centers for Disease Control and Prevention: 2013.
3. Roberts, R. R.; Hota, B.; Ahmad, I.; Scott, R. D.; Foster, S. D.; Abbasi, F.; Schabowski, S.; Kampe, L. M.; Ciavarella, G. G.; Supino, M.; Naples, J.; Cordell, R.; Levy, S. B.; Weinstein, R. A., Hospital and Societal Costs of Antimicrobial-Resistant Infections in a Chicago Teaching Hospital: Implications for Antibiotic Stewardship. *Clin. Infect. Dis.* **2009,** *49*, (8), 1175-1184.
4. Pruden, A.; Pei, R. T.; Storteboom, H.; Carlson, K. H., Antibiotic resistance genes as emerging contaminants: Studies in northern Colorado. *Environ. Sci. Technol.* **2006,** *40*, (23), 7445-7450.
5. McKinney, C. W.; Loftin, K. A.; Meyer, M. T.; Davis, J. G.; Pruden, A., tet and sul Antibiotic Resistance Genes in Livestock Lagoons of Various Operation Type, Configuration, and Antibiotic Occurrence. *Environ. Sci. Technol.* **2010,** *44*, (16), 6102-6109.
6. Czekalski, N.; Berthold, T.; Caucci, S.; Egli, A.; Buergmann, H., Increased levels of multiresistant bacteria and resistance genes after wastewater treatment and their dissemination into Lake Geneva, Switzerland. *Front. Microbiol.* **2012**.
7. Ma, Y. J.; Wilson, C. A.; Novak, J. T.; Riffat, R.; Aynur, S.; Murthy, S.; Prudens, A., Effect of Various Sludge Digestion Conditions on Sulfonamide, Macrolide, and Tetracycline Resistance Genes and Class I Integrons. *Environ. Sci. Technol.* **2011,** *45*, (18), 7855-7861.
8. Luo, Y.; Yang, F.; Mathieu, J.; Mao, D.; Wang, Q.; Alvarez, P. J. J., Proliferation of Multidrug-Resistant New Delhi Metallo-β-lactamase Genes in Municipal Wastewater Treatment Plants in Northern China. *Environ. Sci. Technol. Lett* **2013,** *1*, (1), 26-30.
9. Pei, R. T.; Kim, S. C.; Carlson, K. H.; Pruden, A., Effect of River Landscape on the sediment concentrations of antibiotics and corresponding antibiotic resistance genes (ARG). *Water Res.* **2006,** *40*, (12), 2427-2435.
10. Xi, C. W.; Zhang, Y. L.; Marrs, C. F.; Ye, W.; Simon, C.; Foxman, B.; Nriagu, J., Prevalence of Antibiotic Resistance in Drinking Water Treatment and Distribution Systems. *Appl. Environ. Microbiol.* **2009,** *75*, (17), 5714-5718.
11. Ma, L.; Li, B.; Jiang, X.-T.; Wang, Y.-L.; Xia, Y.; Li, A.-D.; Zhang, T., Catalogue of antibiotic resistome and host-tracking in drinking water deciphered by a large scale survey. *Microbiome* **2017,** *5*, (1), 154.
12. Levy, S. B.; Miller, R. V., *Gene Transfer in the Environment*. McGraw-Hill, Inc.: New York, NY, 1994.
13. Lorenz, M. G.; Wackernagel, W., Bacterial Gene Transfer by Natural Genetic Transformation in the Environment. *Microbiol. Rev.* **1994,** *58*, (3), 563-602.
14. Johnsborg, O.; Eldholm, V.; Havarstein, L. S., Natural genetic transformation: prevalence, mechanisms and function. *Res. Microbiol.* **2007,** *158*, (10), 767-778.
15. Canada, P. H. A. o. Pathogen Safety Data Sheets and Risk Assessment. http://www.phac-aspc.gc.ca/lab-bio/res/psds-ftss/index-eng.php#e
16. Domingues, S.; Harms, K.; Fricke, W. F.; Johnsen, P. J.; da Silva, G. J.; Nielsen, K. M., Natural Transformation Facilitates Transfer of Transposons, Integrons and Gene Cassettes between Bacterial Species. *PLOS Pathog.* **2012**.
17. Lu, N.; Zilles, J. L.; Nguyen, T. H., Adsorption of Extracellular Chromosomal DNA and Its Effects on Natural Transformation of Azotobacter vinelandii. *Appl. Environ. Microbiol.* **2010,** *76*, (13), 4179-4184.

18. Cai, P.; Huang, Q. Y.; Zhang, X. W., Interactions of DNA with clay minerals and soil colloidal particles and protection against degradation by DNase. *Environ. Sci. Technol.* **2006,** *40*, (9), 2971-2976.
19. Yoon, Y.; Chung, H. J.; Di, D. Y. W.; Dodd, M. C.; Hur, H.-G.; Lee, Y., Inactivation efficiency of plasmid-encoded antibiotic resistance genes during water treatment with chlorine, UV, and UV/H2O2. *Water Res.* **2017,** *123*, 783-793.
20. Shih, K. L.; Lederberg, J., Effects of chloramine on Bacillus subtilis deoxyribonucleic acid. *J. Bacteriol.* **1976,** *125*, (3), 934-945.
21. Guo, M.-T.; Yuan, Q.-B.; Yang, J., Distinguishing effects of ultraviolet exposure and chlorination on the horizontal transfer of antibiotic resistance genes in municipal wastewater. *Environ. Sci. Technol.* **2015,** *49*, (9), 5771-5778.
22. Roller, S. D.; Olivieri, V. P.; Kawata, K., Mode of bacterial inactivation by chlorine dioxide. *Water Res.* **1980,** *14*, (6), 635-641.
23. Hamelin, C., Production of Single- and Double-strand Breaks in Plasmid DNA by Ozone. *Int. J. Radiat. Oncol. Biol. Phys.* **1985,** *11*, (2), 253-257.
24. Czekalski, N.; Imminger, S.; Salhi, E.; Veljkovic, M.; Kleffel, K.; Drissner, D.; Hammes, F.; Bürgmann, H.; Von Gunten, U., Inactivation of antibiotic resistant bacteria and resistance genes by ozone: from laboratory experiments to full-scale wastewater treatment. *Environ. Sci. Technol.* **2016,** *50*, (21), 11862-11871.
25. Lerman, L. S.; Tolmach, L. J., Genetic transformation. 2. The significance of damage to the DNA molecule. *Biochim. Biophys. Acta.* **1959,** *33*, (2), 371-387.
26. Setlow, J. K., Shape of UV inactivation curve for transforming DNA. *Nature* **1977,** *268*, (5616), 169-170.
27. Chang, P. H.; Juhrend, B.; Olson, T. M.; Marrs, C. F.; Wigginton, K. R., Degradation of extracellular antibiotic resistance genes with UV254 treatment. *Environ. Sci. Technol.* **2017,** *51*, (11), 6185-6192.
28. Destiani, R.; Templeton, M. R.; Kowalski, W., Relative Ultraviolet Sensitivity of Selected Antibiotic Resistance Genes in Waterborne Bacteria. *Environ. Eng. Sci.* **2017,** *35*, (7), 770-774.
29. McKinney, C. W.; Pruden, A., Ultraviolet disinfection of antibiotic resistant bacteria and their antibiotic resistance genes in water and wastewater. *Environ. Sci. Technol.* **2012,** *46*, (24), 13393-13400.
30. Markham, P. N.; Neyfakh, A. A., Efflux-mediated drug resistance in Gram-positive bacteria. *Curr. Opin. Microbiol.* **2001,** *4*, (5), 509-514.
31. Poole, K., Efflux-mediated antimicrobial resistance. *J. Antimicrob. Chemother.* **2005,** *56*, (1), 20-51.
32. Fluman, N.; Bibi, E., Bacterial multidrug transport through the lens of the major facilitator superfamily. *Biochim. Biophys. Acta Proteins Proteom.* **2009,** *1794*, (5), 738-747.
33. Earl, A. M.; Losick, R.; Kolter, R., Ecology and genomics of Bacillus subtilis. *Trends Microbiol.* **2008,** *16*, (6), 269-275.
34. Ahmed, M.; Lyass, L.; Markham, P. N.; Taylor, S. S.; Vazquezlaslop, N.; Neyfakh, A. A., Two highly similar multidrug transporters of *Bacillus subtilis* whose expression is differentially regulated. *J. Bacteriol.* **1995,** *177*, (14), 3904-3910.
35. Saito, H.; Miura, K., Preparation of transforming deoxyribonucleic acid by phenol treatment. *Biochim. Biophys. Acta.* **1963,** *72*, (4), 619-629.

36. Bott, K. F.; Wilson, G. A., Development of competence in *Bacillus subtilis* transformation system. *J. Bacteriol.* **1967,** *94*, (3), 562-570.
37. Anagnostopoulos, C.; Spizizen, J., Requirements for transformation in *Bacillus subtilis*. *J. Bacteriol.* **1961,** *81*, (5), 741.
38. Shimelis, O.; Giese, R. W., Nuclease P1 digestion/high-performance liquid chromatography, a practical method for DNA quantitation. *J. Chromatogr. A* **2006,** *1117*, (2), 132-136.
39. Dodd, M. C.; Vu, N. V.; Le, V. C.; Kissner, R.; Pham, H. V.; Cao, T. H.; Berg, M.; von Gunten, U., Kinetics and mechanistic aspects of As(III) oxidation by aqueous chlorine, chloramines, and ozone: Relevance to drinking water treatment. *Environmental Science and Technology* **2006,** *40*, (10), 3285-3292.
40. APHA, *Standard Methods for the Examination of Water and Wastewater*. 21 ed.; APHA, AWWA, WPCF: Washington, 2005.
41. Pinkernell, U.; Nowack, B.; Gallard, H.; Von Gunten, U., Methods for the photometric determination of reactive bromine and chlorine species with ABTS. *Water Res.* **2000,** *34*, (18), 4343-4350.
42. Bader, H.; Hoigné, J., Determination of ozone in water by the indigo method. *Water Res.* **1981,** *15*, (4), 449-456.
43. Canonica, S.; Meunier, L.; Von Gunten, U., Phototransformation of selected pharmaceuticals during UV treatment of drinking water. *Water Res.* **2008,** *42*, (1-2), 121-128.
44. Bolton, J. R.; Stefan, M. I.; Shaw, P.-S.; Lykke, K. R., Determination of the quantum yields of the potassium ferrioxalate and potassium iodide–iodate actinometers and a method for the calibration of radiometer detectors. *J. Photochem. Photobiol. A* **2011,** *222*, (1), 166-169.
45. Zepp, R. G., Quantum yields for reaction of pollutants in dilute aqueous solution. *Environ. Sci. Technol.* **1978,** *12*, (3), 327-329.
46. Elovitz, M. S.; von Gunten, U., Hydroxyl radical/ozone ratios during ozonation processes. I. The Rct concept. *Ozone-Sci. Eng.* **1999,** *21*, (3), 239-260.
47. Shioi, J.; Matsuura, S.; Imae, Y., Quantitative measurements of proton motive force and motility in Bacillus subtilis. *J. Bacteriol.* **1980,** *144*, (3), 891-897.
48. Beck, N.; Callahan, K.; Nappier, S.; Kim, H.; Sobsey, M.; Meschke, J., Development of a spot‐titer culture assay for quantifying bacteria and viral indicators. *J. Rapid Methods Autom. Microbiol.* **2009,** *17*, (4), 455-464.
49. Miller, J.; Miller, J. C., *Statistics and chemometrics for analytical chemistry*. Pearson Education: 2018.
50. Ayala-Torres, S.; Chen, Y. M.; Svoboda, T.; Rosenblatt, J.; Van Houten, B., Analysis of gene-specific DNA damage and repair using quantitative polymerase chain reaction. *Methods* **2000,** *22*, (2), 135-147.
51. Sikorsky, J. A.; Primerano, D. A.; Fenger, T. W.; Denvir, J., DNA damage reduces Taq DNA polymerase fidelity and PCR amplification efficiency. *Biochem. Biophys. Res. Commun.* **2007,** *355*, (2), 431-437.
52. Duigou, S.; Ehrlich, S. D.; Noirot, P.; Noirot‐Gros, M. F., DNA polymerase I acts in translesion synthesis mediated by the Y‐polymerases in Bacillus subtilis. *Mol. Microbiol.* **2005,** *57*, (3), 678-690.
53. Filaderli, H. A. Chlorination of Specific Organic Compounds in Water Treatment. Department of Civil Engineering, Imperial College, 1989.

54. Evans, M. D.; Cooke, M. S., *Oxidative damage to nucleic acids*. Springer Science & Business Media: 2007.
55. Law, Y. K.; Forties, R. A.; Liu, X.; Poirier, M. G.; Kohler, B., Sequence-dependent thymine dimer formation and photoreversal rates in double-stranded DNA. *Photoch. Photobio. Sci.* **2013,** *12*, (8), 1431-1439.
56. Prutz, W. A., Hypochlorous acid interactions with thiols, nucleotides, DNA, and other biological substrates. *Arch. Biochem. Biophys.* **1996,** *332*, (1), 110-120.
57. Theruvathu, J. A.; Flyunt, R.; Aravindakumar, C. T.; von Sonntag, C., Rate constants of ozone reactions with DNA, its constituents, and related compounds. *J. Chem. Soc., Perkin Trans. 2* **2001**, (3), 269-274.
58. Masuda, T.; Shinohara, H.; Eda, M.; Kondo, M., Reactivity of nucleotides and polynucleotides toward hydroxyl radical in aqueous solution. *J. Radiat. Res.* **1980,** *21*, (2), 173-179.
59. Udovičić, L.; Mark, F.; Bothe, E., Yields of single-strand breaks in double-stranded calf thymus DNA irradiated in aqueous solution in the presence of oxygen and scavengers. *Radiat. Res.* **1994,** *140*, (2), 166-171.
60. Sivey, J. D.; McCullough, C. E.; Roberts, A. L., Chlorine monoxide (Cl2O) and molecular chlorine (Cl2) as active chlorinating agents in reaction of dimethenamid with aqueous free chlorine. *Environ. Sci. Technol.* **2010,** *44*, (9), 3357-3362.
61. Sivey, J. D.; Roberts, A. L., Assessing the reactivity of free chlorine constituents Cl2, Cl2O, and HOCl toward aromatic ethers. *Environ. Sci. Technol.* **2012,** *46*, (4), 2141-2147.
62. Yoon, Y.; Dodd, M. C.; Lee, Y., Elimination of transforming activity and gene degradation during UV and UV/H2O2 treatment of plasmid-encoded antibiotic resistance genes. *Environ. Sci.: Wat. Res. Technol.* **2018,** *4*, 1239-1251.
63. Patrick, M. H., Studies on Thymine-derived UV photoproducts in DNA —I. Formation and Biological Role of Pyrimidine Adducts in DNA. *Photochem. Photobiol.* **1977,** *25*, (4), 357-372.
64. Douki, T., Low ionic strength reduces cytosine photoreactivity in UVC-irradiated isolated DNA. *Photoch. Photobio. Sci.* **2006,** *5*, (11), 1045-1051.
65. Buxton, G. V.; Greenstock, C. L.; Helman, W. P.; Ross, A. B., Critical review of rate constants for reactions of hydrated electrons, hydrogen atoms and hydroxyl radicals (·OH/·O− in aqueous solution. *J. Phys. Chem. Ref. Data* **1988,** *17*, (2), 513-886.
66. von Sonntag, C., *Free-radical-induced DNA damage and its repair*. Springer: 2006.
67. Napolitano, M. J.; Stewart, D. J.; Margerum, D. W., Chlorine dioxide oxidation of guanosine 5'-monophosphate. *Chem. Res. Toxicol.* **2006,** *19*, (11), 1451-1458.
68. Sugiyama, H.; Saito, I., Theoretical studies of GG-specific photocleavage of DNA via electron transfer: significant lowering of ionization potential and 5 ‘-localization of HOMO of stacked GG bases in B-Form DNA. *J. Am. Chem. Soc.* **1996,** *118*, (30), 7063-7068.
69. Fukuzumi, S.; Miyao, H.; Ohkubo, K.; Suenobu, T., Electron-transfer oxidation properties of DNA bases and DNA oligomers. *J. Phys. Chem. A* **2005,** *109*, (15), 3285-3294.
70. Tataurov, A. V.; You, Y.; Owczarzy, R., Predicting ultraviolet spectrum of single stranded and double stranded deoxyribonucleic acids. *Biophys. Chem.* **2008,** *133*, (1-3), 66-70.
71. Vikesland, P. J.; Pruden, A.; Alvarez, P. J.; Aga, D.; Bürgmann, H.; Li, X.-d.; Manaia, C. M.; Nambi, I.; Wigginton, K.; Zhang, T., Toward a Comprehensive Strategy to Mitigate Dissemination of Environmental Sources of Antibiotic Resistance. *Environ. Sci. Technol.* **2017,** *51*, (22), 13061-13069.

72. Dubnau, D., Genetic exchange and homologous recombination. In *Bacillus subtilis and other gram-positive bacteria: biochemistry, physiology, and molecular genetics.*, Sonenshein, A. L.; Hoch, J. A.; Losick, R., Eds. American Society for Microbiology: Washington D.C, 1993; pp 555-584.
73. Contente, S.; Dubnau, D., Marker rescue transformation by linear plasmid DNA in Bacillus subtilis. *Plasmid* **1979,** *2*, (4), 555-571.
74. Morrison, D. A.; Guild, W. R., Activity of Deoxyribonucleic Acid Fragments of Defined Size in *Bacillus subtilis* Transformation. *J. Bacteriol.* **1972,** *112*, (1), 220-223.
75. Balasubramanian, B.; Pogozelski, W. K.; Tullius, T. D., DNA strand breaking by the hydroxyl radical is governed by the accessible surface areas of the hydrogen atoms of the DNA backbone. *Proc. Natl. Acad. Sci. U.S.A.* **1998,** *95*, (17), 9738-9743.
76. David, S. S.; O'shea, V. L.; Kundu, S., Base-excision repair of oxidative DNA damage. *Nature* **2007,** *447*, (7147), 941.
77. Hadden, C. T., Postreplication repair of ultraviolet-irradiated transforming deoxyribonucleic acid in Bacillus subtilis. *J. Bacteriol.* **1981,** *145*, (1), 434-441.
78. Herbert, M. A.; Hood, D. W.; Moxon, E. R., *Haemophilus influenzae protocols*. Springer Science & Business Media: 2003.
79. Hakenbeck, R.; Chhatwal, S., *Molecular biology of streptococci*. Horizon Scientific Press: 2007.
80. Hamilton, H. L.; Dillard, J. P., Natural transformation of Neisseria gonorrhoeae: from DNA donation to homologous recombination. *Mol. Microbiol.* **2006,** *59*, (2), 376-385.
81. Simpson, D. J.; Dawson, L. F.; Fry, J. C.; Rogers, H. J.; Day, M. J., Influence of flanking homology and insert size on the transformation frequency of Acinetobacter baylyi BD413. *Environ. Biosafety Res.* **2007,** *6*, (1-2), 55-69.
82. Dodd, M. C., Potential impacts of disinfection processes on elimination and deactivation of antibiotic resistance genes during water and wastewater treatment. *J. Environ. Monit.* **2012,** *14*, 1754–1771.
83. Imlay, J. A., Pathways of oxidative damage. *Ann. Rev. Microb.* **2003,** *57*, (1), 395-418.
84. Hawkins, C. L.; Davies, M. J., Hypochlorite-induced damage to DNA, RNA, and polynucleotides: formation of chloramines and nitrogen-centered radicals. *Chem. Res. Toxicol.* **2002,** *15*, (1), 83-92.
85. Manterola, G.; Uriarte, I.; Sancho, L., The effect of operational parameters of the process of sludge ozonation on the solubilisation of organic and nitrogenous compounds. *Water Res.* **2008,** *42*, (12), 3191-3197.
86. EPA *Disinfection profiling and benchmarking guidance manual*; United States Environmental Protection Agency: Office of Water. Washington, DC., 1999.
87. *Ultraviolet Disinfection Guidance Manual for the Final Long Term 2 Enhanced Surface Water Treatment Rule*; United States Environmental Protection Agency: Office of Water. Washington, DC, 2006.
88. Hauchman, F. S.; Noss, C. I.; Olivieri, V. P., Chlorine dioxide reactivity with nucleic acids. *Water Res.* **1986,** *20*, (3), 357-361.
89. Lee, Y.; Gerrity, D.; Lee, M.; Gamage, S.; Pisarenko, A.; Trenholm, R. A.; Canonica, S.; Snyder, S. A.; Von Gunten, U., Organic contaminant abatement in reclaimed water by UV/H2O2 and a combined process consisting of O3/H2O2 followed by UV/H2O2: prediction of abatement efficiency, energy consumption, and byproduct formation. *Environ. Sci. Technol.* **2016,** *50*, (7), 3809-3819.

90. Rosenfeldt, E. J.; Linden, K. G.; Canonica, S.; Von Gunten, U., Comparison of the efficiency of OH radical formation during ozonation and the advanced oxidation processes O3/H2O2 and UV/H2O2. *Water Res.* **2006,** *40*, (20), 3695-3704.
91. Leong, L. Y. C.; Kuo, J.; Tang, C.-C. *Disinfection of Wastewater Effluent - Comparison of Alternative Technologies*; Water Environment Research Foundation: Alexandria, VA, 2008.
92. Pecson, B. M.; Ackermann, M.; Kohn, T., Framework for Using Quantitative PCR as a Nonculture Based Method To Estimate Virus Infectivity. *Environ. Sci. Technol.* **2011,** *45*, (6), 2257-2263.

Supporting Information for Chapter 2

Degradation and deactivation of bacterial antibiotic resistance genes during exposure to free chlorine, monochloramine, chlorine dioxide, ozone, ultraviolet light, and hydroxyl radical

12 narratives, 3 tables, 20 figures, and supporting references

Text S2.1 Chemicals and materials

Free available chlorine (FAC) stock solutions were prepared by diluting a commercial aqueous sodium hypochlorite (NaOCl) stock (~5% w/w, Sigma) in Milli-Q water. Pre-formed aqueous stock solutions of monochloramine (NH_2Cl) were prepared by either slowly pipetting FAC stock (freshly diluted from the commercial stock with Milli-Q water without adjusting pH) into an equal volume of aqueous ammonium chloride (NH_4Cl) (at 2× the molar concentration of FAC, in 20 mM phosphate buffer (PB), at pH 8.5) with vigorous stirring, or mixing the above two solutions through a mixing tee at equal flow rates with a dual-channel syringe pump. The two approaches were found to have no difference in the yield of NH_2Cl according to a 200-600 nm full spectrum scan of the resulting NH_2Cl stock solutions. Aqueous chlorine dioxide (ClO_2) stock solutions were synthesized through the oxidation of chlorite by potassium peroxodisulfate.[1] Pre-dissolved stock solutions of aqueous ozone (O_3) were prepared by bubbling gaseous O_3 (generated by means of a model AC-2025 O_2-fed corona-discharge generator; IN USA, Inc.) through a chilled flask of Milli-Q water.[2] Hydrogen peroxide (H_2O_2) stock solutions were diluted from a commercial stock (30% w/w, J.T. Baker, stabilized) with Milli-Q water. FAC, NH_2Cl, ClO_2, O_3 and H_2O_2 stocks were standardized spectrophotometrically at 292 nm (ε = 350 $M^{-1}cm^{-1}$),[3] 243 nm (ε = 461 $M^{-1}cm^{-1}$),[3] 359 nm (ε = 1200 $M^{-1}cm^{-1}$),[4] 258 nm (ε = 3150 $M^{-1}cm^{-1}$),[5] and 240 nm (ε = 40 $M^{-1}cm^{-1}$),[6] respectively.

Broth and agar growth media for *B. subtilis* 1A189 were prepared using Difco™ antibiotic medium 3 (BD) and Difco™ Tryptose Blood agar (BD), respectively, and autoclaved. To prepare selective medium plates, 4 mg/L acriflavine was dosed to the autoclaved Tryptose Blood agar when it cooled to ~50 °C to avoid heat destruction of acriflavine. Stock solutions of calf thymus DNA were prepared by dissolving the commercially-available DNA sodium salt

(Sigma) in saline-citrate solution (0.15 M NaCl and 0.015 M trisodium citrate, pH=7.0) to yield concentrations of ~200 mg/L as dsDNA. NH_4Cl, sodium thiosulfate ($Na_2S_2O_3$), sodium sulfite (Na_2SO_3), sodium arsenite ($NaAsO_2$), Tris hydrochloride (Tris-HCl), 1,3,5-trimethoxybenzene (TMB), *tert*-Butanol (*t*-BuOH), acriflavine, and competence media (see recipes in Text S3) without magnesium sulfate ($MgSO_4$) were sterilized using 0.22 μm sterile syringe filters (Millex, USA) or 0.2 μm sterile SFCA filter units (Fisher Scientific, USA) depending on the solution volume. Filtered competence medium without $MgSO_4$ was frozen at -20 °C for long-term storage (up to three months). Commercial aqueous $MgSO_4$ solution (2.5 M, for molecular biology, Sigma) was added to the thawed media prior to use. For reagents not amenable to autoclave-sterilization, the Milli-Q water used was pre-autoclaved prior to use in their preparations. Solution pH values were measured using a 5 Star instrument (Thermo Scientific Orion, South Burlington, VT). The pH meter was calibrated prior to each use with pH 4, 7, and 10 buffers.

Text S2.2 DNA extraction protocol

DNA extraction for extracellular ARG (eARG) treatment. *B. subtilis* 1A189 was grown in 500 mL of Difco™ antibiotic medium 3 in a 2 L flask overnight (120 rpm, for 12 ± 0.5 hr) and harvested in the late exponential growth phase. The cells were pelleted by centrifugation (5000 rpm, or 4696 ×g, for 30 min) and washed three times with 25 mL of saline-EDTA (0.15 M NaCl and 0.1 M EDTA, pH=8). The cell pellet was re-suspended in 6 mL of saline-EDTA, containing 12 mg of lysozyme powder (Sigma) and 50 μL proteinase K (600 mAU mL^{-1}, Qiagen) (quickly pre-mixed to avoid lysozyme activity loss due to proteinase K digestion), and incubated in a 37 °C water bath for 60 minutes. Nineteen mL of Tris-SDS buffer (0.1 M Trisbase, 1% SDS and 0.1 M NaCl, pH=9.0) was added, and the mixture was frozen at -80 °C

and then thawed in a 65 °C water bath. This freeze-thaw procedure was repeated (typically 3-4 cycles) until the solution was clear, making sure to cool down the solution at room temperature after the last thawing step. The solution was mixed with an equal volume of phenol:chloroform:isoamyl alcohol (PCI) (25:24:1) (Acros Organics) by gently inverting at room temperature for at least 20 minutes. The mixture was centrifuged at 4696 ×g and 4 °C for ⩾ 90 minutes. The upper aqueous phase (about 23 mL) was then transferred into a new 50 mL centrifuge tube, mixed with an equal volume of chloroform (Fisher) and inverted for 1 min. The mixture was centrifuged (4696 ×g, ⩾ 30 minutes, 4 °C) and the upper aqueous phase (~21 mL) was equally split and transferred into two 50 mL centrifuge tubes. Two-and-a-half volumes of ice cold ethanol were added into each tube, and the mixture was gently inverted until the fibrous DNA precipitates aggregated into a pellet. (Caution: Overdosing of ethanol can lead to cloudiness in the aqueous phase, which may result from fine precipitates of proteins.)[7, 8] The DNA pellet was collected by pipette, washed with 10 mL of 70% ethanol three times, air dried for 15 minutes, and re-dissolved in 25 mL of saline-citrate solution. RNase A (Qiagen) and RNase T1 (Sigma) were each added to a final concentration of 50 μg/mL and the solution was incubated at 37 °C for 60 minutes. Then, the above procedure, including phenol:chloroform:isoamyl extraction, ethanol precipitation plus wash, and re-dissolution was repeated twice. Lastly, the step of ethanol precipitation plus wash was repeated one more time, and the recovered DNA pellet was re-dissolved in 10 mL of saline-citrate solution. The final DNA solution was incubated at 65 °C for 20 minutes (to inactivate potential DNase) and cooled down to room temperature. As a control measurement, 50 μL of the DNA stock was spread plated onto both the selective and non-selective medium (Difco™ Tryptose Blood agar with and

without 4 mg/L acriflavine) used for transformation assays to confirm the absence of vegetative cells or spores in the stock.

Recovery yields. This method could typically recover 10 mL of ~100-150 mg/L linear double-stranded DNA (dsDNA) with a size of ~40-60kbp (as determined by pulsed-field gel electrophoresis, or PFGE; see Text S2.7) from a 1 L overnight culture of *B. subtilis* 1A189.

DNA extraction following intracellular ARG (iARG) treatment. Upon completion of each intracellular treatment experiment, the whole volume of treated cells from the reaction suspension (1 L for FAC, NH_2Cl, ClO_2, and O_3; and 100 mL for UV) was collected on a 0.2 μm track-etched polycarbonate membrane (Whatman, NJ) by vacuum filtration. Then the membrane with the treated cells was placed in a 50 mL sterile centrifuge tube containing 20 mL of 10 mM PB (pH 7). The centrifuge tube was vigorously vortexed for at least 1 min to wash the cells off the membrane. Then the membrane was carefully removed from the tube using a pipette tip, and the cells were pelleted by centrifugation (4696 ×g, 30 min). The cell pellet was re-suspended in 2 mL of saline-EDTA containing lysozyme and proteinase K (quickly premixed at the same concentrations as mentioned above) and then transferred into a 15 mL centrifuge tube. The extraction was processed essentially as described above, but simplified and at smaller scale. Briefly, after cell lysis and one cycle of phenol:chloroform:isoamyl extraction, 2.5 volumes of ice cold ethanol were added to the solution, and the mixture was gently inverted and stored at -20 °C for at least 4 hours to enhance DNA precipitation. The DNA precipitates (usually not visible to the naked eye due to low quantities) were pelleted to the bottom of the tube by centrifugation (4696 ×g, $\geqslant$ 2 hours, 4 °C), and the supernatants were discarded carefully to avoid losing pelleted DNA. The tube was placed upside down to dry any residual ethanol for 15-20 minutes. One mL of saline-citrate pre-mixed with RNase A and RNase T1 (at the same concentrations as

above) was added to the tube. The solution was incubated at 37 °C for 60 minutes and inverted overnight to re-dissolve the DNA.

Recovery yields. This method could typically recover 1 mL of ~10-30 mg/L linear dsDNA with a size of ~40-60kbp (as determined by PFGE; see Text S2.7) from 1L of 10^6 CFU/mL 1A189 cells, or 1 mL of ~7.5-14.4 μM total nucleotides (after nuclease P1 digestion; equivalent to ~2.3-4.5 mg/L as dsDNA) from 100 mL of 10^6 CFU/mL cells. No significant difference was found between the recovery yields of untreated and disinfectant-treated cells.

Text S2.3 Natural transformation assay

Two types of competence media were used for different batches of samples analyzed by this assay. Type I competence medium includes 0.5% glucose, 1.4% potassium phosphate dibasic (K_2HPO_4), 0.6% potassium phosphate monobasic (KH_2PO_4), 0.2% ammonium sulfate ($(NH_4)_2SO_4$), 0.19% trisodium citrate ($C_6H_5Na_3O_7$), 0.02% acid-hydrolysed casein, 50 μg/mL tryptophan, 50 μg/mL histidine, and 6 mM $MgSO_4$. Type II competence medium is generally the same as Type I, except that the acid-hydrolysed casein was replaced by 50 μg/mL each of arginine, valine, lysine, threonine, glycine, aspartic acid and methionine. All the amino acids listed above are in L-form. Replacing commercial acid-hydrolysed casein of unclear composition with the seven amino acids has previously been reported to have stimulatory effects on *B. subtilis* competence as measured by testing of transfection frequency (i.e., frequency of *B. subtilis* transformation with pre-isolated bacteriophage DNA).[9] In the present study, this led to significant enhancement in transformation frequency (and resulting increases in sensitivity), while providing an identical response as the Type I competence medium to changes in normalized transformation frequency (f/f_0) during treatment with selected disinfectants.

The transformation recipient strain *B. subtilis* 1A1 – the non-antibiotic resistant progenitor of strain 1A189 – was cultured on Difco™ Tryptose Blood agar for 16 hours at 37 °C. The cells were transferred into competence medium (with $MgSO_4$ added) to achieve an optical density at 500 nm (OD_{500nm}) of 0.100, which allows for adequate growth and the development of sufficient levels of competence. Five mL of the inoculated medium was transferred into each of a set of 10 mL HACH tubes, and incubated under shaking (at 37 °C, 120 rpm, and an angle of 15°) with OD_{500nm} measured every 30 minutes. Typical growth curves for both types of competence media are shown in Figure S2.1a. Two-and-a-half hours after the fastest growth rate, the competent cell cultures were combined into a 50 mL centrifuge tube and pelleted by centrifugation (4696 ×g, 30 min, 37 °C). Half of the volume of the upper clear media was discarded; then the cells were re-suspended in the remaining half of the competence medium. Three hours after the fastest growth rate, 0.5 mL of the 2× concentrated competent cells and 0.5 mL of the DNA sample were gently mixed in a 50 mL centrifuge tube and incubated under shaking (37 °C, 120 rpm, 90 minutes). A negative control was also processed by mixing 0.5 mL of the 2× concentrated competent cells and 0.5 mL sterilized PB solution (with the same pH as the DNA sample) and incubated under the same conditions as the samples. After 90 minutes of incubation, each solution was dosed with 1 μL of DNase I (1 Unit/μL, Thermo Scientific) and incubated (37 °C, 15 minutes) to quench DNA uptake.

Text S2.4 Measurement of transformation frequency

One-hundred μL of undiluted and 10-fold diluted aliquots of each DNase I-quenched mixture of DNA and competent cells (referred to henceforth as the *transformation mixture* for convenience) – including those prepared from DNA samples and the negative control, were

spread-plated on selective media (Difco™ Tryptose Blood agar with 4 mg/L acriflavine) in duplicate to quantify the cell density of resulting transformant cells bearing the multidrug-resistance phenotype. Serial dilutions (10^0-fold to 10^6-fold) of the transformation mixture of the negative control were also spot-titered on non-selective media (Tryptose Blood agar without acriflavine) to quantify the cell density of non-resistant recipient cells. The transformation frequency (f) for each sample was calculated as the ratio of the transformant cell density on selective media (from which any background signal observed for the negative control on selective media was subtracted) to the recipient cell density on non-selective media. Typical ranges of recipient cell density were $4.75\times10^8 \sim 6.83\times10^8$ CFU/mL for Type I competence medium and $1.08\times10^8 \sim 2.75\times10^8$ for Type II. Typical ranges of transformation frequency for 1 mg/L of untreated DNA were $1.13\times10^{-7} \sim 6.85\times10^{-6}$ for Type I competence medium and $4.35\times10^{-5} \sim 3.40\times10^{-4}$ for Type II. Sample curves of transformation frequency as a function of DNA concentration (ranging from 0.01 to 100 mg/L, before mixing with recipient cells) are provided for Type I and Type II competence media in Figure S2.1b.

Text S2.5 Sequences and locations of *bltR-blt-bltD* gene segment and quantitative polymerase chain reaction (qPCR) amplicons within the *B. subtilis* 168 genome (genome sequence data accessed from GenBank, at http://www.ncbi.nlm.nih.gov/genbank/; accession number: AL009126.3)

bltR gene: from bases 2716035-2716856 (5', 3' termini in bold, blue font)
blt gene: from bases 2716973-2718175 (5', 3' termini in bold, red font)
bltD gene: from bases 2718344-2718802 (5', 3' termini in bold, green font)

Primer set for 266 bp amplicon:
F266 5'-GGTAGGTGGGTTGACCGTTT-3'
R266 5'-CCCGCACCAGGTCCAATAAT-3' => ATTATTGGACCTGGTGCGGG

Primer set for 832 bp amplicon:
F832 5'-TGGGTTATCTTGTTGCGGCT-3'
R832 5'-GGACGTAGCAAATCGAACGC-3' => GCGTTCGATTTGCTACGTCC

Primer set for 870 bp amplicon:
F870 5'-GTTCCCGTGCAAAGATTCCG-3'
R870 5'-CGAAACGGTCAACCCACCTA-3' => TAGGTGGGTTGACCGTTTCG

Primer set for 1017 bp amplicon:
F1017 5'-TCCGGTACGCCTCTTCAGTA-3'
R1017 5'-CGAAACGGTCAACCCACCTA-3' => TAGGTGGGTTGACCGTTTCG

Homologous amplicons symmetrically flanking the point mutation (for model development in Figure 2.4 and Figure S2.19):
800 bp amplicon (5', 3' termini in bold, cyan font)
900 bp amplicon (5', 3' termini in bold, orange font)
1000 bp amplicon (5', 3' termini in bold, purple font)

Site of 1A189/*acfA* point mutation (AT base-pair deletion) in *blt* promoter region:

TTACACCTCTTTAACTTGAAGGAGGATTTTTGCATATGTATTTTCATACCCGTCAACTACCAT
CTCATCCAGCATATATTCCTCATATGCATTTTCCCCTATTTGCATTCCATTTCTTTCAATGAAC
TCAATGATTCTCCGGTACGCCTCTTCAGTATTTCCGCCTATTTCATATCCAACTGCATACAGG
CCTTTTGGCCGTACATGATAATTTATGTTCTCTGCCCCATCTTTTACTTTTATATAAAAGTAAC
TGTAATTGTAGAAGTCTTTTTCTAAGATTTGTTCCCGTGCAAAGATTCCGCCTATCGGATATC
CTTCATCTAATTCATATTGCTGAACTTCATGAATGAGTTCTGAAATGGCTGCCACATATTTTC
GTTCTGGTAAGTTTAATGTTTTTCGGCTTAACATGAATGTTTCTTCATTTAAATATTCAAAAG
AAATTGAGGAAAAATCAGTCTCAAGTGCTTGTTCTGTAAGCGTCACTTTTGTTTGTAAGATC
GTTTGCAACTGCTTAAGCTCATTTATTTTTTTATCAATCTCAATAGACTTTTCTTTTAGAACAT
GCAGGATCTTGTCTGGTGTTTTTCCTTTTATTAGACACTTTATTTCTTTTAATGGAACCCCAAG
CTCTTTAAATAGACTGATGACTTGAAAAGTCTCAAATTGATGATAGGAATAATATCTATACC
CATTTTCTTTTTTTATTTCCGGCGAGAAAAGACCAATCTCATCATAATGAAATAAAGTTTGTT
TTTTTACACGGCAGAGCTTCGAAAACTCCCCTGTTGTGAAATACTTCTTAACATCTTCGCTCA
TAAAAACCTCCTTGACTATACGGTAACCATATACCTTATGATTTGATTGTACTTGAAAAAAG
CTTCAAGCGAAAAGGATAGGTAAAAAGGGTTCAATTGAGTAAAAGGGGAATTCAGATGAAA
AAATCAATAAATGAGCAAAAAACGATATTCATTATACTATTAAGCAACATCTTCGTAGCATT
TCTTGGTATCGGTTTAATCATTCCAGTTATGCCTTCTTTTATGAAAATCATGCATTTATCCGGC
AGCACAATGGGTTATCTTGTTGCGGCTTTGCCATTTCTCAGTTAATTACTTCACCTTTTGCA
GGTAGGTGGGTTGACCGTTTCGGGAGAAAAAAAATGATTATTCTCGGGTTGCTTATATTCAG
TTTATCTGAGTTGATTTTCGGATTAGGGACCCATGTTTCAATATTTTATTTCTCGAGGATATT
GGGTGGTGTAAGTGCGGCTTTTATCATGCCCGCGGTAACAGCATATGTAGCTGATATTACAA
CCCTAAAGGAAAGGTCAAAGGCTATGGGGTATGTTTCTGCTGCAATTAGCACCGGCTTTATT
ATTGGACCTGGTGCGGGAGGATTTATTGCCGGCTTTGGTATCCGCATGCCGTTTTTCTTCGCC
TCCGCCATCGCGTTAATAGCAGCTGTCACTTCCGTTTTTATACTAAAAGAGTCATTGTCGATA
GAAGAACGCCATCAACTCTCATCTCATACAAAGGAATCAAATTTCATTAAAGACTTGAAGAG
ATCCATTCATCCTGTCTATTTCATTGCATTTATTATCGTCTTTGTAATGGCTTTTGGTTTATCA
GCTTATGAAACGGTATTCAGCTTGTTTTCTGATCATAAATTTGGCTTCACACCAAAAGATATT
GCAGCCATTATTACGATTAGTTCCATTGTTGCGGTAGTTATTCAAGTTTTACTATTCGGGAAA
TTGGTCAACAAACTTGGAGAGAAAAGAATGATTCAGCTGTGCTTAATAACCGGTGCGATCTT
GGCTTTCGTGTCTACTGTTATGTCAGGATTTTTAACTGTTTTGCTTGTAACTTGTTTTATTTTT
CTGGCGTTCGATTTGCTACGTCCGGCCTTAACCGCTCATTTATCCAATATGGCCGGTAACCAG
CAGGGTTTCGTAGCAGGCATGAACTCCACATACACCAGCCTGGGAAATATATTTGGACCTGC
TCTAGGCGGTATACTATTTGATCTTAACATTCATTATCCTTTCCTTTTTGCAGGTTTCGTTATG
ATTGTCGGCCTTGGTCTTACAATGGTTTGGAAAGAAAAAAAGAATGATGCTGCAGCTTTGAA
TTAATTCATTTTCTATAAAGTTAAGTCATTTGGATGCAGGGAATGCCCCTGGTTAGGCACAAT

AAGAAAAGGTACTTAATTTGATAGGCTACATGTTGCTTGACGTGAATATAGTATAAGCTGAG
TTTTAGCAATATCAGGATACCGGGATAAGAAAAAAGGAGAATGTAGT**A**TGAGTATAAACAT
AAAAGCAGTAACTGATGATAATCGTGCTGCAATTCTTGATCTACATGTCAGCCAGAATCAAT
TATCATATATTGAATCTACAAAAGTATGTTTAGAAGATGCAAAAGAATGTCACTATTATAAA
CCTGTCGGGCTTTACTATGAAGGAGATCTAGTCGGTTTTGCAATGTATGGATTGTTTCCCGAG
TATGATGAAGATAATAAAAACGGACGAGTCTGGCTTGACCGATTTTTTATTGACGAACGCTA
TCAGGGAAAAGGATTAGGGAAGAAAATGCTTAAAGCCCTCATTCAGCACCTTGCTGAGTTAT
ATAAATGCAAGAGAATTTATTTAAGTATATTTGAAAATAATATTCATGCTATACGCCTTTATC
AAAGGTTTGGTTTTCAATTTAATGGTGAACTCGACTTTAATGGTGAGAAGGTAATGGTAAAA
GAGCTATA**G**

Text S2.6 Protocols of qPCR assays

qPCR mixture compositions and temperature profiles. Each individual 10 μL reaction contained 5 μL of SsoFast™ EvaGreen® Supermix, 1000 nM of forward and reverse primers for the 266 bp amplicon or 500 nM for the other three primer sets (for 832 bp, 870 bp and 1017 bp amplicons), 2 μL of DNA template, and molecular biology grade water (Corning, NY) for the remaining volume. The solutions were mixed in 0.1 mL white PCR tubes with optical caps (USA Scientific, Orlando, FL). The temperature profiles of the qPCR assays for each amplicon are presented in Table S2.2.

Calibration curve and amplification efficiencies. Purified genomic *B. subtilis* 1A189 DNA was used as a qPCR standard. In order to calculate amplicon copy number, DNA standards were assumed to contain only intact genomic DNA carrying one copy of the *bltR-blt-bltD* segment per genome. The calibration curves were conducted in duplicate to cover seven orders of magnitude from 2 to 2×10^6 copies/μL with 10-fold serial dilution, yielding average R^2 values of 0.997 ± 0.002 across all qPCR assays, and amplification efficiencies of 0.91 ± 0.07, 0.89 ± 0.06, 0.84 ± 0.05, and 0.86 ± 0.04 for 266 bp, 832 bp, 870 bp, and 1017 bp amplicons, respectively. Typical calibration curves of the 266 bp and 1017 bp amplicons are provided in Figure S2a,b as examples.

Limits of detection and quantification (LODs & LOQs). The LODs & LOQs of qPCR assays for the shortest and longest amplicons (i.e., 266 bp and 1017 bp) were determined as examples and considered to be representative for the other two amplicons of 832 bp and 870 bp. As per Forootan et al.,[10] a 2-fold dilution series of *B. subtilis* 1A189 DNA standards was prepared, covering the low concentration range of 1 to 32 (i.e., 2^0 to 2^5) copies/µL. Each standard was analyzed in 24 replicates, except that the most diluted one (1 copy/µL) was analyzed in 48 replicates.

The LOD is defined as the lowest concentration at which 95% of the positive samples are detected. In practice, the experimental fraction of positive replicates versus concentration (in log-scale) was fit to a sigmoidal function by non-linear regression. Then, the experimental LOD was either read from the fitted curve or, if smaller than the theoretical LOD of 3 copies per reaction (which equates to 1.5 copies/µL in the present case since 2 µL of DNA template was added per reaction), was rounded up to the theoretical LOD. The LOQ is defined as the lowest concentration at which the coefficient of variation is below the arbitrary threshold of 40%. The coefficient of variation for log-normal distributed concentrations of replicate samples ($CV_{\ln}$) can be calculated from the standard deviation of replicate cycles (SD_{Cq}) and amplification efficiency (E) using $CV_{\ln} = 100\% \cdot \sqrt{(1+E)^{(SD_{Cq})^2 \cdot \ln(1+E)} - 1}$.[10]

The LODs were determined as 3 copies and 5 copies per reaction (i.e., 1.5 copies/µL and 2.5 copies/µL) for 266 bp and 1017 bp amplicons, respectively (Figure S2c,d), and the LOQs were determined as 32 copies per reaction (i.e., 16 copies/µL) for both amplicons (Figure S2e,f).

Text S2.7 Pulsed-field gel electrophoresis (PFGE)

Ten mg/L (for FAC, NH_2Cl, ClO_2, and $^{\bullet}OH$) or 1 mg/L (for O_3 and UV) of extracellular DNA in 10 mM PB solutions was treated at identical conditions as described in the main text (or Text S2.8). The 1 mg/L treated DNA samples from O_3 and UV experiments were then concentrated to 10 mg/L via 3 kDa dialysis membrane (Amicon Ultra-4 Centrifugal Filter, Millipore). DNA concentrations of 10 mg/L were selected here to ensure that the sample loaded per lane – containing 50 μL of 10 mg/L DNA plus 10 μL 6× loading dye (Thermo Scientific) – could yield sufficiently bright bands when exposed to UV light after ethidium bromide staining. PFGE was conducted on a CHEF-DR® II system at 6 V cm^{-1}, 1% Pulsed Field Certified™ Agarose (Bio-Rad), 14 °C, either in 0.5× TBE buffer for 15 hours with switch times of 1–12 seconds if using a LowRange PFG Marker DNA size standard (New England BioLabs), or in 0.5× TAE buffer for 11 hours with switch times of 1–6 seconds if using a 5 kb ladder DNA size standard (Bio-Rad). The gel was stained with 1 μg/mL ethidium bromide for 20-30 min and then exposed to UV light to capture the resulting image.

Text S2.8 Details about treatment of extracellular ARGs (eARGs): reactor configurations, additional control experiments, and determination of disinfectant exposures

Treatment with FAC, NH_2Cl, and ClO_2 in batch reactors. For FAC, NH_2Cl, and ClO_2, the isolated 1A189 DNA stock (in saline-citrate solution at pH 7) was diluted to 1 mg/L as dsDNA (3.2×10^{-6} M based on total nucleotides) in 10 mM phosphate buffer (PB) solution at pH 7 (for FAC and ClO_2) or 8 (for NH_2Cl). Reactions were initiated by mixing the disinfectant stock with the 1 mg/L DNA solution in 25 mL amber bottles using polytetrafluoroethylene (PTFE)-coated magnetic stir bars. Samples were collected at pre-defined times for measurement of residual disinfectant (by adding to sample vessels containing the appropriate colorimetric

reagent), or for subsequent analysis by qPCR or transformation assay (by adding to sample vessels containing amended with sufficient $Na_2S_2O_3$ to yield a 20× molar excess with respect to the disinfectant). Residual disinfectant concentrations were monitored during experiments with colorimetric methods using *N*,*N*-diethyl-*p*-phenylenediamine (DPD) at the wavelength (λ) of 510 nm for FAC and NH_2Cl,[11] and 2,2'-azino-bis(3-ethylbenzthiazoline)-6-sulphonic acid-diammonium salt (ABTS) at λ of 405 nm for ClO_2.[12] Stirring was confirmed to have no effect on transforming activity at the mixing intensities used (200 rpm, data not shown). For NH_2Cl, selected experiments were also conducted in 10 mM PB solutions at pH 7, with all other conditions as above, to confirm consistency with pH 8 results.

For FAC, a number of additional types of experiments were conducted to help explore the mechanism of reaction between FAC and DNA, as follows: **(1)** 1 mg/L of partially denatured 1A189 DNA – prepared by heating a concentrated 1A189 DNA stock (~100 mg/L as dsDNA) in a boiling water bath for 10 min, placing it in an ice bath for 5 min, and then diluting it to 1 mg/L in room temperature PB – was treated as described above. **(2)** 1 mg/L (as dsDNA) of 1A189 DNA in the presence of the radical scavengers methanol (MeOH) or *t*-BuOH (50 mM for each) was treated as described above. **(3)** 1 mg/L (as dsDNA) of 1A189 DNA was treated as described above, and samples collected at pre-defined time intervals were treated with $Na_2S_2O_3$ or various alternate FAC-quenching reagents – including Na_2SO_3, NH_4Cl, H_2O_2, $NaAsO_2$, Tris-HCl, and TMB[13]. Samples quenched with NH_4Cl, H_2O_2, $NaAsO_2$, Tris-HCl, and TMB were immediately diluted by 100-fold to minimize potential further reactions of unstable products (e.g., organochloramines), and analyzed within 20 minutes by qPCR. Subsequently, after approximately three hours, the 100-fold diluted NH_4Cl- and Tris-HCl-quenched samples were re-analyzed with qPCR. **(4)** 90 mg/L (as dsDNA) of 1A189 DNA or calf thymus DNA in PB at pH

7 was subjected to treatment with 320 μM FAC, added in either a single dose (and allowed to react for ~25 minutes after FAC addition), or in six incremental doses of 53 μM FAC at ~10 min intervals (where each dose was allowed to react for ~10 min after addition). The FAC-treated DNA solution was then sampled at pre-defined time intervals for analysis by means of (i) UV absorbance spectrophotometry (using a Shimadzu UV-2700 spectrophotometer), (ii) Hoechst 33258 fluorescence assay with a DNA Quantitation Kit (Bio-Rad) (for measurement of dsDNA levels and dsDNA denaturation), and (iii) DPD colorimetry (for measurement of residual FAC, total available chlorine (TAC), and combined chlorine). After acquisition of UV absorbance spectra for the FAC-treated DNA samples, they were amended with at least 2× molar excesses of $Na_2S_2O_3$ or alternate quenching reagents – including Na_2SO_3, NH_4Cl, H_2O_2, $NaAsO_2$, and Tris-HCl – and re-analyzed by the spectrophotometer in order to assess the impact of quenching reagents on the UV absorbance spectrum of the FAC-treated DNA. Subsequently, the samples quenched with $Na_2S_2O_3$ were passed through a 3 kDa dialysis membrane (Amicon Ultra-4 Centrifugal Filter, Millipore) or a Bio-Rad Bio-Spin P-6 gel column to remove excess $Na_2S_2O_3$ and then re-analyzed by the spectrophotometer. Note that commercially-available calf thymus DNA was used in the majority of these experiments to help preserve the limited quantities of 1A189 DNA isolated through the extraction and purification approaches described in Text S2.

Treatment with O_3 using a continuous-flow, quenched-reaction system. Reactions were initiated by mixing two solutions containing (a) 2 mg/L of 1A189 DNA and 100 mM *t*-BuOH in 20 mM PB at pH 7, and (b) a working solution of O_3 at varying concentrations (≥10-fold molar excess of DNA) in Milli-Q grade H_2O (stabilized by adjustment to pH 4 with sulfuric acid), through a polyether ether ketone (PEEK) or Tefzel™ ethylene-tetrafluoroethylene (ETFE) mixing tee (IDEX) in 1:1 proportion, using a dual-channel syringe pump (Harvard Apparatus).

The mixed reaction solutions subsequently passed through one of several 1 mm or 1/32 inch inner diameter PTFE reaction tubes of lengths ranging from 5 to 75 cm (depending on the desired reaction time), and upon exiting the reaction tube and entering a second PEEK/Tefzel™ ETFE tee, were mixed with a quenching solution containing $Na_2S_2O_3$ in at least 20-fold molar excess of O_3 to stop the reaction prior to sample collection for residual ARG analyses.

Reaction times were calculated based on flow rate and the volumes of the reaction tubes, including the volume of PTFE tubing plus the system dead volume; that is, 1/3 of the swept volume of both the primary and secondary tees. The volumes of PTFE reaction tubes were calibrated by pumping a stock solution of potassium indigo trisulfonate through a given reaction tube connected on each end to two-way shutoff valves, isolating the indigo within the tube by closure of the valves on each end of the tube, and then subsequently flushing the isolated indigo volume out of the tube with Milli-Q grade H_2O. Then the volume of the isolated indigo solution could be determined from the total volume of the flushed effluent (measured using an analytical balance) and the dilution factor of the isolated indigo solution (determined from absorbance measurements as $Abs_{600nm,\ stock}/Abs_{600nm,\ effluent}$). A calibration curve was established for isolated solution volumes vs. a series of PTFE tubing lengths, yielding a slope equal to the volume of PTFE tubing per unit length, and an intercept equal to the total dead volume of the two valves on each end of the tubing used to control the isolation and flushing of indigo trisulfonate. The intercept could be subtracted from the indigo solution volumes isolated with each reaction tube in place in order to obtain the volumes of the reaction tubes themselves.

The swept volumes of the mixing tees were calibrated in a similar manner, where each of three 5 cm lengths of PTFE tubing were connected on one end to one of the three ports of a tee, and on their other end to one of the two-way shutoff valves noted above to control indigo

isolation and flushing. In this case, the overall volume of the isolated solution was taken as the sum of the total volume of 15 cm (3 × 5 cm) of PTFE tubing, the total dead volume of three two-way shutoff valves, and the swept volume of the tee. The swept volume of the tee was in turn calculated by subtracting the total tubing volume and total valve dead volumes from the overall isolated volume of indigo solution.

In this way, the system reaction volumes were calibrated as ranging from 39 to 534 μL (inclusive of PTFE reaction tube volumes and dead volumes of the mixing tees). A flow rate of 12-25 mL/min was used for each of the two channels of the syringe pump driving the DNA and O_3 solutions (confirmed by calibration using Milli-Q water and an analytical balance). Thus, the flow rate passing through the reaction volumes ranged from 24-50 mL/min, so that reaction volume residence times (reaction times) ranged from 0.047 to 1.3 s.

The initial O_3 concentration in the working solution loaded into the O_3 syringe was measured at 258 nm (ε = 3150 $M^{-1}cm^{-1}$),[5] while the residual O_3 concentration remaining at the entrance of the second mixing tee (after reaction with DNA for the residence times noted above) was measured with potassium indigo trisulfonate[2, 11] (in place of $Na_2S_2O_3$), in order to confirm that O_3 concentration did not decrease significantly (less than 10%) over the duration of any experiment and could thus be considered as constant during the reactions (ensuring maintenance of pseudo-first-order conditions).

Overall continuous-flow, quenched-reaction system calibration was also performed by using the reaction between NH_3 and HOCl as a reference according to Dodd et al. (2005).[14] Briefly, the above solutions of DNA and O_3 were replaced with solutions of 70-μM FAC and 1.4-mM NH_4Cl (both buffered with 10mM PB at pH values of 6, 7, or 8). The quenching solution of $Na_2S_2O_3$ utilized in the third syringe channel was replaced with a 3 mM DPD solution

(buffered at pH 6.5 with 0.1 M phosphate, and continuously sparged with N_2 gas to prevent oxidation by O_2 during the experimental time frames). Absorbances at 515 nm were measured for the quenched reaction solutions to determine kinetics of FAC decay, which followed pseudo-first order kinetics due to the large excess of NH_3. Variation in flow rates from 12 to 25 mL/min (for each of the two reactant channels – for FAC and NH_3) was confirmed to have no impact on FAC decay kinetics at a given pH. The pH-independent second-order rate constant determined for the NH_3-HOCl reaction from the measured data was 1.34×10^6 $M^{-1}s^{-1}$, in good agreement with the literature value of 2.62×10^6 $M^{-1}s^{-1}$ for 20 °C.[15]

Treatment with UV irradiation. Monochromatic ultraviolet (UV) light (λ = 254 nm) was generated using a 15-W, low-pressure Hg lamp (UVP, LLC) housed in a quartz immersion well inside of a "merry-go-round" photoreactor apparatus (Ace Glass). The quartz immersion well was wrapped with five layers of 1/16 in. plastic mesh to attenuate lamp output (thus lowering reaction rates) by ~90%. UV irradiation was initiated by placing quartz tubes containing 25-mL of 1 mg/L 1A189 DNA (in pH 7, 10 mM PB) into the photoreactor apparatus with thermostatting at 25 ± 1 °C by means of a recirculating constant temperature water bath. At pre-defined sampling intervals, the quartz tubes were taken out of the photoreactor to terminate the UV irradiation, and 1-mL samples were collected after inverting the irradiated tubes several times to ensure homogeneity of the sampled solutions. Then the quartz tubes were placed back into the photoreactor apparatus to continue the irradiation until the next pre-defined sampling time. Selected experiments were also conducted using 0.1 mg/L DNA (with other conditions identical to those described above) to confirm that a DNA concentration of 1 mg/L had minimal screening effect on UV irradiance (Figure S2.14). Absorbances of 0.1 mg/L and 1 mg/L 1A189 DNA (in pH 7, 10 mM PB) were measured as 0.001 cm^{-1} and 0.022 cm^{-1}, respectively,

corresponding to light-screening factors of 0.9997 and 0.9706 for the optical pathlength of 1.23 cm measured for the quartz tubes (see below).

Fluence rate at 254 nm (I, in mW/cm^2) was measured principally by atrazine actinometry according to the method described by Canonica et al. (2008),[16] with confirmation by potassium iodide/iodate (KI/KIO_3) and potassium ferrioxalate ($Fe^{III}Ox$) actinometry according to the methods described by Rahn (1997)[17, 18] and Bolton et al. (2011),[19] using the same experimental setup as described above for UV irradiation of DNA solutions.

Fluence rate determined by means of atrazine actinometry (under optically dilute conditions, with $\varepsilon_{254,atrazine} l C_{atrazine} \leq 0.02$) was calculated as $I = \left(\frac{k_{254,atrazine}}{2.303 \varepsilon_{254,atrazine} \phi_{254,atrazine}}\right) U_{254}$, where $\varepsilon_{254,atrazine}$ (= 3860 M^{-1}cm^{-1}) is the molar extinction coefficient of atrazine solution at 254 nm,[20] l is the pathlength (= 1.23 cm) of the quartz tubes (see below), $C_{atrazine}$ = 5 × 10^{-6} M, $k_{254,atrazine}$ is the first-order rate constant (s^{-1}) measured for atrazine photolysis in solutions irradiated at 254 nm, U_{254} (= 4.72×10^5 J/Einstein) is the molar photon energy at 254 nm,[17] and $\phi_{254,atrazine}$ (= 0.046 mol/einstein at 254 nm) is the quantum yield for atrazine photolysis at 254 nm.[21] The fluence rate determined by atrazine actinometry was 0.073 mW/cm^2.

Fluence rate determined by means of KI/KIO_3 or $Fe^{III}Ox$ actinometry (under optically opaque conditions, with $\varepsilon_{254,KI/KIO_3} l C_{KI/KIO_3}$ or $\varepsilon_{254,Fe^{III}Ox} l C_{Fe^{III}Ox} > 2$) was calculated as $I = \left(\frac{\Delta Abs_{352nm,I_3^-}}{\Delta t}\left(\frac{1}{\varepsilon_{352,I_3^-} \phi_{254,I_3^-}}\right)\right) U_{254} l$ or $I = \left(\frac{\Delta Abs_{510nm,Fe^{II}Phen}}{\Delta t}\left(\frac{1}{\varepsilon_{510,Fe^{II}Phen} \phi_{254,Fe^{II}}}\right)\right) U_{254} l$, where $\varepsilon_{254,KI/KIO_3}$ (= 220 M^{-1}cm^{-1})[17] or $\varepsilon_{254,Fe^{III}Ox}$ (~ 3200 M^{-1}cm^{-1})[22] are the molar extinction coefficients

for the KI/KIO_3 and $Fe^{III}Ox$ solutions at 254 nm, C_{KI/KIO_3} = 0.6 M KI/0.1 M KIO_3 and $C_{Fe^{III}Ox}$ = 6×10^{-3} M, $\frac{\Delta Abs_{352nm,I_3^-}}{\Delta t}$ and $\frac{\Delta Abs_{510nm,Fe^{II}Phen}}{\Delta t}$ are the rates of absorbance buildup at 352 nm or 510 nm (in units of cm^{-1}) in samples of the irradiated KI/KIO_3 solutions (measured directly) or irradiated $Fe^{III}Ox$ solutions (measured following reaction with acetate-buffered phenanthroline) during exposure to 254 nm UV light (due to generation of I_3^- or Fe^{II}, respectively), ε_{352,I_3^-} (= 26400 $M^{-1}cm^{-1}$)[17] and $\varepsilon_{510,Fe^{II}Phen}$ (= 11100 $M^{-1}cm^{-1}$)[19] are the molar extinction coefficients of triiodide (I_3^-) at 352 nm and Fe^{II}-phenanthroline complex at 510 nm, and Φ_{254,I_3^-} (= 0.72 mol/einstein at 253.7 nm, 25 °C) and $\Phi_{254,Fe^{II}}$ (= 1.38 mol/einstein at 253.7 nm) are the quantum yield for I_3^- and Fe^{II} production as reported by Bolton et al. (2011).[19] U_{254} and l are (as above) the molar photon energy (= 4.72×10^5 J/Einstein) at 254 nm and pathlength (= 1.23 cm) of the quartz tubes (see below). The fluence rates determined by KI/KIO_3 and $Fe^{III}Ox$ actinometry were 0.074 and 0.072 mW/cm^2, respectively, in very good agreement with the value obtained using atrazine actinometry.

The average pathlength (l) of the photolysis cells (i.e., quartz tubes in this study) was determined experimentally with $Fe^{III}Ox$ according to Mill et al (1982),[23] using the method developed by Zepp (1978).[24] Briefly, a series of $Fe^{III}Ox$ solutions with concentrations of 0.5, 0.45, 0.4, 0.35, 0.3, and 0.25 mM was prepared in 0.05 M sulfuric acid (H_2SO_4). Here the $Fe^{III}Ox$ solution of 0.5 mM was considered as an opaque solution, since the estimated absorbance of the solution in the photolysis cell ($\varepsilon_{254,Fe^{III}Ox} C_{Fe^{III}Ox} l$) just exceeds 2.0, and is thus able to absorb essentially all photons of the UV light. The other $Fe^{III}Ox$ solutions of concentrations less than 0.5

mM (and accordingly $\varepsilon_{254,Fe^{III}Ox} C_{Fe^{III}Ox} l < 2.0$) were considered as non-opaque solutions. Each of the $Fe^{III}Ox$ solutions was exposed to 254 nm UV light for up to 5 min in four replicates. The formation of Fe^{II} during irradiation was monitored colorimetrically using 1% phenanthroline at λ = 510 nm.[25] The formation rate of Fe^{II} for each $Fe^{III}Ox$ concentration was calculated as Rate = $\frac{\Delta Abs_{510nm,Fe^{II}Phen}}{\Delta t}$ as above. The formation rate for the opaque solution (0.5 mM $Fe^{III}Ox$) was assigned as $Rate_{max}$. The formation rate for a non-opaque solution *i* at a concentration of $C_{Fe^{III}Ox,\,i}$ was normalized to $Rate_{max}$, and expressed as $Rate_i/Rate_{max}$. By plotting $-\log(1 - Rate_i/Rate_{max})$ versus $\varepsilon_{254,Fe^{III}Ox} C_{Fe^{III}Ox,\,i}$, the slope of the curve equates to the average pathlength. The average pathlength of the quartz tubes (18 mm O.D., 16 mm I.D., Ace Glass) used here for UV irradiations was determined as 1.23 cm.

Treatment with hydroxyl radical. Hydroxyl radical (•OH) was generated via irradiation of hydrogen peroxide (H_2O_2) by near-UV wavelengths (290 nm ⩽ λ ⩽ 400 nm), which were generated as previously described by Forsyth et al.[26] Briefly, a 450-W Xe arc lamp solar simulator (Newport-Oriel Model 66924; Stratford, CT) was equipped with a focusing collimator (50.8 mm diameter), atmospheric attenuation filter (with cutoff of λ < 290 nm to restrict lamp output to near-UV wavelengths), and dichroic mirror (to dissipate infrared-generated heat). Reactions with •OH were undertaken by dosing 10 mM H_2O_2 into 10 mM PB solutions containing 10 mg/L 1A189 DNA and 1 μM *para*-chlorobenzoic acid (*p*CBA), which were placed in a 60-mL crystallization dish (VWR) centered within the quasi-collimated beam of the solar simulator. At pre-defined time intervals, samples were collected and quenched with catalase from bovine liver (aqueous suspension, Sigma) at over 10 units per μmole of H_2O_2 to ensure

quenching within a few seconds (1 unit of bovine catalase quenches 1 μmole of H_2O_2 per min). Residual concentrations of *p*CBA in samples were quantified by high performance liquid chromatography. No ARG degradation or deactivation was noted during additional control experiments in which 10 mg/L DNA was exposed to either 10mM H_2O_2 in the dark or near-UV light alone under the same conditions, confirming that ARG degradation and deactivation during near-UV/H_2O_2 treatment resulted only from reactions with •OH, and not from direct photolysis or reaction with H_2O_2 itself.

A competition kinetics method was used to determine the rate constants for reactions of the amplicons with •OH, with *p*CBA as the reference competitor.[27, 28] The rate constant $k_{\bullet\text{OH, Amp}}$ for each amplicon was in turn calculated as $k_{\bullet\text{OH},p\text{CBA}} \ln(\frac{[\text{Amp}]_t}{[\text{Amp}]_0}) / \ln(\frac{[p\text{CBA}]_t}{[p\text{CBA}]_0})$, where $k_{\bullet\text{OH, }p\text{CBA}} = 5 \times 10^9\ \text{M}^{-1}\text{s}^{-1}$ (see Figure S2.15 for additional details).[29]

•OH exposures were calculated as $\int_0^t [\bullet\text{OH}]dt = -\frac{1}{k_{\bullet\text{OH, }p\text{CBA}}} \ln(\frac{[p\text{CBA}]_t}{[p\text{CBA}]_0})$. H_2O_2 concentrations were monitored during the experiments using Allen's reagent at λ = 350 nm,[6] and confirmed that overall consumption of H_2O_2 was minimal (< 10%) over the course of the experiments.

All of the experiments described above were performed at least in duplicate, at room temperature (20 ± 1 °C) (for FAC, NH_2Cl, ClO_2, O_3, and •OH), or 25 ± 1 °C (for UV). Unless otherwise indicated, results discussed in the main manuscript for eARG treatment were obtained at pH 8 for treatments with NH_2Cl and pH 7 for all other disinfectants, and at 1 mg/L DNA for all disinfectants, except for •OH at 10 mg/L DNA.

Text S2.9 Complex kinetics of reactions between DNA and FAC or NH_2Cl

As shown in Figures 2.1 and S2.3, the rates of qPCR amplicon degradation and transforming activity loss during reactions with FAC were observed to accelerate with time. Previously, Prütz also found the reaction between FAC and DNA to exhibit complex kinetics when monitoring the formation of an associated reaction product at λ = 290 nm.[30] Such kinetics likely reflect the fact that FAC can modify DNA nucleotides by a variety of mechanisms, as well as cause DNA denaturation, which can influence its susceptibility to FAC attack in subsequent reactions.

Several studies have shown that FAC reacts with exocyclic $–NH_2$ and heterocyclic –NH– groups on nucleotide bases to produce organochloramines, and that the reactivity of monomeric nucleotides toward FAC declines in the order of guanosine 5'-monophosphate (GMP) > thymidine 5'-monophosphate (TMP) >> cytidine 5'-monophosphate (CMP) > adenosine 5'-monophosphate (AMP) ($k_{FAC,GMP} = 2.1\times10^4\ M^{-1}s^{-1}$; $k_{FAC,TMP} = 4.3\times10^3\ M^{-1}s^{-1}$; $k_{FAC,CMP} = 66\ M^{-1}s^{-1}$; $k_{FAC,AMP} = 6.4\ M^{-1}s^{-1}$).[30-32] Studies also have shown FAC and organochloramines can halogenate nucleobases to form stable carbon-chlorine bonds,[33-36] and that the major halogenated products include 8-chloroguanine, 5-chloro-6-hydroxy-5-methyldihydro-2,4(1H,3H)-pyrimidinedione, 5-chlorocytosine, and 8-chloroadenine – resulting from halogenation of guanine, thymine, cytosine, and adenine, respectively.[33, 35, 37, 38]

Because a quenching reagent, in this study $Na_2S_2O_3$, was used to terminate reactions and quench excess amounts of FAC, the formation of organochloramines was artificially reversed prior to qPCR analysis (i.e., N-chlorinated nucleotides were reduced back to their parent nucleotides). While this means that measured amplicon damage does not directly reflect the presence of base-centered organochloramines, they likely play an important role in the rates of

irreversible damage observed here. Based on measured FAC-induced DNA denaturation rates, Prütz proposed that the formation of base-centered chloramines disrupts hydrogen-bonds and causes DNA to denature.[31] Prütz also found that FAC reacts with double-stranded DNA (dsDNA) ~10× slower than with single-stranded DNA (ssDNA) (where hydrogen bonds are already disrupted) by measuring the appearance of the associated reaction product at $\lambda = 290$ nm.[30] It was also confirmed in the present study – using heat-denatured DNA – that damage measured by qPCR occurs much faster for partially-denatured DNA than for dsDNA (Figure S2.4, where a rapid, initial drop in qPCR amplicon signal during chlorination of partially-denatured DNA is attributed to reaction of FAC with the fraction of partially-denatured DNA present as ssDNA, and subsequent slower loss of qPCR amplicon signal is attributed to reaction of FAC with the remaining fraction present as dsDNA). In accord with these observations, it is hypothesized here that damage monitored by qPCR occurs through a sequential, two-step process, in which an organochloramine (which can be reduced to the parent nucleobase by reaction with $Na_2S_2O_3$) initially forms and disrupts one or more hydrogen bonds, which in turn activates the unpaired bases associated with a disrupted H-bond toward irreversible halogenation by FAC (presumably to form a carbon-chlorine bond stable toward $Na_2S_2O_3$). Since the continual disruption of hydrogen bonds and activation of bases within an amplicon would accelerate its reactivity towards FAC, this theory is also in agreement with the complex kinetics observed in Figure S2.4.

The observed kinetics do not appear to be attributable to single electron transfer processes initiated by direct reactions of DNA with FAC (leading to either $Cl^{\bullet}$ or $^{\bullet}OH$), as the kinetics of qPCR amplicon loss during exposure to FAC were not influenced by the presence of the radical scavengers methanol (MeOH) or *t*-BuOH (Figure S2.5). Although MeOH or *t*-BuOH

addition may not have been sufficient to ensure scavenging of nitrogen-centered radicals derived from organochloramines species,[39, 40] significant contributions from N-centered radical species (which could be generated through thermal, photochemical, or chemical N-chloro bond homolysis) seem unlikely over the 5-10 minute timescales of the chlorination experiments undertaken here. These experiments were conducted at room temperature and excluded from light, and solutions were furthermore oxygenated and utilized only high-purity reagents, and should therefore also have been free of chemical initiators (e.g., reduced transition metals) of N-chloro bond homolysis. Furthermore, the observed first-order dependence of amplicon decay kinetics on FAC concentrations is also inconsistent with a process governed by N-chloramine decay kinetics.

A variety of additional experiments were undertaken to confirm the $Na_2S_2O_3$-reversible formation of organochloramine species during reaction of DNA with FAC. As shown in Figure S2.6a, after treatment of 90 mg/L calf thymus DNA (~291 μM in dNMPs) with 320 μM FAC for 25 min (to ensure reaction equilibrium was reached) the UV difference spectrum for a treated sample (normalized to the UV absorbance spectrum of untreated 90 mg/L calf thymus DNA) exhibited a build-up of absorbance at 234 nm and 305 nm (Abs_{234nm} and Abs_{305nm}), and bleaching of absorbance at 258 nm (Abs_{258nm}), consistent with changes reported by Prütz[31] under similar conditions (which he attributed to concurrent N-chlorination and denaturation of DNA). After dosing excess $Na_2S_2O_3$ to quench the reaction, a partial reversal of Abs_{305nm} build-up back to the untreated control condition (i.e., the "0" baseline in Figure S2.6a) was observed (Figure S2.6a), although changes of Abs_{258nm} and Abs_{234nm} were obscured by interference from background UV absorbance by $Na_2S_2O_3$ (and/or tetrathionate, $S_4O_6^{2-}$, formed in the reaction of $Na_2S_2O_3$ with FAC[41]) at these wavelengths. Efforts were made to remove the $Na_2S_2O_3$ (and $S_4O_6^{2-}$) using

dialysis membranes or size exclusion columns, but were unsuccessful due to incomplete DNA recovery. As a comparison to $Na_2S_2O_3$, Na_2SO_3 – another strong reductant with much lower UV absorbance at wavelengths below 260 nm – was also used to quench FAC-treated calf thymus DNA solutions. As shown in Figure S2.6a, after dosing excess Na_2SO_3 to quench the reaction, the build-up of Abs_{305nm} and bleaching of Abs_{258nm} due to N-chlorination/denaturation were diminished and the UV difference spectra partially reverted toward the "0" baseline (note that the reverse of the Abs_{234nm} build-up was still difficult to distinguish in this case, due to the background absorbance of Na_2SO_3 below 240 nm). Difference spectra obtained for FAC-treatment and subsequent $Na_2S_2O_3$-quenching of extracellular *B. subtilis* 1A189 DNA under the same conditions were consistent with those observed for calf thymus DNA (Figure S2.6b). Prütz has reported similar observations when reacting FAC-treated DNA or mononucleotides with other reduced sulfur compounds including glutathione and 3,3'-dithio-bis-propionic acid; also noting that reaction of FAC-treated DNA with glutathione yielded only partial (~50%) reversion to the initial absorbance spectrum obtained for untreated DNA.[30]

In comparison with Na_2SO_3 and $Na_2S_2O_3$, "softer" quenching reagents – including NH_4Cl, H_2O_2, $NaAsO_2$, and Tris-HCl – yielded negligible change in the difference spectrum of FAC-treated DNA (aside from a significant increase in absorbance at wavelengths below 230 nm for $NaAsO_2$, due to its background absorbance).

As posited by Prütz[30, 31], the preceding results are consistent with (i) absorbance changes during DNA chlorination due to N-chlorination (presumably of thymine and/or guanine groups) and concurrent denaturation of dsDNA, followed by (ii) a reduction of N-chlorinated functional groups (presumably N-chlorinated thymine and/or guanine) to yield their parent amines through

treatment with Na_2SO_3 or $Na_2S_2O_3$, but not with "softer" quenching reagents such as NH_4Cl, H_2O_2, $NaAsO_2$, and Tris-HCl.

The time profiles of the build-up of Abs_{234nm} and Abs_{305nm}, and the bleaching of Abs_{258nm}, during treatment of ~90 mg/L calf thymus DNA with 320 μM FAC correspond well with the time profile of dsDNA denaturation tracked using the Hoechst 33258 fluorescence assay (Figure S2.7c), as well as with the time profile of combined chlorine (i.e., organochloramine) formation tracked by DPD colorimetry (Figure S2.7a), consistent with concurrent N-chlorination and denaturation of dsDNA. The concurrence of these time profiles was also observed for similar experiments with FAC applied in incremental dosages (53 μM) every ~10 min to reach a total dosed concentration of 320 μM (Figure S2.7b, d). Here, the incremental dosage approach was utilized to examine the kinetics and stoichiometry of the DNA-FAC reaction as FAC concentration was increased from sub-stoichiometric [FAC] levels relative to total [dNMPs] (for 90 mg/L DNA ~ 291 μM [dNMPs]) to slightly above stoichiometric [FAC] levels (i.e., 320 μM FAC). Under these conditions ~1/3 of dosed FAC was converted to organochloramine (through N-chlorination), while the other 2/3 was apparently consumed through irreversible reactions no matter whether FAC or DNA was in excess at the beginning of experiments.

Kinetics of *blt* amplicon degradation observed when using Na_2SO_3 and $Na_2S_2O_3$ to quench FAC were in agreement with each other, but generally slower than those obtained with "softer" quenchers (Figure S2.8), indicating that more qPCR-detectable sites of reversible or irreversible damage remained in N-chlorinated DNA following exposure to the "softer" quenchers, likely due to their inabilities to reduce/revert N-chlorinated sites to their parent amines (consistent with their lack of effects on the difference spectra of FAC-treated DNA; Figure S2.8). Interestingly, if FAC-treated 1A189 DNA samples were treated with NH_4Cl- and

Tris-HCl and then allowed to react for an extended time prior to qPCR analyses (3 hours in this case), the ARG degradation profiles observed for these samples shifted toward to those obtained with Na_2SO_3 and $Na_2S_2O_3$, indicating that N-chlorinated sites *were* very slowly reduced by NH_4Cl and Tris-HCl and that they could ultimately be reverted to their parent amines after long-term storage (Figure S2.8a). These findings suggest that the use of "softer" quenchers to remove FAC residuals from FAC-treated samples could lead to the appearance of faster ARG degradation kinetics than would be observed following quenching with stronger reductants such as Na_2SO_3 or $Na_2S_2O_3$ if samples are analyzed without prior storage for extended periods. The former approach (using "softer" quenchers) likely enables detection of both reversible and irreversible damage sites, whereas the latter approach (utilizing Na_2SO_3 or $Na_2S_2O_3$, as in the present work) provides a more conservative measure of irreversible damage alone (which may more directly relate to conditions likely to be encountered during wastewater chlorination, where FAC-treated effluents would generally be dechlorinated by strong sulfur-based reductants such as bisulfite or metabisulfite prior to discharge).

All of the above observations support the hypothesis that chlorination of DNA proceeds through formation of N-chlorinated nucleotides (most likely from dGMP and/or TMP) with consequent denaturation of the double stranded helix, and that the N-chlorinated products (as identified by UV absorbance spectra and qPCR assays) can be reverted rapidly to their unchlorinated parent amine forms by strong reductants like Na_2SO_3 and $Na_2S_2O_3$, but not by "softer" quenchers, such as NH_4Cl, H_2O_2, $NaAsO_2$, Tris-HCl, and TMB.

In light of the above discussion, the kinetics of qPCR amplicon degradation by FAC were modeled by assuming that FAC attacks the DNA region encompassed by the amplicon of interest according to two separate and sequential steps: (i) N-chlorination of a nucleotide base (leading to

chloramine formation, H-bond disruption, and activation of a nucleotide base and its pairing partner toward irreversible halogenation), which can be reversed by $Na_2S_2O_3$, and (ii) irreversible C-chlorination of one or both of the resulting non-hydrogen-bonded bases, leading to qPCR signal loss due to blockage of amplification by the resulting chlorinated product(s). The N-chlorinated sites (and hence, non-hydrogen-bound bps) on the N-chlorinated amplicons are henceforth described as N-chlorinated base pairs (N-Cl bps).

The first step is treated as second-order overall – first-order in FAC and first-order in amplicon (Amp), as shown in eq S2.1:

$$\mathrm{Amp} + \mathrm{FAC} \underset{\mathrm{Na_2S_2O_3}}{\overset{k_{\mathrm{FAC,Amp}}}{\rightleftharpoons}} \mathrm{Amp_{N\text{-}Cl}} \tag{S2.1}$$

while the second step is also treated as second-order overall – first-order in FAC and first-order in N-chlorinated, activated amplicon ($Amp_{N\text{-}Cl}$), as shown in eq S2.2:

$$\mathrm{Amp_{N\text{-}Cl}} + \mathrm{FAC} \xrightarrow{k_{\mathrm{FAC,\,Amp_{N\text{-}Cl}}}} \mathrm{product} \tag{S2.2}$$

As time proceeds, the proportion of the initial amplicon concentration that has sustained at least one $Na_2S_2O_3$-reversible hit (equal to $[Amp_{N\text{-}Cl}]/[Amp]_0 = 1 - [Amp]/[Amp]_0$) increases according to eq S2.1. Furthermore, the cumulative number of N-chlorinated base pairs (# N-Cl bp) on each amplicon within the resulting population of N-chlorinated amplicons, $[Amp_{N\text{-}Cl}]$, also increases with the same kinetics (recognizing that each amplicon can sustain multiple reversible hits up to a maximum number equal to the length of the amplicon in base pairs (bps)). Since each N-chlorination can be expected to result in the disruption of one H-bond, one can in turn anticipate that the reactivity of each reversibly N-chlorinated amplicon toward irreversible C-chlorination, shown in eq S2.2, will actually increase with time, in proportion to the accumulation of N-Cl bps over the length of the amplicon, as each strand in the double-stranded DNA separates from its partner – rendering it more susceptible to reactions with FAC. Thus,

$k_{\text{FAC,Amp}_{\text{N-Cl}}}$ is actually a variable term proportional to the *extent* of N-chlorination of a given N-chlorinated amplicon. In accord with Pecson et al.,[42] if one assumes that the cumulative number of reversible hits (i.e., # N-Cl bp) sustained by each amplicon within a population of amplicons containing a defined number of bps follows a Poisson distribution, the average number of N-chlorinated bases pairs per N-chlorinated amplicon, $\frac{\text{\#N-Cl bp}}{\text{Amp}_{\text{N-Cl}}}$, within the population of N-chlorinated amplicons resulting from eq S2.1 can be calculated as follows:

$$\frac{\text{\#N-Cl bp}}{\text{Amp}_{\text{N-Cl}}} = -\ln\frac{[\text{Amp}]}{[\text{Amp}]_0} \tag{S2.3}$$

With this information, the rate at which the amplicon of interest sustains irreversible damage can be modeled according to eq S2.4,

$$\frac{d[\text{product}]}{dt} = k_{\text{FAC, Amp}_{\text{N-Cl}}}[\text{FAC}][\text{Amp}_{\text{N-Cl}}] = k_{\text{FAC, N-Cl bp}}\left(\frac{\text{\#N-Cl bp}}{\text{Amp}_{\text{N-Cl}}}\right)[\text{FAC}][\text{Amp}_{\text{N-Cl}}] \tag{S2.4}$$

where [product] represents the concentration of irreversibly damaged qPCR amplicons at a given time, $k_{\text{FAC, N-Cl bp}}$ represents the rate constant for reaction of FAC with a single N-chlorinated bp, which is in turn equal to $k_{\text{FAC, Amp}_{\text{N-Cl}}}$ divided by $\frac{\text{\#N-Cl bp}}{\text{Amp}_{\text{N-Cl}}}$ at a given time, and [$\text{Amp}_{\text{N-Cl}}$] and $\frac{\text{\#N-Cl bp}}{\text{Amp}_{\text{N-Cl}}}$ at a given time can be calculated according to eqs S1 and S3, respectively.

Because there are a finite number of bases in an individual amplicon that can be N-chlorinated, the value of $k_{\text{FAC, Amp}_{\text{N-Cl}}} = k_{\text{FAC, N-Cl bp}}\left(\frac{\text{\#N-Cl bp}}{\text{Amp}_{\text{N-Cl}}}\right)$ should reach a maximum when #N-Cl bp is equal to the total number of base pairs comprising that amplicon (or simply equal to the length of the amplicon in bps). At this condition, eq S2.2 should also become rate limiting, as no further N-chlorination can take place.

As shown in Figure S2.9a-e, the rate at which the 266 bp amplicon was damaged appeared to reach a maximum at extended reaction times during exposure to each of five different FAC concentrations ranging from 70 to 1120 μM. That is, the plots of $\ln([\text{Amp}]/[\text{Amp}]_0)$ versus time were characterized by constant slopes at extended reaction times. The maxima of these slopes were taken to correspond to the maximum values of the pseudo-first-order term $k_{\text{FAC, Amp}_{\text{N-Cl}}}[\text{FAC}] = k_{\text{FAC, N-Cl bp}}\left(\frac{\#\text{N-Cl bp}}{\text{Amp}_{\text{N-Cl}}}\right)[\text{FAC}]$ for amplicon loss in the presence of excess [FAC] at each condition (where [FAC] was confirmed to decrease by no more than 10% over the experimental times monitored). From these data, the value of the N-Cl bp-normalized second-order rate constant, $k_{\text{FAC, N-Cl bp}}$, which is assumed to be independent of amplicon length, was determined by plotting the measured maximum values of $k_{\text{FAC, Amp}_{\text{N-Cl}}}[\text{FAC}]$ (= k_{obs} in Figure S2.9) versus the corresponding FAC concentration at each condition, calculating the slope of the resulting plot by weighted, linear least-squares regression (Figure S2.9f), and dividing the calculated slope by the maximum value of $\frac{\#\text{N-Cl bp}}{\text{Amp}_{\text{N-Cl}}}$; that is, the length of the 266 bp amplicon in this case since the 266 bp amplicon is assumed to be completely N-chlorinated.

In the present work, a maximum value of $k_{\text{FAC, Amp}_{\text{N-Cl}}}$, or $k_{\text{FAC, N-Cl bp}}\left(\frac{\#\text{N-Cl bp}}{\text{Amp}_{\text{N-Cl}}}\right)$, only appeared to have been reached for the 266 bp amplicon, presumably because the qPCR LOD was reached before a maximum rate of loss for the 832 bp, 870 bp, or 1017 bp amplicons could be achieved. Although it is possible that $k_{\text{FAC, N-Cl bp}}$ – like $k_{\text{FAC, Amp}}$ – depends on bps or sequence motifs, the available dataset was not sufficiently large or variable with respect to amplicon sequence composition to permit evaluation of this. Consequently, the $k_{\text{FAC, N-Cl bp}}$ value determined

for the 266 bp amplicon (0.39 ± 0.02 $M^{-1}s^{-1}$) was assumed to represent an "average" value for N-chlorinated bps, and to be the same for all four amplicons. The values of $k_{FAC, Amp}$ (eq S2.1), which are dependent on amplicon length and nucleotide content (as discussed below and also in the main text), were in turn determined for each amplicon by implementing a stepwise numerical analysis of the reaction system comprising eqs S1-S4, fixing $k_{FAC, N\text{-}Cl\ bp}$, and performing non-linear, least-squares regressions of [Amp] versus time against the data shown in Figure S2.3, with $k_{FAC, Amp}$ as the master variable (model fits are depicted as lines in Figure S2.3). The uncertainty in $k_{FAC, Amp}$ was determined by solving for $k_{FAC, Amp}$ with $k_{FAC, N\text{-}Cl\ bp}$ fixed at the values corresponding to its minimum and maximum error bounds. The resulting values of $k_{FAC, Amp}$ were 3.9(±0.3)×10^3, 8.5(±0.5)×10^3, 8.1(±0.5)×10^3, and 9.2(±0.5)×10^3 $M^{-1}s^{-1}$ for the 266 bp, 832 bp, 870 bp, and 1017 bp amplicons, respectively.

Similar to FAC, NH_2Cl also exhibited accelerating kinetics in degrading each of the four qPCR amplicons, as shown in Figure S2.10. Because [NH_2Cl] was found to decay by more than 10% over the duration of the experimental periods (and so cannot be assumed as constant at [NH_2Cl]$_0$), normalized copy numbers were plotted versus the corresponding cumulative CT_{NH2Cl} value at each sampling interval, rather than versus time. In light of these trends, a two-step reaction sequence equivalent to that observed for FAC was also hypothesized to apply to NH_2Cl. Since NH_2Cl is itself generally a very weak oxidant and halogenating agent, a question may be raised as to whether the chlorination of DNA bases in the NH_2Cl system is driven directly by NH_2Cl itself or by low concentrations of FAC in equilibrium with NH_2Cl and NH_3, as per eq S2.5.

$$NH_3 + HOCl \underset{}{\overset{K_{hydrolysis}=1.5\times10^{11}\ M^{-1}}{\rightleftharpoons}} NH_2Cl + H_2O \qquad (S2.5)$$

To explore this question, one can assume that if FAC is the primary driver of DNA damage in the NH_2Cl system, the profile of amplicon degradation (for a certain amplicon) versus *CT* for the equilibrium level of FAC present (CT_{FACeq}) in the NH_2Cl system should match the profile of qPCR degradation (for the same amplicon) versus CT_{FAC} for treatment with FAC itself. In this case, $[FAC_{eq}]$ of the NH_2Cl system can be estimated from the measured $[NH_2Cl]$ according to eq S2.5, whereas [FAC] of the real FAC system can simply be considered as constant at an initial value $[FAC]_0$. By comparing the profiles of amplicon degradation versus CT_{FACeq} (for NH_2Cl treatment) and CT_{FAC} (for FAC treatment), it was clear that at values of $CT_{FACeq} = CT_{FAC}$, amplicon degradation in the NH_2Cl system (i.e., the former profile) was much greater than expected on the basis of reaction with FAC_{eq} alone (i.e., the latter profile) (data not shown), supporting a reaction sequence involving direct amplicon degradation by NH_2Cl. Such a sequence presumably involves direct transfer of chlorine from NH_2Cl to heterocyclic –NH– groups or exocyclic $–NH_2$ groups of the nucleotides in the first step, and to nucleotide carbons in the second step.

In analogy to FAC, the two sequential reactions for NH_2Cl are expressed as in eqs S2.6 and S2.7, respectively. Accordingly, the rate of irreversible damage to a given amplicon (and loss of qPCR signal) can be represented by eq S2.8.

$$\mathrm{Amp} + \mathrm{NH_2Cl} \underset{\mathrm{Na_2S_2O_3}}{\overset{k_{\mathrm{NH_2Cl,\,Amp}}}{\rightleftharpoons}} \mathrm{Amp_{N\text{-}Cl}} \tag{S2.6}$$

$$\mathrm{Amp_{N\text{-}Cl}} + \mathrm{NH_2Cl} \xrightarrow{k_{\mathrm{NH_2Cl,\,Amp_{N\text{-}Cl}}}} \text{product} \tag{S2.7}$$

$$\frac{d[\text{product}]}{dt} = k_{\mathrm{NH_2Cl,\,N\text{-}Cl\ bp}} \left(\frac{\#\text{N-Cl bp}}{\mathrm{Amp_{N\text{-}Cl}}} \right) [\mathrm{NH_2Cl}][\mathrm{Amp_{N\text{-}Cl}}] \tag{S2.8}$$

where, as for FAC, $k_{NH_2Cl,\ N\text{-}Cl\ bp}$ represents the maximum value of $k_{NH_2Cl,\ Amp_{N\text{-}Cl}}$ normalized to the length of the amplicon in bps, and [$Amp_{N\text{-}Cl}$] and $\frac{\#N\text{-}Cl\ bp}{Amp_{N\text{-}Cl}}$ can be calculated at a given time according to eqs S6 and S3, respectively.

A similar approach as applied for FAC was utilized here to determine the rate constants for each step. Since, as for FAC, only the 266 bp amplicon was observed to reach the maximum degradation rate during exposure to NH_2Cl, the "average" length-independent second-order rate constant, $k_{NH_2Cl,\ N\text{-}Cl\ bp}$, for N-chlorinated bps was obtained by linear least-squares regression of the 266 bp amplicon data over its range of maximum slope (Figure S2.11) to determine $k_{NH_2Cl,\ Amp_{N\text{-}Cl}}$, and dividing $k_{NH_2Cl,\ Amp_{N\text{-}Cl}}$ by the length of 266 bp. The values of $k_{NH_2Cl,\ Amp}$ (eq S2.6) were in turn determined for each amplicon by implementing a stepwise numerical analysis of the reaction system comprising equations S3 and S6-S8, fixing $k_{NH_2Cl,\ N\text{-}Cl\ bp}$, and performing non-linear, least-squares regressions of [Amp] versus CT_{NH2Cl} for the data shown in Figure S2.10, with $k_{NH_2Cl,\ Amp}$ as the master variable (model fits are depicted as lines in Figure S2.10). Then the uncertainty of $k_{NH_2Cl,\ Amp}$ was calculated by solving for $k_{NH_2Cl,\ Amp}$ with $k_{NH_2Cl,\ N\text{-}Cl\ bp}$ fixed at the values corresponding to its minimum and maximum error bounds. Note that each linear and non-linear regression of the NH_2Cl data was undertaken by pooling the three datasets obtained for various values of $[NH_2Cl]_0$ (i.e., 300 μM, 580 μM and 880 μM), which were all normalized to CT_{NH2Cl}. The resulting values and uncertainties of $k_{NH_2Cl,\ N\text{-}Cl\ bp}$ and $k_{NH_2Cl,\ Amp}$ are summarized in Table 2.1.

Text S2.10 Calculation of theoretical diffusion-controlled rate constant for the reaction of hydroxyl radical (•OH) with extracellular DNA

The DNA isolated using the extraction procedures described in Text S2.2 was found to be present mainly in linear form with a size of ~40-60 kbp, based on PFGE analyses (see the untreated samples at exposure values of 0 mg/L•min or mJ/cm^2 in Figure S2.18). Robertson et al. (2006) reported the radii of gyration ($R_{G,L}$) and diffusion coefficients (D_L) for a series of linear DNA molecules with varying sizes ranging from 5.9 to 287.1 kbp.[43] By analyzing their data, linear correlations were developed here between $R_{G,L}$ (in μm) and the size of linear-form DNA molecules (*Size*, in kbp) (eq S2.9), and between log-scale diffusion coefficient (logD_L, with D_L in μm^2/s) and log-scale size of linear-form DNA molecules (log*Size*) (eq S2.10).

$$R_{G,L} = 0.00608 \cdot Size + 0.263 \quad (R^2 = 0.99;\ 5.9\ \text{kbp} \le Size \le 287.1\ \text{kbp}) \tag{S2.9}$$

$$\log D_L = -0.568 \cdot \log Size + 0.568 \quad (R^2 > 0.99;\ 5.9\ \text{kbp} \le Size \le 287.1\ \text{kbp}) \tag{S2.10}$$

Assuming the size of a linear molecule of the extracted *B. subtilis* 1A189 DNA investigated here is 50 kbp on average, then its $R_{G,L}$ and D_L can be calculated based on eqs S9 and S10 as 0.568 μm and 0.401 μm^2/s (i.e., 5.68×10^{-5} cm and 4.01×10^{-9} cm^2/s), respectively. Then the hydrodynamic radius ($R_{H,L}$, in cm) for the 50-kbp linear DNA molecule can be determined as 3.76×10^{-5} cm, assuming a constant ratio of $R_{G,L}/R_{H,L}$ (= 1.508) predicted for linear polymers by the Zimm model.[44] The diffusion coefficient of •OH, $D_{\cdot OH}$, has been reported as 2.80×10^{-5} cm^2/s,[45] and – assuming it behaves as a hard sphere – its hydrodynamic radius, $R_{\cdot OH}$, can be calculated as 7.66×10^{-9} cm via the Stokes-Einstein equation[46] (eq S2.11),

$$D_{\cdot OH} = \frac{RT}{6\pi N_{AV}\mu} \cdot \frac{1}{R_{\cdot OH}} \tag{S2.11}$$

where N_{AV} is Avogadro's number, 6.02×10^{23} mol^{-1}, R is the universal gas constant, 8.314 J/(mol·K), T is absolute temperature 20 °C (i.e., 293.15 K), and μ is the solution viscosity, 1.00×10^{-2} g/(cm·s) at 20 °C.

By substituting the above hydrodynamic radii and diffusion coefficients of the 50-kbp linear DNA molecule and •OH into the Smoluchowski equation (eq S2.12),[46]

$$k_{max} = \frac{4\pi}{1000} N_{AV}(R_{H,L} + R_{\cdot OH})(D_L + D_{\cdot OH}) \quad \text{(S2.12)}$$

a diffusion-controlled rate constant (k_{max}) of 7.97×10^{12} $M^{-1}s^{-1}$ can be predicted, which yields a bp-specific value of 1.59×10^{8} $(M\ AT+GC)^{-1}s^{-1}$ when normalized to the length (in AT+GC bps) of the 50-kbp DNA segment. When the preceding bp-specific rate constant is multiplied by the lengths of each of the four qPCR amplicons included in the present study, this approach yields theoretical diffusion-controlled rate constants, k_{max}, of 4.2×10^{10}, 1.3×10^{11}, 1.4×10^{11}, and 1.6×10^{11} $M^{-1}s^{-1}$ for extracellular reactions of •OH with the 266 bp, 832 bp, 870 bp and 1017 bp amplicons, respectively, which agree well with the magnitudes of the measured values listed in Table 2.1.

For comparison, a similar approach was used here to estimate k_{max} for the reaction of •OH with the extracellular pUC4K plasmid utilized in the study of Yoon et al. (2017).[47] Unlike the linear-form genomic DNA extracted from *B. subtilis* 1A189 here, pUC4K plasmids extracted from *Escherichia coli* are primarily in a supercoiled form.[47] Prazeres (2008) has summarized the radii of gyration and diffusion coefficients of supercoiled-form plasmids (here designated as $R_{G,S}$ and D_S, to distinguish from $R_{G,L}$ and D_L for linear-form DNA as noted above, respectively), with varying sizes reported by different investigators.[48] By analyzing their summarized data, it has been determined here that $R_{G,S}$ (in μm) is linearly correlated with the DNA size (again expressed as *Size*, in kbp) for 1.9-6.5 kbp supercoiled plasmids (eq S2.13), and that logD_S (with D_S in $\mu m^2/s$) is linearly correlated with log*Size* for 1.9-287.1 kbp supercoiled plasmids (eq S2.14).

$$R_{G,S} = 0.0115 \cdot Size + 0.0275 \quad (R^2 = 0.89;\ 1.9\ \text{kbp} \le Size \le 6.5\ \text{kbp}) \tag{S2.13}$$

$$\log D_S = -0.663 \cdot \log Size + 0.988 \quad (R^2 > 0.99;\ 1.9\ \text{kbp} \le Size \le 287.1\ \text{kbp}) \tag{S2.14}$$

By substituting the size of the pUC4K plasmid (3.9 kbp) into the above equations, the $R_{G,S}$ and D_S can be calculated as 0.0723 μm and 3.93 $\mu m^2/s$ (i.e., 7.23×10^{-6} cm and 3.93×10^{-8} cm^2/s), respectively. Then the hydrodynamic radius of the pUC4K plasmid (designated as $R_{H,S}$ to distinguish from $R_{H,L}$) can be determined as 2.23×10^{-6} cm, assuming a ratio of $R_{G,S}/R_{H,S}$ (= 1.8^2 = 3.24) measured for a 7-kbp plasmid in TE buffer by Ke et al. (2010).[49] By substituting $R_{H,S}$ and D_S of the pUC4K plasmid and $R_{\cdot OH}$ and $D_{\cdot OH}$ of $^{\bullet}$OH into eq S2.12, the k_{max} for pUC4K plasmid reacting with $^{\bullet}$OH can be calculated as 4.73×10^{11} $M^{-1}s^{-1}$. By normalizing for the length of the pUC4K plasmid (3914 bp) and multiplying by the lengths of the *kan*^{R} 806 bp and *amp*^{R} 850 bp amplicons studied by Yoon et al. (2017),[47] k_{max} values of 9.75×10^{10} $M^{-1}s^{-1}$ and 1.03×10^{11} $M^{-1}s^{-1}$ can be calculated for extracellular reactions of $^{\bullet}$OH with the *kan*^{R} 806 bp and *amp*^{R} 850 bp amplicons, respectively. These values differ by a factor of ~5 from the approximate value of 2×10^{10} $M^{-1}s^{-1}$ estimated by Yoon et al. (2017),[47] which is reasonably close, considering model and experimental uncertainties.

Text S2.11 Possible interpretations of the residual intercepts ($k_{Disinfectant,0}$) yielded by linear regressions of $k_{Disinfectant,Amp}$ versus amplicon nucleotide content for each disinfectant

In the event that linear regressions of $k_{Disinfectant,Amp}$ according to eq 2.9 in the main text account for all DNA constituents that contribute significantly to the reactivity of a given amplicon, they should yield values of $k_{Disinfectant,0}$ that are close to zero (or small enough relative to the magnitudes of $k_{Disinfectant,Amp}$ that they can be neglected), as appears to be the case for ClO_2,

UV, O_3, and $^{\bullet}OH$ (Figure 2.2c-f and Table 2.1; note that the standard error for $k_{O_3,0}$ is relatively large). Put another way, the reactivity of a hypothetical segment of DNA containing none of the putative "reactive" constituents included in the regression should be effectively zero in such a case (i.e., $k_{Disinfectant,Amp}$ should be zero at an x-axis value of zero in Figure 2.2). However, as apparent from Figure 2.2a,b and Table 2.1, the linear regressions of rate constants, $k_{Disinfectant,Amp}$, versus specific amplicon nucleotide content for FAC and NH_2Cl each yield relatively large, positive intercepts, $k_{Disinfectant,0}$. Comparison with the much smaller values of $k_{Disinfectant,0}$ obtained from linear regressions for ClO_2, UV, O_3, and $^{\bullet}OH$ suggests that the values of $k_{Disinfectant,0}$ for FAC and NH_2Cl are not likely attributable to experimental or regression errors alone.

Although the reasons for the relatively high magnitudes of $k_{Disinfectant,0}$ for FAC and NH_2Cl are currently uncertain, it is possible that they may arise at least in part from reactivities of specific sequence elements (e.g., nucleotide singlets, doublets, triplets, etc.), that are not accounted for in the relatively simple one-parameter linear regression model applied here (eq 2.9), which accounts for only one sequence descriptor at a time – that being total AT+GC bps (amplicon length) in the case of FAC and NH_2Cl.

Another possible explanation for the non-zero $k_{Disinfectant,0}$ values is that they indicate that reactions for a particular disinfectant involve not only a specific nucleotide (or nucleotides), but specific nucleotide sequences. For example, the strong correlation of $k_{FAC,Amp}$ with AT+GC content indicates that $k_{FAC,Amp}$ is proportional to the number of dGMPs (Gs) and TMPs (Ts) within a strand of DNA. However, it is possible that reactivity might not depend simply on number of Gs and Ts in a given DNA segment, but on the relative molar contents of specific sequences incorporating G or T, such as isolated (non-contiguous) guanine or thymine singlets,

doublets, triplets, and quadruplets (or combinations thereof), considering that G and T multiplets are known to exhibit varying susceptibilities to oxidative attack compared to G and T singlets.[50-54] NH_2Cl might exhibit similar dependencies on recurring sequences of G and/or T multiplets that are likewise not captured by the single-parameter regression of $k_{NH_2Cl,Amp}$ vs. AT+GC bps according to eq 2.9. This possibility seems to be supported by the particularly strong correlations observed for $k_{FAC,Amp}$ and $k_{NH_2Cl,Amp}$ versus 5'-GT-3' and 5'-AG-3', respectively.

Confirmation of either of the above hypotheses would require the application of more robust, multi-parameter linear regressions incorporating the contents of multiple interstrand bps, intrastrand doublets, and/or other sequence elements. Although this approach is currently not feasible due to the limited number of amplicons investigated in the current work, it is highly recommended that future work addresses this topic if and when kinetics data becomes available for a wider array of DNA amplicons.

Text S2.12 Dependence of $k_{UV,Amp}$ on 5'-bipyrimidine-3' doublet contents

Yoon et al. (2018) recently employed a theoretical approach to estimate amplicon photoreactivities based on previously reported molar extinction coefficients, quantum yields, and knowledge of the specific content of various 5'-bipyrimidine-3' doublets for a given amplicon.[55] A similar approach was used here to evaluate the dependence of the 266-1017 bp amplicons' photoreactivities on their 5'-bipyrimidine-3' contents. According to this approach, the theoretical overall rate constant, $k_{all\ lesions,f}$ (in cm^2/mJ), for degradation of a given amplicon by UV (due to lesion formation at 5'-bipyrimidine-3' doublets) can be calculated as

$$k_{all\ lesions,f} = \sum_{bipyrimidine = TT, TC, CT, CC} (2.303 \varepsilon_{254,\ 5'\text{-bipyrimidine-}3'} \Phi_{254,\ 5'\text{-bipyrimidine-}3'} / U_{254}) (\#_{5'\text{-bipyrimidine-}3'}) \quad \text{(S2.15)}$$

where, for each type of 5'-bipyrimidine-3' doublet (with bipyrimidine = TT, TC, CT, or CC), $f_{254,\ 5'\text{-bipyrimidine-}3'}$ is the quantum yield (in mol/einstein) for *overall lesion formation* at 254 nm – including cyclobutane pyrimidine dimers (CPDs) and (6-4) photoproducts ((6-4)PPs) (determined as described below), $\varepsilon_{254,\ 5'\text{-bipyrimidine-}3'}$ is the molar extinction coefficient (in $M^{-1}cm^{-1}$) at 254 nm (also determined as described below), and $\#_{5'\text{-bipyrimidine-}3'}$ is the number of 5'-bipyrimidine-3' doublets in the amplicon. U_{254} (= 4.72×10^5 J/Einstein) is the molar photon energy at 254 nm (as specified above in Text S2.8).[17]

For each 5'-bipyrimidine-3' doublet, quantum yields of various photoproducts, including *cis,syn* CPDs, *trans,syn* CPDs, and (6–4)PPs, were based on the data set reported by Douki (2006)[56] for irradiation of 50 mg/L calf thymus DNA by 254 nm UV light in the presence of 0.02 M NaCl at 30°C (close to the ionic strength and temperature used here). The quantum yield for *overall lesion formation*, $f_{254,\ 5'\text{-bipyrimidine-}3'}$, at a certain 5'-bipyrimidine-3' doublet was obtained by summing the specific quantum yields for *cis,syn* CPDs, *trans,syn* CPDs, and (6–4)PPs.

It is important to note that in Douki (2006),[56] quantum yields were reported with respect to overall photon absorbance by all DNA nucleotides (here designated as $f^{\text{nucleotides}}_{254,\ 5'\text{-bipyrimidine-}3'}$), rather than with respect to photon absorbance by the 5'-bipyrimidine-3' doublets specifically.[56] In order to re-express these values in terms of 254 nm photon absorbance by each type of 5'-bipyrimidine-3' doublet, one can consider the general expressions in eqs S16a and S16b,[24] for the rate of lesion formation from a specific type of 5'-bipyrimidine-3' doublet during monochromatic 254 nm irradiation of a solution of DNA with volume, V (in cm^3) and irradiated surface area, A (in cm^2) – expressed either with respect to photon absorbance by all DNA nucleotides (eq S2.16a) or by the specified type of 5'-bipyrimidine-3' doublet (eq S2.16b).

$$\frac{d\left[\text{lesions}\right]_{\text{5'-bipyrimidine-3'}}}{dt} = f^{\text{nucleotides}}_{\text{254, 5'-bipyrimidine-3'}}\left(\frac{I}{\text{U}_{254}}\right)\left(\frac{\text{A}}{\text{V}}\right)F_{254,\,S}F_{\text{254, nucleotides}} \quad \text{(S2.16a)}$$

(with respect to photon absorbance by all DNA nucleotides)

$$\frac{d\left[\text{lesions}\right]_{\text{5'-bipyrimidine-3'}}}{dt} = f_{\text{254, 5'-bipyrimidine-3'}}\left(\frac{I}{\text{U}_{254}}\right)\left(\frac{\text{A}}{\text{V}}\right)F_{254,\,S}F_{\text{254, 5'-bipyrimidine-3'}} \quad \text{(S2.16b)}$$

(with respect to photon absorbance by 5'-bipyrimidine-3' doublets of the specified type)

In eqs S16a and S16b, $f^{\text{nucleotides}}_{\text{254, 5'-bipyrimidine-3'}}$, $f_{\text{254, 5'-bipyrimidine-3'}}$, and I are as defined above (see Text S2.8 for discussion of the fluence rate, I), and $F_{254,S}$ (= $1 - 10^{-\text{Abs}_{254\text{nm},\,S}}$) represents the overall fraction of light passing through the irradiated solution that is absorbed by solution constituents, with $\text{Abs}_{254\text{nm},S}$ representing the overall solution absorbance. Assuming that DNA is the only UV-absorbing constituent of the irradiated solution, $\text{Abs}_{254\text{nm},S}$ can be approximated as $\text{Abs}_{254\text{nm,nucleotides}} = \varepsilon_{254,\text{nucleotides}} C_{\text{nucleotides}} l$. For the experimental system utilized by Douki et al. in determining $f^{\text{nucleotides}}_{\text{254, 5'-bipyrimidine-3'}}$ values,[56, 57] $C_{\text{nucleotides}}$ = 50 mg/L (= 1.6×10^{-4} M) and the pathlength, l = 1 cm. Thus, for $\varepsilon_{254,\text{nucleotides}} = 7.59\times10^{3}$ $\text{M}^{-1}\text{cm}^{-1}$ (determined as described below), the value of $\text{Abs}_{254\text{nm,nucleotides}}$ can be calculated as 1.2, yielding a value of $F_{254,S}$ = 0.94, which can in turn be approximated as ~1 for purposes of simplifying the determination of $f_{\text{254, 5'-bipyrimidine-3'}}$ from $f^{\text{nucleotides}}_{\text{254, 5'-bipyrimidine-3'}}$.

$F_{254,\text{nucleotides}}$ and $F_{254,\text{5'-bipyrimidine-3'}}$ in eqs S16a and S16b represent the respective fractions of light absorbed during passage through the irradiated DNA solution that are absorbed by DNA nucleotides in general or by the specified type of 5'-bipyrimidine-3' doublet. These values can in turn be expressed as $\frac{\text{Abs}_{254\text{nm, nucleotides}}}{\text{Abs}_{254\text{nm},\,S}}$ and $\frac{\text{Abs}_{254\text{nm, 5'-bipyrimidine-3'}}}{\text{Abs}_{254\text{nm},\,S}}$, respectively, where

$Abs_{254nm,nucleotides}$ and $Abs_{254nm,5'\text{-bipyrimidine-}3'}$ represent absorbances attributable to all DNA nucleotides or to the specified type of 5'-bipyrimidine-3' doublet. Again, assuming DNA is the only UV-absorbing constituent of the irradiated solution, $Abs_{254nm,S} \sim Abs_{254nm,nucleotides}$, so that

$$F_{254,\ \text{nucleotides}} = \frac{\text{Abs}_{254\text{nm},\ \text{nucleotides}}}{\text{Abs}_{254\text{nm},\ S}} \sim \frac{\text{Abs}_{254\text{nm},\ \text{nucleotides}}}{\text{Abs}_{254\text{nm},\ \text{nucleotides}}} = 1.$$

Furthermore, since $Abs_{254nm,nucleotides} = \varepsilon_{254,nucleotides} C_{nucleotides} l$

and

$Abs_{254nm,5'\text{-bipyrimidine-}3'} = \varepsilon_{254,\ 5'\text{-bipyrimidine-}3'} C_{5'\text{-bipyrimidine-}3'} l$,

it follows that

$$F_{254,\ 5'\text{-pyrimidine-}3'} = \frac{\text{Abs}_{254\text{nm},\ 5'\text{-bipyrimidine-}3'}}{\text{Abs}_{254\text{nm},\ S}} = \frac{\varepsilon_{254,\ 5'\text{-bipyrimidine-}3'} C_{5'\text{-bipyrimidine-}3'} l}{\varepsilon_{254,\ \text{nucleotides}} C_{\text{nucleotides}} l} = \frac{\varepsilon_{254,\ 5'\text{-bipyrimidine-}3'}}{\varepsilon_{254,\ \text{nucleotides}}} f_{5'\text{-bipyrimidine-}3'},$$

where $\varepsilon_{254,nucleotides}$ and $\varepsilon_{254,\ 5'\text{-bipyrimidine-}3'}$ are the average molar extinction coefficient for all nucleotides and the molar extinction coefficient for the specified 5'-bipyrimidine-3' doublet (determined as described below), respectively, and $f_{5'\text{-bipyrimidine-}3}$ is the fractional molar content of 5'-bipyrimidine-3' doublets relative to all nucleotides in the irradiated DNA. The value of $f_{254,\ 5'\text{-bipyrimidine-}3'}$ can in turn be obtained from $f^{\text{nucleotides}}_{254,\ 5'\text{-bipyrimidine-}3'}$ by equating, simplifying, and rearranging the expressions in eqs S2.16a and S2.16b to yield eq S2.17.

$$f_{254,\ 5'\text{-bipyrimidine-}3'} = \frac{f^{\text{nucleotides}}_{254,\ 5'\text{-bipyrimidine-}3'}}{F_{254,\ 5'\text{-bipyrimidine-}3'}} = f^{\text{nucleotides}}_{254,\ 5'\text{-bipyrimidine-}3'} \left(\frac{\varepsilon_{254,\ 5'\text{-bipyrimidine-}3'}}{\varepsilon_{254,\ \text{nucleotides}}} f_{5'\text{-bipyrimidine-}3'} \right)^{-1} \qquad \text{(S2.17)}$$

The ratio $\frac{\varepsilon_{254,\ 5'\text{-bipyrimidine-}3'}}{\varepsilon_{254,\ \text{nucleotides}}} f_{5'\text{-bipyrimidine-}3'}$, was determined based on the nearest-neighbor model developed by Tataurov et al. (2008)[58] as,

$$\frac{\varepsilon_{254,\ 5'\text{-bipyrimidine-}3'}}{\varepsilon_{254,\ \text{nucleotides}}} f_{5'\text{-bipyrimidine-}3'} = \frac{(1-h_{5'\text{-bipyrimidine-}3'})(\varepsilon_{260,\ 5'\text{-bipyrimidine-}3'} R_{254/260,\ 5'\text{-bipyrimidine-}3'})}{(1-h_{\text{DNA}}) \sum_{i,j\ =\ \text{A, T, G, C}} (\varepsilon_{260,\ 5'\text{-}ij\text{-}3'} f_{5'\text{-}ij\text{-}3'}) \sum_{i,j\ =\ \text{A, T, G, C}} (R_{254/260,\ 5'\text{-}ij\text{-}3'} f_{5'\text{-}ij\text{-}3'})} f_{5'\text{-bipyrimidine-}3'} \quad \text{(S2.18)}$$

where $\varepsilon_{260,\ 5'\text{-}ij\text{-}3'}$ is the extinction coefficient (in $M^{-1}cm^{-1}$) at 260 nm for each type of nucleotide doublet 5'-*ij*-3' within the DNA duplex (with *i* and *j* = A, T, G, or C), $R_{254/260,\ 5'\text{-}ij\text{-}3'}$ is the ratio of absorbance at 254 nm over that at 260 nm for 5'-*ij*-3' within the DNA duplex, $f_{5'\text{-}ij\text{-}3'}$ is the fractional content (in mol *ij* per mol nucleotides) of 5'-*ij*-3' (including $f_{5'\text{-bipyrimidine-}3'}$ for 5'-bipyrimidine-3') appearing in the two complementary strands of the DNA molecule(s), and h_{DNA} and $h_{5'\text{-bipyrimidine-}3'}$ are the hypochromicities for duplex DNA and duplex 5'-bipyrimidine-3' doublets, respectively. Values of $\varepsilon_{260,\ 5'\text{-}ij\text{-}3'}$ and $R_{254/260,\ 5'\text{-}ij\text{-}3'}$ for all types of 5'-*ij*-3' doublets are available in Tataurov et al. (2008),[58] including those for 5'-bipyrimidine-3' doublets (i.e., $\varepsilon_{260,\ 5'\text{-bipyrimidine-}3'}$ and $R_{254/260,\ 5'\text{-bipyrimidine-}3'}$). $f_{5'\text{-}ij\text{-}3'}$ was determined by analyzing the whole genome of *Bos taurus* breed Hereford, including 30 pairs of chromosomes (sequences available in GenBank), as an approximation of the calf thymus DNA used in Douki (2006).[56] h_{DNA} is dependent on the fraction of AT and GC bps, according to the relationship $h_{\text{DNA}} = 0.287 f_{\text{AT}} + 0.059 f_{\text{GC}}$,[58] and was determined as 0.192, whereas respective $h_{5'\text{-bipyrimidine-}3'}$ values for 5'-TT -3', 5'-TC -3', 5'-CT -3', and 5'-CC -3' were determined from the same relationship as 0.287, 0.173, 0.173, and 0.059 (assuming duplex pairing of each doublet with its corresponding complement). The average extinction coefficient for all nucleotides, $\varepsilon_{254,\ \text{nucleotides}}$, was calculated as 7.59×10^3 $M^{-1}cm^{-1}$, and extinction coefficients for each type of 5'-bipyrimidine-3' doublet, $\varepsilon_{254,\ 5'\text{-bipyrimidine-}3'}$ (accounting for the hypochromism effect), were calculated as

5.36×10^3, 6.16×10^3, 6.32×10^3, and 7.19×10^3 $M^{-1}cm^{-1}$ for 5'-TT -3', 5'-TC -3', 5'-CT -3', and 5'-CC -3', respectively.

Quantum yields for *overall lesion formation*, $f_{254,\ 5'\text{-bipyrimidine-}3'}$, were in turn obtained via eq S2.17, by dividing the values of $f^{\text{nucleotides}}_{254,\ 5'\text{-bipyrimidine-}3'}$ from Douki (2006)[56] by $\frac{e_{254,\ 5'\text{-bipyrimidine-}3'}}{e_{254,\ \text{nucleotides}}} f_{5'\text{-bipyrimidine-}3'}$, yielding 0.0096, 0.0102, 0.0017, and 0.0005 for 5'-TT -3', 5'-TC -3', 5'-CT -3', and 5'-CC -3', respectively.

These values of $f_{254,\ 5'\text{-bipyrimidine-}3'}$ were then used to obtain respective values of $e_{254,\ 5'\text{-bipyrimidine-}3'} f_{254,\ 5'\text{-bipyrimidine-}3'}$ = 52, 63, 11, and 3.3 for 5'-TT -3', 5'-TC -3', 5'-CT -3', and 5'-CC -3'. Theoretical values of $k_{\text{all lesions},\ f}$ were then determined for the investigated amplicons by substituting $e_{254,\ 5'\text{-bipyrimidine-}3'} f_{254,\ 5'\text{-bipyrimidine-}3'}$, U_{254}, and the $\#_{5'\text{-bipyrimidine-}3'}$ values summarized in Table S2.1 into eq S2.15, and plotted versus measured values of $k_{\text{UV,Amp}}$ (Figure S2.16a). As shown in Figure S2.16a, the theoretical values of $k_{\text{all lesions},\ f}$ are higher than, but still close to (~1.1-1.6×) the measured values of $k_{\text{UV,\ Amp}}$ for each amplicon, suggesting that it may be possible to predict values of $k_{\text{UV,\ Amp}}$ for various amplicons using the approach described above, as long as amplicon doublet contents are known.

From eq S2.15, it also follows that the relative contribution of each type of 5'-bipyrimidine-3' doublet to the magnitude of $k_{\text{all lesions},\ f}$ can be expressed by eq S2.19.

$$\frac{k_{5'\text{-bipyrimidine-}3',\ f}}{k_{\text{all lesions},\ f}} = \frac{(e_{254,\ 5'\text{-bipyrimidine-}3'} f_{254,\ 5'\text{-bipyrimidine-}3'})(\#_{5'\text{-bipyrimidine-}3'})}{\sum_{\substack{\text{bipyrimidine} \\ = \text{TT, TC, CT, CC}}} (e_{254,\ 5'\text{-bipyrimidine-}3'} f_{254,\ 5'\text{-bipyrimidine-}3'})(\#_{5'\text{-bipyrimidine-}3'})} \qquad \text{(S2.19)}$$

where $k_{\text{5'-bipyrimidine-3'},f}$ is the theoretical rate constant for lesion formation from each type of 5'-bipyrimidine-3' doublet. Based on eq S2.19, lesions formed from 5'-TT-3', 5'-TC-3', 5'-CT-3', and 5'-CC-3' are predicted to account for ~58-61%, ~33-35%, ~5-6%, and ~1-3% of the overall value of $k_{\text{all lesions},f}$, respectively, for the 266-1017 bp amplicons investigated here, with TT-CPDs by far the dominant type of lesion – accounting for 56-59% of total lesion formation. This is consistent with the strong correlations of measured $k_{\text{UV, Amp}}$ values versus 5'-TT-3' content (Figure 2e), and suggests that reasonable theoretical estimates of $k_{\text{UV, Amp}}$ may also be obtained from 5'-TT-3' content alone for amplicons in which photoreactivity is dominated by 5'-TT-3' doublets.

Assuming that 5'-TT-3' cyclobutane pyrimidine dimers (TT-CPD) are the predominant lesions during UV irradiation of an amplicon, $k_{\text{all lesions},f}$ may be approximated as

$$k_{\text{all lesions},f} \approx k_{\text{TT-CPD},f} = 2.303(\varepsilon_{254,\text{ 5'-TT-3'}} f_{254,\text{ TT-CPD}}/\text{U}_{254})(\#_{\text{5'-TT-3'}}) \quad \text{(S2.20)}$$

where $k_{\text{TT-CPD},f}$ is the theoretical rate constant for TT-CPD formation, $\varepsilon_{254,\text{ 5'-TT-3'}}$ is the molar extinction coefficient of 5'-TT-3' doublets, $f_{254,\text{ TT-CPD}}$ is the quantum yield of TT-CPD formation at 254 nm (including *cis,syn* CPDs and *trans,syn* CPDs), and $\#_{\text{5'-TT-3'}}$ is the number of 5'-TT-3' doublets in the amplicon.

The theoretical values of $k_{\text{TT-CPD},f}$ obtained for each amplicon with eq S2.20 – using a value of $\varepsilon_{254,\text{ 5'-TT-3'}} f_{254,\text{ TT-CPD}}$ = 48 (determined by the same procedures described above) – underpredict the $k_{\text{UV, Amp}}$ values measured for the 266-1017 bp amplicons by ~0.6-0.9× (Figures 2.2g and S2.16b), in reasonably good agreement with the experimental values. In comparison, when substituting values reported by Patrick (1977)[59] for $\varepsilon_{254,\text{ 5'-TT-3'}}$ (= 8.4×10^3 $\text{M}^{-1}\text{cm}^{-1}$) and

$f_{254,\,\text{TT-CPD}}$ (= 0.019) into eq S2.20, as done by Yoon et al. (2018)[55], the resulting $k_{\text{TT-CPD},\,f}$ values *overpredict* $k_{\text{UV, Amp}}$, by ~2.0-2.8× (Figures 2.2g and S2.16b). Although elucidation of the possible reasons for the differences between the $\varepsilon_{254,\,5'\text{-TT-}3'}$ and $f_{254,\,\text{TT-CPD}}$ values estimated here and those reported by Patrick (1977)[59] is beyond the scope of the present work, it is worth pointing out that similarly wide variations in reported values of $\varepsilon_{254,\,5'\text{-TT-}3'}$ and $f_{254,\,\text{TT-CPD}}$ have been previously noted by other investigators.[60, 61]

These findings highlight that the accuracy of *predicted theoretical* values of $k_{\text{all lesions},\,f}$ or $k_{\text{TT-CPD},\,f}$ in comparison to *measured* values of $k_{\text{UV, Amp}}$ will strongly depend on the input values used for $\phi_{254,\,5'\text{-bipyrimidine-}3'}$ and $\varepsilon_{254,\,5'\text{-bipyrimidine-}3'}$, or for $f_{254,\,\text{TT-CPD}}$ and $\varepsilon_{254,\,5'\text{-TT-}3'}$, potentially leading to significant uncertainties in the resulting predictions. Therefore, it is highly recommended that continued efforts be directed at more precisely determining values of $\phi_{254,\,5'\text{-bipyrimidine-}3'}$ and $\varepsilon_{254,\,5'\text{-bipyrimidine-}3'}$ (expressed with respect to photon absorbance by a given type of 5'-bipyrimidine-3' doublet) for *all four* 5'-bipyrimidine-3' doublets, in both plasmid and chromosomal dsDNA, under a range of conditions representative of those likely to be encountered in water and wastewater treatment.

Table S2.1. Specific nucleotide contents for the qPCR amplicons (266 bp, 832 bp, 870 bp, and 1017 bp) and the homologous *acf*A-centered amplicons (800 bp, 900 bp, and 1000 bp) used for transformation frequency modeling. Nucleotide contents were counted using the on-line tool of Wageningen University Bioinformatics group (http://www.bioinformatics.nl/cgi-bin/emboss/wordcount#forms::wordcount).

Specific nucleotide base pairs or doublets		qPCR amplicons				Homologous *acfA*-flanking sequences[a]		
		266 bp	832 bp	870 bp	1017 bp	800 bp	900 bp	1000 bp
AT bp	#	152	503	572	666	530	592	654
	% of total bps[c]	57.14	60.46	65.75	65.49	66.25	65.78	65.40
GC bp	#	114	329	298	351	270	308	346
	% of total bps[c]	42.86	39.54	34.25	34.51	33.75	34.22	34.60
AT+GC bp	#	266	832	870	1017	800	900	1000
5'-GG-3' doublet	#[b]	16	49	37	47	30	35	41
	% of total bases[c]	3.01	2.94	2.13	2.31	1.88	1.94	2.05
5'-TT-3' doublet	#[b]	52	188	237	270	222	248	268
	% of total bases[c]	9.77	11.30	13.62	13.27	13.88	13.78	13.40
5'-TC-3' doublet	#[b]	25	93	109	123	99	110	119
	% of total bases[c]	4.70	5.59	6.26	6.05	6.19	6.11	5.95
5'-CT-3' doublet	#[b]	25	86	95	113	88	95	108
	% of total bases[c]	4.70	5.17	5.46	5.56	5.50	5.28	5.40
5'-CC-3' doublet	#[b]	37	74	56	69	55	64	72
	% of total bases[c]	6.95	4.45	3.22	3.39	3.44	3.56	3.60

[a] Homologous *acfA*-flanking regions were centered at the *acfA* mutation (i.e., with symmetrical, 400, 450, or 500 bp flanks located on either side of the mutation). [b] Contents of 5'-GG-3', 5'-TT-3', 5'-TC-3', 5'-CT-3', 5'-CC-3' doublets (i.e., # of doublets per amplicon) represent the total doublet contents of both of the two complementary strands of DNA comprising a given amplicon region. For example, the total number of 5'-TT-3' doublets within an amplicon was taken to equal the sum of 5'-TT-3' doublets plus 5'-AA-3' doublets in the sequence (Text S5) within one strand of the dsDNA comprising the amplicon region. Here 5'-GG-3' doublet contents comprise only non-contiguous 5'-GG-3' doublets (not adjacent to any guanosine bases up- or downstream) in the amplicon sequence, while excluding those within 5'-GGG-3' or 5'-GGGG-3' sequences. In contrast, 5'-TT-3' doublet contents comprise those within 5'-TTT-3' and 5'-TTTT-3' sequences, which were counted as containing two and three 5'-TT-3' doublets, respectively. [c] For a given amplicon, relative AT and GC bp contents (in % of total bps) were determined by dividing # of AT or GC bps by # of total bps (i.e., # of AT+GC bps, or amplicon length), while relative contents of 5'-GG-3', 5'-TT-3', 5'-TC-3', 5'-CT-3', and 5'-CC-3' doublets (in % of total bases) were determined by dividing # of doublets by # of total bases (i.e., 2× # of AT+GC bps).

Table S2.2. qPCR reaction temperature profile.

Amplicon	1 cycle	40 cycles			
blt 266 bp or 832 bp	95 °C	95 °C	55 °C	68 °C	Melting curve (from 60 °C to 95 °C; 20 min)
	5 min	15 sec	30sec	1 min	
blt 870 bp	98 °C	98 °C	60 °C	68 °C	
	5 min	15 sec	20 sec	1 min	
blt 1017 bp	98 °C	98 °C	60 °C	70 °C	
	5 min	15 sec	20 sec	1 min	

Table S2.3. Summary of kinetic parameters for ARG degradation and deactivation measured or estimated in this study, and reported in the literature: Including second-order rate constants (in units of $M^{-1}s^{-1}$) for FAC, NH_2Cl, ClO_2, O_3 and $^{\bullet}OH$, fluence-based first-order rate constants (in units of cm^2/mJ) for UV, and *CT* (in units of mg/L•min for FAC, NH_2Cl, ClO_2, O_3, and units of M•s for $^{\bullet}OH$) and *IT* (in units of mJ/cm^2 for UV) values required for 2 log_{10} ARG degradation (for qPCR amplicons) or deactivation (for transforming activity).

Disinfectant	Reference; DNA source and treatment condition studied	Monitored target (i.e., ARG amplicon and length, ARG biological activity, and/or bulk DNA concentration)	Extracellular treatment		Intracellular treatment	
			k [a]	***CT* or *IT* required for 2-log_{10} ARG degradation or deactivation** [b]	***k*** [a]	***CT* or *IT* required for 2-log_{10} ARG degradation or deactivation** [b]
FAC	This study; genomic DNA or intact cells of *B. subtilis* 1A189, PB pH 7	*blt* 266 bp	$3.9(\pm0.3)\times10^3$	100	N.A.	N.A.
		blt 832 bp	$8.5(\pm0.5)\times10^3$	70	N.A.	N.A.
		blt 870 bp	$8.1(\pm0.5)\times10^3$	67	N.A.	N.A.
		blt 1017 bp	$9.2(\pm0.5)\times10^3$	65	N.A.	N.A.
		blt transforming activity	N.A.	> 60 (1.5 log_{10})	N.A.	> 46 (1 log_{10})
	Yoon et al. (2017);[47] plasmid DNA or intact cells of *E. coli* strain, PB pH 7	kan^R 806 bp	$2.5(\pm0.1)\times10^2$	28; 2 log_{10}	$1.2(\pm0.1)\times10^2$	26; 2 log_{10}
		amp^R 850 bp	$3.7(\pm0.2)\times10^2$	22; 2 log_{10}	$1.2(\pm0.1)\times10^2$	21; 2 log_{10}
	Prütz (1996);[31] calf thymus DNA, pH 7	bulk DNA denaturation (spectra)	~10 [d]	N.A.	N.A.	N.A.
NH_2Cl	This study; genomic DNA or intact cells of *B. subtilis* 1A189, PB pH 8	*blt* 266 bp	1.7(±0.1)	2.2×10^5	N.A.	N.A.
		blt 832 bp	3.6(±0.1)	1.5×10^5	N.A.	N.A.
		blt 870 bp	3.8(±0.2)	1.4×10^5	N.A.	N.A.
		blt 1017 bp	4.4(±0.2)	1.3×10^5	N.A.	N.A.
		blt transforming activity	N.A.	> 7.8×10^5 (0.8 log_{10})	N.A.	> 5.1×10^3 (0.4 log_{10})
	Shih and Lederberg (1976);[62] genomic DNA or intact cells of *B. subtilis*, PB pH 7 (37 °C)	Transforming activity of chromosomal prototroph- encoding genes ($aroB^+$, $hisB^+$, and $tyrA^+$)	N.A.	> 4000 (<0.8 log_{10})	N.A.	> 170 (0.6-0.7 log_{10})
ClO_2	This study; genomic DNA or intact cells of *B. subtilis* 1A189, PB pH 7	*blt* 266 bp	3.5(±0.3)	> 1,032 (1.5 log_{10})	N.A.	N.A.
		blt 832 bp	$1.2(\pm0.2)\times10^1$	400	N.A.	N.A.
		blt 870 bp	8.9(±0.2)	575	N.A.	N.A.

		blt 1017 bp	$1.2(\pm0.1)\times10^{1}$	430	N.A.	N.A.
		blt transforming activity	N.A.	> 1,134 (1.5 $\log_{10}$)	N.A.	>> 20 (negligible)
	Roller et al. (1980);[63] genomic DNA of streptomycin-resistant *H. influenzae*	Transforming activity of streptomycin resistance gene	N.A.	> 75 (less than 1 $\log_{10}$)	N.A.	N.A.
O_3	This study; genomic DNA or intact cells of *B. subtilis* 1A189, PB pH 7	*blt* 266 bp	$1.8(\pm0.5)\times10^{4}$	> 0.12 (1.7 $\log_{10}$)	N.A.	N.A.
		blt 832 bp	$6.1(\pm1.2)\times10^{4}$	0.067	N.A.	N.A.
		blt 870 bp	$5.3(\pm0.8)\times10^{4}$	0.066	N.A.	N.A.
		blt 1017 bp	$6.9(\pm0.8)\times10^{4}$	0.058	N.A.	N.A.
		blt transforming activity	N.A.	> 0.032 (1 $\log_{10}$)	N.A.	0.100
	Czekalski et al. (2016);[64] intact cells of *E. coli* J53 strain (carrying plasmid-borne ARG *sul*1) in secondary wastewater effluent	*sul*1 827 bp	N.A.	N.A.	$9.6(\pm0.0)\times10^{4}$	0.050
		16S rRNA 457 bp			$4.8(\pm2.9)\times10^{4}$	0.092
	Czekalski et al. (2016);[64] native bacterial cells in secondary wastewater effluent	*sul*1 827 bp	N.A.	N.A.	$2.9(\pm0.5)\times10^{5}$	0.029
		16S rRNA 457 bp			$2.4(\pm1.0)\times10^{5}$	0.035
	Theruvathu et al. (2001);[65] calf thymus DNA, pH 7 (*k* measured from O_3 consumption kinetics with DNA in excess)	bulk DNA	410 [d]	N.A.	N.A.	N.A.
UV	This study; genomic DNA of *B. subtilis* 1A189, PB pH 7	*blt* 266 bp	$2.0(\pm0.1)\times10^{-2}$	> 88 (0.6 $\log_{10}$)	N.A.	N.A.
		blt 832 bp	$5.2(\pm0.2)\times10^{-2}$	> 88 (1.6 $\log_{10}$)	N.A.	N.A.
		blt 870 bp	$7.8(\pm 0.4)\times10^{-2}$	66	N.A.	N.A.
		blt 1017 bp	$8.8(\pm 0.4)\times10^{-2}$	53	N.A.	N.A.
		blt transforming activity	N.A.	109	N.A.	> 66 (1.9 $\log_{10}$)

	This study; ranges of *theoretical* rate constants of TT-cyclobutane pyrimidine dimer (CPD) formation ($k_{\text{TT-CPD},f}$) for ARG amplicons on genomic DNA of *B. subtilis* 1A189 calculated using data either from Patrick (1977),[59] or from Douki (2006)[56] and Tataurov et al. (2008)[65] (Text S2.12)	*blt* 266 bp *blt* 832 bp *blt* 870 bp *blt* 1017 bp	$1.2\times10^{-2} – 4.0\times10^{-2}$ $4.4\times10^{-2} – 1.5\times10^{-1}$ $5.6\times10^{-2} – 1.8\times10^{-1}$ $6.3\times10^{-2} – 2.1\times10^{-1}$	N.A.	N.A.	N.A.
	Yoon et al. (2017);[47] plasmid DNA or intact cells of *E. coli* strain, PB pH 7 [c]	amp^R 806 bp amp^R 850 bp	$1.5\ (\pm0.06)\times10^{-1}$ $1.1\ (\pm0.01)\times10^{-1}$	31 42	$9.0\ (\pm1.4)\times10^{-2}$ $7.0\ (\pm0.3)\times10^{-2}$	51 66
	Yoon et al. (2017);[47] plasmid DNA or intact cells of *E. coli* strain, PB pH 8 [c]	kan^R 806 bp amp^R 850 bp	$1.3(\pm0.1)\times10^{-1}$ $1.0\ (\pm0.06)\times10^{-1}$	35 46	$7.2\ (\pm0.9)\times10^{-2}$ $6.5(\pm0.9)\times10^{-2}$	64 71
	Yoon et al. (2018);[55] plasmid DNA or intact cells of *E. coli* strain, PB pH 7 [c]	amp^R 192 bp amp^R 400 bp amp^R 603 bp amp^R 851 bp amp^R transforming activity *ori* 190 bp *ori* 390 bp *ori* 530 bp	$1.9\ (\pm0.11)\times10^{-2}$ $3.1\ (\pm0.09)\times10^{-2}$ $5.4\ (\pm0.16)\times10^{-2}$ $1.0(\pm0.03)\times10^{-1}$ $6.1(\pm0.25)\times10^{-2}$ $1.7\ (\pm0.69)\times10^{-2}$ $2.9\ (\pm0.12)\times10^{-2}$ $4.0\ (\pm0.24)\times10^{-2}$	242 149 85 46 75 271 159 115	$1.7(\pm0.09)\times10^{-2}$ $2.8\ (\pm0.06)\times10^{-2}$ $4.6\ (\pm0.18)\times10^{-2}$ $7.2(\pm0.35)\times10^{-2}$ $6.2\ (\pm0.44)\times10^{-2}$ N.A. N.A. N.A.	271 164 100 64 74 N.A. N.A. N.A.
	Chang et al. (2017);[66] plasmid DNA of *A. baylyi* strain, PB pH 7 [c]	$bla_{\text{TEM-1}}$ 209 bp $bla_{\text{TEM-1}}$ 861 bp $bla_{\text{TEM-1}}$ transforming activity *tet*A 216 bp *tet*A 1200 bp *tet*A transforming activity	$5.5(\pm0.6)\times10^{-3}$ $6.8(\pm0.4)\times10^{-2}$ $1.13(\pm0.09)\times10^{-1}$ $4.0\ (\pm0.5)\times10^{-3}$ $5.8\ (\pm0.6)\times10^{-2}$ $1.02(\pm0.19)\times10^{-1}$	> 430 (1 $\log_{10}$) 68 40 >430 (0.75 $\log_{10}$) >108 (1.7 $\log_{10}$) 45	N.A.	N.A.

	McKinney and Pruden (2012);[67] genomic or plasmid DNA of various ARB strains or their intact cells, PB pH 7	*amp*C 1006 bp *mec*A 1018 bp *tet*A 1054 bp *van*A 1030 bp	N.A.	~180 ~70 ~180 ~75	N.A.	~240 ~70 ~200 ~80
$^{\bullet}$OH	This study; genomic DNA of *B. subtilis* 1A189, PB pH 7	*blt* 266 bp *blt* 832 bp *blt* 870 bp *blt* 1017 bp *blt* transforming activity	$5.9(\pm0.8)\times10^{10}$ $1.9(\pm0.2)\times10^{11}$ $2.0(\pm0.2)\times10^{11}$ $2.3(\pm0.3)\times10^{11}$ N.A.	$> 2.6\times10^{-11}$ (0.8 $\log_{10}$) 2.1×10^{-11} 2.1×10^{-11} 1.8×10^{-11} $> 6.5\times10^{-12}$ (1.7 $\log_{10}$)	N.A.	N.A.
	This study; *theoretical* diffusion-controlled limit for *blt* 266-1017 bp amplicons on genomic DNA of *B. subtilis* 1A189, and kan^R 806 bp and amp^R 850 bp amplicons carried on plasmid DNA (Text S2.10)	*blt* 266 bp *blt* 832 bp *blt* 870 bp *blt* 1017 bp kan^R 806 bp amp^R 850 bp	4.2×10^{10} 1.3×10^{11} 1.4×10^{11} 1.6×10^{11} 9.75×10^{10} 1.03×10^{11}	N.A.	N.A.	N.A.
	Yoon et al. (2017);[47] plasmid DNA of *E. coli* strain, PB pH7 (UV/H_2O_2)	kan^R 806 bp/ amp^R 850 bp	2×10^{10}	N.A.	N.A.	N.A.
	Masuda et al. (1980);[45] calf thymus DNA pH 7	bulk DNA (absorbance at 260nm)	1.1×10^{8} [d]	N.A.	N.A.	N.A.
	Udovicic et al. (1994);[68] calf thymus DNA pH 7.6	bulk DNA (laser light-scattering)	2.5–4.6 ($\times10^{8}$) [d]	N.A.	N.A.	N.A.

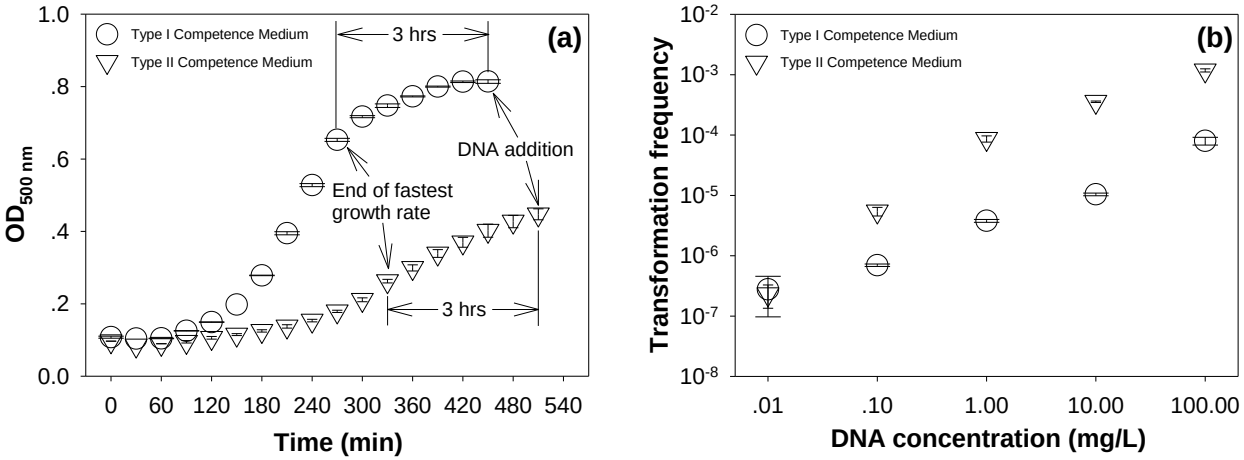

Figure S2.1. Determination (a) Sample growth curves of *B. subtilis* 1A1 (transformation recipient cell) in competence media incubated at 37 °C, 120 rpm, angle of 15°. Error bars represent one standard deviation from the mean, obtained from multiple broth cultures originating from the same source inoculum of *B. subtilis* 1A1. (b) Sample curves of transformation frequency as a function of DNA concentration (in units of mg/L). *B. subtilis* 1A189 DNA (0.01, 0.1, 1, 10, and 100 mg/L) was mixed with equal volumes of *B. subtilis* 1A1 cells prepared according to Text S2.3, followed by 90-min incubation at 37 °C with 120-rpm shaking. Error bars represent one standard deviation from the mean, obtained from at least duplicate transformation assays conducted at each concentration of DNA (i.e., transformation assays conducted on duplicate aliquots of the same DNA standard solution at each concentration level.

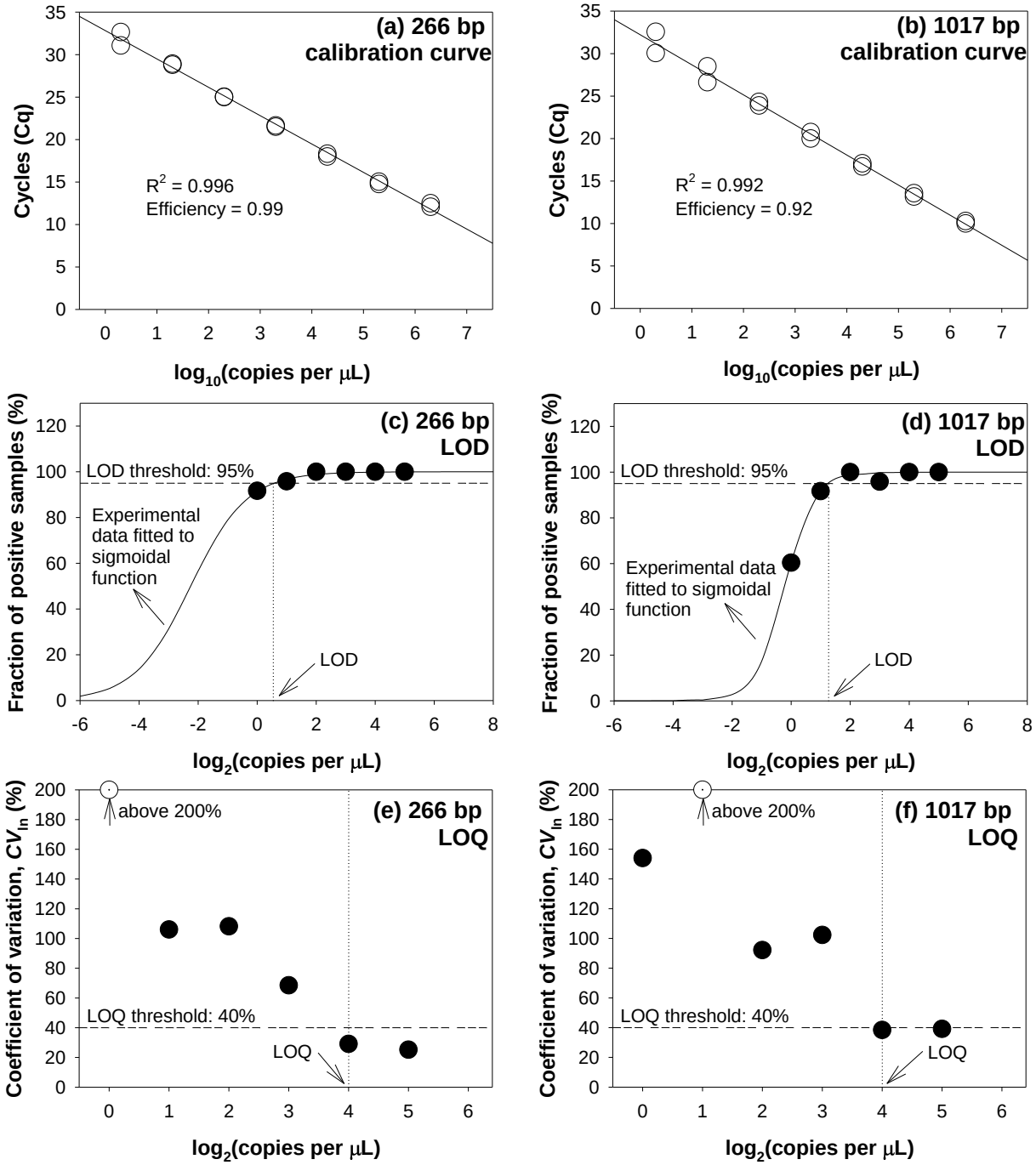

Figure S2.2. Determination of LODs and LOQs for qPCR assays: (a) and (b) typical calibration curves of 1A189 DNA standards containing from 2 to 2×10^6 copies μL^{-1} (linear regressions were performed by pooling data from duplicate assays), (c) and (d) fraction of positive samples, (e) and (f) coefficient of variation for 1A189 DNA standards containing from 1 to 32 copies μL^{-1}, for 266 bp amplicon and 1017 bp amplicon, respectively.

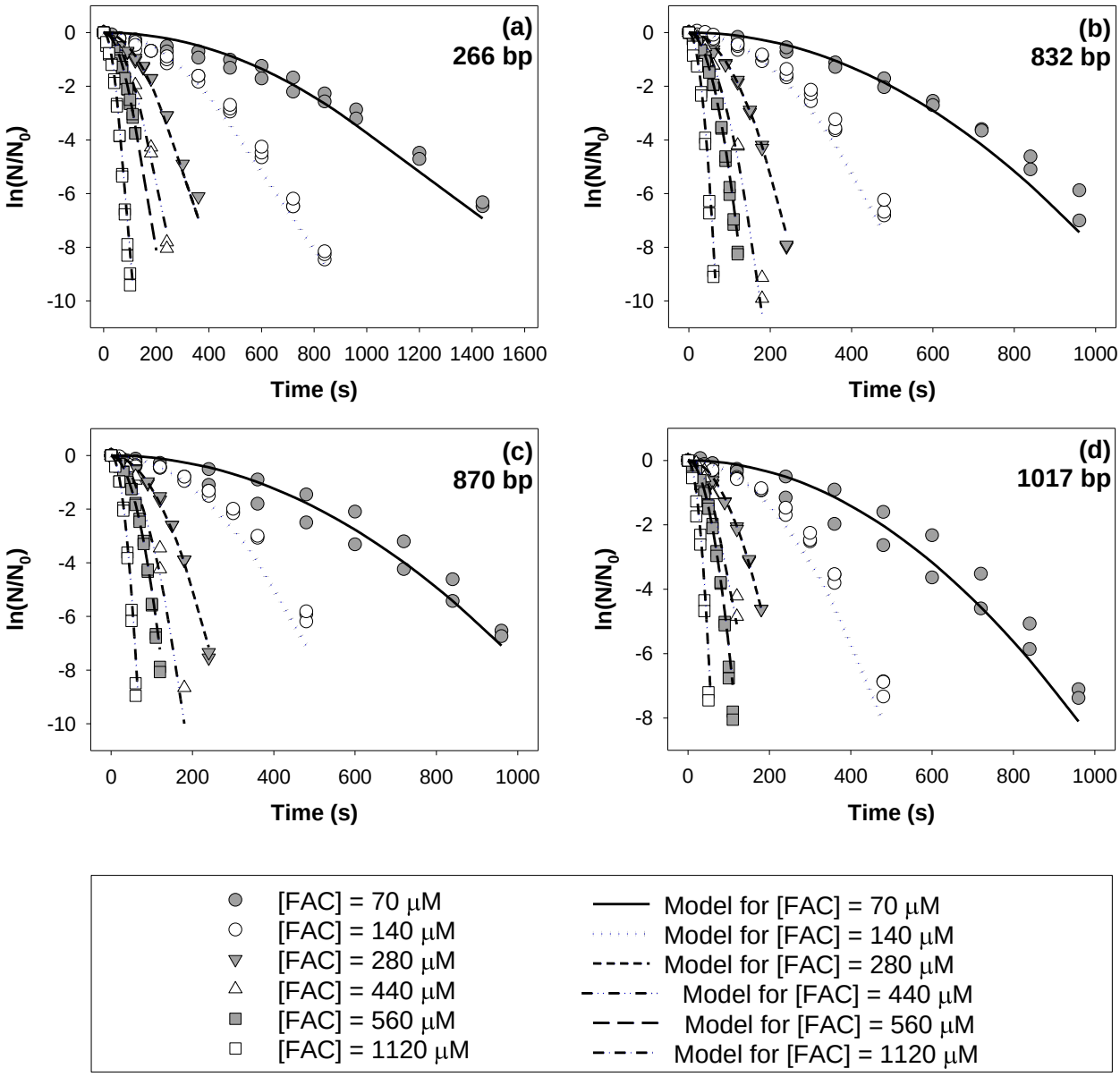

Figure S2.3. Degradation of (a) 266 bp amplicon, (b) 832 bp amplicon, (c) 870 bp amplicon, and (d) 1017 bp amplicon in 1 mg/L dsDNA reacting with FAC in excess. Residual FAC concentrations were confirmed to be constant (< 10% loss) over the treatment periods. All data were obtained by treatment of extracellular *B. subtilis* 1A189 DNA in 10-mM phosphate buffer at pH 7. Data were pooled from at least duplicate experiments.

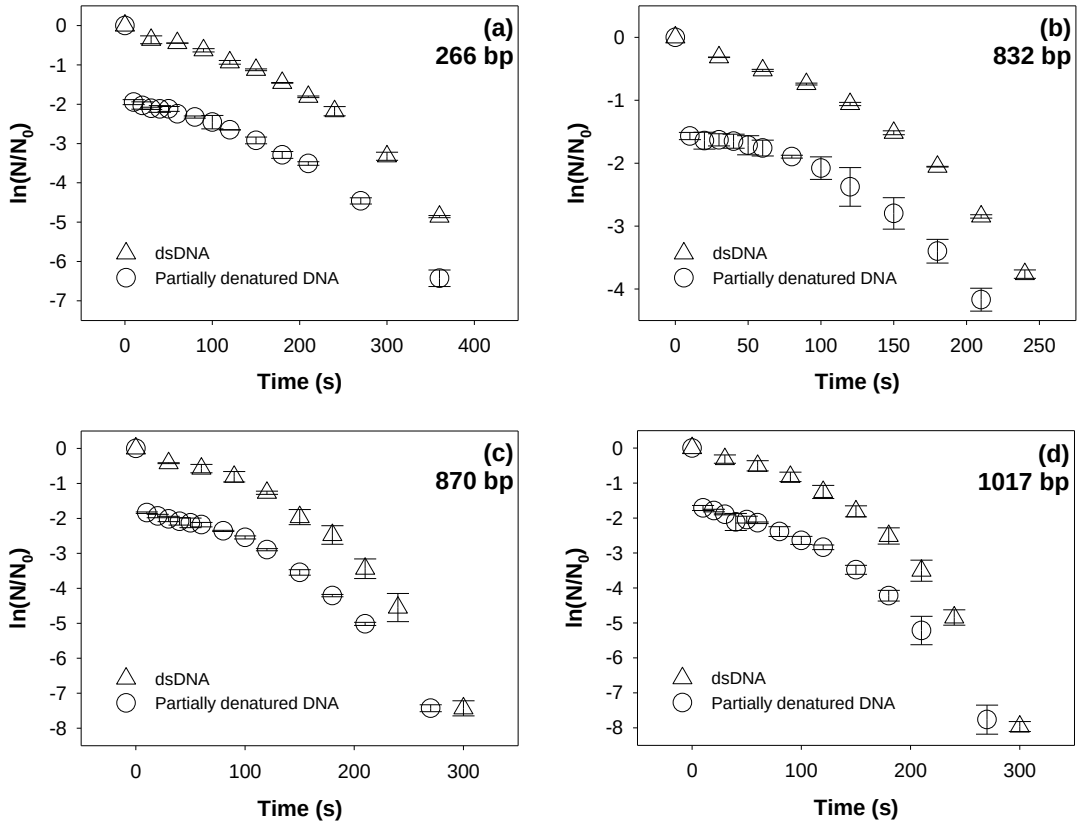

Figure S2.4. Degradation of (a) 266 bp amplicon, (b) 832 bp amplicon, (c) 870 bp amplicon, and (d) 1017 bp amplicon in 1 mg/L dsDNA and partially denatured DNA reacting with 280 μM FAC. All data were obtained by treatment of extracellular *B. subtilis* 1A189 DNA in 10-mM phosphate buffer at pH 7. Error bars represent one standard deviation from the mean, obtained from at least duplicate experiments.

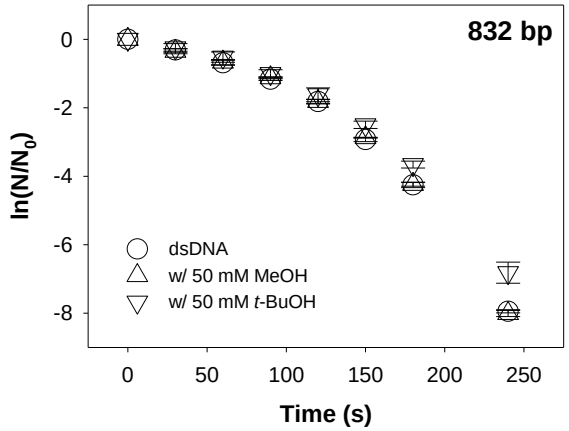

Figure S2.5. Degradation of 832 bp amplicon in 1 mg/L dsDNA reacting with 280 μM FAC, with and without 50 mM MeOH or 50 mM *t*-BuOH. All data were obtained by treatment of extracellular *B. subtilis* 1A189 DNA in 10-mM phosphate buffer at pH 7. Error bars represent one standard deviation from the mean, obtained from at least duplicate experiments.

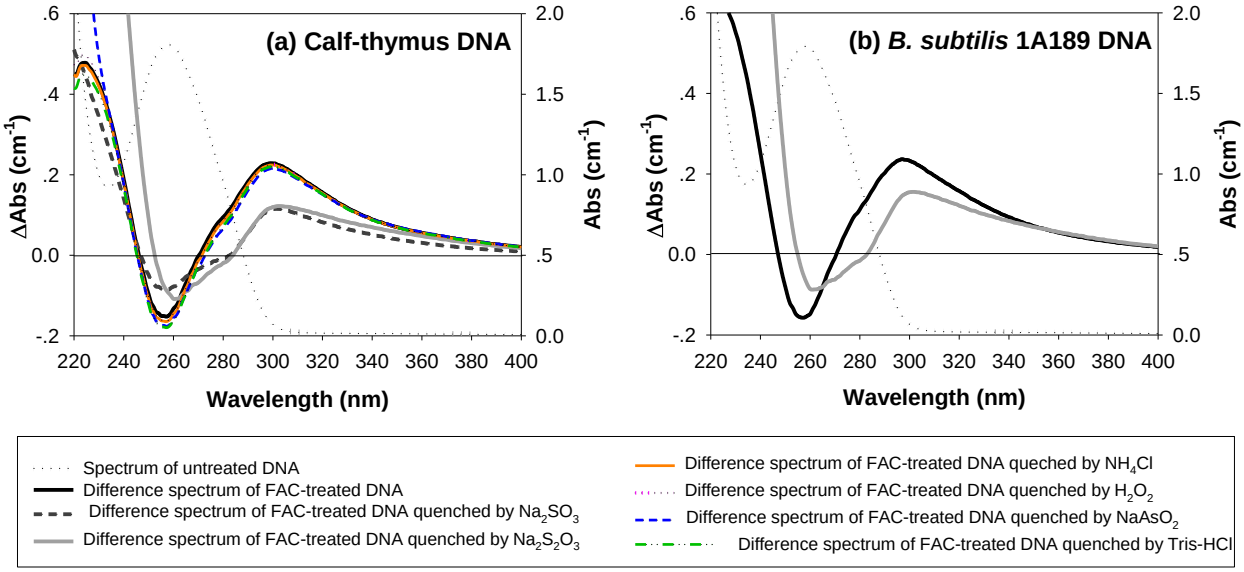

Figure S2.6. UV absorbance and difference spectra of ~90 mg/L (a) calf-thymus DNA and (b) *B. subtilis* 1A189 DNA after reaction with 320 μM FAC for 25 min and after subsequent quenching with various quenching reagents (including Na_2SO_3, $Na_2S_2O_3$, NH_4Cl, H_2O_2, $NaAsO_2$, and Tris-HCl). Difference spectra were obtained by subtracting the spectrum of untreated DNA (thick dotted gray line) from the spectra of treated DNA samples.

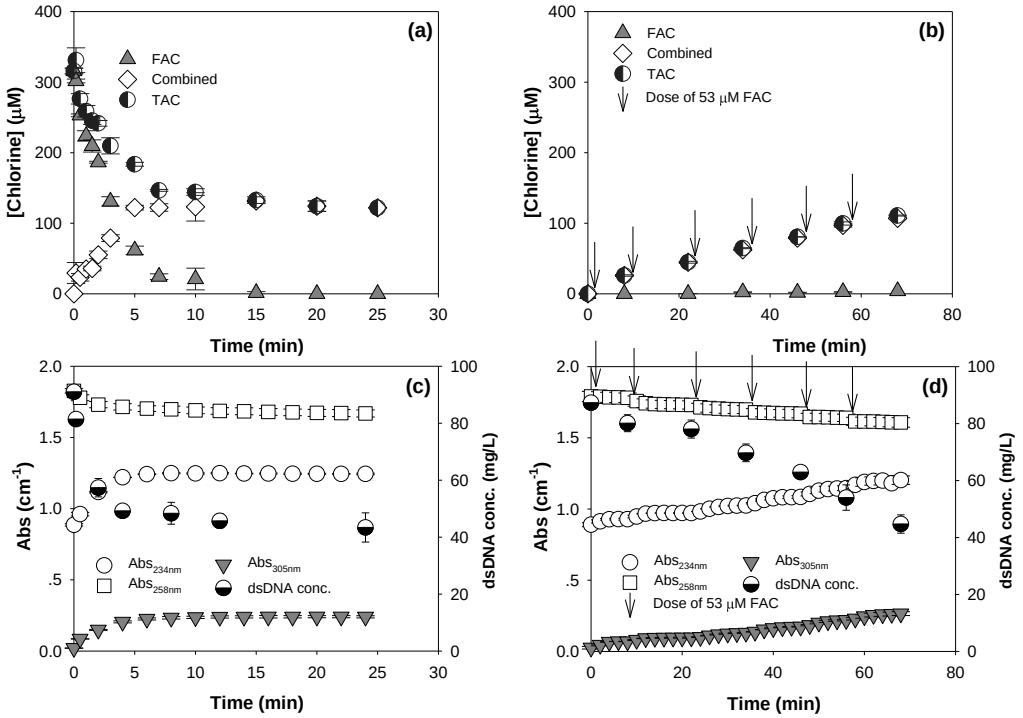

Figure S2.7. Residual concentrations of chlorine species (including FAC, combined chlorine, and total available chlorine, or TAC), dsDNA concentrations, and UV absorbances at 234 nm, 258 nm, and 305 nm (Abs_{234nm}, Abs_{258nm}, and Abs_{305nm}), as a function of time for 90 mg/L calf thymus DNA reacting with FAC. (a), (c) 320 μM FAC added to DNA solutions in one dose; (b), (d) FAC added to DNA solutions in six incremental doses of 53 μM every ~10 min (for ~320 μM in total). Arrows in panels (b) and (d) indicate the moment of FAC dosage after each measurement of residual chlorine concentration. All data were obtained by treatment of calf thymus DNA in 10-mM phosphate buffer at pH 7. Error bars represent one standard deviation from the mean, obtained from duplicate experiments.

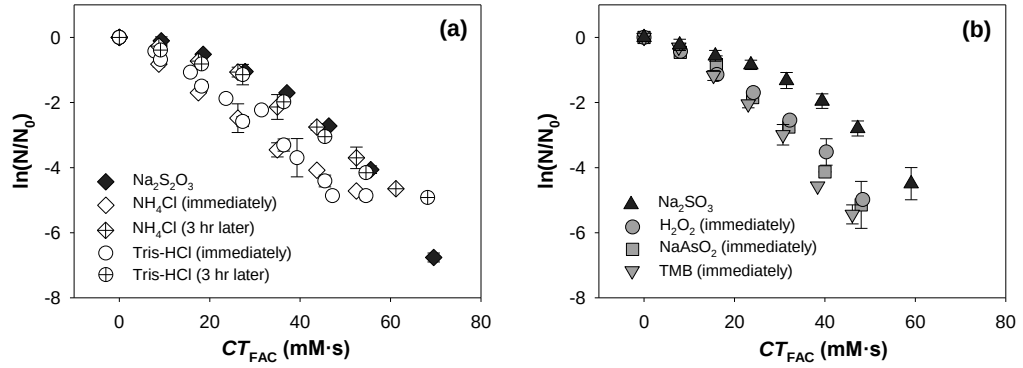

Figure S2.8. Degradation of 1017 bp amplicon in samples containing 1 mg/L dsDNA and 140 μM FAC, using various reagents to quench residual FAC prior to qPCR analyses, with various quenching reagents including (a) $Na_2S_2O_3$, NH_4Cl, Tris-HCl, and (b) Na_2SO_3, H_2O_2, $NaAsO_2$, and TMB. Samples treated with the "soft quenchers" (i.e., NH_4Cl, Tris-HCl, H_2O_2, $NaAsO_2$, and TMB) were diluted by 100-fold after quenching and analyzed immediately. The diluted samples obtained using NH_4Cl and Tris-HCl were also re-analyzed after three hours. All data were obtained by treatment of extracellular *B. subtilis* 1A189 DNA in 10-mM phosphate buffer at pH 7. Error bars represent one standard deviation from the mean, obtained from duplicate experiments.

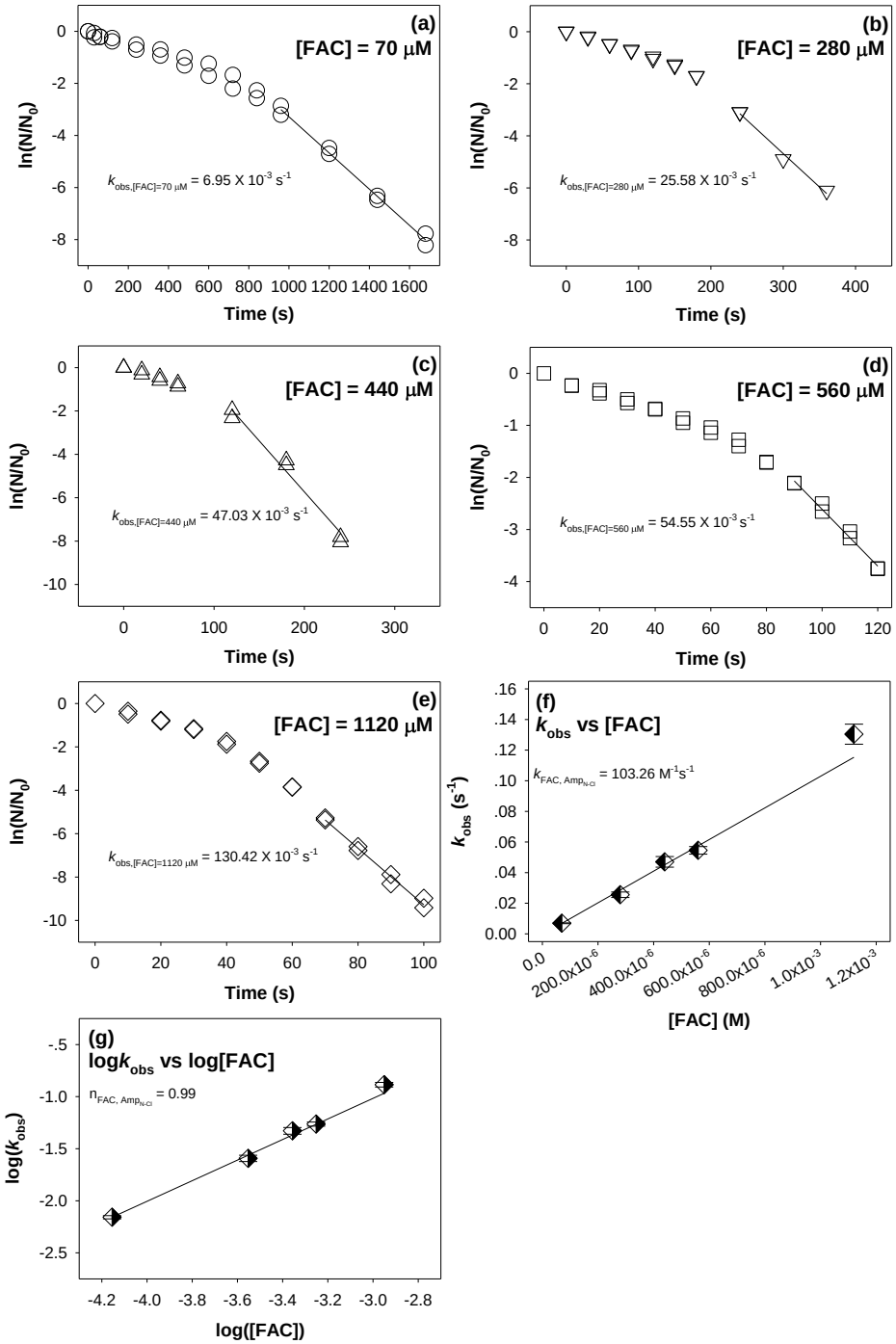

Figure S2.9. Degradation of 266 bp amplicon in 1 mg/L dsDNA reacting with (a) 70 μM, (b) 280 μM, (c) 440 μM, (d) 560 μM, and (e) 1120 μM FAC. Observed rate constants ($k_{obs,\ [FAC]}$) were determined for (a)-(e) by regression over the linear regions corresponding to maximal slopes of the ln(N/N$_0$) data versus time. Residual FAC concentrations were confirmed to be constant (< 10% loss) over the treatment periods. The value of $k_{FAC,\ Amp_{N-Cl}}$ (Text S2.9) and corresponding reaction order ($n_{FAC,\ Amp_{N-Cl}}$) were determined through weighted linear regressions of data obtained from (a)-(e), as plotted in (f) and (g), respectively. All data were obtained by treatment of extracellular *B. subtilis* 1A189 DNA in 10-mM phosphate buffer at pH 7. Data were pooled from duplicate experiments in panels (a)-(e). Error bars in panels (f) and (g) represent standard errors of observed rate constants obtained from (a)-(e).

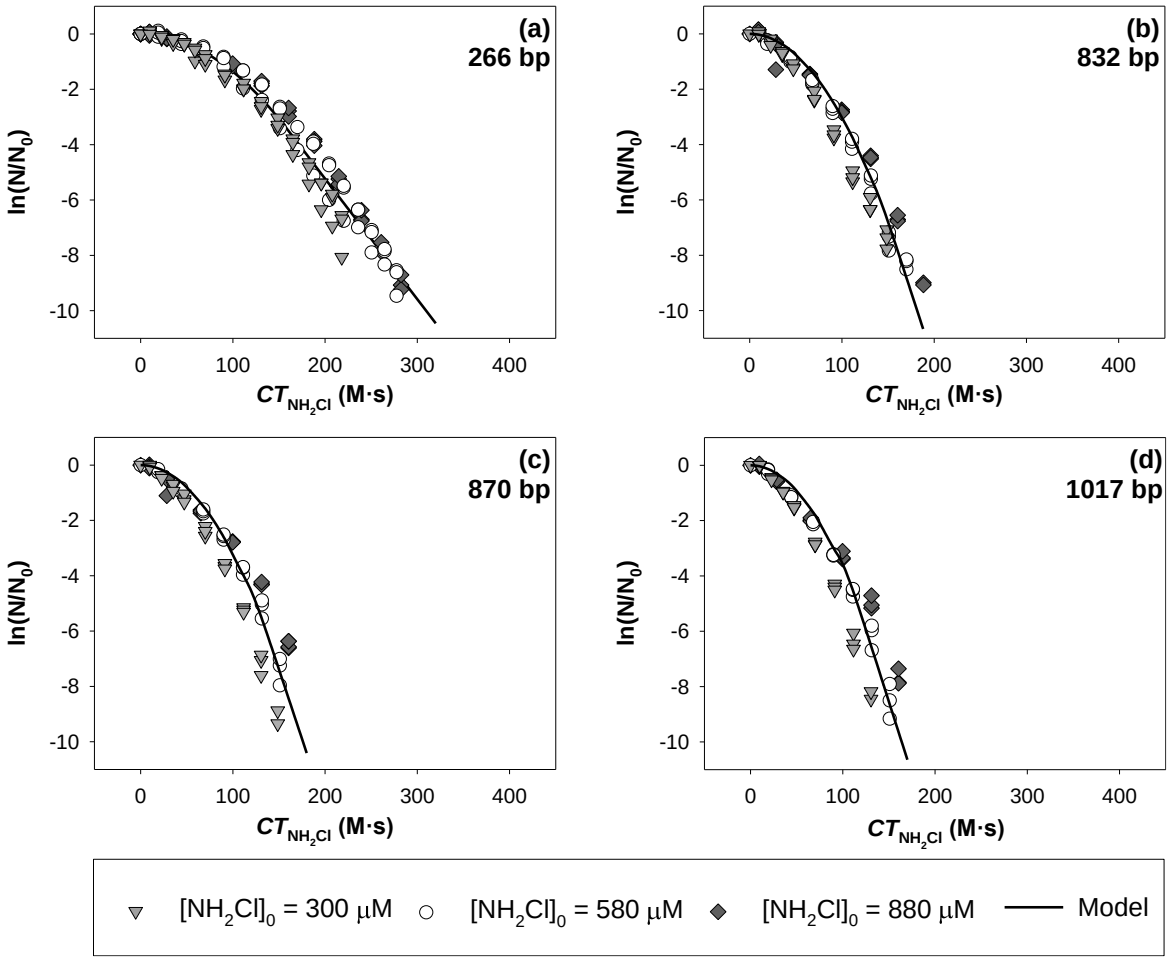

Figure S2.10. Degradation of (a) 266 bp amplicon, (b) 832 bp amplicon, (c) 870 bp amplicon, and (d) 1017 bp amplicon in 1 mg/L dsDNA reacting with NH_2Cl at initial concentrations of 300 μM, 580 μM, and 880 μM. The data were plotted as $\ln(N/N_0)$ versus CT_{NH2Cl} instead of time because residual NH_2Cl concentrations could not be assumed constant (> 10% loss) over the treatment periods. All data were obtained by treatment of extracellular *B. subtilis* 1A189 DNA in 10-mM phosphate buffer at pH 8. Data were pooled from triplicate experiments.

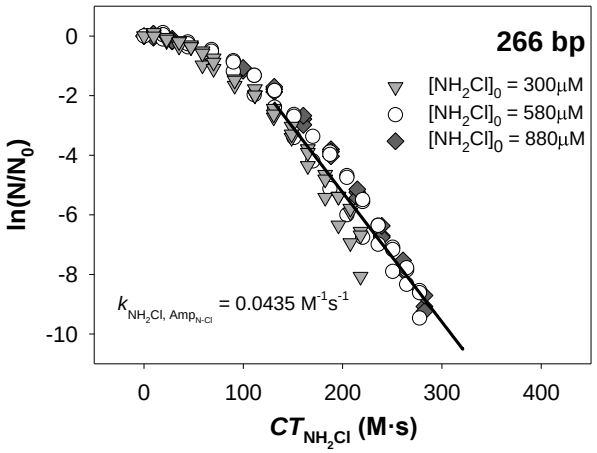

Figure S2.11. Degradation of 266 bp amplicon in 1 mg/L dsDNA reacting with NH_2Cl at initial concentrations of 300 μM, 580 μM, and 880 μM. The value of $k_{NH_2Cl,\ Amp_{N\text{-}Cl}}$ (Text S2.9) was determined by regression over the linear region corresponding to the maximal slope of the pooled $\ln(N/N_0)$ data versus time. All data were obtained by treatment of extracellular *B. subtilis* 1A189 DNA in 10-mM phosphate buffer at pH 8. Linear regression was performed by pooling data from triplicate experiments.

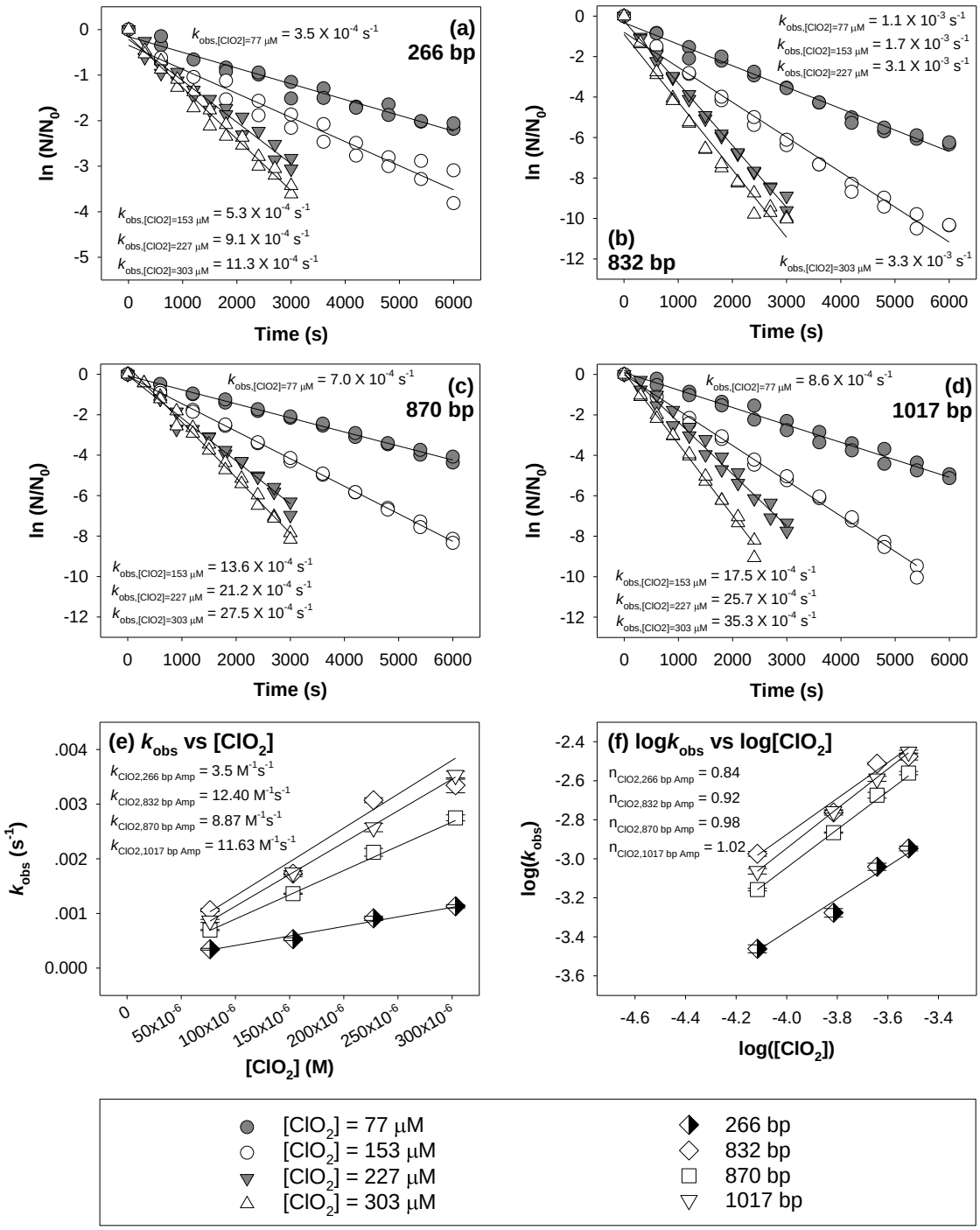

Figure S2.12. Degradation of (a) 266 bp amplicon, (b) 832 bp amplicon, (c) 870 bp amplicon, and (d) 1017 bp amplicon in 1 mg/L dsDNA reacting with ClO_2 in excess. Observed rate constants ($k_{obs,\,[ClO2]}$) were determined for (a)-(d) by linear regressions of $\ln(N/N_0)$ versus time. Residual ClO_2 concentrations were confirmed to be constant (< 10% loss) over the treatment periods. Second-order rate constants ($k_{ClO2,\,Amp}$) and reaction orders ($n_{ClO2,\,Amp}$) were determined through weighted linear regressions of data obtained from (a)-(d), as plotted in (e) and (f), respectively. All data were obtained by treatment of extracellular *B. subtilis* 1A189 DNA in 10-mM phosphate buffer at pH 7. Data were pooled from duplicate experiments in panels (a)-(d). Error bars in panels (e) and (f) represent standard errors of observed rate constants obtained from (a)-(d).

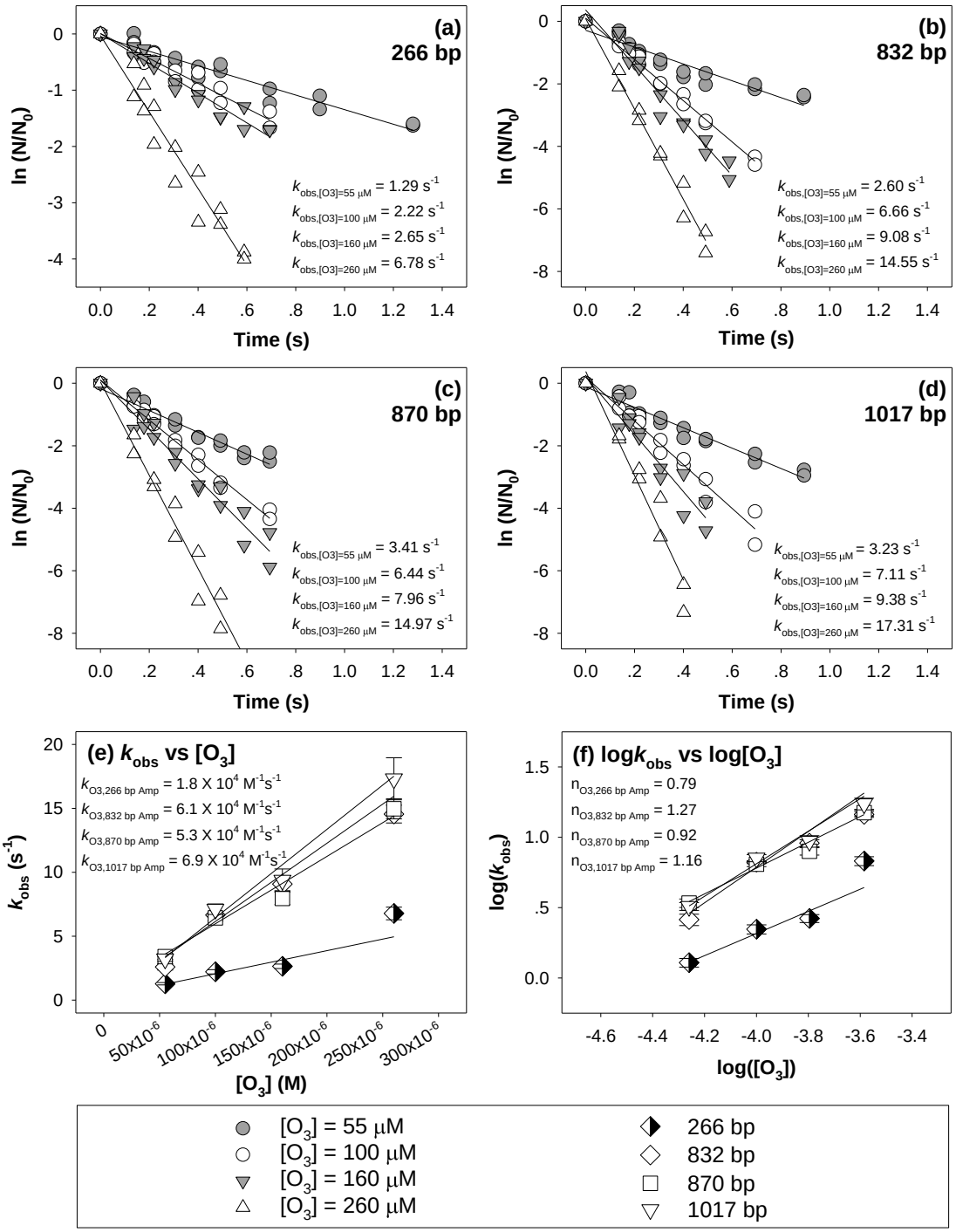

Figure S2.13. Degradation of (a) 266 bp amplicon, (b) 832 bp amplicon, (c) 870 bp amplicon, and (d) 1017 bp amplicon in 1 mg/L dsDNA reacting with O_3 in excess. Observed rate constants ($k_{obs,\,[O3]}$) were determined for (a)-(d) by linear regressions of $\ln(N/N_0)$ versus time. Residual O_3 concentrations were confirmed to be constant (< 10% loss) over the treatment periods. Second-order rate constants ($k_{O3,\,Amp}$) and reaction orders ($n_{O3,\,Amp}$) were determined through weighted linear regressions of data obtained from (a)-(d), as plotted in (e) and (f), respectively. All data were obtained by treatment of extracellular *B. subtilis* 1A189 DNA in 10-mM phosphate buffer containing 50-mM *t*-BuOH at pH 7. Data were pooled from duplicate experiments in panels (a)-(d). Error bars in panels (e) and (f) represent standard errors of observed rate constants obtained from (a)-(d).

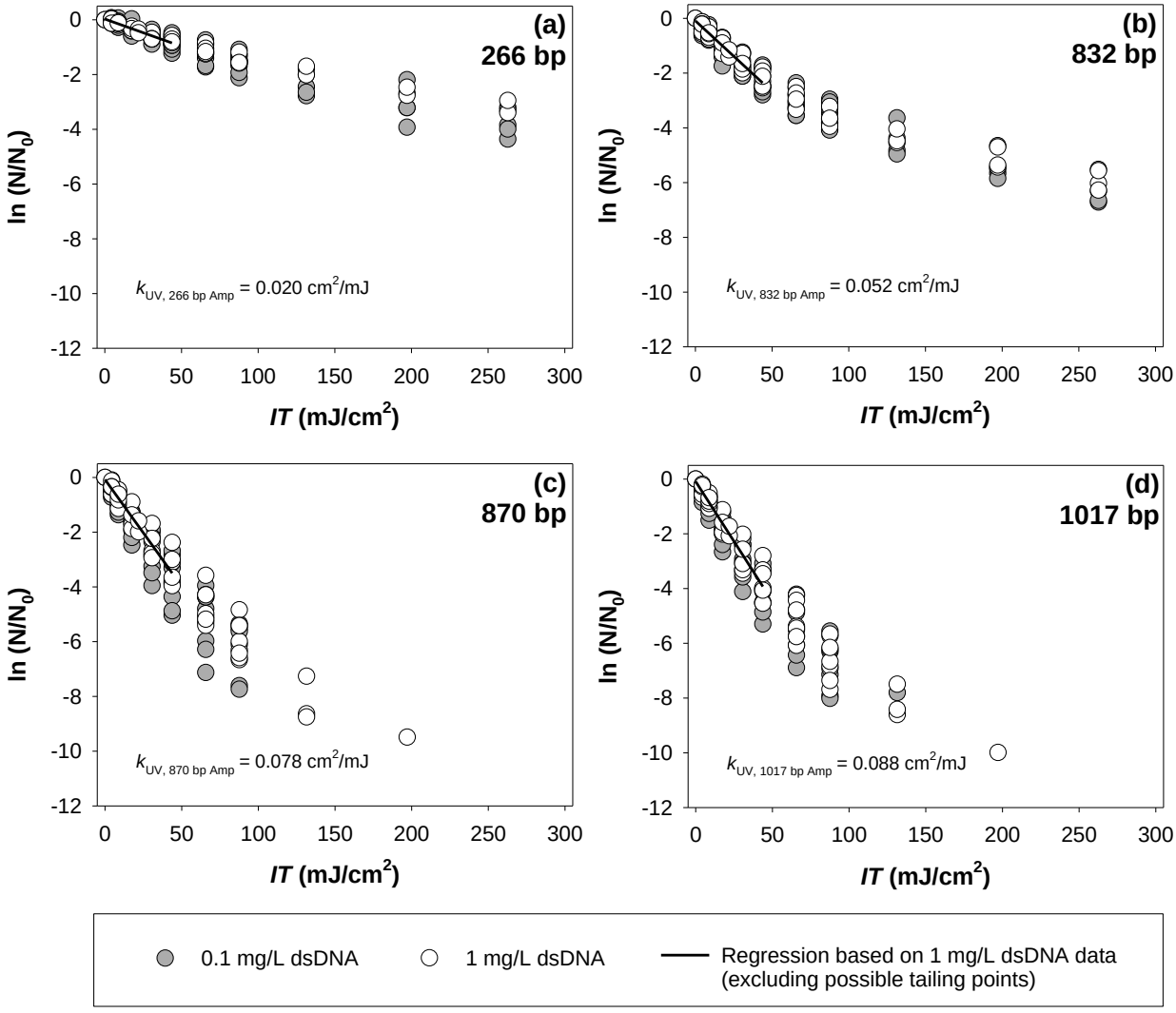

Figure S2.14. Degradation of (a) 266 bp amplicon, (b) 832 bp amplicon, (c) 870 bp amplicon, and (d) 1017 bp amplicon in 1 mg/L dsDNA treated by UV light. Fluence-based first-order rate constants ($k_{UV, Amp}$) were determined by linear regressions of $\ln(N/N_0)$ versus *IT* over *IT* values below 45 mJ/cm^2 to exclude minor tailing effects (potentially arising from CPD photoreversal at higher exposures). Selected experiments were also conducted using 0.1 mg/L dsDNA to confirm that 1 mg/L dsDNA concentration had minimal screening effect on UV irradiance. All data were obtained by treatment of extracellular *B. subtilis* 1A189 DNA in 10-mM phosphate buffer at pH 7. Linear regressions were performed by pooling data from independently conducted experiments undertaken on three separate dates, with experiments undertaken at least in duplicate on each date. Slopes (i.e., $k_{UV, Amp}$) obtained from 1 mg/L and 0.1 mg/L dsDNA were compared by two-tailed *t*-test, yielding $p > 0.05$ (i.e., no significant difference) for each panel.

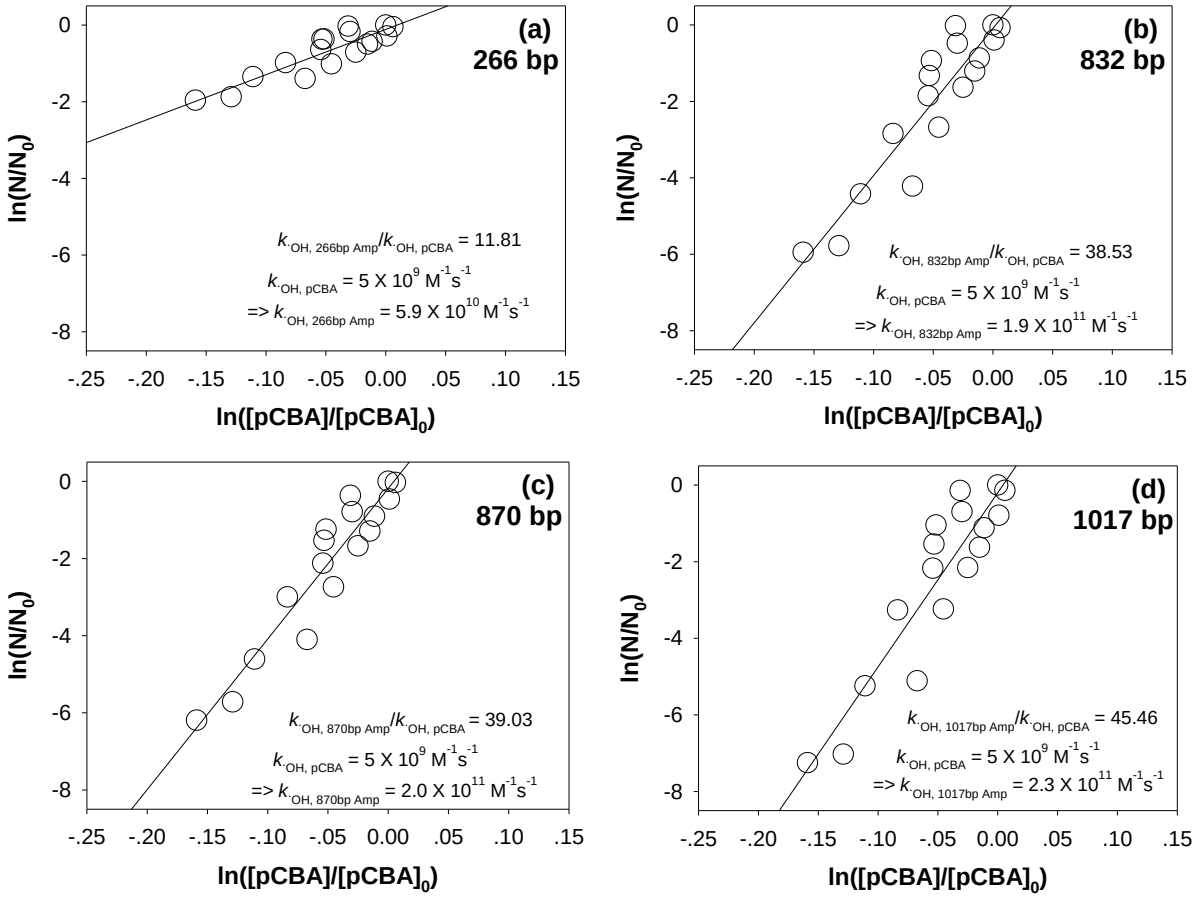

Figure S2.15. Competition plots for degradation of (a) 266 bp amplicon, (b) 832 bp amplicon, (c) 870 bp amplicon, and (d) 1017 bp amplicon in 10 mg/L dsDNA treated by $^{\cdot}$OH. The slope of the regression line in each panel equals the ratio of the second-order rate constant for reaction of the qPCR amplicon with $^{\cdot}$OH ($k_{\cdot OH, Amp}$) over that for reaction of pCBA with $^{\cdot}$OH ($k_{\cdot OH, pCBA}$). All data were obtained by treatment of extracellular *B. subtilis* 1A189 DNA in 10-mM phosphate buffer at pH 7. Linear regressions were performed by pooling data from duplicate experiments.

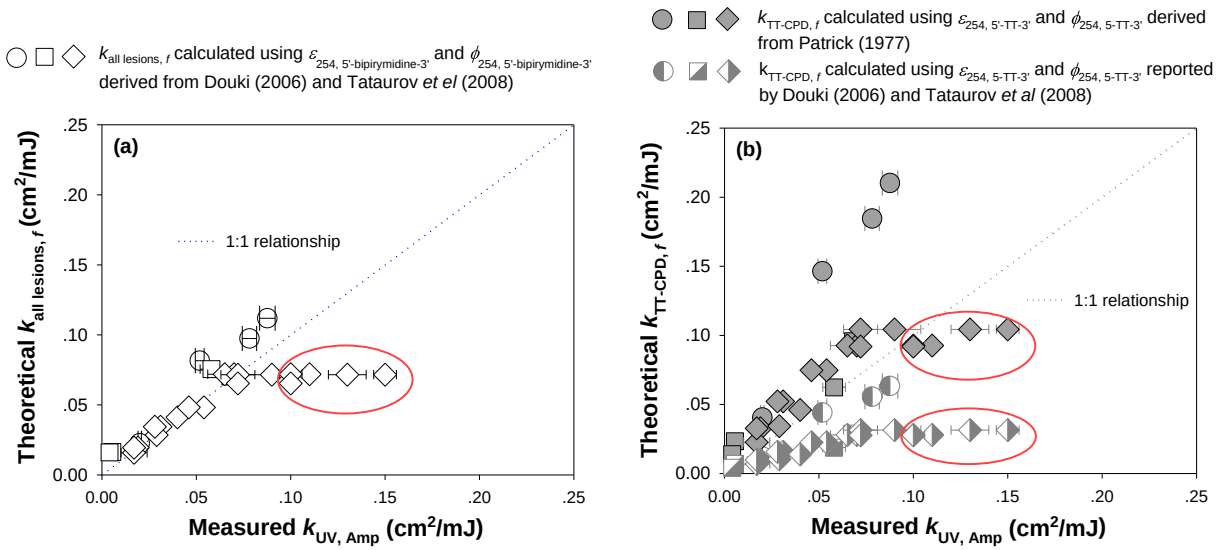

Figure S2.16. Theoretical rate constants of (a) overall lesion formation ($k_{\text{all lesions, } f}$) or (b) TT-CPD formation ($k_{\text{TT-CPD, } f}$) versus measured rate constants of amplicon degradation ($k_{\text{UV, Amp}}$) during UV treatment. Measured $k_{\text{UV, Amp}}$ values were collected from this study (circles), Chang et al. (2017)[66] (squares), and Yoon et al. (2017)[47] and Yoon et al. (2018)[55] (diamonds). Measured $k_{\text{UV, Amp}}$ values from this study were obtained by treatment of 1 mg/L of extracellular *B. subtilis* 1A189 dsDNA in 10-mM phosphate buffer at pH 7. Predicted $k_{\text{all lesions, } f}$ and $k_{\text{TT-CPD, } f}$ values were obtained according to the procedures described in Text S2.12, using the 5'-bipyrimidine-3' doublet contents provided in Table S2.1 or reported in the previous studies.[47,55,66] The apparent outliers (circled in red) are $k_{\text{UV, Amp}}$ measurements for >800 bp eARG amplicons obtained from the works by Yoon et al., which may have been influenced by incidental photochemical generation of radicals from trace transition metals remaining in DNA extracts.[55] Error bars in the *x*-direction represent standard errors of measured $k_{\text{UV, Amp}}$ as summarized in Table 2.1. The dotted line represents a theoretical 1:1 relationship, as opposed to a regression line.

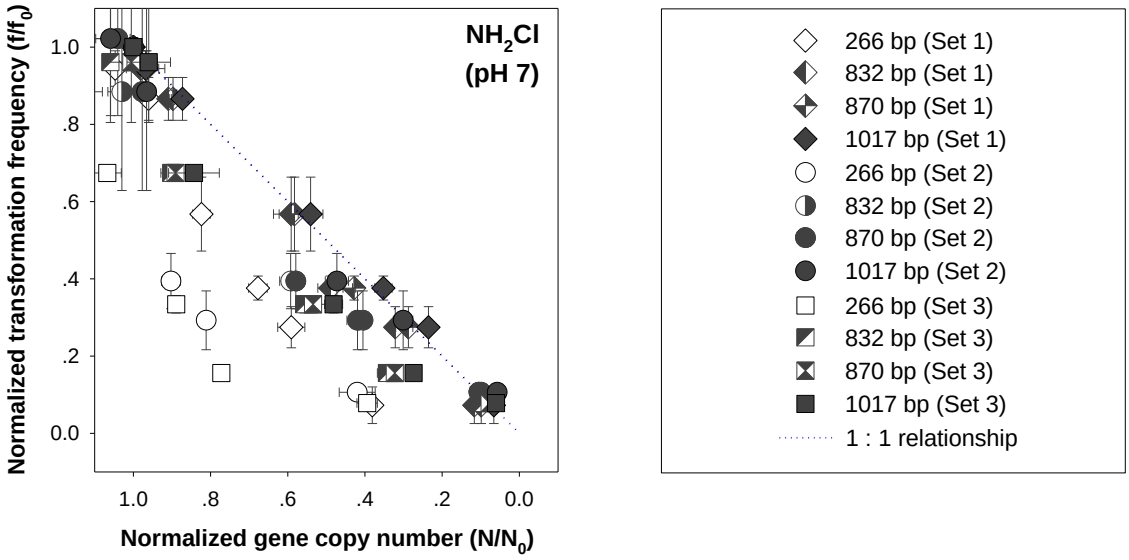

Figure S2.17. Normalized transformation frequency (f/f_0) plotted versus normalized copy number (N/N_0) of 266 bp, 832 bp, 870 bp and 1017 bp amplicons for extracellular ARG treatment with NH_2Cl. All data were obtained by treatment of 1 mg/L of extracellular *B. subtilis* 1A189 dsDNA in 10-mM phosphate buffer at pH 7. Sets 1, 2, and 3 (plotted using different symbol shapes) represent independent experiments undertaken under the same conditions but on different dates, each in at least duplicate. Error bars represent one standard deviation from the mean, obtained from at least duplicate experiments undertaken on the same date. The dotted line represents a theoretical 1:1 relationship, as opposed to a regression line.

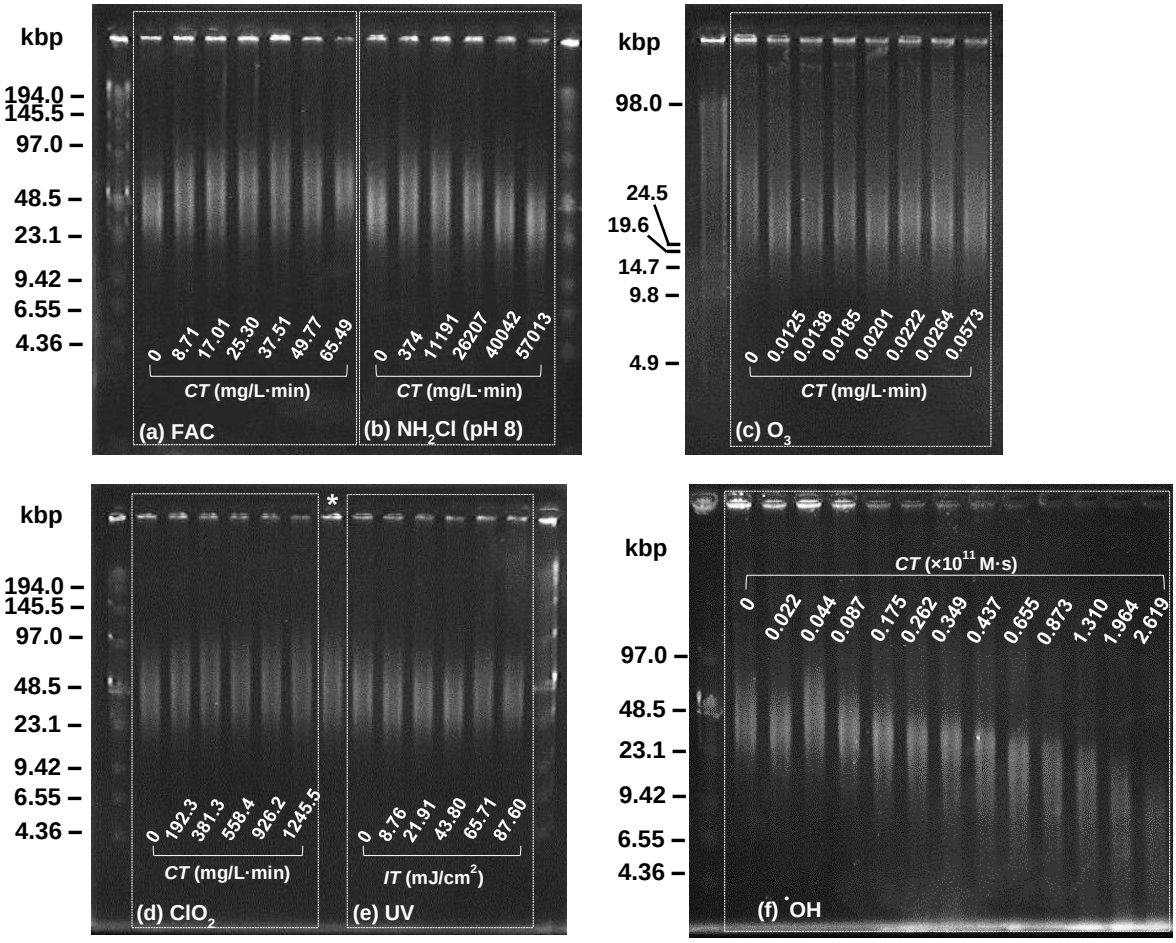

Figure S2.18. Pulsed-field gel electrophoresis for extracellular 1A189 DNA treated by (a) FAC, (b) NH_2Cl, (c) O_3, (d) ClO_2, (e) UV and (f) $^{\bullet}OH$ in 10-mM phosphate buffer at pH 7 (FAC, O_3, ClO_2, UV, and $^{\bullet}OH$) or 8 (NH_2Cl only). LowRange PFG Marker (NEB) was used for (a), (b) and (d)-(f) and 5 Kb ladder DNA size standard (Bio-Rad) for (c) as references. Ten mg/L dsDNA was used for all treatments except O_3 and UV, for which 1 mg/L was used instead. The lane between (d) and (e), labeled as *, was loaded with 10 mg/L DNA with no treatment, which indicates that dialysis pre-concentration had no impact on DNA fragment size as compared with the first lane in (e) (1 mg/L DNA with no treatment and pre-concentrated to 10 mg/L).

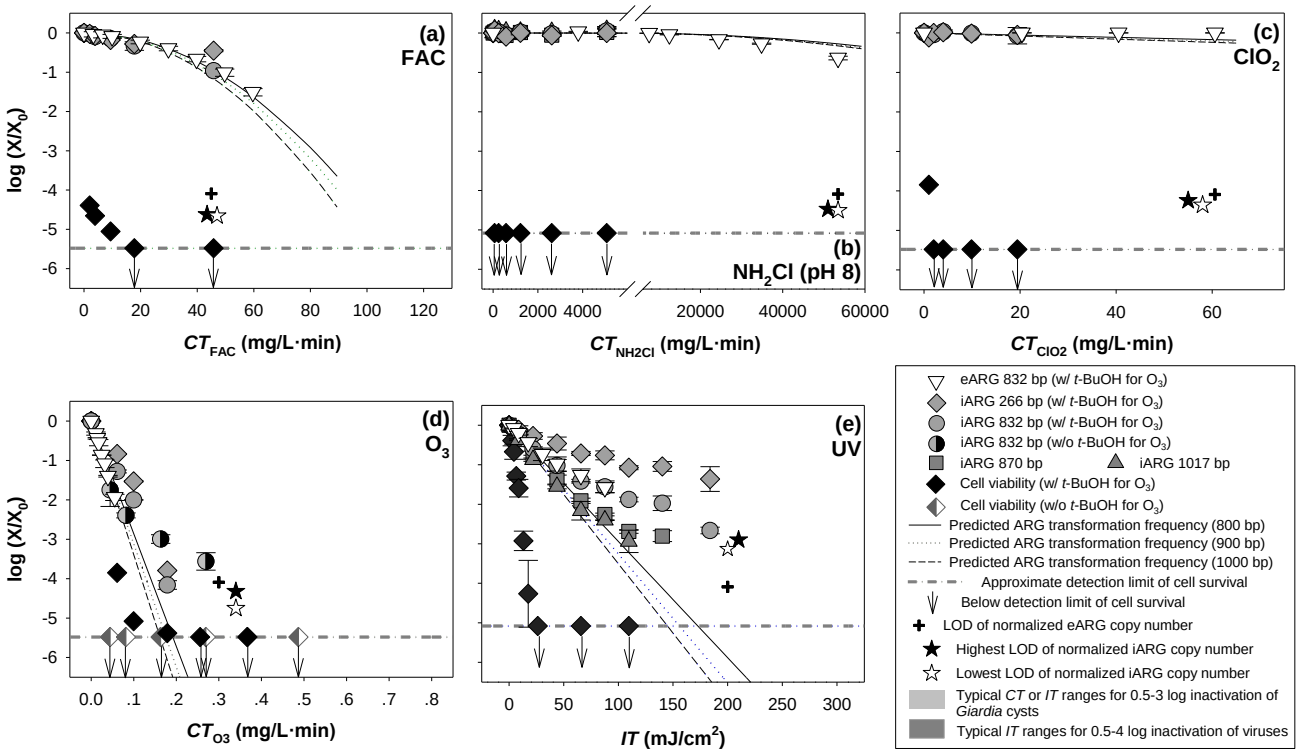

Figure S2.19. Normalized copy numbers (for 266 bp, 832 bp, 870 bp and 1017 bp amplicons), normalized cell survival, and normalized *modeled* (predicted) transformation frequency (with the latter obtained using 800 bp, 900 bp, and 1000 bp homologous *acfA*-flanking sequences) versus disinfectant exposure for (a) FAC, (b) NH_2Cl, (c) ClO_2, (d) O_3, and (e) UV, during exposure of extracellular *B. subtilis* 1A189 DNA (1 mg/L dsDNA) or intact *B. subtilis* 1A189 cells (~1×10^6 CFU/mL) to each disinfectant in 10-mM phosphate buffer at pH 7 (FAC, ClO_2, O_3, and UV) or 8 (NH_2Cl only). qPCR results of intracellular ARG treatment were only available for 266 bp and 832 bp amplicons in plots of (a) FAC, (c) ClO_2 and (d) O_3 (w/ *t*-BuOH), and only for 832 bp in (d) O_3 (w/o *t*-BuOH). Typical *CT* and *IT* ranges applied in practice when using each disinfectant to inactivate *Giardia* cysts[69] or viruses[70] are indicated by light gray and dark gray shaded areas, respectively. Kinetics-based predictions of transformation frequency losses were obtained using the model in Text S2.9 for FAC and NH_2Cl, eq 2.7 for ClO_2 and O_3, and eq 2.8 for UV, where theoretical degradation rate constants, $k_{\text{Disinfectant,Amp}}$, for the 800 bp, 900 bp and 1000 bp homologous *acfA*-flanking sequences (Scheme 2.1, Text S2.5) were calculated by means of eq 2.9, using the values of $k_{\text{Disinfectant,Specific}}$ and $k_{\text{Disinfectant,0}}$ provided in Table 2.1, and specific nucleotide contents of the homologous sequences (Table S2.1). LODs of normalized iARG copy numbers varied for treatment with different disinfectants (due to varying intracellular DNA extraction yields) and for different amplicons. The highest and lowest LOD values for the four amplicons are shown for each disinfectant. Error bars (representing one standard deviation from the mean) for qPCR copy numbers and cell survivals were obtained from duplicate experiments conducted independently, except that cell viabilities for (c) ClO_2 were only measured for one of the duplicate experiments (and are thus shown without error bars).

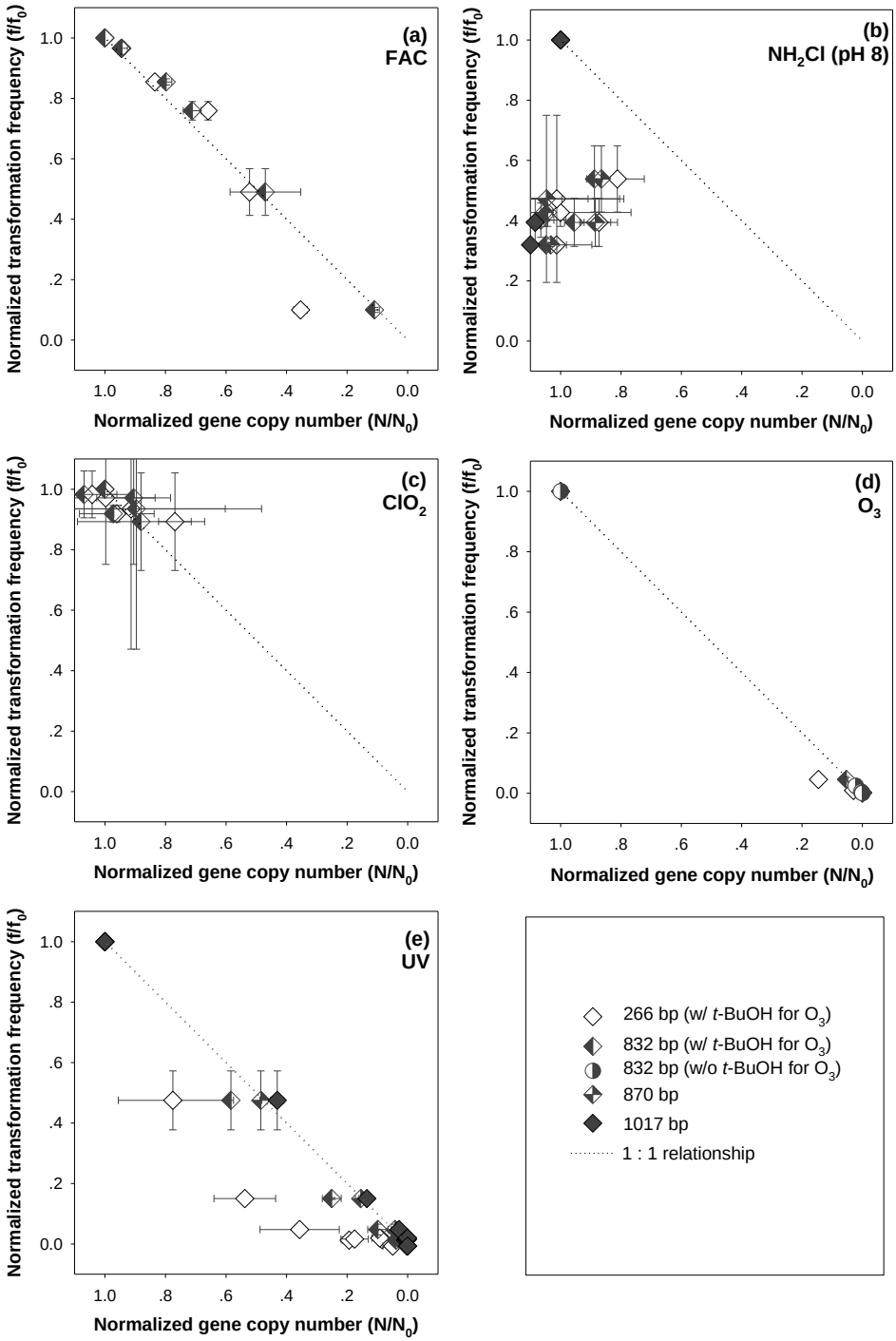

Figure S2.20. Normalized transformation frequency (f/f_0) plotted versus normalized copy number (N/N_0) of 266 bp, 832 bp, 870 bp and 1017 bp amplicons for intracellular ARG treatment with (a) FAC, (b) NH_2Cl, (c) ClO_2, (d) O_3, and (e) UV. In plots of (a) FAC, (c) ClO_2 and (d) O_3, normalized copy number measurements were only available for 266 bp and 832 bp amplicons. All data were obtained by treatment of ~1×10^6 CFU/mL of intact *B. subtilis* 1A189 cells in 10-mM phosphate buffer at pH 7 (FAC, ClO_2, O_3, and UV) or 8 (NH_2Cl only). Error bars represent one standard deviation from the mean, obtained from at least duplicate experiments. The dotted lines represent theoretical 1:1 relationships, as opposed to regression lines.

References

1. Huber, M. M.; Korhonen, S.; Ternes, T. A.; von Gunten, U., Oxidation of pharmaceuticals during water treatment with chlorine dioxide. *Water Res.* **2005,** *39*, (15), 3607-3617.
2. Bader, H.; Hoigné, J., Determination of ozone in water by the indigo method. *Water Res.* **1981,** *15*, (4), 449-456.
3. Kumar, K.; Day, R. A.; Margerum, D. W., Atom-transfer redox kinetics: General-acid-assisted oxidation of iodide by chloramines and hypochlorite. *Inorg. Chem.* **1986,** *25*, 4344-4350.
4. Hoigne, J.; Bader, H., Kinetics of reactions of chlorine dioxide (OClO) in water. 1. Rate constants for inorganic and organic compounds. *Water Res.* **1994,** *28*, (1), 45-55.
5. Hoigné, J., Chemistry of aqueous ozone and transformation of pollutants by ozonation and advanced oxidation processes. In *The Handbook of Environmental Chemistry*, Hrubec, J., Ed. Springer Verlag: Berlin, Germany, 1998; pp 83-141.
6. Allen, A. O.; Hochanadel, C.; Ghormley, J.; Davis, T., Decomposition of water and Aqueous solutions under mixed fast neutron and γ-radiation. *J. Phys. Chem.* **1952,** *56*, (5), 575-586.
7. Spizizen, J., Transformation of biochemically deficient strains of Bacillus subtilis by deoxyribonucleate. *Proc. Natl. Acad. Sci. U.S.A.* **1958,** *44*, (10), 1072-1078.
8. Yoshikawa, H.; Hirano, A.; Arakawa, T.; Shiraki, K., Mechanistic insights into protein precipitation by alcohol. *Int. J. Biol. Macromol.* **2012,** *50*, (3), 865-871.
9. Wilson, G. A.; Bott, K. F., Nutritional factors influencing the development of competence in the Bacillus subtilis transformation system. *J. Bacteriol.* **1968,** *95*, (4), 1439-1449.
10. Forootan, A.; Sjöback, R.; Björkman, J.; Sjögreen, B.; Linz, L.; Kubista, M., Methods to determine limit of detection and limit of quantification in quantitative real-time PCR (qPCR). *Biomol. Detect. Quantif.* **2017,** *12*, 1-6.
11. APHA, *Standard Methods for the Examination of Water and Wastewater*. 21 ed.; APHA, AWWA, WPCF: Washington, 2005.
12. Pinkernell, U.; Nowack, B.; Gallard, H.; Von Gunten, U., Methods for the photometric determination of reactive bromine and chlorine species with ABTS. *Water Res.* **2000,** *34*, (18), 4343-4350.
13. Lau, S. S.; Dias, R. P.; Martin-Culet, K. R.; Race, N. A.; Schammel, M. H.; Reber, K. P.; Roberts, A. L.; Sivey, J. D., 1, 3, 5-Trimethoxybenzene (TMB) as a new quencher for preserving redox-labile disinfection byproducts and for quantifying free chlorine and free bromine. *Environ. Sci.: Wat. Res. Technol.* **2018,** *4*, 926-941
14. Dodd, M. C.; Shah, A. D.; von Gunten, U.; Huang, C.-H., Interactions of Fluoroquinolone Antibacterial Agents with Aqueous Chlorine: Reaction Kinetics, Mechanisms, and Transformation Pathways. *Environ. Sci. Technol.* **2005,** *39*, (18), 7065-7076.
15. Qiang, Z.; Adams, C. D., Determination of Monochloramine Formation Rate Constants with Stopped-Flow Spectrophotometry. *Environ. Sci. Technol.* **2004,** *38*, (5), 1435-1444.
16. Canonica, S.; Meunier, L.; Von Gunten, U., Phototransformation of selected pharmaceuticals during UV treatment of drinking water. *Water Res.* **2008,** *42*, (1-2), 121-128.
17. Rahn, R. O., Potassium iodide as a chemical actinometer for 254 nm radiation: Use of iodate as an electron scavenger. *Photochem. Photobiol.* **1997,** *66*, (4), 450-455.

18. Rahn, R. O., Potassium iodide as a chemical actinometer for 254 nm radiation: Use of iodate as an electron scavenger (vol. 66, pg. 450, 1997). *Photochem. Photobiol.* **1997,** *66*, (6), 885-885.
19. Bolton, J. R.; Stefan, M. I.; Shaw, P.-S.; Lykke, K. R., Determination of the quantum yields of the potassium ferrioxalate and potassium iodide–iodate actinometers and a method for the calibration of radiometer detectors. *J. Photochem. Photobiol. A* **2011,** *222*, (1), 166-169.
20. Nick, K.; Schöler, H.; Mark, G.; Söylemez, T.; Akhlaq, M.; Schuchmann, H.; Von Sonntag, C., Degradation of some triazine herbicides by UV radiation such as used in the UV disinfection of drinking water. *J. Water Supply Res. T.* **1992,** *41*, (2), 82-87.
21. Hessler, D.; Gorenflo, V.; Frimmel, F., Degradation of Aqueous Atrazine and Metazachlor Solutions by UV and UV/H2O2—Influence of pH and Herbicide Concentration Abbau von Atrazin und Metazachlor in wäßriger Lösung durch UV und UV/H2O2—Einfluß von pH und Herbizid‐Konzentration. *Acta Hydrochim. Hydrobiol.* **1993,** *21*, (4), 209-214.
22. Goldstein, S.; Rabani, J., The ferrioxalate and iodide–iodate actinometers in the UV region. *J. Photochem. Photobiol. A* **2008,** *193*, (1), 50-55.
23. Mill, T.; Mabey, W.; Bomberger, D.; Chou, T.-W.; Hendry, D., Laboratory protocols for evaluating the fate of organic chemicals in air and water. *EPA-600/3-82-022 July 1982. Environmental Research Laboratory, Athens, GA. 329 p, 21 Fig, 46 Tab, 287 Ref. Contract/Grant* **1982**, (68-03).
24. Zepp, R. G., Quantum yields for reaction of pollutants in dilute aqueous solution. *Environ. Sci. Technol.* **1978,** *12*, (3), 327-329.
25. Montalti, M.; Credi, A.; Prodi, L.; Gandolfi, M. T., *Handbook of photochemistry*. CRC press: 2006.
26. Forsyth, J. E.; Zhou, P.; Mao, Q.; Asato, S. S.; Meschke, J. S.; Dodd, M. C., Enhanced inactivation of Bacillus subtilis spores during solar photolysis of free available chlorine. *Environ. Sci. Technol.* **2013,** *47*, (22), 12976-12984.
27. Huber, M. M.; Canonica, S.; Park, G.-Y.; Von Gunten, U., Oxidation of pharmaceuticals during ozonation and advanced oxidation processes. *Environ. Sci. Technol.* **2003,** *37*, (5), 1016-1024.
28. Dodd, M. C.; Buffle, M.-O.; Von Gunten, U., Oxidation of antibacterial molecules by aqueous ozone: moiety-specific reaction kinetics and application to ozone-based wastewater treatment. *Environ. Sci. Technol.* **2006,** *40*, (6), 1969-1977.
29. Elovitz, M. S.; von Gunten, U., Hydroxyl radical/ozone ratios during ozonation processes. I. The Rct concept. *Ozone-Sci. Eng.* **1999,** *21*, (3), 239-260.
30. Prutz, W. A., Interactions of hypochlorous acid with pyrimidine nucleotides, and secondary reactions of chlorinated pyrimidines with GSH, NADH, and other substrates. *Arch. Biochem. Biophys.* **1998,** *349*, (1), 183-191.
31. Prutz, W. A., Hypochlorous acid interactions with thiols, nucleotides, DNA, and other biological substrates. *Arch. Biochem. Biophys.* **1996,** *332*, (1), 110-120.
32. Hawkins, C. L.; Davies, M. J., Hypochlorite-Induced Damage to Nucleosides: Formation of Chloramines and Nitrogen-Centered Radicals. *Chem. Res. Toxicol.* **2001,** *14*, (8), 1071-1081.
33. Evans, M. D.; Cooke, M. S., *Oxidative damage to nucleic acids*. Springer Science & Business Media: 2007.

34. Henderson, J. P.; Byun, J.; Heinecke, J. W., Chlorination of nucleobases, RNA and DNA by myeloperoxidase: a pathway for cytotoxicity and mutagenesis by activated phagocytes. *Redox Rep.* **1999,** *4*, (6), 319-320.
35. Whiteman, M.; Jenner, A.; Halliwell, B., 8-Chloroadenine: a novel product formed from hypochlorous acid-induced damage to calf thymus DNA. *Biomarkers* **1999,** *4*, (4), 303-310.
36. Whiteman, M.; Jenner, A.; Halliwell, B., Hypochlorous Acid-Induced Base Modifications in Isolated Calf Thymus DNA. *Chem. Res. Toxicol.* **1997,** *10*, 1240-1246.
37. Filaderli, H. A. Chlorination of Specific Organic Compounds in Water Treatment. Department of Civil Engineering, Imperial College, 1989.
38. Whiteman, M.; Hong, H. S.; Jenner, A.; Halliwell, B., Loss of oxidized and chlorinated bases in DNA treated with reactive oxygen species: implications for assessment of oxidative damage in vivo. *Biochem. Biophys. Res. Commun.* **2002,** *296*, (4), 883-889.
39. Pattison, D. I.; Davies, M. J.; Asmus, K.-D., Absolute rate constants for the formation of nitrogen-centred radicals from chloramines/amides and their reactions with antioxidants. *J. Chem. Soc., Perkin Trans. 2* **2002**, (8), 1461-1467.
40. Hawkins, C. L.; Davies, M. J., Hypochlorite-induced damage to DNA, RNA, and polynucleotides: formation of chloramines and nitrogen-centered radicals. *Chem. Res. Toxicol.* **2002,** *15*, (1), 83-92.
41. Hu, Y.; Xie, G.; Stanbury, D. M., Oxidations at sulfur centers by aqueous hypochlorous acid and hypochlorite: Cl+ versus O atom transfer. *Inorg. Chem.* **2017,** *56*, (7), 4047-4056.
42. Pecson, B. M.; Ackermann, M.; Kohn, T., Framework for Using Quantitative PCR as a Nonculture Based Method To Estimate Virus Infectivity. *Environ. Sci. Technol.* **2011,** *45*, (6), 2257-2263.
43. Robertson, R. M.; Laib, S.; Smith, D. E., Diffusion of isolated DNA molecules: dependence on length and topology. *Proc. Natl. Acad. Sci. U.S.A.* **2006,** *103*, (19), 7310-7314.
44. Fukatsu, M.; Kurata, M., Hydrodynamic Properties of Flexible ‐ Ring Macromolecules. *J. Chem. Phys.* **1966,** *44*, (12), 4539-4545.
45. Masuda, T.; Shinohara, H.; Eda, M.; Kondo, M., Reactivity of nucleotides and polynucleotides toward hydroxyl radical in aqueous solution. *J. Radiat. Res.* **1980,** *21*, (2), 173-179.
46. Benjamin, M. M.; Lawler, D. F., *Water quality engineering: Physical/chemical treatment processes*. John Wiley & Sons: 2013.
47. Yoon, Y.; Chung, H. J.; Di, D. Y. W.; Dodd, M. C.; Hur, H.-G.; Lee, Y., Inactivation efficiency of plasmid-encoded antibiotic resistance genes during water treatment with chlorine, UV, and UV/H2O2. *Water Res.* **2017,** *123*, 783-793.
48. Prazeres, D., Prediction of diffusion coefficients of plasmids. *Biotechnol. Bioeng.* **2008,** *99*, (4), 1040-1044.
49. Ke, F.; Luu, Y. K.; Hadjiargyrou, M.; Liang, D., Characterizing DNA condensation and conformational changes in organic solvents. *PLoS One* **2010,** *5*, (10), e13308.
50. Sugiyama, H.; Saito, I., Theoretical studies of GG-specific photocleavage of DNA via electron transfer: significant lowering of ionization potential and 5 ‘-localization of HOMO of stacked GG bases in B-Form DNA. *J. Am. Chem. Soc.* **1996,** *118*, (30), 7063-7068.
51. Fukuzumi, S.; Miyao, H.; Ohkubo, K.; Suenobu, T., Electron-transfer oxidation properties of DNA bases and DNA oligomers. *J. Phys. Chem. A* **2005,** *109*, (15), 3285-3294.

52. Joy, A.; Ghosh, A. K.; Schuster, G. B., One-electron oxidation of DNA oligomers that lack guanine: Reaction and strand cleavage at remote thymines by long-distance radical cation hopping. *J. Am. Chem. Soc.* **2006,** *128*, (16), 5346-5347.
53. Ghosh, A.; Joy, A.; Schuster, G. B.; Douki, T.; Cadet, J., Selective one-electron oxidation of duplex DNA oligomers: reaction at thymines. *Org. Biomol. Chem.* **2008,** *6*, (5), 916-928.
54. Joseph, J.; Schuster, G. B., One-electron oxidation of DNA: reaction at thymine. *Chem. Commun.* **2010,** *46*, (42), 7872-7878.
55. Yoon, Y.; Dodd, M. C.; Lee, Y., Elimination of transforming activity and gene degradation during UV and UV/H2O2 treatment of plasmid-encoded antibiotic resistance genes. *Environ. Sci.: Wat. Res. Technol.* **2018,** *4*, 1239-1251.
56. Douki, T., Low ionic strength reduces cytosine photoreactivity in UVC-irradiated isolated DNA. *Photoch. Photobio. Sci.* **2006,** *5*, (11), 1045-1051.
57. Douki, T., Effect of denaturation on the photochemistry of pyrimidine bases in isolated DNA. *J. Photochem. Photobiol. B* **2006,** *82*, (1), 45-52.
58. Tataurov, A. V.; You, Y.; Owczarzy, R., Predicting ultraviolet spectrum of single stranded and double stranded deoxyribonucleic acids. *Biophys. Chem.* **2008,** *133*, (1-3), 66-70.
59. Patrick, M. H., Studies on Thymine-derived UV photoproducts in DNA —I. Formation and Biological Role of Pyrimidine Adducts in DNA. *Photochem. Photobiol.* **1977,** *25*, (4), 357-372.
60. Garces, F.; Davila, C. J. P.; photobiology, Alterations in DNA irradiated with ultraviolet radiation—I. The formation process of cyclobutylpyrimidine dimers: cross sections, action spectra and quantum yields. **1982,** *35*, (1), 9-16.
61. Görner, H., New trends in photobiology: Photochemistry of DNA and related biomolecules: Quantum yields and consequences of photoionization. *J. Photochem. Photobiol. B* **1994,** *26*, (2), 117-139.
62. Shih, K. L.; Lederberg, J., Effects of chloramine on Bacillus subtilis deoxyribonucleic acid. *J. Bacteriol.* **1976,** *125*, (3), 934-945.
63. Roller, S. D.; Olivieri, V. P.; Kawata, K., Mode of bacterial inactivation by chlorine dioxide. *Water Res.* **1980,** *14*, (6), 635-641.
64. Czekalski, N.; Imminger, S.; Salhi, E.; Veljkovic, M.; Kleffel, K.; Drissner, D.; Hammes, F.; Bürgmann, H.; Von Gunten, U., Inactivation of antibiotic resistant bacteria and resistance genes by ozone: from laboratory experiments to full-scale wastewater treatment. *Environ. Sci. Technol.* **2016,** *50*, (21), 11862-11871.
65. Theruvathu, J. A.; Flyunt, R.; Aravindakumar, C. T.; von Sonntag, C., Rate constants of ozone reactions with DNA, its constituents, and related compounds. *J. Chem. Soc., Perkin Trans. 2* **2001**, (3), 269-274.
66. Chang, P. H.; Juhrend, B.; Olson, T. M.; Marrs, C. F.; Wigginton, K. R., Degradation of extracellular antibiotic resistance genes with UV254 treatment. *Environ. Sci. Technol.* **2017,** *51*, (11), 6185-6192.
67. McKinney, C. W.; Pruden, A., Ultraviolet disinfection of antibiotic resistant bacteria and their antibiotic resistance genes in water and wastewater. *Environ. Sci. Technol.* **2012,** *46*, (24), 13393-13400.
68. Udovičić, L.; Mark, F.; Bothe, E., Yields of single-strand breaks in double-stranded calf thymus DNA irradiated in aqueous solution in the presence of oxygen and scavengers. *Radiat. Res.* **1994,** *140*, (2), 166-171.

69. EPA *Disinfection profiling and benchmarking guidance manual*; United States Environmental Protection Agency: Office of Water. Washington, DC., 1999.
70. *Ultraviolet Disinfection Guidance Manual for the Final Long Term 2 Enhanced Surface Water Treatment Rule*; United States Environmental Protection Agency: Office of Water. Washington, DC, 2006.

Chapter 3. Validation and Application of a Kinetics-Based Modeling Approach to Predict Antibiotic Resistance Gene Degradation during UV- and Chlorine-Based Wastewater Disinfection Processes: from Bench-Scale to Full-Scale

He, H.; Wu, S.J.; Fang, X.; Anderson, A.K.; Roberts, M.C.; Lee, Y.; Dodd, M. C.. *In preparation.*

ABSTRACT

This study investigated antibiotic resistance gene (ARG) degradation profiles in wastewater matrixes during bench- and full-scale treatment with two commonly-applied disinfectants – UV and chlorine – with the latter (dosed as NaOCl) maintained as free available chlorine (FAC) in nitrified/denitrified (low-ammonia) wastewater, while completely converted into monochloramine (NH_2Cl) in non-nitrified (high-ammonia) wastewater. A suite of (clinically-relevant) ARGs – including *blt*, *mec*A, *van*A, *tet*(A), *amp*C, bla_{NDM}, and bla_{KPC} – were employed as disinfection targets, in addition to a "ladder" of variable-length 16S rRNA gene segments – used here as surrogates for total bacterial DNA. Their associated ARB strains (including *Bacillus subtilis*, *Staphylococcus aureus*, *Enterococcus faecium*, *Escherichia coli*, *Pseudomonas aeruginosa*, and *Klebsiella pneumoniae*) exhibited variable inactivation kinetics toward each disinfectant, which all outpaced degradation of intracellular ARG/16S rRNA gene amplicons. A kinetics-based quantitative framework was validated and utilized to predict rate constants for degradation of 21 separate ARG/16S rRNA gene amplicons (ranging from 143-1509 bp) by each disinfectant based on the amplicons' sequences, and to predict ARG/16S rRNA gene degradation kinetics during treatment with each disinfectant. Degradation of these amplicons by UV and FAC could be accurately predicted up to 1–2-log_{10} losses during bench-scale treatment of different reaction matrixes (clean buffers or wastewaters), whereas treatment with NH_2Cl yielded no degradation even over extended exposure ranges (also in agreement with model predictions). Bench-scale experimental and modeling results supported observations of ARG fate during full-scale disinfection at local WWTPs, where UV provided ~1-log_{10} ARG elimination, and chlorination of high-ammonia wastewater dominated by NH_2Cl yielded no significant ARG removal.

3.1 INTRODUCTION

Since the first half of the 20th century, antibiotic resistance has been a growing challenge in public-health and environmental sectors. Studies over the past decades have confirmed that the increase of antibiotic resistance gene (ARG) levels in aquatic-associated environments is intimately linked with the increase in antibiotic resistance gene (ARB) proportions relative to total bacterial populations in clinical isolates.[1, 2] Recent studies have highlighted that aquatic environments serve as recipients, reservoirs, and sources of ARGs of clinical concern, and at the same time receive inputs of antibiotics from wastewater treatment plants (WWTPs), livestock operations, aquaculture, and industry, which contribute to selection pressure for elevation of resistance levels in native bacteria.[3-6] It is apparent that ARB and ARGs can be transported amongst various aquatic systems (including those directly connected with healthcare facilities) via multiple pathways, considering the interconnectivity of these systems driven by natural and urban water cycling.[7] Moreover, ARB and ARGs are able to propagate and disseminate amongst aquatic environments and clinical settings through vertical (i.e., cell division) and horizontal gene transfer (HGT – including conjugation, transduction, and natural transformation).[7]

Numerous studies over the past decade have investigated occurrences of ARB/ARGs in different compartments of WWTPs by applying cultivation-based approaches and/or molecular tools such as (quantitative) polymerase chain reaction ((q)PCR) and metagenomic analyses,[8-11] which have shown that **(1)** WWTPs play an important role as environmental "hot spots" in promoting antibiotic resistance dissemination, and **(2)** ARGs can persist even after effective ARB inactivation by disinfection processes and be released through discharge of final effluents, potentially resulting in HGT events (e.g., natural transformation) in downstream aquatic environments.[12, 13] Therefore, besides ARB inactivation, recent attention has also been

increasingly paid to ARG elimination during bench- or full-scale disinfection of wastewaters (and associated sludges) with such disinfectants as 254 nm UV light (henceforth referred to as UV),[14-21] chlorine[14, 16, 17, 19, 21-25], and ozone (O_3).[19, 20, 25, 26] Conflicting results have been reported on the effectiveness of chlorination in eliminating ARGs (and their biological activities) in wastewater matrixes,[14, 16, 17, 22-24] which requires further investigation and fundamental explanation. Only a limited number of the recent studies have explicitly quantified ARG degradation kinetics during bench-scale wastewater disinfection processes or derived fundamental kinetics parameters (e.g., rate constants, disinfectant exposures) that can be used to enable modeling and/or prediction of full-scale treatment efficiencies.[15, 25-27] Further, fewer of these kinetics studies employed ARGs harbored by clinically-relevant pathogens as disinfection targets,[15, 27] leading to a relatively weak connection of (waste)water treatment researches to public health issues.

In this context, this study was undertaken to investigate ARG degradation kinetics in wastewater matrixes during bench/full-scale disinfection by UV and chlorine, the two most-commonly applied disinfectants in wastewater treatment. A suite of ARGs – including the *blt* gene harbored by non-pathogenic *Bacillus subtilis*, and the pathogen-related ARGs *mec*A, *van*A, *tet*(A), *amp*C, bla_{NDM}, and bla_{KPC} – were employed as disinfection targets, in addition to a "ladder" of variable-length 16S rRNA gene segments as surrogates for total bacterial DNA, either deriving from the model ARB strains or from native biomass in wastewaters. The ARGs of *blt*, *mec*A, *van*A, *tet*(A), and *amp*C, in association with their host ARB strains, were selected as model targets on account of their use in prior disinfection studies,[15, 27, 28] in order to allow inter-study/inter-laboratory comparisons; bla_{NDM} and bla_{KPC} were also investigated here because of their significance in clinical concerns[29] and expanding occurrence in aquatic environments.[24, 30-32]

Water quality parameters such as nutrient levels (e.g, ammonia), suspended solids, and UV transmittance were evaluated with respect to their impact on ARG degradation kinetics. A quantitative framework developed in previous work[28] was utilized to model degradation kinetics of ARGs or 16S rRNA gene segments by using rate constants predicted from their specific nucleotide sequences. The predicted degradation kinetics were then compared with measurements in bench-scale experiments for model validation. Results of the bench-scale kinetics studies were utilized to explain efficacies of ARG elimination by full-scale UV-and chlorine-based disinfection processes at two regional WWTPs.

3.2 MATERIALS AND METHODS

3.2.1 *Chemical reagents and growth media.*

All chemical reagents were purchased from Sigma-Aldrich, and were of molecular biology grade purity, or reagent grade purity if the former was not available. The working stocks of chemical reagents (except disinfectants) used in bacteria culturing, disinfection treatment and DNA extraction were sterilized either through autoclaving or 0.2 μm membrane filtration if not amenable to autoclaving, as in the case of antibiotics and redox reactive reagents (e.g., ammonium chloride (NH_4Cl), sodium thiosulfate ($Na_2S_2O_3$), etc.). Free available chlorine (FAC) was prepared by dilution of an aqueous ~5% (w/w) sodium hypochlorite (NaOCl) stock. Monochloramine (NH_2Cl) was pre-formed by mixing NH_4Cl with FAC at a 2:1 molar ratio at pH 8.5 as previously described.[28] FAC and NH_2Cl stocks were standardized spectrophotometrically at 292 nm (ε = 350 $M^{-1}cm^{-1}$) and 243 nm (ε = 461 $M^{-1}cm^{-1}$), respectively.[33] Broth and agar media were all purchased from BD Difco™. Selective media were prepared by adding required

antibiotics (see Table S3.1) into autoclaved broth or (liquefied) agar after cooling to ~50 °C to avoid heat destruction of the antibiotics.

3.2.2 *Bacterial strains and genes.*

Disinfection target ARGs and host ARB strains. The ARGs *blt*, *mec*A, *van*A, *tet*(A), *amp*C, bla_{NDM}, and bla_{KPC} were selected as disinfection targets in bench- or full-scale wastewater disinfection treatment. The host ARB strains for *blt*, *mec*A, *van*A, *tet*(A), and *amp*C – *Bacillus subtilis* 1A189, methicillin-resistant *Staphylococcus aureus* (MRSA, ATCC BAA-1556), vancomycin-resistant *Enterococci faecium* (VRE, ATCC 700221), *Escherichia coli* SMS-3-5 (ATCC BAA-1743), and *Pseudomonas aeruginosa* O1 (PAO1, ATCC 47085), respectively – were adopted as model bacteria for use in bench-scale disinfection experiments investigating degradation of intracellular ARGs, whereas bla_{NDM} and bla_{KPC} were only monitored as targets in full-scale disinfection processes due to the expensive cultivation cost of their host strains, *Klebsiella pneumoniae* 1.53 and ATCC BAA-1705, respectively.

Internal standards. Two ARB strains and their associated genes were used as internal standards to evaluate DNA recoveries in full-scale wastewater sample extractions. One was *B. subtilis* 1A189 carrying *blt*, and the other was *E. coli* ECE228, an NEB 5*α* strain cloned with the *pCFPamy* plasmid carrying the *cfp* gene (encoding cyan fluorescent protein) fused with the upstream *amyE* gene of *B. subtilis*.[34] Detailed information of the above strains and associated genes (including strain resources, growth media, gene locations, resistance mechanisms, etc.) is provided in Supporting Information (SI) Table S3.1.

3.2.3 *DNA extraction.*

A FastDNA Spin Kit (MP Biomedicals) was used to perform DNA extractions in most intracellular ARG experiments according to the manufacturer's protocol, optimized with additional steps of cell lysis and DNA purification. Alternatively, a modified phenol-chloroform-isoamyl alcohol extraction method[28, 35] was applied to extract high-purity DNA for use in all extracellular ARG experiments, or when the former method could not provide satisfactory extraction yields in intracellular experiments (i.e., in the case of FAC disinfection of ARB strains). Details of the two above methods and their application in this study are provided in SI Text S3.1.

3.2.4 *Quantitative polymerase chain reaction (qPCR).*

qPCR assays were performed with SsoFast™ EvaGreen® Supermix[15] (Bio-Rad, Hercules, CA) on an Eppendorf RealPlex[4] Mastercycler (Hauppauge, NY) or a Roche LightCycler® 96 Instrument (Pleasanton, CA), to analyze copy numbers of ARGs, 16S rRNA gene segments, and internal standard genes in DNA extracts obtained from bench/full-scale disinfection treatment. Primer pairs were either obtained from the literature or designed herein through primer-BLASTs based on the gene sequences, to target **(1)** varying-length *blt* amplicons (266 bp, 832 bp, 870 bp, and 1017 bp) as previously described,[28] and long amplicons of the other pathogen-related ARGs, including *mec*A 1018 bp,[15, 36, 37] *van*A 1030 bp,[15, 38] *tet*(A) 1054 bp,[15, 39, 40] *amp*C 1006 bp,[15, 41, 42] bla_{NDM} 807 bp,[24] and bla_{KPC} 805 bp; **(2)** a ladder of bacterial 16S rRNA gene amplicons (142 bp, 534 bp, 734 bp, 1068 bp, and 1509 bp on average for the five model ARB strains used in bench-scale experiments),[43-45] which served as surrogates for total bacterial DNA (Note the sequences and lengths of the 16S rRNA gene segments vary for different strains, as shown in Tables S3.2-S3.3); and **(3)** two internal standard genes – a 1017 bp *blt* amplicon on

the *B. subtilis* 1A189 chromosome (as above) and a 663 bp *cfpamy* amplicon (encompassing the ligation site of *cfp* and *amyE* front) on the *E. coli* ECE228 *pCFPamy* plasmid. Sequences, annealing temperatures, and locations on the targeted genes are displayed for the primer pairs in SI Table S3.2. Nucleotide contents of the qPCR amplicons, including numbers of AT, GC, and AT+GC bps per amplicon, as well as numbers of 5'-T/C-3' doublets (designated as 5'-bipyrimidine-3' previously,[28] with T/C = bipyrimidine = TT, TC, CT, or CC) per amplicon, are provided in SI Table S3.3. qPCR assay protocols (including standard preparation, temperature profiles, and LOD & LOQ determination) have been described previously for the four *blt* amplicons (266-1017 bp)[28] and in SI Text S3.2 for the others.

3.2.5 *Other analyses.*

Double-stranded DNA (dsDNA) concentrations were measured by Hoechst 33258 fluorescence assay, using a DNA Quantitation Kit (Bio-Rad). qPCR products of DNA extracts from full-scale wastewater samples were verified by agarose gel electrophoresis, and sent to Eurofin Genomics for Sanger sequencing to confirm their identities. Residual viabilities of ARB cells treated in bench-scale wastewater disinfection experiments were measured by spot-titering[46] on agar plates (with selective agent if required) (see Table S3.1), which were incubated in the dark at 37 °C overnight until colonies were visible.

3.2.6 *Full-scale disinfection treatment: wastewater sampling and DNA recovery yield.*

Pre and post-disinfection secondary effluents were collected from two local wastewater treatment plants (WWTPs, named as 1 and 2 here) in WA, applying chlorine and UV as disinfectant, respectively. WWTP 1 provides additional nitrification/denitrification processes applied through aeration and anoxic basins, respectively, with the result that the ammonia level

of its secondary effluent (< 0.4 mg N/L) is much lower than that of WWTP 2 (~27 mg N/L), where only traditional aerated activated sludge treatment is employed. Other water quality parameters (e.g., pH, dissolved organic carbon (DOC), absorbance at 254 nm (Abs_{254}), alkalinity, bromide concentration, etc.) for the pre-disinfection effluents from each WWTP are provided in SI Table S3.4. For each secondary effluent, a composite sample was collected by obtaining an equal volume (~300 mL) of effluent every 10 minutes over the span of 1 hour. Samples were transported to the laboratory on ice, stored at 4 °C, and processed for DNA extraction within 24 hours. Prior to processing for DNA extraction, intact cells of the two internal standards, *B. subtilis* 1A189 and *E. coli* ECE228, were dosed to the wastewaters to evaluate DNA recovery yields. The wastewaters (spiked with internal standards) were then concentrated through filtration with 0.2 μm polycarbonate membranes (Whatman, NJ) to recover biomass containing intracellular and cell/particle-associated DNA (noting that extracellular DNA could have passed through membranes).[10] Concentrated wastewaters were transferred to lysis buffer contained in extraction tubes obtained from the FastDNA Spin Kit, and stored at -80 °C until extraction. Detailed procedures of internal standard doses and determination of DNA recovery yields are provided in SI Text S3.3, and the resulting recovery yields for the full-scale samples in SI Table S3.5. Actual levels of ARG and 16S rRNA gene amplicons (in units of copies/mL) in pre- and post-disinfection secondary effluents from each WWTP were back-calculated by dividing by fractional DNA recoveries (see Text S3.3).

3.2.7 *Bench-scale disinfection treatment. Treatment of extra- and intracellular ARGs (eARGs and iARGs) in phosphate buffers.*

DNA carrying the ARGs *blt*, *mec*A, *van*A, *tet*(A), and *amp*C genes was pre-isolated from vegetative cells of *B. subtilis* 1A189, MRSA, VRE, *E. coli* SMS-3-5 and PAO1, respectively,

according to the phenol-chloroform-isoamyl alcohol method described above. The isolated DNA was then dosed to 10 mM phosphate buffer (PB) at 1 mg/L as double-stranded DNA (dsDNA) and exposed to UV light, FAC, or *pre-formed* NH_2Cl up to and beyond exposures typical of (waste)water treatment, as previously described.[28] Similar intracellular experiments were conducted by treating vegetative cells of each strain, combined or individually, at total initial cell concentrations of ~10^7 CFU/mL for FAC and NH_2Cl or ≤ ~10^6 CFU/mL for UV (to ensure >95% transmittance), also in 10 mM PB solutions, but in larger volumes.

3.2.8 *Treatment of iARGs and native bacterial DNA in wastewaters.*

The above iARG experiments by UV, FAC, and NH_2Cl were also conducted using pre-disinfection secondary effluents collected from WWTPs 1 or 2 buffered with 10 mM PB, with or without suspended solids (i.e., *unfiltered* or 0.2-μm *filtered*). For FAC and NH_2Cl, disinfection treatments were initiated by dosing NaOCl into samples of the effluents from WWTPs 1 and 2 (already spiked with ARB cells) at 10–16 mg Cl_2/L (i.e., at [FAC]:[NH_3-N] ≥ 1.5) for WWTP 1 to ensure FAC residual over the treatment period and at 2–3 mg/L mg Cl_2/L (i.e., at [FAC]:[NH_3-N] << 1.5) for WWTP 2 to yield *in-situ formation* of an equivalent concentration of NH_2Cl (by exceeding the chlorination breakpoint or not) (see SI Text S3.4). Treatments were also conducted by UV irradiation or chlorination of *unfiltered* pre-disinfection effluents as above, but without spiking ARB cells, to assess degradation kinetics of native bacterial DNA in wastewaters. More details of reactor configurations and experimental setups of the above bench-scale experiments treating eARGs, iARGs, or native biomasses are provided in SI Text S3.4.

At pre-determined time intervals, samples were quenched with excess $Na_2S_2O_3$ (> 20× molar ratio) for FAC and NH_2Cl experiments. The treated model ARB and/or native biomasses obtained from bench-scale experiments were recovered on 0.2 μm polycarbonate membrane

filters, and then processed with DNA extraction using either the FastDNA Spin Kit or the phenol-chloroform-isoamyl alcohol method (see Text S3.1). A separate set of experiments was conducted by treating vegetative cells of each strain *individually* in *filtered* wastewaters without pre-concentration and recovery of cells by filtration, to assess survival of each model ARB strain during treatment with each disinfectant.

All bench-scale experiments were buffered at pH 7 (for UV and FAC) or 8 (for NH_2Cl), and performed in at least duplicate at 25±1 °C (UV) or 20±1 °C (FAC and NH_2Cl). Normalized gene copy numbers (N/N_0) or normalized cell viabilities (X/X_0) were calculated as gene copy number or ARB cell viability of a given sample divided by that of a corresponding untreated control, respectively.

Scheme S3.1 provides an overview of the major procedures of wastewater sampling from local WWTPs and bench-scale disinfection experiments described above, plus the subsequent steps of DNA extraction and analyses.

3.2.9 *Determination of disinfectant exposures.*

Residual concentrations of FAC, NH_2Cl, and total available chorine (TAC) were monitored by means of *N*,*N*-diethyl-*p*-phenylenediamine colorimetry over the treatment period.[47] Cumulative integrated exposures (or *CT* values, in mg/L•min) for chlorine species were calculated as $\int_0^t [\text{Disinfectant}]\,dt$. Fluence rates ($I$, in mW/cm^2) of 254 nm UV light were measured using atrazine actinometry.[48] UV fluences (or *IT* values, in mJ/cm^2) were determined as $I \times t$ (for clean buffers) or $I \times t \times$ WF (for *filtered* or *unfiltered* wastewaters), where WF (water factor) was calculated as $(1-10^{-Abs_{254}\cdot l})/(Abs_{254}\cdot l\cdot \ln 10)$,[49] using Abs_{254} (cm^{-1}) of the wastewater

and pathlength (l in cm) of the quartz tubes used with the "merry-go-round" reactor apparatus in experiments (previously measured as 1.23 cm).[28]

3.2.10 *Statistical Analysis.*

Data from independent replicate experiments were pooled in order to perform least-squares linear or nonlinear regressions using Microsoft Excel 365 (through LINEST function or SOLVER, respectively), for determining second-order or fluence-based first-order rate constants (and associated uncertainties) for degradation of each amplicon by each disinfectant. Weighted linear regressions[50] were performed for measured amplicon rate constants (carrying uncertainties) versus amplicon nucleotide contents in Excel spreadsheets as previously described.[28] Mean values of paired datasets (e.g., ARG levels in pre- and post-disinfection effluents from WWTPs) were compared using two-tailed t-tests with $p < 0.05$ and a null hypothesis of no significant difference existing between means of the two datasets.

3.3 RESULTS AND DISCUSSION

3.3.1 *Validation and improvement of kinetic models for DNA segment degradation by UV, FAC, and NH_2Cl using an expanded array of ARG/16S rRNA gene amplicons: determination of kinetics and rate constants.*

Prior work by the authors has evaluated degradation of four varying-length *blt* amplicons (266-1017 bp) carried on *B. subtilis* 1A189 chromosomal DNA as model ARG segments, to investigate the mechanisms and kinetics of DNA segment degradation by various disinfectants, including UV light, FAC, and NH_2Cl.[28] It has been found that DNA segment degradation (as measured by qPCR) during UV irradiation follows fluence-based first-order kinetics at UV fluences up to ~50 mJ/cm^2, characterized by an apparent rate constant $k_{UV,Amp,app}$ (previously

designated as $k_{UV,Amp}$), where the normalized residual gene copy number $\ln(N/N_0)$ during UV irradiation is linearly related to *IT* according to (eqs 3.1-3.2),

$$Amp + UV \xrightarrow{k_{UV,Amp,app}} product \quad \text{(eq 3.1)}$$

$$\ln(N/N_0) = -k_{UV,Amp,app} \times IT \quad \text{(eq 3.2)}$$

DNA segment degradation only adheres to the above linear kinetic model (eqs 3.1-3.2) up to UV fluences of ~50 mJ/cm^2, beyond which moderate to significant tailing was observed in the kinetics – potentially due to photoreversal of cyclobutane pyrimidine dimers (CPDs), the primary UV-induced lesions.[51] To address this tailing effect, a modified kinetics model was proposed in a later study by Choi et el. (2020)[27] using *mec*A as model gene, that DNA segment degradation by UV consists of **(i)** formation of photo-reversible CPD lesions, characterized by $k_{UV,Amp\text{-}CPD,f}$ and $k_{UV,single\text{-}CPD,r}$ for the forward and reverse reactions (eq 3.3), respectively, and **(ii)** formation of irreversible lesions primarily as (6-4) photo-products (6-4PPs), characterized by $k_{UV,single6\text{-}4PP}$ (eq 3.4), with each elementary reaction following fluence-based first-order kinetics.

$$Amp + UV \underset{k_{UV,singleCPD,r}}{\overset{k_{UV,Amp\text{-}CPD,f}}{\rightleftharpoons}} Amp_{CPD} \quad \text{(eq 3.3)}$$

$$Amp + UV \xrightarrow{k_{UV,\,single6\text{-}4PP}} Amp_{6\text{-}4PP} \quad \text{(eq 3.4)}$$

In regards to FAC and NH_2Cl, DNA segment degradation measured by qPCR was found to follow accelerating kinetics with increasing disinfectant exposures, which has previously been hypothesized to involve a two-step sequence of **(i)** reversible N-chlorination, forming N-chlorinated amplicons ($Amp_{N\text{-}Cl}$) – non-detectable by qPCR after sample quenching with $Na_2S_3O_3$, followed by **(ii)** irreversible C-chlorination of the N-chlorinated base pairs (N-Cl bps), forming stable halogenated products detectable by qPCR,[27, 28] with each of the sequential

reactions following second-order kinetics characterized by $k_{\text{FAC or NH}_2\text{Cl,Amp}}$ and $k_{\text{FAC or NH}_2\text{Cl,N-Cl bp}}$, respectively (eqs 3.5-3.6).

$$\text{Amp} + \text{FAC/NH}_2\text{Cl} \underset{\text{Na}_2\text{S}_2\text{O}_3}{\overset{k_{\text{FAC or NH}_2\text{Cl,Amp}}}{\rightleftharpoons}} \text{Amp}_{\text{N-Cl}} \quad \text{(eq 3.5)}$$

$$\text{Amp}_{\text{N-Cl}} + \text{FAC/NH}_2\text{Cl} \xrightarrow{k_{\text{FAC or NH}_2\text{Cl,N-Cl bp}}} \text{product} \quad \text{(eq 3.6)}$$

In this study, the aforementioned degradation kinetics of DNA segments toward UV, FAC, and NH_2Cl have been verified using a larger array of qPCR amplicons, targeting various chromosomal or plasmid-borne ARGs (*mec*A 1018 bp, *van*A 1030 bp, *tet*(A) 1054 bp, and *amp*C 1006 bp) plus varying lengths of 16S rRNA gene segments (142-1509 bp). The results are plotted as $\ln(N/N_0)$ versus disinfectant exposures (*IT* or *CT* values) in Figures S3.1-S3.3 for UV, Figure S3.4 for FAC, and Figures S3.5-S3.6 for NH_2Cl. Rate constants for degradation of selected *blt* amplicons by each disinfectant were also re-measured as self-validation(s) for each disinfectant, and found to be in generally good agreement with prior values. For UV, the rate constants of all four *blt* amplicons were re-measured and found to be ~20–35% higher than the previous results (Figures S3.1 and S3.2; see further discussion in Text S3.5). For FAC and NH_2Cl, degradation kinetics of the *blt* gene were within ±5% of the previous results,[28] as verified by *blt* 1017 bp (Figures S3.4 and S3.5, respectively).

Procedures used to measure rate constants for degradation of the ARG/16S rRNA amplicons (including the four *blt* amplicons if necessary) by each disinfectant are described in detail in SI Text S3.5 and Figure S3.1-S3.7. The resulting values with standard errors are summarized in Table 3.1. Briefly, the apparent rate constant $k_{\text{UV,Amp,}app}$ for each amplicon was determined according to eq 3.2 through linear regression of data within *IT* of ~50 mJ/cm^2 (Figure S3.1). Rate constants of $k_{\text{UV,Amp-CPD,}f}$ (variable to each amplicon) and $k_{\text{UV,single-CPD,}r}$ (a constant specific to photoreversal of each single CPD lesion) were determined by means of numerical

solution of eqs 3.3-3.4 via non-linear regressions (Figure S3.2), with $k_{UV,single\text{-}6,4PPs}$ (a constant specific to formation of each single 6,4-PP) pre-determined via linear regression of data for selected amplicons at extended fluence range ($\geq$ ~150 mJ/cm^2) (Figure S3.3) according to Choi et al. (2020).[27] For FAC (Figure S3.4) and NH_2Cl (Figure S3.5), the amplicon-specific rate constants, $k_{FAC\text{ or }NH_2Cl,Amp}$, were determined through numerical solution of eqs 3.5-3.6 via non-linear regression, assuming $k_{FAC\text{ or }NH_2Cl,N\text{-}Cl\text{ bp}}$ is a constant specific to each individual N-chlorinated base pair (N-Cl bp), as previously described.[28] For FAC, the previously-determined $k_{FAC,N\text{-}Cl\text{ bp}}$ is still in use here to solve $k_{FAC,Amp}$, while for NH_2Cl, $k_{NH_2Cl,N\text{-}Cl\text{ bp}}$ was re-determined using data for the 142 bp 16S rRNA gene amplicon to improve the model accuracy (Figures S3.6-S3.7). The rate constants for the previously-investigated *blt* amplicons (266-1017 bp) were also selectively re-determined as appropriate (e.g., for $k_{UV,Amp,app}$ and $k_{NH_2Cl,Amp}$).

3.3.2 *Validation and improvement of kinetic models for DNA segment degradation by UV, FAC, and NH_2Cl using an expanded array of ARG/16S rRNA gene amplicons: dependence of rate constants on amplicon nucleotide content*

Prior work using the *blt* gene as a model ARG has demonstrated that the reactivity of DNA sequences toward UV, FAC, and NH_2Cl strongly depends on the DNA sequences' lengths and/or nucleotide contents, as can be described according to a linear model (eq 3.7),

$$k_{Disinfectant,Amp} = k_{Disinfectant,Specific} \cdot (\text{mol X/mol Amp}) + k_{Disinfecant,0} \quad \text{(eq 3.7)}$$

where mol X/mol Amp represents the molar content of type X nucleotide bps or doublets per mole amplicon (with X = 5'-TT-3' for UV, or AT+GC bp for FAC and NH_2Cl); $k_{Disinfectant,Specific}$ characterizes DNA segment reactivity toward a given disinfectant normalized to specific nucleotide content; and $k_{Disinfectant,0}$ represents residual ARG reactivity not fully accounted for by the single-parameter linear model (potentially due to reactions occurring at unidentified

Table 3.1. Kinetics parameters (as mean ± standard error) for degradation of ARG/16S rRNA gene amplicons toward UV, FAC, and NH_2Cl [a]

qPCR amplicons of ARGs/16S rRNA gene	Host ARB strain for eDNA isolation	$k_{UV,Amp,\ app}$ (cm^2/mJ) (eqs 3.1-3.2)	$k_{UV,Amp\text{-}CPD,f}$ [b] (cm^2/mJ) (eq 3.3 forward)	$k_{UV,singleCPD,r}$ (cm^2/mJ) (eq 3.3 reverse)	$k_{UV,single6,4\text{-}PP}$ (cm^2/mJ) (eq 3.4)	$k_{FAC,Amp}$ [b] ($M^{-1}s^{-1}$) (eq 3.5)	$k_{FAC,N\text{-}Cl\ bp}$ ($M^{-1}s^{-1}$) (eq 3.6)	$k_{NH_2Cl,Amp}$ [b] ($M^{-1}s^{-1}$) (eq 3.5)	$k_{NH_2Cl,N\text{-}Cl\ bp}$ ($M^{-1}s^{-1}$) (eq 3.6)
***blt* 266 bp**		$2.5(\pm0.1)\times10^{-2}$	$3.8(\pm0.1)\times10^{-2}$			$3.9(\pm0.3)\times10^{3}$		$5.7(\pm0.3)\times10^{-1}$	
***blt* 832 bp**	*B. subtilis*	$6.1(\pm0.2)\times10^{-2}$	$6.7(\pm0.1)\times10^{-2}$			$8.5(\pm0.5)\times10^{3}$		$1.4(\pm0.1)$	
***blt* 870 bp**	1A189	$1.1(\pm0.1)\times10^{-1}$	$1.5(\pm0.1)\times10^{-1}$			$8.1(\pm0.5)\times10^{3}$		$1.5(\pm0.1)$	
***blt* 1017 bp**		$1.2(\pm0.1)\times10^{-1}$	$1.6(\pm0.1)\times10^{-1}$			$9.2(\pm0.5)\times10^{3}$		$1.7(\pm0.1)$	
***mec*A 1018 bp**	MRSA	$8.9(\pm0.2)\times10^{-2}$	$1.2(\pm0.1)\times10^{-1}$			$7.3(\pm0.4)\times10^{3}$		$1.9(\pm0.1)$	
***van*A 1030 bp**	VRE	$8.2(\pm0.2)\times10^{-2}$	$1.1(\pm0.1)\times10^{-1}$			$9.9(\pm0.5)\times10^{3}$		$2.2(\pm0.1)$	
***tet*(A) 1054 bp**	*E. coli* SMS-3-5	$4.2(\pm0.2)\times10^{-2}$	$2.8(\pm0.4)\times10^{-2}$			$9.4(\pm0.5)\times10^{3}$		$2.1(\pm0.1)$	
***amp*C 1006 bp**	PAO1	$3.4(\pm0.2)\times10^{-2}$	$2.7(\pm0.3)\times10^{-2}$			$9.8(\pm0.5)\times10^{3}$		$1.1(\pm0.1)$	
	B. subtilis 1A189	$1.2(\pm0.2)\times10^{-2}$	$1.2(\pm0.1)\times10^{-2}$			$4.2(\pm0.5)\times10^{3}$		$5.1(\pm0.2)\times10^{-1}$	
16S rRNA gene 142 bp	MRSA	$1.2(\pm0.1)\times10^{-2}$	$1.4(\pm0.1)\times10^{-2}$			$3.4(\pm0.3)\times10^{3}$		$6.0(\pm0.3)\times10^{-1}$	
	VRE	$1.3(\pm0.2)\times10^{-2}$	$1.3(\pm0.1)\times10^{-2}$			$3.3(\pm0.4)\times10^{3}$		$5.4(\pm0.2)\times10^{-1}$	
	E. coli SMS-3-5	$1.3(\pm0.2)\times10^{-2}$	$1.4(\pm0.1)\times10^{-2}$	$1.7(\pm0.1)\times10^{-2}$	$1.2(\pm0.1)\times10^{-4}$	$3.3(\pm0.3)\times10^{3}$	$3.9(\pm0.2)\times10^{-1}$	$4.8(\pm0.2)\times10^{-1}$	$4.3(\pm0.2)\times10^{-4}$
	PAO1	$2.6(\pm2.3)\times10^{-3}$	$6.6(\pm0.1)\times10^{-3}$			$2.9(\pm0.2)\times10^{3}$		$4.4(\pm0.2)\times10^{-1}$	
16S rRNA gene 536 bp	*B. subtilis* 1A189	$3.2(\pm0.3)\times10^{-2}$	$3.0(\pm0.1)\times10^{-2}$			$6.6(\pm0.3)\times10^{3}$		$1.6(\pm0.1)$	
16S rRNA gene 734 bp	*B. subtilis* 1A189	$4.7(\pm0.4)\times10^{-2}$	$5.9(\pm0.1)\times10^{-2}$			$8.6(\pm0.4)\times10^{3}$		$2.1(\pm0.1)$	
16S rRNA gene 1068 bp	*B. subtilis* 1A189	$6.6(\pm0.4)\times10^{-2}$	$6.9(\pm0.2)\times10^{-2}$			$1.1(\pm0.6)\times10^{4}$		$2.7(\pm0.1)$	
	B. subtilis 1A189	$8.9(\pm0.6)\times10^{-2}$	$9.3(\pm0.2)\times10^{-2}$			$1.4(\pm0.7)\times10^{4}$		$4.2(\pm0.2)$	
16S rRNA gene 1509 bp	MRSA	$1.1(\pm0.1)\times10^{-1}$	$1.2(\pm0.1)\times10^{-1}$			$1.3(\pm0.7)\times10^{4}$		$4.8(\pm0.2)$	
	VRE	$1.1(\pm0.1)\times10^{-1}$	$1.2(\pm0.1)\times10^{-1}$			$1.3(\pm0.7)\times10^{4}$		$4.8(\pm0.2)$	
	E. coli SMS-3-5	$9.6(\pm0.4)\times10^{-2}$	$1.0(\pm0.1)\times10^{-2}$			$1.5(\pm0.8)\times10^{4}$		$3.3(\pm0.2)$	
	PAO1	$8.5(\pm0.5)\times10^{-2}$	$8.6(\pm0.3)\times10^{-2}$			$1.5(\pm0.7)\times10^{4}$		$1.4(\pm0.1)$	
	$k_{Disinfectant,Specific}$ [b]	$3.9(\pm0.2)\times10^{-4}$ (M 5'-TT-3'/M amplicon)$^{-1}$ (cm^2/mJ)	$5.3(\pm0.3)\times10^{-4}$ (M 5'-TT-3'/M amplicon)$^{-1}$ (cm^2/mJ)	N.A.	N.A.	7.3±0.4 (M AT+GC)$^{-1}s^{-1}$	N.A.	$1.9(\pm0.2)\times10^{-3}$ (M AT+GC)$^{-1}s^{-1}$	N.A.
	$k_{Disinfectant,0}$ [b]	$7.1(\pm2.7)\times10^{-3}$ cm^2/mJ	$4.6(\pm0.6)\times10^{-3}$ cm^2/mJ	N.A.	N.A.	$2.2(\pm0.3)\times10^{4}$ $M^{-1}s^{-1}$	N.A.	$2.1(\pm0.6)\times10^{-1}$ $M^{-1}s^{-1}$	N.A.

[a] All data were obtained by treatment of extracellular DNA of *B. subtilis* 1A189, MRSA, VRE, *E. coli* SMS-3-5, and PAO1 in 10 mM PB at pH 7 (UV and FAC) or 8 (NH_2Cl). Significands of standard errors of $k_{Disinfectant,\ Amp}$ were rounded up to 0.1 if below 0.1. [b] For each disinfectant, $k_{Disinfectant,\ Specific}$ and $k_{Disinfectant,\ 0}$ are, respectively, the slope and intercept of the correlations obtained by weighted linear regression of the rate constants, $k_{Disinfectant,\ Amp}$, for the 21 amplicons versus corresponding specific nucleotide contents (Figure 3.1), with data points of *amp*C 1006 bp and 16S rRNA gene 1509 bp excluded for NH_2Cl. $k_{Disinfectant,\ Specific}$ represents the sequence-independent, bp- or doublet-specific rate constant for each disinfectant, and $k_{Disinfectant,\ 0}$ is attributed to factors influencing DNA reactivity (e.g., secondary targets, specific sequence elements) that are not fully accounted for by eq 3.7.

secondary targets within specific nucleotide sequences). $k_{\text{Disinfectant,Specific}}$ and $k_{\text{Disinfectant,0}}$ can in turn be calculated as the slope and intercept obtained from weighted linear regressions of $k_{\text{Disinfectant,Amp}}$ versus mol X/mol Amp.[28]

As illustrated in Figure 3.1a, a strong correlation was found between the apparent rate constants $k_{\text{UV,Amp,}app}$ (eqs 3.1-3.2) and 5'-TT'-3 doublet content for the expanded array of 21 ARG/16S rRNA gene amplicons ($R^2 = 0.94$), consistent with findings reported when using the four *blt* amplicons only ($R^2 = 0.96$). As also shown in Figure 3.1a, the rate constants for CPD lesion formation, $k_{\text{UV,Amp-CPD,}f}$ (eqs 3.3-3.4), also strongly correlate with 5'-TT'-3 doublet contents ($R^2 = 0.95$) for the 21 amplicons in the regression analyses. Both correlations support the mechanism that 5'-TT-3' doublets are the most susceptible 5'-bipyrimidine-3' sites for generation of CPDs – the primary DNA lesions induced by UV.[15, 52] In addition, the regression line of $k_{\text{UV,Amp-CPD,}f}$ versus 5'-TT'-3 generates a larger slope (defined as $k_{\text{UV,Specific}}$ according to eq 3.7) than that of $k_{\text{UV,Amp,}app}$. This can be attributed to the fact that $k_{\text{UV,Amp,}app}$ characterizes the *aggregate* effect of CPD formation (plus minor contribution of 6-4PP formation) *and* CPD photoreversal, resulting in a generally smaller value than for $k_{\text{UV,Amp-CPD,}f}$, which quantifies the effect of CPD formation alone.

Linear regression of the two sets of measured rate constants $k_{\text{UV,Amp,}app}$ or $k_{\text{UV,Amp-CPD,}f}$ was also performed using eq 3.7 with mol X/mol Amp representing the *total* number of all 5'- T/C-3' doublets weighted by the corresponding molar extinction coefficients ($\varepsilon_{254,\ 5'\text{-T/C-}3'}$) and quantum yields ($\phi_{254,\ 5'\text{-T/C-}3'}$) of lesion formation at 254 nm UV light for each type of 5'-T/C-3' doublets (derived from Douki (2006)[52] and Tataurov (2008);[53] see SI Text S3.6). As shown in Figure S3.8, each regression yielded strong correlations ($R^2 \geq 0.95$). In addition as shown in Figure

S3.8, the *measured* rate constants agreed well with *theoretical* rate constants of *overall* 5'-T/C-3' *lesion* formation ($k_{UV,all\ lesions,f}$)[28], but were significantly larger than those of theoretical TT-CPD formation ($k_{UV,TT\text{-}CPD,f}$), where $k_{UV,all\ lesions,f}$ and $k_{UV,TT\text{-}CPD,f}$ were estimated using the same $\varepsilon_{254,\ 5'\text{-}T/C\text{-}3'}$ and $\phi_{254,\ 5'\text{-}T/C\text{-}3'}$ values[52, 53] noted above, according to previously reported methods.[28, 54] These trends are consistent with 5'-TT-3' doublets representing the predominant sites of UV-induced lesion formation, with the other types of 5'-T/C-3' doublets (i.e., 5'-TC-3', 5'-CT-3', and 5'-CC-3') also contributing to varying degrees to formation of UV-induced lesions, including both CPDs and 6-4PPs.[52, 55] Further discussions on regression analyses of $k_{UV,Amp,app}$ and $k_{UV,Amp\text{-}CPD,f}$ versus 5'-TT-3' or *weighted* 5'-T/C-3' doublet contents, as well as comparisons with *theoretical* $k_{UV,all\ lesions,f}$ and $k_{UV,TT\text{-}CPD,f}$, are provided in Text S3.6.

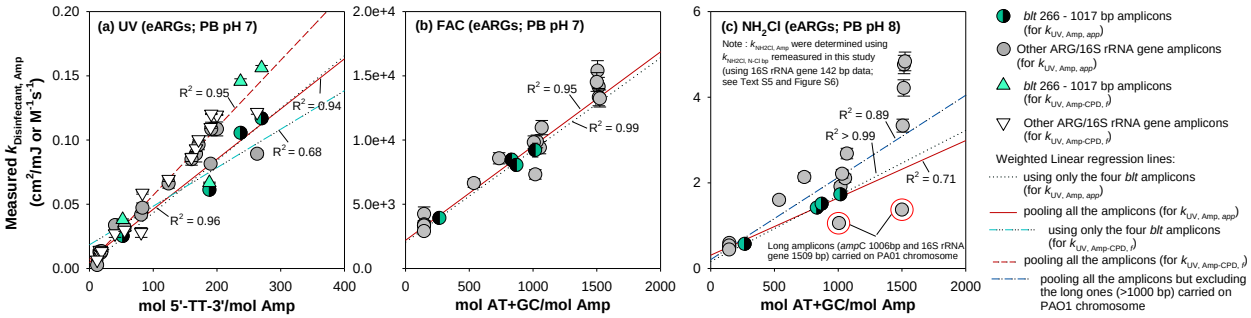

Figure 3.1. Plots of fluence-based first-order or second-order rate constants ($k_{Disinfectant,\ Amp}$) versus molar contents of 5'-TT-3' doublets or nucleotide bps (mol X/mol Amp), for various qPCR amplicons of ARGs and 16S rRNA gene segments for **(a)** UV, **(b)** FAC, and **(c)** NH_2Cl. All data were obtained by treatment of extracellular DNA pre-isolated from *B. subtilis* 1A189, MRSA, VRE, *E. coli* SMS-3-5, and PA01 individually in 10-mM phosphate buffer at pH 7 (UV and FAC) or 8 (NH_2Cl). Measured values of $k_{Disinfectant,\ Amp}$ and associated standard errors (illustrated as error bars) are summarized in Table 3.1. Trendlines and R^2 in panels **(a)-(c)** were obtained via weighted linear regressions of $k_{Disinfectant,\ Amp}$ versus specific nucleotide contents.

The strong correlation of $k_{FAC,Amp}$ values with AT+GC bp content reported previously for the four *blt* amplicons ($R^2 = 0.99$) has been validated here with the expanded array of 21 ARG/16S rRNA gene amplicons ($R^2 = 0.95$), as shown in Figure 3.1b. In contrast, a poorer correlation was observed between $k_{NH_2Cl,Amp}$ and AT+GC bp content after expanding the weighted

linear regression from the four *blt* amplicons ($R^2 = 0.99$) evaluated in our previous study to encompass all 21 amplicons used here ($R^2 = 0.71$), as shown in Figure 3.1c. This could be attributable in part to relatively large uncertainties in measuring $k_{NH_2Cl,Amp}$ values with very small magnitudes over the extremely long periods of NH_2Cl experiments. Notably, correlation of $k_{NH_2Cl,Amp}$ with AT+GC bp was significantly improved by excluding the data for long amplicons of gene targets (*amp*C 1006 bp and 16S rRNA gene 1509 bp) on the PAO1 chromosome ($R^2 = 0.89$), which were found to exhibit 1.5–2-fold slower degradation kinetics than similar-length amplicons of gene targets on chromosomes or plasmids from other microorganisms (Figure S3.5). The reasons for these latter observations are currently unclear, but may be due to incomplete purification of DNA extracted from PAO1.

Following the above analyses, the *sequence-independent* rate constants $k_{Disinfectant, Specific}$ and $k_{Disinfectant, 0}$ were obtained from weighted linear regressions of the $k_{Disinfectant, Amp}$ values measured for degradation of the 21 amplicons by each disinfectant (with values for the >1000-bp amplicons on the PAO1 chromosome excluded for NH_2Cl), and summarized in Table 3.1. In general, the weighted linear regressions in Figure 3.1 for the expanded array of qPCR amplicons are consistent with the previously-proposed hypothesis that DNA segments' reactivities toward each disinfectant are predictable based on their sequences. These findings also indicate that the linear-relationship model can be applied not only to amplicons of the *blt* gene on the *B. subtilis* 1A189 chromosome, but also to other ARG and 16S rRNA gene segments (including chromosome- or plasmid-borne segments) harbored by various bacterial strains. It is important to note, however, that the two plasmid-borne ARGs *van*A and *tet*(A) investigated here are both located on moderate- to large-size plasmids (39.1 kbp and 130.4 kbp) harbored by VRE and *E. coli* SMS-3-5, respectively. Due to their sizes, these plasmids may exhibit diffusion rates and reactivities

toward FAC and NH_2Cl that are more similar to chromosomal DNA than typical plasmid DNA (typically in forms of 50-Kbp linear DNA molecule after extraction).[28, 56] Future studies are recommended to focus on smaller plasmids (down to several kbp) to confirm whether there are inherent differences in plasmid and genomic DNA reactivities in chemical reactions.

3.3.3 *Predictions of ARG degradation kinetics during bench-scale disinfection*

The *sequence-independent* rate constants determined as described above were used in eq 3.7 to calculate *theoretical* rate constants $k_{\text{Disinfectant,Amp}}$ for each ARG/16S rRNA gene amplicon on the basis of the appropriate nucleotide content term (mol X/mol Amp) of the amplicon (Table S3.3). The *theoretical* $k_{\text{Disinfectant,Amp}}$ values were then utilized in eqs 3.1-3.2 or eqs 3.3-3.4 (for UV irradiation) or eqs 3.5-3.6 (for FAC and NH_2Cl treatment) to predict degradation of both extra- and intracellular ARG/16S rRNA gene amplicons during exposure to each disinfectant. The resulting *predicted* profiles of ARG degradation are summarized in Figure 3.2 for the long amplicons (>1000 bp) of the five model ARGs, as well as the shortest and longest amplicons (142 bp and 1509 bp) of 16S rRNA gene (carried on *B. subtilis* 1A189 or PAO1 chromosomes) as examples.

Extracellular ARGs in phosphate buffer. Predicted gene degradation profiles based on the approach described above were firstly compared with measured degradation kinetics for each of the individual ARG/16S rRNA gene amplicons during extracellular treatment with each disinfectant in phosphate buffer (Figure 3.2). For UV (Figure 3.2-I), eqs 3.1-3.2 (linear UV model) accurately predicted extracellular gene degradation up to 2–3-$\log_{10}$ loss (corresponding to ~50–100 mJ/cm^2), but significantly overpredicted degradation levels at higher fluences on account of tailing effects in the measured degradation profiles, especially for longer amplicons with higher 5'-TT-3' content (e.g., *mec*A 1018 bp, *van*A 1030 bp, and 16S rRNA gene 1509 bp).

In comparison, eqs 3.3-3.4 (expanded UV model) enable accurate predictions of extracellular gene degradation kinetics (including the tailing region) for the whole monitored fluence range up to 300 mJ/cm^2, greatly extending the models' applicability. For FAC and NH_2Cl (Figure 3.2-II and III, respectively), the two-step reaction model represented by eqs 3.5-3.6 performed well in predicting degradation kinetics of all the extracellular genes treated in phosphate buffers by either disinfectant, except for the 1006 bp *amp*C amplicon at extremely high exposures ($\geq \sim 10^5$ mg/L•min) of NH_2Cl. This latter finding likely resulted from the weaker correlation of $k_{NH_2Cl,Amp}$ with AT+GC bp content (Figure 3.1c) and exclusion of the 1006 bp *amp*C amplicon from regression analyses (Table 3.1).

Intracellular ARGs in phosphate buffer and wastewater matrixes (effects of host cells, reaction matrixes, and/or suspended solids). The resulting *predicted* profiles of ARG degradation were then compared with their *measured* degradation kinetics during intracellular treatment in phosphate buffer and several wastewater effluent samples, to assess the effects of host cells, reaction matrixes, and suspended solids. In phosphate buffer, degradation kinetics of ARGs/16SrRNA gene amplicons harbored by vegetative ARB cells generally exhibited stronger tailing effects than their extracellular forms during UV irradiation. Prior studies have also highlighted the tailing phenomenon when using qPCR to monitor intracellular gene degradation during UV irradiation,[15, 18, 57] which was likely attributable to one or both of two possible causes: (1) photoreversal of the formed CPDs by photolytic cleavage of the dimers bonds to yield the unreacted parent doublets (likely also responsible for the tailing effects observed in extracellular cases),[51, 57] and (2) dark- and/or photo-repair of damaged intracellular DNA by viable ARB cells,[58, 59] noting that ARB samples were periodically exposed to ambient light for a cumulative

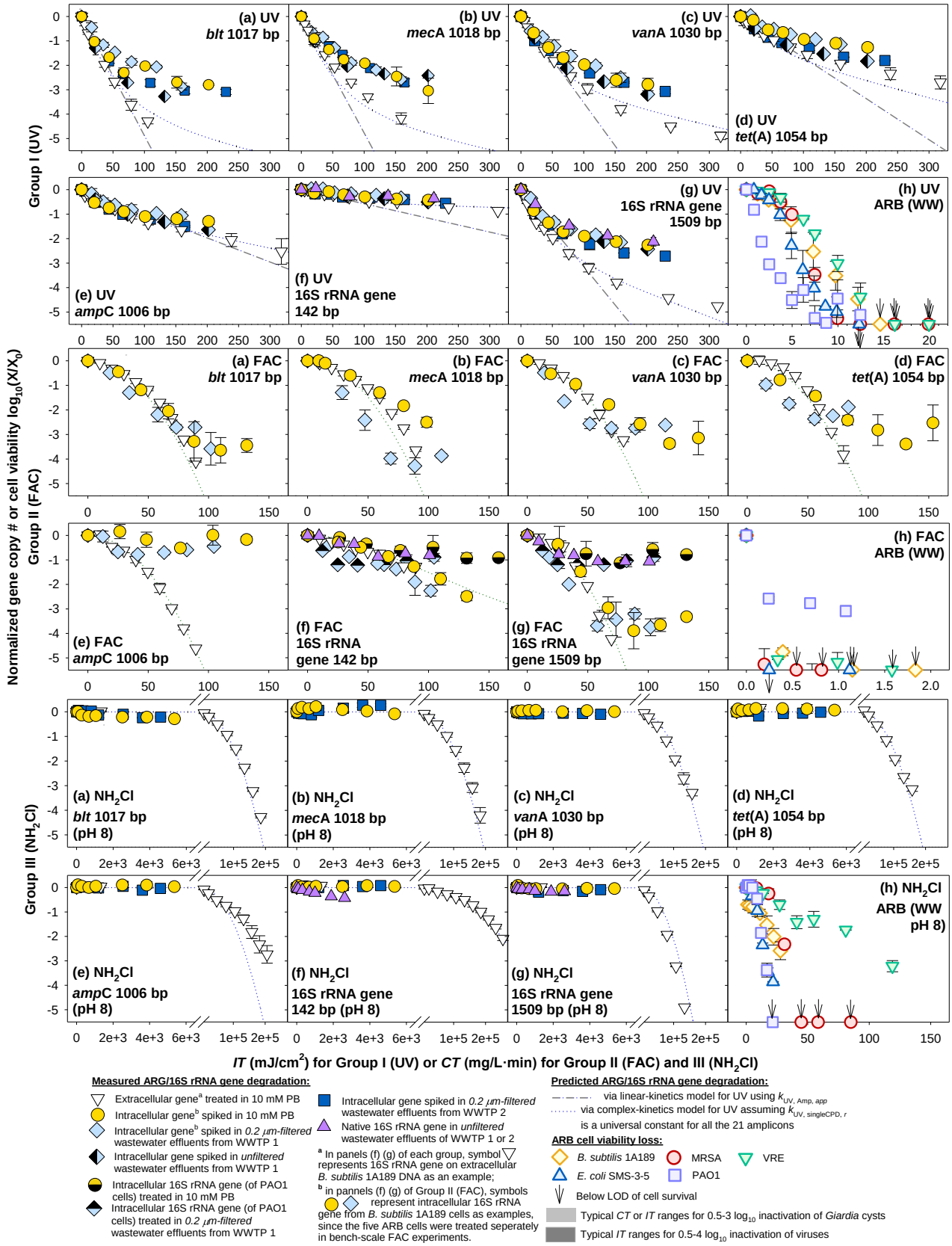

Figure 3.2. Normalized (log_{10}-scale) *measured* and *predicted* copy numbers of various ARG or 16S rRNA gene amplicons and their host ARB cell survival versus disinfectant exposures of **(Group I)** UV,

(Group II) FAC, and **(Group III)** NH_2Cl, during treatment of intact cells of *B. subtilis* 1A189, MRSA, VRE, *E. coli* SMS-3-5, and PAO1, individually or combined, in 10 mM PB solutions or secondary effluents of local WWTPs, or during treatment of native bacterial DNA in unfiltered secondary effluents. Each group includes 8 panels for **(a)** *blt* 1017 bp, **(b)** *mec*A 1018bp, **(c)** *van*A 1030 bp, **(d)** *tet*(A) 1054 bp, **(e)** *amp*C 1006 bp, **(f)** 16S rRNA gene 142 bp, **(g)** 16S rRNA gene 1509 bp, and **(h)** ARB viability loss. In each panel, typical *CT* and *IT* ranges applied in drinking water practice when using each disinfectant to inactivate *Giardia* cysts[60] or viruses[61] are indicated by light and dark gray shaded areas, respectively. Kinetics-based predictions of ARG/16S rRNA degradation were obtained via eqs 3.1-3.2 for fluence-based first-order kinetics model of UV, eqs 3.3-3.4 for complex kinetics model of UV, or eqs 3.5-3.6 for accelerating kinetics model of FAC and NH_2Cl, using theoretical degradation rate constants calculated according to eq 3.7. Error bars (representing standard deviations) for normalized gene copy number and cell survival were obtained from duplicate experiments conducted independently.

total of ~20–30 min during sample recovery and processing (due to the need to maintain room lighting under biosafety level 2 conditions).

Degradation kinetics of intracellular ARGs/16S rRNA gene amplicons during UV irradiation in phosphate buffer were compared with those obtained in different wastewater matrixes, including *unfiltered* and *filtered* effluents from WWTP 1, as well as *filtered* effluents from WWTP 2, with UV fluences corrected by water factor for each wastewater (Figure 3.2-I). General consistency was found between the four datasets for each amplicon after correcting for water factors in each matrix, implying minimal impacts of different aqueous matrixes (see *wastewaters versus clean buffers*) or the presence of suspended solids (see *filtered versus unfiltered wastewater*) on intracellular gene degradation by UV irradiation. In addition, the degradation kinetics of intracellular *blt* 1017 bp, *amp*C 1006 bp, and 16S rRNA gene 142 bp and 1509 bp segments observed when treating cells of the five ARB strains added together within the same matrix agreed well with those obtained by treating *B. subtilis* 1A189 or PAO1 cells individually, in either phosphate buffers and wastewaters (Text S3.4; Figure S3.9), indicating that co-existence of other ARB cells in the matrixes had no significant influence on intracellular gene degradation.

For FAC, treatment of the intracellular ARGs *blt*, *mec*A, *van*A, and *tet*(A) in phosphate buffer resulted in degradation measurements in agreement with predictions up to ~1–2-$\log_{10}$ losses, followed tailing effects at higher *CT*s (above 50–60 mg/L•min), leading to overprediction of the actual degradation levels by the models at the higher fluence ranges. One potential explanation for these observations could be accelerated FAC consumption within the cell matrix of the ARB cells due to solubilization of reactive biomolecules at higher exposures (similar to prior observations during treatment with O_3).[28] In contrast with the above four ARGs, the intracellular *amp*C 1006 bp harbored by PAO1 exhibited tailing even at very low *CT* values, resulting in limited degradation (< 0.2 $\log_{10}$) over the whole of the investigated *CT* range. The much more significant tailing for *amp*C 1006 bp likely resulted from production of high levels of extracellular polymeric substances (EPS) by PAO1, as such EPS can be highly reactive toward FAC, leading to rapid consumption of FAC at the cell surface and functioning as a permeability barrier to FAC diffusion into the cell and reaction with DNA inside.[62]

Consistent with the above findings, variable extents of tailings were also observed in degradation profiles of 16S rRNA gene segments (Figure 3.2-IIf,g), for which the same-length segment harbored by PAO1 exhibited more significant tailing at lower *CT* ranges than that harbored by *B. subtilis* 1A189, likely due to the same reasons discussed above. The variable tailing patterns in Figure 3.2-II demonstrate that intracellular gene degradation toward FAC may be greatly affected by the susceptibilities of the host cells to FAC.

During bench-scale chlorination of effluents from WWTPs 1 and 2, the added chlorine residuals were predominantly present in the forms of FAC and NH_2Cl, respectively (Figure S3.10). For FAC in WWTP 1 effluent, degradation kinetics of intracellular genes treated in wastewaters were significantly accelerated in comparison with those obtained in phosphate

buffers (Figure 3.2-II), possibly due to permeation of DNases present in wastewaters into damaged cell envelopes[27] leading to enhanced DNA degradation. For NH_2Cl, no significant loss of intracellular ARGs/16S rRNA gene amplicons in either phosphate buffer or wastewater matrixes was observed (Figure 3.2-III), consistent with model predictions within the monitored *CT* ranges and with the extremely low reactivity of NH_2Cl toward DNA.[28]

Native bacterial DNA in unfiltered wastewater matrixes. 16S rRNA gene amplicons associated with native bacterial DNA exhibited degradation kinetics consistent with those associated with spiked ARB cells during UV treatment, indicating that DNA within native biomass in the wastewater matrixes exhibits similar sensitivities to UV compared with the DNA from model strains. For FAC, the degradation profiles of 16S rRNA gene segments obtained using unfiltered wastewaters exhibited similar trends as observed for PAO1 cells, implying the presence of FAC-resistant bacterial populations (e.g., *Pseudomonas* spp. or bacterial endospores)[63] in these wastewaters. None of the native 16S rRNA gene amplicons were significantly degraded by NH_2Cl in the non-nitrified/denitrified wastewater matrix, consistent with model predictions and results obtained with spiked ARB cells.

3.3.4 *Intracellular ARG/16S rRNA gene amplicon degradation versus ARB inactivation in wastewater matrixes.*

Measurements of normalized ARB cell viabilities are plotted versus disinfectant exposures for bench-scale wastewater disinfection with UV, FAC, and NH_2Cl in Figure 3.2 (panel (h) for each Group). UV irradiation achieved >5-$\log_{10}$ inactivation at *IT* of 10-20 mJ/cm^2 for all five of the model ARB strains (Figure 3.2-I-h), through the strains exhibited variable inactivation kinetics. The Gram-positive ARB strains (VRE, *B. subtilis* 1A189, and MRSA) appeared to exhibit higher resistance to UV inactivation (with longer lag phases) than the Gram-

negative strains (*E. coli* SMS-3-5 and PAO1). These results agree well with prior findings by McKinney and Pruden (2012),[15] where the same four pathogenic ARB (MRSA, VRE, *E. coli* SMS-3-5, and PAO1) were exposed to UV irradiation in filtered wastewaters. These trends may be attributable to two primary factors: (1) the Gram-negative ARB strains investigated here possess larger genome sizes (*E. coli* SMS-3-5: 5.1 Mbp; PAO1: 6.3 Mbp) than the Gram-positive strains (VRE: 2.8 Mbp; MRSA: 2.9 Mbp; *B. subtilis* 1A189: 4.2 Mbp), and thus sustain more rapid accumulation of lethal DNA damage upon UV exposure; and (2) the thicker peptidoglycan layer of Gram-positive bacteria, potentially containing higher levels of chromophores, absorbs more photons and shields the contents of the cytoplasm (specifically DNA) from UV light,[15, 64] conferring upon them intrinsically stronger resistance against UV light, which has been commonly observed in other prior studies.[65-67] Although PAO1 appears to be the most directly susceptible strain to UV, with no lag phase, the residual viability of PAO1 appeared to exhibit tailing at higher fluences, likely resulting from a high photoadaptation ability of PAO1,[67] as also noted by McKinney and Pruden (2012).[15]

During treatment with FAC (in WWTP 1 effluent), all ARB strains were rapidly inactivated (> 5-$\log_{10}$) within a *CT* range of 1–2 mg/L•min (Figure 3.2-II-h), except that PAO1 exhibited two-stage inactivation kinetics with a fast initial drop of viability followed by tailing at higher exposures. Prior studies have reported similar multi-phase kinetics for PAO1 viability loss during exposure to FAC.[68] Although gram-positive strains are typically reported to be more resistant to chlorine than gram-negative strains,[69] here PAO1 exhibited higher resistance to FAC than all the other four ARB, which might be ascribed to enhancement of PAO1's resistance toward FAC by its capsular EPS as discussed above.[62]

Compared to FAC, exposure to NH_2Cl (in WWTP 2 effluent) required much higher *CT* ranges to achieve the same levels of ARB inactivation (Figure 3.2-III-h), which is consistent with the much lower reactivity of NH_2Cl than FAC toward biomolecules.[7] Gram-positive ARB strains displayed higher resistance to NH_2Cl than gram-negative strains, indicating that the thicker peptidoglycan layer of the gram-positive microorganisms may limit NH_2Cl access to or diffusion through the plasma membrane.[62] VRE in particular was much more resistant to NH_2Cl than the other four ARB, requiring extremely high *CT*s (~120 mg/L•min) to reach ~3-$\log_{10}$ inactivation, highlighting the possibility of VRE cells surviving during chlorination of high-ammonia wastewater and disseminating into downstream aqueous systems – consistent with its reported occurrences in coastal marine environments of the northwestern United States.[70, 71]

Degradation of intracellular ARGs/16S rRNA gene amplicons lagged far behind host cell inactivation for all five ARB strains during treatment with UV, FAC, and NH_2Cl in each wastewater matrix. These results demonstrate that ARGs could persist and potentially disseminate into non-resistant bacterial populations (e.g., by natural transformation) after effluent discharge even though ARB cells are fully inactivated by these disinfection processes. Furthermore, the 16S rRNA gene data represent degradation profiles of the bulk pool of intracellular DNA harbored by these (pathogenic) ARB, indicating that other genes in the bulk DNA pool, such as bacterial virulence genes encoding virulence factors (e.g., toxin production, biofilm formation, etc.) responsible for clinical infections, could also survive these disinfection processes and spread into downstream environments.

3.3.5 *Predictions of ARG degradation level during full-scale wastewater disinfection and practical implications.*

Measured concentrations of each of the pathogen-related ARGs as well as the monitored 16S rRNA gene amplicons are shown in Figure 3.3 for full-scale pre- and post-disinfection effluents from each WWTP. Amongst the six clinically-relevant ARGs, three – *van*A 1030 bp, ampC 1006 bp, and bla_{KPC} 805 bp – were detected above or around approximate LOQs (~160 copies/mL) in effluents from both WWTPs, with identities of their corresponding qPCR products confirmed by means of gel electrophoresis analyses and Sanger sequencing (SI Figure S3.11; sequence similarities of 90% and 95% for *van*A, 76% and 96% for *amp*C, and 82% and 96% for bla_{KPC} were found for pre-disinfection samples of WWTPs 1 and 2, respectively). Concentrations of *mec*A 1018 bp were below approximate LODs (~30 copies/mL), and its absence in effluents from either WWTP was confirmed on gel (with no band shown at ~1000 bp in Figure S3.11a). Although *tet*(A) 1054 bp and bla_{NDM} 807 bp were seemingly detected at high concentrations according to qPCR signals, their occurrences were ruled out by gel analyses (shown as smeared bands) and Sanger sequencing (no significant similarities found) (Figure S3.11). These findings highlight the importance of evaluating detections of putative qPCR products in complex matrixes using confirmatory analyses.

The levels of degradation of total bacterial DNA during the full-scale disinfection processes were calculated from measured concentrations of the 1059 bp 16S rRNA gene amplicon in pre-and post-disinfection effluents from each WWTP (Figure 3.3), yielding elimination of 0.96-$\log_{10}$ and 0.15-$\log_{10}$ during full-scale disinfection with UV (WWTP 1) and chlorination (WWTP 2), respectively. (It is notable that after normalizing recoveries to dsDNA to exclude contributions from physical biomass losses (26% and 23%), the actual *degradation* efficiency of total bacterial DNA turned out to be 0.83-$\log_{10}$ and 0.04-$\log_{10}$ by full-scale UV and

chlorination processes, respectively.) The distinct efficacies of ARG removal by full-scale UV and chlorination processes can be explained by the observations in bench-scale experiments that chlorine-based disinfection in WWTP 2 was in fact governed by NH_2Cl due to the rapid conversion of FAC to NH_2Cl by excess NH_3 in the secondary effluent matrix (Figure S3.10b), and the very short residence time of chlorination contactor at WWTP 2 (~15 min from the point of NaOCl dosage to the point of dechlorination with $Na_2S_2O_3$). Based on these conditions, CT_{NH2Cl} at the WWTP 2 would have been no larger than ~10 mg/L•min for an average exit total chlorine concentration of 0.65 mg/L as Cl_2 over the duration of the sample collection, far below CT_{NH2Cl} levels required to yield more than marginal DNA degradation (based on Figure 3.2-III).

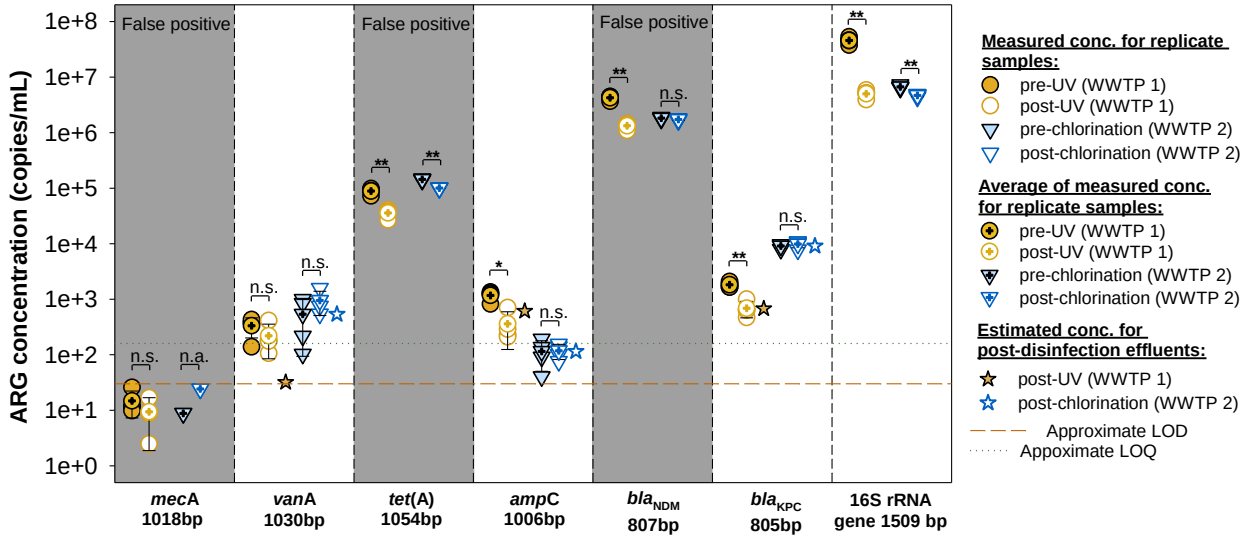

Figure 3.3. Concentrations of ARGs (*blt* 1017 bp, *mec*A 1018bp, *van*A 1030 bp, *tet*(A) 1054 bp, *amp*C 1006 bp, bla_{NDM} 807 bp, bla_{KPC} 805 bp) and 16S rRNA gene (1509 bp) in pre- and post-disinfection secondary effluents collected from two WWTPs in Seattle area, WA. Error bars represent standard deviations obtained from measured ARG/16S rRNA gene concentrations of four replicates (duplicate effluent samples pre-concentrated through 0.2 μm filtration, each of which was then split into duplicate DNA extractions).

Although the applied UV fluence at WWTP 1 was not directly available from the plant, it was estimated as ~29 mJ/cm^2 from eq 3.2 by using the removal efficiency of the 1509 bp 16S rRNA gene amplicon (0.96-$\log_{10}$) and its predicted rate constant $k_{UV,Amp,app}$ (= 0.076 cm^2/mJ on

average for the five model ARB strains) to back-calculate *IT*, since the amplicon removal (≤ 1-$\log_{10}$) was still within the linear range of the amplicon's decay kinetics (according to Figure 3.2-I-g). The estimated UV fluence (~29 mJ/cm^2) and CT_{NH2Cl} (~10 mg/L•min) values were then applied to predict ARG removal efficiencies by UV disinfection of WWTP 1 and chlorination of WWTP 2 according to eqs 3.1-3.2 and eqs 3.5-3.6, respectively. The resulting predicted ARG concentrations in the post-disinfection effluents of each WWTP are shown in comparison to the corresponding measured ARG concentrations in Figure 3.3. As shown in the figure, the kinetic modeling approaches yielded estimates that were generally in good agreement with measurements for removal of *amp*C, *van*A, and bla_{KPC} by full-scale UV- and chlorine-based disinfection processes, though a lower than anticipated loss was measured for *van*A degradation by UV disinfection in WWTP 1.

More generally, the full-scale data (Figure 3.3) and bench-scale data (Figure 3.2-I and 3.2-III) demonstrate that chlorination of effluents from conventional WWTPs not practicing secondary nutrient removal is unlikely to yield significant ARG degradation, whereas UV is likely to yield from ~0.5-1.5 $\log_{10}$ ARG degradation under typical operational conditions, and hence to provide a more reliable barrier to antibiotic resistance dissemination. UV irradiation also has the advantage of being relatively insensitive to high levels of ammonia as compared to chlorination, as evident when comparing ARG degradation during UV irradiation of the effluents from WWTPs 1 and 2 (Figure 3.2-I). The ineffectiveness of NH_2Cl-dominated chlorination in degrading DNA might pose concerns related to downstream ARG dissemination not only with respect to conventional WWTPs, but also to reclaimed and potable water distribution systems, where chlorine species are often dominated by NH_2Cl either due to incidental formation of chloramines following chlorination in the presence of residual ammonia or when using

monochloramine purposefully for maintenance of total chlorine residuals, respectively. This could in turn result in persistence of intra- or extracellular ARGs in such systems even when the ARB cells from which they originate are inactivated, as revealed by recent studies.[72, 73]

ACKNOWLEDGEMENTS

This material is based upon work supported by the National Science Foundation under Grant Number CBET-1254929. Dr. Daniel R. Zeigler (Bacillus Genetic Stock Center), Dr. J. Scott Meschke (UW), Dr. Mari Winkler (UW), David No (Research Scientist of the Roberts lab), and graduate students in the Winkler lab including Bao Nguyen Quoc, Stephany Wei, and Kathryn Cogert, are greatly acknowledged for their technical support and advice. Staffs at local WWTPs are greatly thanked for wastewater sampling.

REFERENCES

1. Knapp, C. W.; Dolfing, J.; Ehlert, P. A.; Graham, D. W., Evidence of increasing antibiotic resistance gene abundances in archived soils since 1940. *Environ. Sci. Technol. Lett* **2009,** *44*, (2), 580-587.
2. Thevenon, F.; Adatte, T.; Wildi, W.; Poté, J., Antibiotic resistant bacteria/genes dissemination in lacustrine sediments highly increased following cultural eutrophication of Lake Geneva (Switzerland). *Chemosphere* **2012,** *86*, (5), 468-476.
3. Martinez, J. L., The role of natural environments in the evolution of resistance traits in pathogenic bacteria. *Proceedings of the Royal Society B: Biological Sciences* **2009,** *276*, (1667), 2521-2530.
4. Wright, G. D., Antibiotic resistance in the environment: a link to the clinic? *Curr. Opin. Microbiol.* **2010,** *13*, (5), 589-594.
5. Chee-Sanford, J. C.; Mackie, R. I.; Koike, S.; Krapac, I. G.; Lin, Y.-F.; Yannarell, A. C.; Maxwell, S.; Aminov, R. I., Fate and transport of antibiotic residues and antibiotic resistance genes following land application of manure waste. *Journal of environmental quality* **2009,** *38*, (3), 1086-1108.
6. Pruden, A.; Larsson, D. J.; Amézquita, A.; Collignon, P.; Brandt, K. K.; Graham, D. W.; Lazorchak, J. M.; Suzuki, S.; Silley, P.; Snape, J. R., Management options for reducing the release of antibiotics and antibiotic resistance genes to the environment. *Environmental health perspectives* **2013,** *121*, (8), 878-885.

7. Dodd, M. C., Potential impacts of disinfection processes on elimination and deactivation of antibiotic resistance genes during water and wastewater treatment. *J. Environ. Monit.* **2012,** *14*, 1754–1771.
8. Szczepanowski, R.; Linke, B.; Krahn, I.; Gartemann, K.-H.; Guetzkow, T.; Eichler, W.; Pühler, A.; Schlueter, A., Detection of 140 clinically relevant antibiotic-resistance genes in the plasmid metagenome of wastewater treatment plant bacteria showing reduced susceptibility to selected antibiotics. *Microbiology* **2009,** *155*, (7), 2306-2319.
9. Czekalski, N.; Berthold, T.; Caucci, S.; Egli, A.; Buergmann, H., Increased levels of multiresistant bacteria and resistance genes after wastewater treatment and their dissemination into Lake Geneva, Switzerland. *Front. Microbiol.* **2012**.
10. Zhang, Y.; Li, A.; Dai, T.; Li, F.; Xie, H.; Chen, L.; Wen, D., Cell-free DNA: a neglected source for antibiotic resistance genes spreading from WWTPs. *Environ. Sci. Technol.* **2018,** *52*, (1), 248-257.
11. Ju, F.; Beck, K.; Yin, X.; Maccagnan, A.; McArdell, C. S.; Singer, H. P.; Johnson, D. R.; Zhang, T.; Bürgmann, H., Wastewater treatment plant resistomes are shaped by bacterial composition, genetic exchange, and upregulated expression in the effluent microbiomes. *The ISME journal* **2019,** *13*, (2), 346.
12. Pruden, A., Balancing water sustainability and public health goals in the face of growing concerns about antibiotic resistance. *Environ. Sci. Technol.* **2014,** *48*, (1), 5-14.
13. Vikesland, P. J.; Pruden, A.; Alvarez, P. J.; Aga, D.; Bürgmann, H.; Li, X.-d.; Manaia, C. M.; Nambi, I.; Wigginton, K.; Zhang, T., Toward a Comprehensive Strategy to Mitigate Dissemination of Environmental Sources of Antibiotic Resistance. *Environ. Sci. Technol.* **2017,** *51*, (22), 13061-13069.
14. Munir, M.; Wong, K.; Xagoraraki, I., Release of antibiotic resistant bacteria and genes in the effluent and biosolids of five wastewater utilities in Michigan. *Water Res.* **2011,** *45*, (2), 681-693.
15. McKinney, C. W.; Pruden, A., Ultraviolet disinfection of antibiotic resistant bacteria and their antibiotic resistance genes in water and wastewater. *Environ. Sci. Technol.* **2012,** *46*, (24), 13393-13400.
16. Guo, M.-T.; Yuan, Q.-B.; Yang, J., Distinguishing effects of ultraviolet exposure and chlorination on the horizontal transfer of antibiotic resistance genes in municipal wastewater. *Environ. Sci. Technol.* **2015,** *49*, (9), 5771-5778.
17. Zhang, Y.; Zhuang, Y.; Geng, J.; Ren, H.; Zhang, Y.; Ding, L.; Xu, K., Inactivation of antibiotic resistance genes in municipal wastewater effluent by chlorination and sequential UV/chlorination disinfection. *Science of the Total Environment* **2015,** *512*, 125-132.
18. Destiani, R.; Templeton, M. R.; Kowalski, W., Relative Ultraviolet Sensitivity of Selected Antibiotic Resistance Genes in Waterborne Bacteria. *Environ. Eng. Sci.* **2017,** *35*, (7), 770-774.
19. Lamba, M.; Ahammad, S. Z., Performance comparison of secondary and tertiary treatment systems for treating antibiotic resistance. *Water Res.* **2017,** *127*, 172-182.
20. Jäger, T.; Hembach, N.; Elpers, C.; Wieland, A.; Alexander, J.; Hiller, C.; Krauter, G.; Schwartz, T., Reduction of antibiotic resistant bacteria during conventional and advanced wastewater treatment, and the disseminated loads released to the environment. *Front. Microbiol.* **2018,** *9*.
21. Destiani, R.; Templeton, M., Chlorination and ultraviolet disinfection of antibiotic-resistant bacteria and antibiotic resistance genes in drinking water. **2019**.

22. Huang, J.-J.; Hu, H.-Y.; Tang, F.; Li, Y.; Lu, S.-Q.; Lu, Y., Inactivation and reactivation of antibiotic-resistant bacteria by chlorination in secondary effluents of a municipal wastewater treatment plant. *Water Res.* **2011,** *45*, (9), 2775-2781.
23. Shi, P.; Jia, S.; Zhang, X.-X.; Zhang, T.; Cheng, S.; Li, A., Metagenomic insights into chlorination effects on microbial antibiotic resistance in drinking water. *Water Res.* **2013,** *47*, (1), 111-120.
24. Luo, Y.; Yang, F.; Mathieu, J.; Mao, D.; Wang, Q.; Alvarez, P. J. J., Proliferation of Multidrug-Resistant New Delhi Metallo-β-lactamase Genes in Municipal Wastewater Treatment Plants in Northern China. *Environ. Sci. Technol. Lett* **2013,** *1*, (1), 26-30.
25. Pak, G.; Salcedo, D. E.; Lee, H.; Oh, J.; Maeng, S. K.; Song, K. G.; Hong, S. W.; Kim, H.-C.; Chandran, K.; Kim, S. J. E. S.; Technology, Comparison of antibiotic resistance removal efficiencies using ozone disinfection under different pH and suspended solids and humic substance concentrations. **2016,** *50*, (14), 7590-7600.
26. Czekalski, N.; Imminger, S.; Salhi, E.; Veljkovic, M.; Kleffel, K.; Drissner, D.; Hammes, F.; Bürgmann, H.; Von Gunten, U., Inactivation of antibiotic resistant bacteria and resistance genes by ozone: from laboratory experiments to full-scale wastewater treatment. *Environ. Sci. Technol.* **2016,** *50*, (21), 11862-11871.
27. Choi, Y.; Dodd, M. C.; Lee, Y., Degradation kinetics of antibiotic resistance gene (mecA) of methicillin-resistant Staphylococcus aureus (MRSA) during water disinfection with chlorine, ozone, and ultraviolet light. *In preparation* **2020**.
28. He, H.; Zhou, P.; Shimabuku, K. K.; Fang, X.; Li, S.; Lee, Y.; Dodd, M. C., Degradation and deactivation of bacterial antibiotic resistance genes during exposure to free chlorine, monochloramine, chlorine dioxide, ozone, ultraviolet light, and hydroxyl radical. *Environ. Sci. Technol.* **2019,** *53*, (4), 2013-2026.
29. Gupta, N.; Limbago, B. M.; Patel, J. B.; Kallen, A. J., Carbapenem-resistant Enterobacteriaceae: epidemiology and prevention. *Clin. Infect. Dis.* **2011,** *53*, (1), 60-67.
30. Yang, F.; Huang, L.; Li, L.; Yang, Y.; Mao, D.; Luo, Y., Discharge of KPC-2 genes from the WWTPs contributed to their enriched abundance in the receiving river. *Science of the Total Environment* **2017,** *581*, 136-143.
31. Mathys, D. A.; Mollenkopf, D. F.; Feicht, S. M.; Adams, R. J.; Albers, A. L.; Stuever, D. M.; Grooters, S. V.; Ballash, G. A.; Daniels, J. B.; Wittum, T. E., Carbapenemase-producing Enterobacteriaceae and Aeromonas spp. present in wastewater treatment plant effluent and nearby surface waters in the US. *PloS one* **2019,** *14*, (6), e0218650.
32. Zhang, A.; Call, D. R.; Besser, T. E.; Liu, J.; Jones, L.; Wang, H.; Davis, M. A., β-lactam resistance genes in bacteriophage and bacterial DNA from wastewater, river water, and irrigation water in Washington State. *Water Res.* **2019**.
33. Kumar, K.; Day, R. A.; Margerum, D. W., Atom-transfer redox kinetics: General-acid-assisted oxidation of iodide by chloramines and hypochlorite. *Inorg. Chem.* **1986,** *25*, 4344-4350.
34. Bisicchia, P.; Botella, E.; Devine, K. M., Suite of novel vectors for ectopic insertion of GFP, CFP and IYFP transcriptional fusions in single copy at the amyE and bglS loci in Bacillus subtilis. *Plasmid* **2010,** *64*, (3), 143-149.
35. Saito, H.; Miura, K., Preparation of transforming deoxyribonucleic acid by phenol treatment. *Biochim. Biophys. Acta.* **1963,** *72*, (4), 619-629.

36. Volkmann, H.; Schwartz, T.; Bischoff, P.; Kirchen, S.; Obst, U., Detection of clinically relevant antibiotic-resistance genes in municipal wastewater using real-time PCR (TaqMan). *Journal of microbiological methods* **2004,** *56*, (2), 277-286.
37. Oliveira, D. C.; de Lencastre, H., Multiplex PCR strategy for rapid identification of structural types and variants of the mec element in methicillin-resistant Staphylococcus aureus. *Antimicrobial agents and chemotherapy* **2002,** *46*, (7), 2155-2161.
38. Clark, N.; Cooksey, R.; Hill, B.; Swenson, J.; Tenover, F., Characterization of glycopeptide-resistant enterococci from US hospitals. *Antimicrobial Agents and Chemotherapy* **1993,** *37*, (11), 2311-2317.
39. Dalsgaard, A.; Forslund, A.; Sandvang, D.; Arntzen, L.; Keddy, K., Vibrio cholerae O1 outbreak isolates in Mozambique and South Africa in 1998 are multiple-drug resistant, contain the SXT element and the aadA2 gene located on class 1 integrons. *J. Antimicrob. Chemother.* **2001,** *48*, (6), 827-838.
40. Ng, L.-K.; Martin, I.; Alfa, M.; Mulvey, M., Multiplex PCR for the detection of tetracycline resistant genes. *Molecular and cellular probes* **2001,** *15*, (4), 209-215.
41. Dumas, J.-L.; Van Delden, C.; Perron, K.; Köhler, T., Analysis of antibiotic resistance gene expression in Pseudomonas aeruginosa by quantitative real-time-PCR. *FEMS microbiology letters* **2006,** *254*, (2), 217-225.
42. Tam, V.; Schilling, A.; LaRocco, M.; Gentry, L.; Lolans, K.; Quinn, J.; Garey, K., Prevalence of AmpC over‐expression in bloodstream isolates of Pseudomonas aeruginosa. *Clinical microbiology and infection* **2007,** *13*, (4), 413-418.
43. Devereux, R.; Willis, S. G., Amplification of ribosomal RNA sequences. In *Molecular microbial ecology manual*, Springer: 1995; pp 277-287.
44. Suzuki, M. T.; Taylor, L. T.; DeLong, E. F., Quantitative analysis of small-subunit rRNA genes in mixed microbial populations via 5′-nuclease assays. *Applied environmental microbiology* **2000,** *66*, (11), 4605-4614.
45. Baker, G.; Smith, J. J.; Cowan, D. A., Review and re-analysis of domain-specific 16S primers. *Journal of microbiological methods* **2003,** *55*, (3), 541-555.
46. Beck, N.; Callahan, K.; Nappier, S.; Kim, H.; Sobsey, M.; Meschke, J., Development of a spot‐titer culture assay for quantifying bacteria and viral indicators. *J. Rapid Methods Autom. Microbiol.* **2009,** *17*, (4), 455-464.
47. APHA, *Standard Methods for the Examination of Water and Wastewater*. 21 ed.; APHA, AWWA, WPCF: Washington, 2005.
48. Canonica, S.; Meunier, L.; Von Gunten, U., Phototransformation of selected pharmaceuticals during UV treatment of drinking water. *Water Res.* **2008,** *42*, (1-2), 121-128.
49. Bolton, J. R.; Linden, K. G., Standardization of methods for fluence (UV dose) determination in bench-scale UV experiments. *Journal of environmental engineering* **2003,** *129*, (3), 209-215.
50. Miller, J.; Miller, J. C., *Statistics and chemometrics for analytical chemistry*. Pearson Education: 2018.
51. Law, Y. K.; Forties, R. A.; Liu, X.; Poirier, M. G.; Kohler, B., Sequence-dependent thymine dimer formation and photoreversal rates in double-stranded DNA. *Photoch. Photobio. Sci.* **2013,** *12*, (8), 1431-1439.
52. Douki, T., Low ionic strength reduces cytosine photoreactivity in UVC-irradiated isolated DNA. *Photoch. Photobio. Sci.* **2006,** *5*, (11), 1045-1051.

53. Tataurov, A. V.; You, Y.; Owczarzy, R., Predicting ultraviolet spectrum of single stranded and double stranded deoxyribonucleic acids. *Biophys. Chem.* **2008,** *133*, (1-3), 66-70.
54. Yoon, Y.; Dodd, M. C.; Lee, Y., Elimination of transforming activity and gene degradation during UV and UV/H2O2 treatment of plasmid-encoded antibiotic resistance genes. *Environ. Sci.: Wat. Res. Technol.* **2018,** *4*, 1239-1251.
55. Matallana-Surget, S.; Meador, J. A.; Joux, F.; Douki, T., Effect of the GC content of DNA on the distribution of UVB-induced bipyrimidine photoproducts. *Photoch. Photobio. Sci.* **2008,** *7*, (7), 794-801.
56. Robertson, R. M.; Laib, S.; Smith, D. E., Diffusion of isolated DNA molecules: dependence on length and topology. *Proc. Natl. Acad. Sci. U.S.A.* **2006,** *103*, (19), 7310-7314.
57. Poepping, C.; Beck, S. E.; Wright, H.; Linden, K. G., Evaluation of DNA damage reversal during medium-pressure UV disinfection. *Water Res.* **2014,** *56*, 181-189.
58. Sinha, R. P.; Häder, D.-P., UV-induced DNA damage and repair: a review. *Photoch. Photobio. Sci.* **2002,** *1*, (4), 225-236.
59. Hijnen, W.; Beerendonk, E.; Medema, G. J., Inactivation credit of UV radiation for viruses, bacteria and protozoan (oo) cysts in water: a review. *Water Res.* **2006,** *40*, (1), 3-22.
60. EPA *Disinfection profiling and benchmarking guidance manual*; United States Environmental Protection Agency: Office of Water. Washington, DC., 1999.
61. *Ultraviolet Disinfection Guidance Manual for the Final Long Term 2 Enhanced Surface Water Treatment Rule*; United States Environmental Protection Agency: Office of Water. Washington, DC, 2006.
62. Xue, Z.; Hessler, C. M.; Panmanee, W.; Hassett, D. J.; Seo, Y., Pseudomonas aeruginosa inactivation mechanism is affected by capsular extracellular polymeric substances reactivity with chlorine and monochloramine. *FEMS microbiology ecology* **2013,** *83*, (1), 101-111.
63. Forsyth, J. E.; Zhou, P.; Mao, Q.; Asato, S. S.; Meschke, J. S.; Dodd, M. C., Enhanced inactivation of Bacillus subtilis spores during solar photolysis of free available chlorine. *Environ. Sci. Technol.* **2013,** *47*, (22), 12976-12984.
64. Williams, P. D.; Eichstadt, S. L.; Kokjohn, T. A.; Martin, E. L., Effects of ultraviolet radiation on the gram-positive marine bacterium Microbacterium maritypicum. *Current microbiology* **2007,** *55*, (1), 1-7.
65. Arrange, A. A.; Phelps, T. J.; Benoit, R. E.; Palumbo, A. V.; White, D. C., Bacterial sensitivity to UV light as a model for ionizing radiation resistance. *Journal of microbiological methods* **1993,** *18*, (2), 127-136.
66. Arrage, A.; Phelps, T.; Benoit, R.; White, D., Survival of subsurface microorganisms exposed to UV radiation and hydrogen peroxide. *Appl. Environ. Microbiol.* **1993,** *59*, (11), 3545-3550.
67. Sheldon, J. L.; Kokjohn, T. A.; Martin, E. L., The effects of salt concentration and growth phase on MRSA solar and germicidal ultraviolet radiation resistance. *Ostomy/wound management* **2005,** *51*, (1), 36-8, 42-4, 46 passim.
68. Mao, G.; Song, Y.; Bartlam, M.; Wang, Y., Long-term effects of residual chlorine on Pseudomonas aeruginosa in simulated drinking water fed with low AOC medium. *Front. Microbiol.* **2018,** *9*.
69. Virto, R.; Manas, P.; Alvarez, I.; Condon, S.; Raso, J., Membrane damage and microbial inactivation by chlorine in the absence and presence of a chlorine-demanding substrate. *Applied Environmental Microbiology* **2005,** *71*, (9), 5022-5028.

70. Roberts, M. C.; No, D. B.; Marzluff, J. M.; Delap, J. H.; Turner, R., Vancomycin resistant Enterococcus spp. from crows and their environment in metropolitan Washington State, USA: Is there a correlation between VRE positive crows and the environment? *Veterinary microbiology* **2016,** *194*, 48-54.
71. Roberts, M.; Soge, O.; Giardino, M.; Mazengia, E.; Ma, G.; Meschke, J., Vancomycin‐resistant Enterococcus spp. in marine environments from the West Coast of the USA. *Journal of applied microbiology* **2009,** *107*, (1), 300-307.
72. Garner, E.; Chen, C.; Xia, K.; Bowers, J.; Engelthaler, D. M.; McLain, J.; Edwards, M. A.; Pruden, A., Metagenomic characterization of antibiotic resistance genes in full-scale reclaimed water distribution systems and corresponding potable systems. *Environ. Sci. Technol.* **2018,** *52*, (11), 6113-6125.
73. Sakcham, B.; Kumar, A.; Cao, B., Extracellular DNA in monochloraminated drinking water and its influence on DNA-based profiling of a microbial community. *Environ. Sci. Technol. Lett* **2019,** *6*, (5), 306-312.

Supporting Information for Chapter 3

Validation and application of a kinetics-based modeling approach to predict antibiotic resistance gene degradation during UV- and chlorine-based wastewater disinfection processes: from bench-scale to full-scale

6 narratives, 6 tables, 11 figures, and supporting references

Text S3.1. DNA extraction methods

Method I: DNA extraction using FastDNA Spin Kit. Biomass, including (un)treated ARB cells and/or native bacteria associated with suspended solids, either obtained from bench-scale experiments or full-scale wastewater samples (with or without spiking internal standards), were transferred into Lysing Matrix A 2.0 mL tubes containing 1 mL CLS-TC lysing buffer (MP Biomedicals) and stored at -80 °C until extraction. DNA extraction was performed following the manufacturer's protocol with optimizations as below.

Samples were taken out of storage at -80 °C and thawed at room temperature, then dosed with proteinase K stock (> 600 mAU/mL, Qiagen) to target a final concentration of ~1.5 mAU/mL. The samples were homogenized (6.0 m/s, 40 sec) on a FastPrep® Instrument (MP Bio) three times (allowing ~5 min rest between each cycle to avoid overheating of the samples). The homogenized samples were then incubated at 37 °C water bath for at least 1 hour, and then frozen and thawed (-80 °C/65 °C) through 3-4 cycles. The above steps of multiple homogenizations, proteinase K digestion and freeze-thaws were found to enhance DNA extraction yield significantly. After the last thaw step at 65 °C, the samples were cooled down and centrifuged (14000 ×g, ≥ 15 min) at room temperature, and 0.9 mL supernatants were transferred into 2.0 mL flat-bottom centrifuge tubes (while avoiding any cell debris floating on the supernatant surface). The supernatants were centrifuged again (14000 ×g, ≥ 15 min) at room temperature, and 0.8 mL of the resulting supernatants were then transferred to 2.0 mL flat-bottom centrifuge tubes containing 0.8 mL Binding Matrix. The mixed solutions went through the remaining procedures as instructed by the manufacturer's protocol, except that the washing step using SEWS-M solution (amended with ethanol) was conducted three times to minimize qPCR inhibitors.

Method II: DNA extraction using phenol-chloroform method. The protocol for the modified phenol-chloroform-isoamyl alcohol extraction method[1] has been previously described for extraction of *Bacillus subtilis* 1A189 DNA.[2] The same protocol was applied in this work **(1)** to prepare DNA stocks for ***extracellular*** experiments, which requires large quantities of high purity DNA, or **(2)** to extract DNA from treated ARB cells obtained from ***intracellular*** FAC experiments, for which the FastDNA Spin Kit could not provide high enough recovery yield for accurate quantification of the recovered DNA concentrations (except for intracellular FAC experiments treating *E. coli* SMS-3-5, since the pSMS35_130 plasmid carrying *tet*(A) gene, harbored by *E. coli* SMS-3-5, were found to yield inconsistent recoveries by this method before and after FAC treatment for reasons unclear to the authors).

For recovery of DNA from intracellular FAC experiments, modifications were made to the cell lysis step of the previously reported protocol when processing cells of methicillin-resistant *Staphylococcus aureus* (MRSA, ATCC BAA-1556). For DNA extraction for ***extracellular*** experiments, overnight broth culture of MRSA cells was washed with saline-EDTA, pelleted, and resuspended in saline-EDTA solution containing lysozyme powder (Sigma) and proteinase K (Qiagen), as previously described.[2] The cell suspensions were then amended with lysostaphin from *Staphylococcus staphylolyticus* (lyophilized powder, Sigma L7386; pre-dissolved in saline-EDTA), and incubated at 37 °C water bath overnight (~12 hours). Typically, 1 mg lysostaphin powder was dissolved in 1mL saline-EDTA, and capable to lyse MRSA cells harvested from 1 L overnight culture. For ***intracellular*** FAC experiments, lysostaphin was also applied in addition to lysozyme and proteinase K in the step of cell lysis followed with overnight incubation (37 °C). Typically, 1 mg lysostaphin powder (also pre-dissolved in 1mL saline-EDTA) was used for incubation of 14-16 samples obtained from FAC treatment, with each

sample containing treated MRSA cells recovered from ~150 mL reaction solutions dosed with ~10^7 CFU/mL cells. After incubation, the remainder of the freeze-thaw procedures, phenol:chloroform:isoamyl alcohol extractions, RNase A&T1 digestion, ethanol precipitation, and re-dissolution were conducted according to the original protocol.[2]

Text S3.2. Protocols of qPCR assays

Preparation of qPCR standards and calibration curves. qPCR standards of ARG amplicons, including *blt* 266-1017 bp, *mec*A 1018 bp, *tet*(A), and *amp*C 1006 bp, were prepared with total DNA, including chromosome and plasmids (if applicable), of *B. subtilis* 1A189, MRSA, *E. coli* SMS-3-5, and PAO1, respectively, extracted using FastDNA Spin Kit as described in Text S3.1. qPCR standards of the other plasmid-borne ARGs were cloned using a TOPO™ TA Cloning™ Kit (Invitrogen™), due to uncertainty of their locations on chromosome or plasmid when developing methodology of this work (in the case of *van*A), or unknown sequences of their plasmid carriers (for bla_{NDM} and bla_{KPC}). Briefly, total DNA of VRE was extracted using FastDNA Spin Kit, and plasmids of *K. pneumoniae* 1.53 and ATCC BAA-1705 were extracted using RapidPure Plasmid Mini Kit (MP Biomedicals), to obtain DNA templates carrying *van*A, bla_{NDM}, and bla_{KPC}, respectively. The PCR products of *van*A (1030 bp), bla_{NDM} (807 bp), and bla_{KPC} (805 bp), were amplified from corresponding templates with primers specified in Table S3.2, and each inserted into pCR™4-TOPO® TA vectors, which were then transformed into One Shot™ TOP10 chemically competent *E. coli* cells. The constructed plasmids were extracted (as above) from the *E. coli* positive clones (grown in LB broth w/ 100 μg/mL ampicillin overnight), and used as qPCR standards of *van*A, bla_{NDM}, or bla_{KPC}. qPCR standards of the other internal standard gene, *cfpamy*, was prepared with the pCFPamy plasmids

extracted from *E. coli* ECE228. Amplicon copy numbers of the targeted genes were calculated assuming the DNA standards contain only intact genomic and/or plasmid DNA carrying one copy of the gene per genome (for total DNA) or plasmid (for plasmid DNA). (Note: *E. coli* SMS-3-5 was reported to harbor one copy of pSMS35_130 plasmid per cell, which carries one copy of *tet*(A)).[3] qPCR standards of the 16S rRNA gene segments were prepared using chromosomal DNA of *B. subtilis* 1A189 (knowing that *B. subtilis* DNA carries 10 copies of 16S rRNA gene per genome), which yielded consistent amplification efficiencies and melting curves when compared with chromosomal DNA from the other model ARB. qPCR calibration curves were conducted in duplicate to cover at least seven orders of magnitude with 10-fold serial dilution, yielding average R^2 values ≥ 0.99 across all assays, and amplification efficiencies of 0.98 ± 0.05 for short amplicons (*blt* 266 bp and 16S rRNA gene 142 bp), and 0.86 ± 0.07 for the other longer (> 600 bp) amplicons.

qPCR mixture compositions and temperature profiles. Each individual 10 μL reaction contained 5 μL of SsoFast™ EvaGreen® Supermix, 400 nM of forward and reverse primers, 0.5 μL of DNA template, and molecular biology grade water (Corning, NY) for the remaining volume,[4] which were mixed in 0.1 mL white PCR tubes with clear caps (USA Scientific, Orlando, FL). The temperature profiles of qPCR assays were optimized as one cycle of enzyme activation at 98 °C for 5 min, and 40 cycles of denaturation at 98 °C for 10 s, annealing at annealing temperature (T_A; see Table S3.2) for 20 s, plus extension at 72 °C for 1 min, followed by a melting curve (60 °C to 95 °C); except for the four *blt* amplicons (266 – 1017 bp), which were analyzed according to previously reported protocols.[2]

Limits of detection and quantification (LOD & LOQ). LODs and LOQs of the qPCR assays were determined according to Czekalski et al. (2016).[5] Briefly, LOD for each assay was

defined by the lowest threshold cycles (Cq) determined in qPCR-or extraction blanks, while LOQ was determined by the lowest concentrated standard dilution with a standard deviation of quadruplicate Cq values smaller than 0.5.[5] The LODs and LOQs were typically determined as 3 copies/μL and 16 copies/μL, respectively, for most qPCR assays.

Text S3.3. Internal standard dose and evaluation of DNA recovery yield for full-scale samples.

The two internal standards, i.e., *B. subtilis* 1A189 and *E. coli* ECE228, were streaked on agar plates (Tryptose Blood agar w/ 4 μg/mL acriflavine and Luria-Bertani, or LB, w/ 100 μg/mL ampicillin, respectively), cultured for 16 hours at 37 °C, and transferred to broth media (Antibiotic Medium #3 broth, and LB broth w/ 100 μg/mL ampicillin, respectively) to target optical densities at 600 nm (OD600nm) of 0.100 (using corresponding clean broths as blanks), and grown for ~3.5 hours at 37 °C to reach mix-exponential phases. The exponential-phase cells were washed by 10 mM PB at pH 7 by three times, pelleted (via centrifugation at 5000 rmp for 30 min), and resuspended in 10 mM PB (pH 7) in 1/10 volume of the original broth culture. Then the 10× concentrated internal standard stocks were stored at 4 °C (no longer than 2 hours) until spiking into wastewaters samples.

Prior to processing DNA extraction, duplicate volumes (200 mL) of wastewater effluents were spiked with the two internal standard stocks, to target DNA concentrations roughly equivalent to the native DNA level in the wastewaters. The native biomasses associated with suspended solids in wastewater (as well as the internal standard cells) in each duplicate sample were collected on 0.2 μm polycarbonate membranes (Whatman, NJ) through vacuum filtration, and washed off the membrane into a 50 mL sterile centrifuge tube containing 5-7 mL of 10 mM

PB (pH 7) by vigorous vortexing for at least 1 min. After removing the membrane from the tube using a pipette tip, the biomasses were pelleted by centrifugation (5000 rpm, or 4696 ×g, ≥ 1 hour), and resuspended in ~400 μL 10 mM PB (pH 7). Next, each of the ~400 μL concentrated duplicate samples was further split into duplicate aliquots and processed with DNA extraction using a FastDNA Spin Kit as described in Text S3.1. This method ultimately resulted in four replicates of 100μL DNA extracts for the original 400 mL wastewater, thus DNA in the original sample was concentrated by 1000 fold. The wastewater samples were also processed with the above filtration and DNA extraction procedure without spiking internal standards, for use as negative controls.

DNA recovery yield (η) was determined as below (eq S3.1),

$$\eta_{\text{dsDNA/gene}} = \frac{[\text{dsDNA/gene}]_{\text{WW w/ IS}} - [\text{dsDNA/gene}]_{\text{WW w/o IS}}}{[\text{dsDNA/gene}]_{\text{IS stock}}} \times 100\% \qquad \text{(eq S3.1)}$$

where $[\text{dsDNA/gene}]_{\text{WW w/ IS}}$ and $[\text{dsDNA/gene}]_{\text{WW w/o IS}}$ represent measured concentrations of double-stranded DNA (dsDNA, in units of ng/μL) or internal standard genes *blt* 1017 bp or *cfpamy* 663 bp (in units of copies/μL) in DNA extracts recovered from wastewater biomass, with and without spiking internal standards, respectively, and $[\text{dsDNA/gene}]_{\text{IS stock}}$ represents those concentrations in DNA extracts directly originating from internal standard stocks with the same cell amounts, but which were not subjected to filtration. In this way, the recovery yields account for potential losses of DNA due to filtration, nuclease degradation, and other factors during the above wastewater processing.

The η values based on [dsDNA], [*blt* 1017 bp], and [*cfpamy* 663 bp] represent recoveries of total, chromosomal, and plasmid-borne DNA, respectively, which are summarized in Table S3.5 for each wastewater sample.

Generally, DNA recoveries based on internal standard genes aligned well with those calculated based on dsDNA concentrations (though inconsistence existed probably due to systematic errors during DNA extraction or qPCR analyses), demonstrating the reliability of the extraction method. In the main text, the original concentrations of native ARGs or 16S rRNA gene segments in wastewater samples ($[gene]_{WW\ original}$, in units of copies/μL or copies/mL), were back-calculated using the concentrations measured in DNA extracts ($[gene]_{WW\ original}$, generated from wastewater samples without spiking internal standards), the recovery yield based on [dsDNA] (η_{dsDNA}), and the pre-concentration factor (i.e., 1000-fold), as below (eq S3.2),

$$[gene]_{WW\ original} = \frac{[gene]_{DNA\ extract}}{\eta_{dsDNA}} \times 1000 \quad \text{(eq S3.2)}$$

Text S3.4. Details about reactor configurations, experimental setup, additional control experiments, and selection of NaOCl doses for bench-scale disinfection treatment

Treatment of extracellular ARGs (eARGs) in phosphate buffers. Chromosomal DNA plus plasmids (if there are) of *B. subtilis* 1A189, MRSA, VRE, *E. coli* SMS-3-5 or PAO1 were pre-isolated from vegetative cells of each ARB strain, and diluted to 1 mg/L as double-stranded DNA (dsDNA) in 10 mM phosphate buffer (PB) at pH 7 (for UV and FAC) or 8 (for NH_2Cl, to minimize NH_2Cl self-decomposition over the extremely long treatment period). The 1-mg/L DNA solutions of each ARB strain were individually irradiated by 254 nm UV light in a in a "merry-go-round" photoreactor apparatus equipped with a low-pressure Hg lamp, or exposed to FAC and *pre-formed* NH_2Cl in amber bottles with continuous stirring, over or beyond exposures typical of (waste)water treatment, as previously described.[2]

Treatment of intracellular ARGs (iARGs) in phosphate buffers. Intracellular ARGs, contained within the DNA of intact ARB cells, were treated by each disinfectant in 10 mM PB at

the same pH conditions as the extracellular experiments but in larger volumes, also as previously described.[2] Vegetative cells of the above five ARB strains, from overnight broth cultures washed three times with PB, were treated as a combined mixture (with roughly equal cell dose for each strain) by UV and *pre-formed* NH_2Cl, or individually by FAC, in which case host cells considerably affected iARG degradation kinetics (as discussed in the main text). Cell concentrations of ~10^7 CFU/mL for each strain or in total after combining were applied for FAC and NH_2Cl, respectively, while lower concentrations ($\leq$ ~10^6 CFU/mL in total) were used for UV to limit any increase in background Abs_{254} to less than 0.04, to ensure no significant change in matrix transmittance. Additional control experiments for UV were also conducted by treating vegetative cells of *B. subtilis* 1A189 and PAO1 separately in 10 mM PB (pH 7), to confirm iARG degradation kinetics during UV irradiation in clean buffers would not be affected by conditions of treating the five ARB strains together or individually. Here *blt* 1017 bp and *amp*C 1006 bp, harbored by *B. subtilis* 1A189 and PAO1, respectively, were selected as examples of the most and least susceptible iARGs toward UV irradiation (as discussed in the main text).

Treatment of iARGs in wastewaters (and selection of NaOCl doses). The above iARG experiments were repeated in the same manners as above, but using pre-disinfection secondary effluents collected from WWTP 1 or WWTP 2 as reaction matrixes, 0.2-μm *filtered* (to remove native biomass) or *unfiltered*, and buffered at pH 7 or 8 with 10 mM PB as specified above. For UV, experiments were conducted by treating vegetative cells of the 5 ARB strains together (at total cell doses of $\leq$ ~10^6 CFU/mL as mentioned above), in matrixes of 0.2-μm *filtered* effluents from WWTP 1 and WWTP 2, as well as *unfiltered* effluents from WWTP 1, to investigate the effects of different wastewater matrixes and presence of suspended solids on iARG degradation kinetics, respectively. Additional UV experiments were conducted by treating vegetative cells of

B. subtilis 1A189 and PAO1 separately in 0.2-μm *filtered* effluents from WWTP 1 (buffered at pH 7), in order to confirm that iARG degradation kinetics during UV irradiation of wastewater matrixes were consistent whether the five ARB strains were treated together or individually.

FAC and NH_2Cl experiments were initiated by dosing 10–16 mg Cl_2/L or 2–3 mg Cl_2/L NaOCl into corresponding effluents (already spiked with ARB cells), to ensure either FAC or NH_2Cl residuals, respectively (see discussion below). The doses of NaOCl were selected based on ammonia levels of the effluents and whether or not exceedance of the chlorination breakpoint was desired, in addition to combined or (post-breakpoint) free available chlorine consumption kinetics. Example consumption curves of chlorine species, including FAC, NH_2Cl, and total available chlorine (TAC), are provided for disinfection using each WWTP matrix in Figure S3.8. As shown in Figure S3.8, under the dosage conditions used for the high-ammonia effluent from WWTP 2 (27.4 mg N/L), free available chlorine (FAC) was rapidly and completely converted into combined chlorine (predominantly NH_2Cl), according to eq S3.3. In contrast, under the dosage conditions used for the low-ammonia effluent from WWTP 1 (< 0.4 mg N/L), the dosed FAC was able to overcome the chlorination breakpoint to maintain a free chlorine (FAC) residual over the experimental period. Thus, in the discussion of the main text, bench-scale chlorination experiments using effluents from WWTP 1 and WWTP 2 are designated as treatment with "FAC" and "NH_2Cl", respectively. "FAC" treatment was not conducted using WWTP 2 effluents since the necessary dose of NaOCl to overcome the NH_3-N breakpoint (molar ratio of $[FAC]_{total} : [NH_3]_{total} \geq 1.5 :1$; weight ratio of $[FAC]_{total} : [NH_3]_{total} \geq 7.6 :1$)[6] would have been extremely high, which is not representative of typical chlorine dosages (typically ~4 mg/L as Cl_2 at both WWTPs) in practical treatment scenarios.

$$NH_3 + HOCl \underset{}{\overset{K_{hydrolysis}=1.5\times10^{11}\,M^{-1}}{\rightleftharpoons}} NH_2Cl + H_2O \qquad \text{(eq S3.3)}$$

Treatment of native bacterial DNA in wastewaters. The above wastewater experiments were also conducted by using *unfiltered* pre-disinfection effluents (from WWTP 1 for UV and FAC, and from WWTP 2 for NH_2Cl) without spiking ARB cells, to assess degradation kinetics of native bacterial DNA in wastewaters. For all UV experiments using *unfiltered* wastewaters (with or without spiking ARB cells), micro-stir plates were installed at the bottom of the "merry-go-round" system to provide continuous stirring of the reaction solutions containing suspended solids within the quartz reactor tubes.

Text S5. Determination of rate constants for degradation of 21 ARG/16S rRNA gene amplicons by UV, FAC, and NH_2Cl

Determination of fluence-based first-order rate constants for UV. The fluence-based first-order apparent rate constants, $k_{UV,Amp,app}$ (and associated uncertainties), were determined for each amplicon according to eq 3.2 through linear regression analyses of $\ln(N/N_0)$ versus *IT* over the *linear-kinetics* region (*IT* <~50 mJ/cm^2), as depicted in Figure S3.1. $k_{UV,Amp,app}$ was re-determined for the four *blt* amplicons using the measurements obtained in this study (Figure S3.1a), and found to be ~20-35% higher than the previously reported values (i.e., $2.0(\pm0.1)\times10^{-2}$, $5.2(\pm0.2)\times10^{-2}$, $7.8(\pm0.4)\times10^{-2}$, and $8.8(\pm0.4)\times10^{-2}$ cm^2/mJ for *blt* 266 bp, 832 bp, 870 bp, and 1017 bp, respectively),[2] following re-measurement of UV fluence rates in the merry-go-round reactor system. The $k_{UV,Amp,app}$ values and associated uncertainties of the 21 amplicons are summarized in Table 3.1.

For the *complex-kinetics* UV model, the fluence-based first-order rate constants $k_{UV,Amp\text{-}CPD,f}$, $k_{UV,single\text{-}CPD,r}$, and $k_{UV,single\text{-}6,4PPs}$ – characterizing formation of cyclobutane pyrimidine dimers (CPDs) on a given DNA segment, photoreversal of each single CPD, and formation of each single (6-4) photo-product (6-4PP), respectively – were determined according to Choi et al.

(2020).[7] In brief, the degradation rate of qPCR amplicons ($d[\text{Amp}]/dt$) during UV irradiation can be derived from eqs 3.3-3.4 in the main text, by using the following expressions (eqs S3.3-S3.4),

$$\frac{d[\text{Amp}]}{dt} = -k_{\text{UV,Amp-CPD},f}[\text{Amp}] + k_{\text{UV,singleCPD},r}(f_{\text{singleCPD}})[\text{Amp}_{\text{CPD}}] - k_{\text{UV,single6-4PP}}\left(\frac{\#5'\text{-TC-}3'}{\text{Amp}}\right)[\text{Amp}] \quad \text{(eq S3.3)}$$

$$\frac{d[\text{Amp}_{\text{CPD}}]}{dt} = k_{\text{UV,Amp-CPD},f}[\text{Amp}] - k_{\text{UV,singleCPD},r}(f_{\text{singleCPD}})[\text{Amp}_{\text{CPD}}] - k_{\text{UV,single6-4PP}}\left(\frac{\#5'\text{-TC-}3'}{\text{Amp}}\right)[\text{Amp}_{\text{CPD}}] \quad \text{(eq S3.4)}$$

where $\frac{\#5'\text{-TC-}3'}{\text{Amp}}$ is the number of 5'-TC-3' doublets (the primary sites for 6-4PP lesion formation) per amplicon; and $f_{\text{singleCPD}}$ is the fraction of amplicons sustaining a single CPD lesion ($\text{Amp}_{\text{singleCPD}}$) over the whole population of CPD-containing amplicons (Amp_{CPD}) (noting that neither $\text{Amp}_{\text{singleCPD}}$ nor Amp_{CPD} sustain 6-4PP lesions), which can be calculated according to eq S3.5 using the average number of CPD lesions per Amp_{CPD} (λ_{CPDs}), which equals $-\ln([\text{Amp}]/[\text{Amp}]_0)$ – assuming CPD lesion formation on DNA segments follows a Poisson distribution.[8]

$$f_{\text{singleCPD}} = \lambda_{\text{CPDs}} \cdot \exp(-\lambda_{\text{CPDs}}) = -\ln\left(\frac{\text{Amp}}{\text{Amp}_0}\right) \cdot \exp\left[\ln\left(\frac{\text{Amp}}{\text{Amp}_0}\right)\right] \quad \text{(eq S3.5)}$$

Here, $k_{\text{UV,Amp-CPD},f}$ (for CPD lesion formation on the whole amplicon sequence) varies for different amplicons, while $k_{\text{UV,single-CPD},r}$ (specific to photo-reversal of each single CPD lesion) and $k_{\text{UV,single6-4PP}}$ (specific to 6-4PP formation at each single 5'-TC-3' site on amplicons) are considered to be constants and independent of amplicon lengths or nucleotide contents. According to Choi et al. (2020),[7] after the reactions of CPD formation and photo-reversal (eq 3.3) reach equilibrium, degradation kinetics of the given DNA segment would be solely governed by the formation of 6-4PPs, and would exhibit linear-kinetics at extended UV fluences. Among the investigated

amplicons, only *tet*(A) 1054 bp and *amp*C 1006 bp had visually reached this pseudo-equilibrium *linear-kinetics* region at fluences higher than ~150 mJ/cm^2 (Figure S3.2, panels (e) and (f) of either Group I or II). According to eq S3.3, the amplicon degradation rate constant at the pseudo-equilibrium *linear-kinetics* region equals $k_{\text{UV,single6-4PP}}\left(\frac{\#5'\text{-TC-}3'}{\text{Amp}}\right)$, which could be determined via linear regression of the data over this region ($IT \geq$ ~150 mJ/cm^2) as 1.28(±0.16)×10^{-2} cm^2/mJ and 1.42(±0.23)×10^{-2} cm^2/mJ for *tet*(A) 1054 bp and *amp*C 1006 bp, respectively, as provided in Figure S3.3. Then $k_{\text{UV,single6-4PP}}$ was calculated as 9.5(±1.2)×10^{-5} cm^2/mJ and 1.3(±0.2)×10^{-4} cm^2/mJ for *tet*(A) 1054 bp and *amp*C 1006 bp, respectively, by dividing the above degradation rate constants by $\frac{\#5'\text{-TC-}3'}{\text{Amp}}$ for each amplicon (i.e., 135 and 106, respectively; Table S3.3). The average of the two values was taken as 1.2(±0.1)×10^{-4} cm^2/mJ and used as $k_{\text{UV,single6-4PP}}$ for all 21 the amplicons, which is smaller but in relatively good agreement with the value of 1.6(±0.2)×10^{-4} cm^2/mJ reported by Choi et al (2020) (obtained using a 212 bp amplicon of the *mec*A gene).[7]

The $k_{\text{UV,single6-4PP}}$ above was then applied to determine $k_{\text{UV,Amp-CPD},f}$ (an amplicon-dependent variable) for the 21 amplicons and $k_{\text{UV,single-CPD},r}$ (an amplicon-independent universal constant) together through numerical solution of eqs S3-S4 via a master non-linear regression by Excel Solver. The upper and lower error bounds of $k_{\text{UV,single-6,4PPs}}$ were used to determine error bounds of $k_{\text{UV,Amp-CPD}}$ and $k_{\text{UV,single-CPD},r}$. The non-linear regression fits are depicted as lines in Figure S3.2, Group I, and the values of $k_{\text{UV,Amp-CPD},f}$ (for 21 amplicons) and $k_{\text{UV,single-CPD},r}$ are summarized with their uncertainties in Table 3.1.

It is worthwhile noting that in this study, to allow establishment of a universal model in predicting reactivity of a given DNA segment toward UV, $k_{\text{UV,single-CPD},r}$ is assumed to be a constant

independent of amplicon sequences, which may not be completely accurate. It has been found that the photoreversal reaction kinetics of thymine-thymine cyclobutane pyrimidine dimers (TT-CPD) depends strongly on the identity of the nearest-neighbor bases on the 5' and 3' side of the 5'-TT-3' doublet; for example, the photoreversal kinetics of a 5'-GTTC-3' tetrad is reported to be ~ 6–7× higher than that of a 5'-ATTA-3' tetrad.[9] Based on this principle, alternative sets of $k_{\text{UV,Amp-CPD},f}$ and $k_{\text{UV,single-CPD},r}$ values were determined by treating both rate constants as amplicon-dependent variables, and solving for their values by non-linear regressions as described above but individually for each amplicon, with results summarized in Table S3.6 and the corresponding regression lines depicted in Figure S3.2, Group II. The resulting $k_{\text{UV,single-CPD},r}$ values for the 21 amplicons varied widely ranging from 0.0046 – 0.035 cm^2/mJ, supporting the above principle. Further studies are recommended to analyze the contents of neighboring bases on the 5' and 3' sides of all 5'-T/C-3' doublets on the 21 amplicons investigated here, and to use them to develop a universal model for predicting $k_{\text{UV,single-CPD},r}$ for various amplicons.

Determination of second-order rate constants for FAC and NH_2Cl. Determination of second-order rate constants $k_{\text{FAC or NH}_2\text{Cl,Amp}}$ and $k_{\text{FAC or NH}_2\text{Cl,N-Cl bp}}$ (and their associated uncertainties) for the sequential reactions (N-chlorination followed by C-chlorination) of DNA segments with FAC or NH_2Cl have been previously described in He et el. (2019).[2] Briefly, according to eqs 3.5-3.6, the formation rates of reversible N-chlorinated amplicons and irreversible halogenated products (captured as amplicon loss by qPCR assays) can be expressed as below,

$$\frac{d[\text{Amp}_{\text{N-Cl}}]}{dt} = k_{\text{FAC or NH}_2\text{Cl,Amp}}[\text{FAC/NH}_2\text{Cl}][\text{Amp}] - \frac{d[\text{product}]}{dt} \qquad \text{(eq S3.6)}$$

$$\frac{d[\text{product}]}{dt} = -\frac{d[\text{Amp}]}{dt} = k_{\text{FAC or NH}_2\text{Cl,N-Cl bp}}\left(\frac{\#\text{N-Cl bp}}{\text{Amp}_{\text{N-Cl}}}\right)[\text{FAC/NH}_2\text{Cl}][\text{Amp}_{\text{N-Cl}}] \qquad \text{(eq S3.7)}$$

where $\frac{\#\text{N-Cl bp}}{\text{Amp}_{\text{N-Cl}}}$ represents the average number of N-chlorinated base pairs (N-Cl bps) per N-chlorinated amplicon ($\text{Amp}_{\text{N-Cl}}$), which equals $-\ln([\text{Amp}]/[\text{Amp}]_0)$, again assuming that accumulation of N-Cl bps on $\text{Amp}_{\text{N-Cl}}$ follows a Poisson distribution.[8]

The *blt* gene degradation kinetics by FAC and NH_2Cl have been confirmed to be highly consistent with previous results, as shown in Figures S3.4a and S3.5b for the *blt* 1017 bp amplicon. Thus, the previously-determined $k_{\text{FAC,Amp}}$ for the four *blt* amplicons and $k_{\text{FAC,N-Cl bp}}$ (specific to individual N-chlorinated bps, and thus an amplicon-independent constant) based on *blt* 266 bp data are retained here from He et el. (2019).[2] The upper and lower bounds of $k_{\text{FAC,N-Cl bp}}$ (= 0.39 ± 0.02 $M^{-1}s^{-1}$) were applied to obtain the lower and upper bounds of $k_{\text{FAC,Amp}}$, respectively, for each of the other 17 amplicons by performing numerical solutions of eqs S3.6-S3.7 via non-linear regressions with Excel Solver. The non-linear regression fits are depicted as lines in Figure S3.3, and values of $k_{\text{FAC,Amp}}$ and $k_{\text{FAC,N-Cl bp}}$ (as mean ± standard error) are summarized in Table 3.1.

Similarly, the previously-determined $k_{\text{NH}_2\text{Cl,Amp}}$ for the four *blt* amplicons and $k_{\text{NH}_2\text{Cl,N-Cl bp}}$ (= $1.6(\pm0.1)\times10^{-4}$, obtained from *blt* 266 bp kinetics data) were also initially retained here, with the latter being applied to obtain $k_{\text{NH}_2\text{Cl,Amp}}$ for the other 17 amplicons by means of the numerical approach described above, with the resulted values and uncertainties also summarized in Table S3.6. However, by using the previous $k_{\text{NH}_2\text{Cl,N-Cl bp}}$ value, the solution of $k_{\text{NH}_2\text{Cl,Amp}}$ found for 16S rRNA gene 142 bp amplicons was not able to fit the measured data at *CT*s > ~200 M·s (shown in Figure S3.6), with the modeled kinetics always slower than measurements for each model strain. According to eq S3.7, the slopes of qPCR amplicon degradation kinetics (normalized to *CT*) during NH_2Cl treatment can be expressed as $-k_{\text{NH}_2\text{Cl,N-Cl bp}}\left(\frac{\#\text{N-Cl bp}}{\text{Amp}_{\text{N-Cl}}}\right)$. At *CT*s > ~200 M·s,

the slope of degradation kinetics for 16S rRNA gene 142 bp has reached its maximum value (Figure S3.6), corresponding to *complete* N-chlorination of the amplicon (i.e., $\frac{\text{\#N-Cl bp}}{\text{Amp}_{\text{N-Cl}}}$ = ampicon length). The poor model prediction over this region may be attributable to the following: (1) the previous measurement of $k_{NH_2Cl,\text{N-Cl bp}}$ underestimates its actual value, potentially due to incompleteness of N-chlorination of the whole amplicon sequence, or systematic errors in the extremely long period of NH_2Cl experiments; or (2) the intrinsic reactivity of an N-chlorinated GC bp toward NH_2Cl might be different from (and potentially higher than) that of an N-chlorinated AT bp. Accordingly, 16S rRNA gene 142 bp – a more GC-enriched amplicon (44.52% AT bp; 55.48% GC bp), possessed a higher "average" reactivity toward NH_2Cl when normalized to individual N-Cl bps (characterized by $k_{NH_2Cl,\text{N-Cl bp}}$) than *blt* 266 bp, a more AT-enriched amplicon (57.14% AT bp; 42.86% GC bp). The above explanations require future confirmation by analyzing a larger array of short amplicons with varying AT/GC ratios (all < 300 bps in length, to ensure that amplicon degradation kinetics can reach their maximum slopes prior to reaching qPCR detection limit).

To address the above problem, a new $k_{NH_2Cl,\text{N-Cl bp}}$ value was determined by using the kinetics data of 16S rRNA gene 142 bp measured in this study. In brief, the maximum slopes were determined through linear regression of the "linear" region at *CT*s > ~200 M·s (Figure S3.6) as 0.062(±0.003), 0.069(±0.007), 0.063(±0.008), 0.051(±0.002), and 0.029(±0.027) $M^{-1}s^{-1}$ for 16S rRNA gene 142 bp amplicons of *B. subtilis* 1A189, MRSA, VRE, *E. coli* SMS-3-5, and PAO1, respectively. Then, by dividing the absolute value of the maximum slope for each amplicon (i.e., $k_{NH_2Cl,\text{N-Cl bp}}\left(\frac{\text{\#N-Cl bp}}{\text{Amp}_{\text{N-Cl}}}\right)$) over the maximum $\frac{\text{\#N-Cl bp}}{\text{Amp}_{\text{N-Cl}}}$ (i.e., amplicon length of 143, 143, 142, 142, and 142 bp), $k_{NH_2Cl,\text{N-Cl bp}}$ was calculated as $4.3(\pm0.2)\times10^{-4}$, $4.8(\pm0.5)\times10^{-4}$,

$4.5(\pm0.6)\times10^{-4}$, $3.6(\pm0.1)\times10^{-4}$, and $2.0(\pm1.9)\times10^{-4}$ $M^{-1}s^{-1}$, respectively, for the five strains. An average value of $k_{NH_2Cl,N\text{-}Cl\ bp}$ was then calculated as $4.3(\pm0.2)\times10^{-4}$ $M^{-1}s^{-1}$ by excluding the value generated from PAO1 data (= $2.0(\pm1.9)\times10^{-4}$ $M^{-1}s^{-1}$), which is far lower than the other four and characterized by much larger uncertainty (potentially due to impurities within the extracellular DNA extracted from PAO1 cells). Finally, the newly-determined $k_{NH_2Cl,N\text{-}Cl\ bp}$ was applied to solve for a new set of $k_{NH_2Cl,Amp}$ values for each of the 21 amplicons (including the four *blt* amplicons, using their previously measured kinetics data). This new set of $k_{NH_2Cl,Amp}$ values (determined using the new $k_{NH_2Cl,N\text{-}Cl\ bp}$ value) yields a stronger correlation with amplicon length (i.e., AT+GC bp content) than the older set (determined using the previous $k_{NH_2Cl,N\text{-}Cl\ bp}$), as obtained through weighted linear regressions. The differences in the new and old data sets are evident in Figure S3.7 (with $R^2 = 0.71$ and 0.49 for the new and old sets of $k_{NH_2Cl,Amp}$, respectively), suggesting that modeling efforts in the present work could be improved by adopting the new set of $k_{NH_2Cl,Amp}$ values. Therefore, in this study, the newly-determined $k_{NH_2Cl,N\text{-}Cl\ bp}$ and its corresponding $k_{NH_2Cl,Amp}$ values were adopted to derive sequence-independent rate constants, as summarized in Table 3.1, where the corresponding non-linear regression fits are depicted as lines in Figure S3.5.

Text S6. Dependence of rate constants $k_{UV,Amp,app}$ or $k_{UV,Amp\text{-}CPD,f}$ on amplicon contents of 5'-TT-3' and *weighted* 5'-T/C-3', and comparison of the *measured* rate constants with *theoretical* rate constants of overall lesion formation ($k_{UV,all\ lesions,f}$) and TT-CPD formation ($k_{UV,TT\text{-}CPD,f}$).

In this study, the total numbers of 5'-T/C-3' doublets (where T/C = bipyrimidine = TT, TC, CT, or CC) per amplicon were weighted by the extinction coefficients and quantum yields of lesion formation at 254 nm UV light ($\varepsilon_{254,\ 5'\text{-}T/C\text{-}3'}$ and $\phi_{254,\ 5'\text{-}T/C\text{-}3'}$, respectively) for each type of 5'-T/C-3' doublets, to account for their contributions to overall formation of UV-induced lesions in

target amplicons. The *weighted* 5'-T/C-3' doublet content for each amplicon was calculated as below (eq S3.8),

$$weighted\ \#5'\text{-T/C-3}' = \sum_{\substack{\text{T/C = TT,}\\ \text{TC, CT, CC}}} \left(\#5'\text{-T/C-3}' \cdot weight_{5'\text{-T/C-3}'}\right) \quad \text{(eq S3.8)}$$

where $\#5'\text{-T/C-3}'$ is the number of each type of 5'-T/C-3' doublet contained in the given amplicon, and $weight_{5'\text{-T/C-3}'}$ represents the weight for each type of 5'-T/C-3' doublet and was evaluated as (eq S3.9),

$$weight_{5'\text{-T/C-3}'} = \frac{\varepsilon_{254,\ 5'\text{-T/C-3}'}\phi_{254,\ 5'\text{-T/C-3}'}}{\sum_{\substack{\text{T/C = TT,}\\ \text{TC, CT, CC}}} \left(\varepsilon_{254,\ 5'\text{-T/C-3}'}\phi_{254,\ 5'\text{-T/C-3}'}\right)} \quad \text{(eq S3.9)}$$

where $\varepsilon_{254,\ 5'\text{-T/C-3}'}$, represents the molar extinction coefficients for each 5'-T/C-3' doublet (with consideration of the hypochromism effect) at 254 nm – derived from the data of Tataurov et al. (2008)[10] as 5.36×10^3, 6.16×10^3, 6.32×10^3, 7.19×10^3 $M^{-1}cm^{-1}$ for 5'-TT-3', 5'-TC-3', 5'-CT-3', and 5'-CC-3', respectively; and $\phi_{254,\ 5'\text{-T/C-3}'}$, represents the quantum yields for *overall lesion formation* for each 5'-T/C-3' doublet at 254 nm – derived from the data of Douki (2006)[11] as 0.0096, 0.0102, 0.0017, 0.0005 for 5'-TT-3', 5'-TC-3', 5'-CT-3', and 5'-CC-3', respectively. Derivations of the values of $\varepsilon_{254,\ 5'\text{-T/C-3}'}$ and $\phi_{254,\ 5'\text{-T/C-3}'}$ were previously described in He et al. (2019).[2] The values of $e_{254,\ 5'\text{-bipyrimidine-3}'}f_{254,\ 5'\text{-bipyrimidine-3}'}$ were in turn calculated as 52, 63, 11, and 3.3 for 5'-TT -3', 5'-TC -3', 5'-CT -3', and 5'-CC -3', respectively, and the values of $weight_{5'\text{-T/C-3}'}$ as 0.40, 0.49, 0.08, and, 0.03, respectively.

The method of estimating amplicon photoreactivities based on previously reported molar extinction coefficients, quantum yields, and the specific content of 5'-T/C-3' doublets for a given amplicon was originally proposed by Yoon et al. (2018),[12] and then applied in He et al. (2019)[2]

to calculate *theoretical* rate constants of overall lesion formation ($k_{UV,all\ lesions,f}$) and TT-CPD formation ($k_{UV,TT\text{-}CPD,f}$), with the equations given below (eqs S3.10-S3.11),

$$k_{UV,all\ lesions,f} = \sum_{\substack{T/C = TT,\\ TC, CT, CC}} (2.303 e_{254,\ 5'\text{-}T/C\text{-}3'} f_{254,\ 5'\text{-}T/C\text{-}3'} / U_{254})(\#_{5'\text{-}T/C\text{-}3'}) \quad \text{(eq S3.10)}$$

$$k_{UV,TT\text{-}CPD,f} = 2.303 (e_{254,\ 5'\text{-}TT\text{-}3'} f_{254,\ 5'\text{-}TT\text{-}3'} / U_{254})(\#_{5'\text{-}TT\text{-}3'}) \quad \text{(eq S3.11)}$$

where U_{254} (= 4.72×10^5 J/Einstein) is the molar photon energy at 254 nm.[13]

As shown in the main text, linear regression of the rate constants $k_{UV,Amp,app}$ or $k_{UV,Amp\text{-}CPD,f}$ (assuming $k_{UV,single\text{-}CPD,r}$ is a universal constant for the 21 amplicons; Table 3.1) was performed versus 5'-TT-3' doublet contents (Figure 3.1a). Here, a more complete analysis of the linear-relationship models is provided in Figure S3.8, where weighted linear regressions of $k_{UV,Amp}$ were performed for three different sets of rate constants – including (1) $k_{UV,Amp,app}$ (Table 3.1), (2) $k_{UV,Amp\text{-}CPD,f}$ determined with a fixed universal $k_{UV,single\text{-}CPD,r}$ (Table 3.1), and (3) $k_{UV,Amp\text{-}CPD,f}$ determined with variable $k_{UV,single\text{-}CPD,r}$ (Text S3.5 and Table S3.6) – versus 5'-TT-3' doublet content or *weighted* 5'-T/C-3' doublet content. As shown in Figure S3.8 (Groups I and II), the three different sets of $k_{UV,Amp}$, determined based on different kinetic models, generally exhibited strong correlations ($R^2 \geq 0.91$) with 5'-TT-3' doublet content, as well as with *weighted* 5'-T/C-3' doublet content, after pooling the data for all 21 amplicons together. Furthermore, for each dataset, $k_{UV,Amp}$ visually appears to align more closely with *weighted* 5'-T/C-3' doublet content than with 5'-TT-3' doublet content (though this is not directly reflected in the R^2 values of the weighted linear regressions). This is most obvious for the third dataset of $k_{UV,Amp\text{-}CPD,f}$ determined with variable $k_{UV,single\text{-}CPD,r}$ (by comparing Figure S3.8-Ic and IIc). One explanation for this trend may be that $k_{UV,Amp\text{-}CPD,f}$ determined with variable $k_{UV,single\text{-}CPD,r}$ (Table S3.6) more accurately captures the *real* photoreactivity of CPD formation for each amplicon than either $k_{UV,Amp,app}$, or

$k_{UV,Amp\text{-}CPD,f}$ determined with a fixed universal $k_{UV,single\text{-}CPD,r}$, since the former excludes not only the contribution of 6-4PP formation, but also the varying effects of photoreversal for different amplicons, and the latter excludes the varying effects of photoreversal for different amplicons. Clearly in Figure S3.8-Ic, the more GC-enriched amplicons (GC content = 50-57%) exhibit higher photoreactivities per unit of molar 5'-TT-3' content than the more AT-enriched ones (GC content = 30-45%, e.g., *blt* 266-1017 bp, *mec*A 1018 bp, v*an*A 1030 bp), likely due to the fact that the more GC-enriched amplicons possess higher frequencies of 5'-TC-3', 5'-CT-3', 5'-CC-3' doublets within the total 5'-T/C-3' doublet populations.[14] These latter three doublets (5'-TC-3', 5'-CT-3', and 5'-CC-3') also play significant roles in UV-induced lesion formation[11, 14] but were not taken into account in the simple linear-regression model incorporating only molar 5'-TT-3' content. The discrepancies between GC-enriched and AT-enriched amplicons were reconciled by plotting $k_{UV,Amp\text{-}CPD,f}$ (determined with variable $k_{UV,single\text{-}CPD,r}$) versus *weighted* 5'-T/C-3' doublet content, which enables consideration of the contributions of all types of 5'-T/C-3' doublets (Figure S3.8-IIc). This is consistent with the above discussions of 5'-T/C-3' reactivities and indicates that *weighted* 5'-T/C-3' doublet content could be a better predictor in estimating the photoreactivities of DNA segments, as also demonstrated in Figure S3.8-IIa and IIb.

Theoretical values of $k_{UV,all\ lesions,f}$ and $k_{UV,TT\text{-}CPD,f}$ were also calculated for all 21 amplicons based on eqs S3.10 and S3.11, respectively, using the above $\varepsilon_{254,\ 5'\text{-}T/C\text{-}3'}$ and $\phi_{254,\ 5'\text{-}T/C\text{-}3'}$ values derived from Douki (2006)[11] and Tataurov et al. (2008).[10] The resulting values of $k_{UV,all\ lesions,f}$ and $k_{UV,TT\text{-}CPD,f}$ were then compared with the three sets of *measured* $k_{UV,Amp}$ values. As illustrated in Figure S3.8 (Group IV), for each data set, the *theoretical* values of $k_{UV,TT\text{-}CPD,f}$ were found to significantly underpredict the *measured* $k_{UV,Amp}$ values for the 21 amplicons, while the *theoretical* values of $k_{UV,all\ lesions,f}$ are in much better agreement with the experimental values, further

supporting the importance of considering contributions of all 5'-T/C-3' doublet types to UV-induced lesion formation. In comparison, the *theoretical* values of $k_{UV,TT\text{-}CPD,f}$ were also calculated using $\varepsilon_{254,\ 5'\text{-}TT\text{-}3'}$ (= $8.4\times10^3\ M^{-1}cm^{-1}$) and $\phi_{254,\ 5'\text{-}TT\text{-}3'}$ (= 0.019) reported by an earlier study of Patrick (1977)[15], which were adopted by Yoon et al. (2018).[12] As also shown in Figure S3.8 (Group IV), the data of Patrick (1977)[15] yielded *theoretical* $k_{UV,TT\text{-}CPD,f}$ values that significantly overpredicted the *measured* $k_{UV,Amp}$ values. These findings highlight the need for more precise determination of $\varepsilon_{254,\ 5'\text{-}T/C\text{-}3'}$ and $\phi_{254,\ 5'\text{-}T/C\text{-}3'}$ when applying this approach, as also noted previously by He et al. (2019).[2]

Table S3.1. Information of bacterial strains and associated genes

ARB strain (Gram+/–; resources, where ATCC = American Type Culture Center, and BGSC = Bacillus Genome Strain Center)	ARG or internal standard gene (location)	Use in this study	Resistance	Resistance mechanism	Growth media (and antibiotics)
Bacillus subtilis 1A189 (Gram +; BGSC)	*blt* (chromosome)	Disinfection target ARB/ARG [b] and internal standard for DNA extraction [d]	fluoroquinolones, chloramphenicol, doxorubicin, and acriflavine	Efflux pump	Antibiotic medium #3 broth; Tryptose Blood agar + 4 μg/mL acriflavine
Methicillin-resistant *Staphylococcus aureus* (MRSA) ATCC BAA-1556 (Gram +; ATCC)	*mec*A (chromosome)	Disinfection target ARB/ARG [b]	Methicillin, penicillin-like antibiotics	Penicillin-binding protein 2A	Brain Heart Infusion (BHI) broth/agar
Vancomycin-resistant Enterococci faecium (VRE) ATCC 700221 (Gram +; ATCC)	*van*A (plasmid)	Disinfection target ARB/ARG [b]	Vancomycin, teicoplanin	Alteration of cell wall (protein/peptidoglycan structure)	BHI broth/agar
Escherichia coli SMS-3-5 (ATCC BAA-1743; Gram –)	*tet*(A) (plasmid)	Disinfection target ARB/ARG [b]	Tetracyclines	Efflux pump	Luria-Bertani (LB) broth/agar
Pseudomonas aeruginosa O1 (PAO1) ATCC 47085 (Gram –; ATCC)	*amp*C (chromosome)	Disinfection target ARB/ARG [b]	Most penicillins, cephalothin, cefazolin	Class C β-lactamases	LB broth/agar + 10 μg/mL tetracycline
Klebsiella pneumoniae 1.53 (Gram –; donated) [a]	bla_{NDM} (plasmid)	Disinfection target ARG [c]	Carbapenems	Carbapenemases	BHI broth/agar + 1 μg/mL imipenem
K. pneumoniae ATCC BAA-1705 (Gram –; donated) [a]	bla_{KPC} (plasmid)	Disinfection target ARG [c]	Carbapenems	Carbapenemases	BHI broth/agar + 1 μg/mL meropenem
E. coli ECE228 (Gram –; BGSC)	*cfpamy* (plasmid)	Internal standard for DNA extraction [d]	Ampicillin (encoded by amp^R on its plasmid)	Not of interest here	LB broth/agar + 100 μg/mL ampicillin

[a] The two *K. pneumoniae* strains were kindly donated by Dr. Marilyn C. Roberts (UW), and neither of their complete genome sequences were available until preparation of this manuscript. *Klebsiella pneumoniae* 1.53, harboring bla_{NDM} (or more specifically bla_{NDM-1}), was firstly reported in Lascols et al. (2009)[16] and characterized by Ramirez et al. (2012).[17] Whole-genome draft sequence (shotgun) of *K. pneumoniae* ATCC BAA-1705, harboring bla_{KPC} (or more specifically bla_{KPC-2}) is reported by Broberg et al. (2013).[18] [b] The ARB and associated ARGs were used as disinfection model ARB/ARG pairs in bench-scale experiments, and the ARGs were also monitored for wastewater samples obtained from full-scale disinfection treatment. [c] The two ARGs (bla_{NDM} and bla_{KPC}) were monitored as disinfection targets for full-scale disinfection treatment, while the associated ARB strains were only utilized to prepare qPCR standards. [d] The internal standard genes, ARG *blt a*nd non-ARG *cfpamy*, were used in DNA extraction of full-scale wastewater samples.

Table S3.2. Sequences of ARGs and 16S rRNA genes and locations of qPCR amplicons used as disinfection targets in this study (genome sequence data accessed from GenBank, at http://www.ncbi.nlm.nih.gov/genbank/)

Amplicon (length in bp)	**Sequence (5'-3') of forward or reverse primer (FP or RP)**	T_A	**Reference(s)**
blt **266 bp**	FP: 5'-GGTAGGTGGGTTGACCGTTT-3'	55.0 °C	He et al. (2019)[2]
	RP: 5'-CCCGCACCAGGTCCAATAAT-3' => ATTATTGGACCTGGTGCGGG		
blt **832 bp**	FP: 5'-TGGGTTATCTTGTTGCGGCT-3'	55.0 °C	
	RP: 5'-GGACGTAGCAAATCGAACGC-3' => GCGTTCGATTTGCTACGTCC		
blt **870 bp**	FP: 5'-GTTCCCGTGCAAAGATTCCG-3'	60.0 °C	
	RP: 5'-CGAAACGGTCAACCCACCTA-3' => TAGGTGGGTTGACCGTTTCG		
blt **1017 bp**	FP: 5'-TCCGGTACGCCTCTTCAGTA-3'	60.0 °C	
	RP: 5'-CGAAACGGTCAACCCACCTA-3' => TAGGTGGGTTGACCGTTTCG		
	Note: locations of the four *blt* amplicons and corresponding primers on the *bltR-blt-bltD* gene segment of *B. subtilis* 168 chromosome (GenBank Accession No.: AL009126.3) were provided previously.[2] *bltR* gene: region 2716035-2716856 *blt* gene: region 2716973-2718175 *bltD* gene: region 2718344-2718802		
mec**A 1018 bp**	FP: 5'-CGCAACGTTCAATTTAATTTTGTTAA-3'	51.7 °C	Volkmann et al. (2004)[19]
	RP: 5'-CCACTTCATATCTTGTAACG-3' => CGTTACAAGATATGAAGTGG		Oliveira and de Lencastre (2002)[20]
	Staphylococcus aureus **subsp. *aureus* USA300_FPR3757, complete genome (GenBank Accession No.: CP000255.1)** ***mec*****A gene: region 39127 – 41133, 2007 bp (5', 3' termini in bold, red font)** ATGAAAAAGATAAAAATTGTTCCACTTATTTTAATAGTTGTAGTTGTCGGGTTTGGTATATATTTTTATGCTTCAAAAGATAAAGAAATTAAT AATACTATTGATGCAATTGAAGATAAAAATTTCAAACAAGTTTATAAAGATAGCAGTTATATTTCTAAAAGCGATAATGGTGAAGTAGAAAT GACTGAACGTCCGATAAAAATATATAATAGTTTAGGCGTTAAAGATATAAACATTCAGGATCGTAAAATAAAAAAAGTATCTAAAAATAAA AAACGAGTAGATGCTCAATATAAAATTAAAACAAACTACGGTAACATTGATCGCAACGTTCAATTTAATTTTGTTAAAGAAGATGGTATGTG GAAGTTAGATTGGGATCATAGCGTCATTATTCCAGGAATGCAGAAAGACCAAAGCATACATATTGAAAATTTAAAATCAGAACGTGGTAAA ATTTTAGACCGAAACAATGTGGAATTGGCCAATACAGGAACAGCATATGAGATAGGCATCGTTCCAAAGAATGTATCTAAAAAAGATTATAA AGCAATCGCTAAAGAACTAAGTATTTCTGAAGACTATATCAAACAACAAATGGATCAAAATTGGGTACAAGATGATACCTTCGTTCCACTTA AAACCGTTAAAAAAATGGATGAATATTTAAGTGATTTCGCAAAAAAATTTCATCTTACAACTAATGAAACAGAAAGTCGTAACTATCCTCTA GGAAAAGCGACTTCACATCTATTAGGTTATGTTGGTCCCATTAACTCTGAAGAATTAAAACAAAAAGAATATAAAGGCTATAAAGATGATGC AGTTATTGGTAAAAAGGGACTCGAAAAACTTTACGATAAAAAGCTCCAACATGAAGATGGCTATCGTGTCACAATCGTTGACGATAATAGCA ATACAATCGCACATACATTAATAGAGAAAAAGAAAAAAGATGGCAAAGATATTCAACTAACTATTGATGCTAAAGTTCAAAAGAGTATTTAT AACAACATGAAAAATGATTATGGCTCAGGTACTGCTATCCACCCTCAAACAGGTGAATTATTAGCACTTGTAAGCACACCTTCATATGACGTC TATCCATTTATGTATGGCATGAGTAACGAAGAATATAATAAATTAACCGAAGATAAAAAAGAACCTCTGCTCAACAAGTTCCAGATTACAAC TTCACCAGGTTCAACTCAAAAAATATTAACAGCAATGATTGGGTTAAATAACAAAACATTAGACGATAAAACAAGTTATAAAATCGATGGTA AAGGTTGGCAAAAAGATAAATCTTGGGGTGGTTACAACGTTACAAGATATGAAGTGGTAAATGGTAATATCGACTTAAAACAAGCAATAGA ATCATCAGATAACATTTTCTTTGCTAGAGTAGCACTCGAATTAGGCAGTAAGAAATTTGAAAAAGGCATGAAAAAACTAGGTGTTGGTGAAG ATATACCAAGTGATTATCCATTTTATAATGCTCAAATTTCAAACAAAAATTTAGATAATGAAATATTATTAGCTGATTCAGGTTACGGACAAG		

	GTGAAATACTGATTAACCCAGTACAGATCCTTTCAATCTATAGCGCATTAGAAAATAATGGCAATATTAACGCACCTCACTTATTAAAAGAC ACGAAAAACAAAGTTTGGAAGAAAAATATTATTTCCAAAGAAAATATCAATCTATTAACTGATGGTATGCAACAAGTCGTAAATAAAACAC ATAAAGAAGATATTTATAGATCTTATGCAAACTTAATTGGCAAATCCGGTACTGCAGAACTCAAAATGAAACAAGGAGAAACTGGCAGACA AATTGGGTGGTTTATATCATATGATAAAGATAATCCAAACATGATGATGGCTATTAATGTTAAAGATGTACAAGATAAAGGAATGGCTAGCT ACAATGCCAAAATCTCAGGTAAAGTGTATGATGAGCTATATGAGAACGGTAATAAAAAATACGATATAGATGAATA**A**		
***van*A** **1030 bp**	FP: 5'-CATGAATAGAATAAAAGTTGCAATA-3'	55.7 °C	Clark et al. (1993)[21]
	RP: 5'-CCCCTTTAACGCTAATACGATCAA-3' => TTGATCGTATTAGCGTTAAAGGGG		
	***Enterococcus faecium* strain ATCC 700221 plasmid unnamed3, complete sequence (GenBank Accession No.: CP014452.1)** ***van*A gene: region 33682 – 34713, 1032 bp (5', 3' termini in bold, red font)** Note: the forward primer targets sequence beyond *van*A gene by one bp. GACAGGAGC**A**TGAATAGAATAAAAGTTGCAATACTGTTTGGGGGTTGCTCAGAGGAGCATGACGTATCGGTAAAATCTGCAATAGAGATAG CCGCTAACATTAATAAAGAAAAATACGAGCCGTTATACATTGGAATTACGAAATCTGGTGTATGGAAAATGTGCGAAAAACCTTGCGCGGAA TGGGAAAACGACAATTGCTATTCAGCTGTACTCTCGCCGGATAAAAAAATGCACGGATTACTTGTTAAAAAGAACCATGAATATGAAATCAA CCATGTTGATGTAGCATTTTCAGCTTTGCATGGCAAGTCAGGTGAAGATGGATCCATACAAGGTCTGTTTGAATTGTCCGGTATCCCTTTTGTA GGCTGCGATATTCAAAGCTCAGCAATTTGTATGGACAAATCGTTGACATACATCGTTGCGAAAAATGCTGGGATAGCTACTCCCGCCTTTTGG GTTATTAATAAAGATGATAGGCCGGTGGCAGCTACGTTTACCTATCCTGTTTTTGTTAAGCCGGCGCGTTCAGGCTCATCCTTCGGTGTGAAA AAAGTCAATAGCGCGGACGAATTGGACTACGCAATTGAATCGGCAAGACAATATGACAGCAAAATCTTAATTGAGCAGGCTGTTTCGGGCTG TGAGGTCGGTTGTGCGGTATTGGGAAACAGTGCCGCGTTAGCTGTTGGCGAGGTGGACCAAATCAGGCTGCAGTACGGAATCTTTCGTATTC ATCAGGAAGTCGAGCCGGAAAAAGGCTCTGAAAACGCAGTTATAACCGTTCCCGCAGACCTTTCAGCAGAGGAGCGAGGACGGATACAGGA AACGGCAAAAAAAATATATAAAGCGCTCGGCTGTAGAGGTCTAGCCCGTGTGGATATGTTTTTACAAGATAACGGCCGCATTGTACTGAACG AAGTCAATACTCTGCCCGGTTTCACGTCATACAGTCGTTATCCCCGTATGATGGCCGCTGCAGGTATTGCACTTCCCGAACTGATTGACCGC**T** TGATCGTATTAGCGTTAAAGGGGTG**A**		
***tet*(A)** **1054 bp**	FP: 5'-GTAATTCTGAGCACTGTCGC-3'	57.2 °C	Dalsgaard et al. (2001);[22] and modified by McKinney and Pruden (2012)[4]
	RP: 5'-CATAGATCGCCGTGAAGAGG-3' => CCTCTTCACGGCGATCTATG		Ng et al. (2001)[23]
	***Escherichia coli* SMS-3-5 plasmid pSMS35_130, complete sequence (GenBank Accession No.: CP000971.1)** ***tet*(A) gene: region 120487 – 121761; length 1275 bp (5', 3' termini in bold, red font)** **GenBank: CP000971.1 (Region: 120487 – 121761; Gene length: 1275 bp; Amplicon length: 1054 bp)** **A**TGTCCACCAACTTATCAGTGATAAAGAATCCGCGCGTTCAATCGGACCAGCGGAGGCTGGTCCGGAGGCCAGACGTGAAACCCAACAGAC CCCTGATCGTAATTCTGAGCACTGTCGCGCTCGACGCTGTCGGCATCGGCCTGATTATGCCGGTGCTGCCGGGCCTCCTGCGCGATCTGGTTC ACTCGAACGACGTCACCGCCCACTATGGCATTCTGCTGGCGCTGTATGCGTTGATGCAATTTGCCTGCGCACCTGTGCTGGGCGCGCTGTCGG ATCGTTTCGGGCGGCGGCCGGTCTTGCTCGTCTCGCTGGCCGGCGCTGCTGTCGACTACGCCATCATGGCGACGGCGCCTTTCCTTTGGGTTCT CTATATCGGGCGGATCGTGGCCGGCATCACCGGGGCGACTGGGGCGGTAGCCGGCGCTTATATTGCCGATATCACTGATGGCGATGAGCGCG CGCGGCACTTCGGCTTCATGAGCGCCTGTTTCGGGTTCGGGATGGTCGCGGGACCTGTGCTCGGTGGGCTGATGGGCGGTTTCTCCCCCCACG CTCCGTTCTTCGCCGCGGCAGCCTTGAACGGCCTCAATTTCCTGACGGGCTGTTTCCTTTTGCCGGAGTCGCACAAAGGCGAACGCCGGCCGT TACGCCGGGAGGCTCTCAACCCGCTCGCTTCGTTCCGGTGGGCCCGGGGCATGACCGTCGTCGCCGCCCTGATGGCGGTCTTCTTCATCATGC AACTTGTCGGACAGGTGCCGGCCGCGCTTTGGGTCATTTTCGGCGAGGATCGCTTTCACTGGGACGCGACCACGATCGGCATTTCGCTTGCCG CATTTGGCATTCTGCATTCACTCGCCCAGGCAATGATCACCGGCCCTGTAGCCGCCCGGCTCGGCGAAAGGCGGGCACTCATGCTCGGAATG		

	ATTGCCGACGGCACAGGCTACATCCTGCTTGCCTTCGCGACACGGGGATGGATGGCGTTCCCGATCATGGTCCTGCTTGCTTCGGGTGGCATC GGAATGCCGGCGCTGCAAGCAATGTTGTCCAGGCAGGTGGATGAGGAACGTCAGGGGCAGCTGCAAGGCTCACTGGCGGCGCTCACCAGCC TGACCTCGATCGTCGGACCCCTCCTCTTCACGGCGATCTATGCGGCTTCTATAACAACGTGGAACGGGTGGGCATGGATTGCAGGCGCTGCCC TCTACTTGCTCTGCCTGCCGGCGCTGCGTCGCGGGCTTTGGAGCGGCGCAGGGCAACGAGCCGATCGCTGA		
***amp*C** **1006 bp**	FP: 5'-CGGCTCGGTGAGCAAGACCTTC-3' RP: 5'-GAAGCGCTCATGGCACCATCATAGCC-3' => GGCTATGATGGTGCCATGAGCGCTTC	70.9 °C	Dumas et al. (2006)[24] Tam et al. (2007)[25]
	***Pseudomonas aeruginosa* PAO1, complete genome (GenBank Accession No.: AE004091.2)** ***ampC* gene: region 4594029 – 4595222, 1194 bp (5', 3' termini in bold, red font)** Note: the reverse primer targets sequence beyond *amp*C gene. ATGCGCGATACCAGATTCCCCTGCCTGTGCGGCATCGCCGCTTCCACACTGCTGTTCGCCACCACCCCGGCCATTGCCGGCGAGGCCCCGGCG GATCGCCTGAAGGCACTGGTCGACGCCGCCGTACAACCGGTGATGAAGGCCAATGACATTCCGGGCCTGGCCGTAGCCATCAGCCTGAAAG GAGAACCGCATTACTTCAGCTATGGGCTGGCCTCGAAAGAGGACGGCCGCCGGGTGACGCCGGAGACCCTGTTCGAGATCGGCTCGGTGAG CAAGACCTTCACCGCCACCCTCGCCGGCTATGCCCTGACCCAGGACAAGATGCGCCTCGACGACCGCGCCAGCCAGCACTGGCCGGCACTGC AGGGCAGCCGCTTCGACGGCATCAGCCTGCTCGACCTCGCGACCTATACCGCCGGCGGCTTGCCGCTGCAGTTCCCCGACTCGGTGCAGAAG GACCAGGCACAGATCCGCGACTACTACCGCCAGTGGCAGCCGACCTACGCGCCGGGCAGCCAGCGCCTCTATTCCAACCCGAGCATCGGCCT GTTCGGCTATCTCGCCGCGCGCAGCCTGGGCCAGCCGTTCGAACGGCTCATGGAGCAGCAAGTGTTCCCGGCACTGGGCCTCGAACAGACCC ACCTCGACGTGCCCGAGGCGGCGCTGGCGCAGTACGCCCAGGGCTATGGCAAGGACGACCGCCCGCTACGGGTCGGTCCCGGCCCGCTGGA TGCCGAAGGCTACGGGGTGAAGACCAGCGCGGCCGACCTGCTGCGCTTCGTCGATGCCAACCTGCATCCGGAGCGCCTGGACAGGCCCTGGG CGCAGGCGCTCGATGCCACCCATCGCGGTTACTACAAGGTCGGCGACATGACCCAGGGCCTGGGCTGGGAAGCCTACGACTGGCCGATCTCC CTGAAGCGCCTGCAGGCCGGCAACTCGACGCCGATGGCGCTGCAACCGCACAGGATCGCCAGGCTGCCCGCGCCACAGGCGCTGGAGGGCC AGCGCCTGCTGAACAAGACCGGTTCCACCAACGGCTTCGGCGCCTACGTGGCGTTCGTCCCGGGCCGCGACCTGGGCCTGGTGATCCTGGCC AACCGCAACTATCCCAATGCCGAGCGGGTGAAGATCGCCTACGCCATCCTCAGCGGCCTGGAGCAGCAGGGCAAGGTGCCGCTGAAGCGCT GAAGCGCGCTCGCGAGGGCGACGGAGCGTAGCGGCGCGGGACGCCGGTCCTGGCTATGATGGTGCCATGAGCGCTTCCCCGCCCCTCCGCCA GCCCTGCCCGCCCGGCGCCTG		
***bla*$_{NDM}$** **807 bp**	FP: 5'-GGAATTGCCCAATATTATGC-3' RP: 5'-CGCAGCTTGTCGGCCATG-3' => CATGGCCGACAAGCTGCG	61.2 °C	Luo et el. (2013)[26]
	***Klebsiella pneumoniae* strain ATCC BAA-2146 plasmid pNDM-US, complete sequence (GenBank Accession No.: CP006661.1)** ***bla*$_{NDM}$ gene: region 122191-123003, 813 bp (5', 3' termini in bold, red font)** Note: the primer pair was designed based on the sequence of *bla*$_{NDM-1}$,[26] while primer-BLAST indicates it can amplify *bla*$_{NDM}$ variants from *bla*$_{NDM-1}$ to *bla*$_{NDM-29}$. ATGGAATTGCCCAATATTATGCACCCGGTCGCGAAGCTGAGCACCGCATTAGCCGCTGCATTGATGCTGAGCGGGTGCATGCCCGGTGAAAT CCGCCCGACGATTGGCCAGCAAATGGAAACTGGCGACCAACGGTTTGGCGATCTGGTTTTCCGCCAGCTCGCACCGAATGTCTGGCAGCACA CTTCCTATCTCGACATGCCGGGTTTCGGGGCAGTCGCTTCCAACGGTTTGATCGTCAGGGATGGCGGCCGCGTGCTGGTGGTCGATACCGCCT GGACCGATGACCAGACCGCCCAGATCCTCAACTGGATCAAGCAGGAGATCAACCTGCCGGTCGCGCTGGCGGTGGTGACTCACGCGCATCA GGACAAGATGGGCGGTATGGACGCGCTGCATGCGGCGGGGATTGCGACTTATGCCAATGCGTTGTCGAACCAGCTTGCCCCGCAAGAGGGG ATGGTTGCGGCGCAACACAGCCTGACTTTCGCCGCCAATGGCTGGGTCGAACCAGCAACCGCGCCCAACTTTGGCCCGCTCAAGGTATTTTA CCCCGGCCCCGGCCACACCAGTGACAATATCACCGTTGGGATCGACGGCACCGACATCGCTTTTGGTGGCTGCCTGATCAAGGACAGCAAGG CCAAGTCGCTCGGCAATCTCGGTGATGCCGACACTGAGCACTACGCCGCGTCAGCGCGCGTTTGGTGCGGCGTTCCCCAAGGCCAGCATG ATCGTGATGAGCCATTCCGCCCCCGATAGCCGCGCCGCAATCACTCATACGGCCCGCATGGCCGACAAGCTGCCCTGA		
***bla*$_{KPC}$** **805 bp**	FP: 5'-CGCGGAACCATTCGCTAAACTC-3' RP: 5'-TTCAGAGCCTTACTGCCCGTTG-3' => CAACGGGCAGTAAGGCTCTGAA	64.5 °C	This study
	***Klebsiella pneumoniae* strain ATCC BAA-1705 carbapenem-hydrolyzing beta-lactamase (blaKPC-2) gene (GenBank Accession No.: FJ665695.1)**		

	KPC-2 gene: region 1-842, 842 bp (5', 3' termini in bold, red font) Note: the primer pair was designed based on the sequence of *bla*$_{KPC-2}$ in this study, while primer-BLAST indicates it can amplify *bla*$_{KPC}$ variants including *bla*$_{NDM-1}$ to *bla*$_{NDM-5}$, as well as *bla*$_{NDM-14}$, *bla*$_{NDM-18}$, and *bla*$_{NDM-33}$. CGCGCTGACCAACCTCGTCGCGGAACCATTCGCTAAACTCGAACAGGACTTTGGCGGCTCCATCGGTGTGTACGCGATGGATACCGGCTCAG GCGCAACTGTAAGTTACCGCGCTGAGGAGCGCTTCCCACTGTGCAGCTCATTCAAGGGCTTTCTTGCTGCCGCTGTGCTGGCTCGCAGCCAGC AGCAGGCCGGCTTGCTGGACACACCCATCCGTTACGGCAAAAATGCGCTGGTTCCGTGGTCACCCATCTCGGAAAAATATCTGACAACAGGC ATGACGGTGGCGGAGCTGTCCGCGGCCGCCGTGCAATACAGTGATAACGCCGCCGCCAATTTGTTGCTGAAGGAGTTGGGCGGCCCGGCCGG GCTGACGGCCTTCATGCGCTCTATCGGCGATACCACGTTCCGTCTGGACCGCTGGGAGCTGGAGCTGAACTCCGCCATCCCAGGCGATGCGC GCGATACCTCATCGCCGCGCGCCGTGACGGAAAGCTTACAAAAACTGACACTGGGCTCTGCACTGGCTGCGCCGCAGCGGCAGCAGTTTGTT GATTGGCTAAAGGGAAACACGACCGGCAACCACCGCATCCGCGCGGCGGTGCCGGCAGACTGGGCAGTCGGAGACAAAACCGGAACCTGCG GAGTGTATGGCACGGCAAATGACTATGCCGTCGTCTGGCCCACTGGGCGCGCACCTATTGTGTTGGCCGTCTACACCCGGGCGCCTAACAAG GATGACAAGCACAGCGAGGCCGTCATCGCCGCTGCGGCTAGACTCGCGCTCGAGGGATTGGGCGTCAACGGGCAGTAAGGCTCTGAAAATC ATCTATTGGCCCACC		
16S rRNA gene 142 bp	FP (1369F) [a]: 5'-CGGTGAATACGTTCYCGG-3' RP (1492R) [a]: 5'-GGWTACCTTGTTACGACTT-3' => **AAGTCGTAACAAGGTAWCC**	57.5 °C	Suzuki et al. (2000)[27]
16S rRNA gene 534 bp	FP (27F) [a]: 5'-**AGAGTTTGATCCTGGCTCAG**-3' RP (534R) [a]: 5'-GWATTACCGCGGCKGCTG-3' => CAGCMGCCGCGGTAATWC	62.5 °C	Devereux and Wilkinson (1995)[28] Baker et al. (2003)[29]
16S rRNA gene 734 bp	FP (779F) [a]: 5'-GCTAASSGGATTAGATACCC-3' RP (1510R) [a]: 5'-GGTTACCTTGTTACGACTT-3' => AAGTCGTAACAAGGTAACC	61.0 °C	Baker et al. (2003)[29]
16S rRNA gene 1068 bp	FP (341F) [a]: 5'-CCTACGGGRSGCAGCAG-3' RP (1406R) [a]: 5'-GACGGGCGGTGTGTRCA-3' => TGYACACACCGCCCGTC	64.6 °C	Baker et al. (2003)[29]
16S rRNA gene 1509 bp	FP (27F) [a]: 5'-**AGAGTTTGATCCTGGCTCAG**-3' RP (1492R) [a]: 5'-GGWTACCTTGTTACGACTT-3' => **AAGTCGTAACAAGGTAWCC**	57.0 °C	Devereux and Wilkinson (1995)[28] Suzuki et al. (2000)[27]
	***Bacillus subtilis* subsp. subtilis str. 168 chromosome, complete genome (GenBank Accession No.: AL009126.3)** **16S rRNA gene: region 9810 – 11364, 1555 bp (5', 3' termini in bold, red font)** Note: *B. subtilis* 168 chromosome contains 10 copies of 16S rRNA gene (≥ 99% identity). Here shows the 1st one as the example. Amplicon lengths: 143, 536, 734, 1068, and 1511 bp ATTTATCGG**AGAGTTTGATCCTGGCTCAG**GACGAACGCTGGCGGCGTGCCTAATACATGCAAGTCGAGCGGACAGATGGGAGCTTGCTCCC TGATGTTAGCGGCGGACGGGTGAGTAACACGTGGGTAACCTGCCTGTAAGACTGGGATAACTCCGGGAAACCGGGGCTAATACCGGATGGT TGTTTGAACCGCATGGTTCAAACATAAAAGGTGGCTTCGGCTACCACTTACAGATGGACCCGCGGCGCATTAGCTAGTTGGTGAGGTAACGG CTCACCAAGGCGACGATGCGTAGCCGACCTGAGAGGGTGATCGGCCACACTGGGACTGAGACACGGCCCAGACTCCTACGGGAGGCAGCAG TAGGGAATCTTCCGCAATGGACGAAAGTCTGACGGAGCAACGCCGCGTGAGTGATGAAGGTTTTCGGATCGTAAAGCTCTGTTGTTAGGGAA GAACAAGTGCCGTTCGAATAGGGCGGTACCTTGACGGTACCTAACCAGAAAGCCACGGCTAACTACGTGCCAGCAGCCGCGGTAATACGTA GGTGGCAAGCGTTGTCCGGAATTATTGGGCGTAAAGGGCTCGCAGGCGGTTTCTTAAGTCTGATGTGAAAGCCCCCGGCTCAACCGGGGAGG GTCATTGGAAACTGGGGAACTTGAGTGCAGAAGAGGAGAGTGGAATTCCACGTGTAGCGGTGAAATGCGTAGAGATGTGGAGGAACACCAG TGGCGAAGGCGACTCTCTGGTCTGTAACTGACGCTGAGGAGCGAAAGCGTGGGGAGCGAACAGGATTAGATACCCTGGTAGTCCACGCCGT AAACGATGAGTGCTAAGTGTTAGGGGGTTTCCGCCCCTTAGTGCTGCAGCTAACGCATTAAGCACTCCGCCTGGGGAGTACGGTCGCAAGAC TGAAACTCAAAGGAATTGACGGGGGCCCGCACAAGCGGTGGAGCATGTGGTTTAATTCGAAGCAACGCGAAGAACCTTACCAGGTCTTGAC ATCCTCTGACAATCCTAGAGATAGGACGTCCCCTTCGGGGGCAGAGTGACAGGTGGTGCATGGTTGTCGTCAGCTCGTGTCGTGAGATGTTG GGTTAAGTCCCGCAACGAGCGCAACCCTTGATCTTAGTTGCCAGCATTCAGTTGGGCACTCTAAGGTGACTGCCGGTGACAAACCGGAGGAA		

	GGTGGGGATGACGTCAAATCATCATGCCCCTTATGACCTGGGCTACACACGTGCTACAATGGACAGAACAAAGGGCAGCGAAACCGCGAGG TTAAGCCAATCCCACAAATCTGTTCTCAGTTCGGATCGCAGTCTGCAACTCGACTGCGTGAAGCTGGAATCGCTAGTAATCGCGGATCAGCAT GCCGCGGTGAATACGTTCCCGGGCCTTGTACACACCGCCCGTCACACCACGAGAGTTTGTAACACCCGAAGTCGGTGAGGTAACCTTTTAGG AGCCAGCCGCCGAAGGTGGGACAGATGATTGGGGTGAAGTCGTAACAAGGTAGCCGTATCGGAAGGTGCGGCTGGATCACCTCCTTTCTA
	***Staphylococcus aureus* subsp. aureus USA300_FPR3757, complete genome (GenBank Accession No.: CP000255.1)** **16S rRNA gene: region 512890 – 514444, 1555 bp (5', 3' termini in bold, red font)** Note: MRSA chromosome contains 5 copies of 16S rRNA gene (100% identity). Here shows the 1st one as the example. Amplicon lengths: 143, 536, 736, 1069, and 1513 bp TTTTATGGAGAGTTTGATCCTGGCTCAGGATGAACGCTGGCGGCGTGCCTAATACATGCAAGTCGAGCGAACGGACGAGAAGCTTGCTTCT CTGATGTTAGCGGCGGACGGGTGAGTAACACGTGGATAACCTACCTATAAGACTGGGATAACTTCGGGAAACCGGAGCTAATACCGGATAA TATTTTGAACCGCATGGTTCAAAAGTGAAAGACGGTCTTGCTGTCACTTATAGATGGATCCGCGCTGCATTAGCTAGTTGGTAAGGTAACGGC TTACCAAGGCAACGATGCATAGCCGACCTGAGAGGGTGATCGGCCACACTGGAACTGAGACACGGTCCAGACTCCTACGGGAGGCAGCAGT AGGGAATCTTCCGCAATGGGCGAAAGCCTGACGGAGCAACGCCGCGTGAGTGATGAAGGTCTTCGGATCGTAAAACTCTGTTATTAGGGAA GAACATATGTGTAAGTAACTGTGCACATCTTGACGGTACCTAATCAGAAAGCCACGGCTAACTACGTGCCAGCAGCCGCGGTAATACGTAGG TGGCAAGCGTTATCCGGAATTATTGGGCGTAAAGCGCGCGTAGGCGGTTTTTTAAGTCTGATGTGAAAGCCCACGGCTCAACCGTGGAGGGT CATTGGAAACTGGAAAACTTGAGTGCAGAAGAGGAAAGTGGAATTCCATGTGTAGCGGTGAAATGCGCAGAGATATGGAGGAACACCAGTG GCGAAGGCGACTTTCTGGTCTGTAACTGACGCTGATGTGCGAAAGCGTGGGGATCAAACAGGATTAGATACCCTGGTAGTCCACGCCGTAAA CGATGAGTGCTAAGTGTTAGGGGGTTTCCGCCCCTTAGTGCTGCAGCTAACGCATTAAGCACTCCGCCTGGGGAGTACGACCGCAAGGTTGA AACTCAAAGGAATTGACGGGGACCCGCACAAGCGGTGGAGCATGTGGTTTAATTCGAAGCAACGCGAAGAACCTTACCAAATCTTGACATC CTTTGACAACTCTAGAGATAGAGCCTTCCCCTTCGGGGGACAAAGTGACAGGTGGTGCATGGTTGTCGTCAGCTCGTGTCGTGAGATGTTGG GTTAAGTCCCGCAACGAGCGCAACCCTTAAGCTTAGTTGCCATCATTAAGTTGGGCACTCTAAGTTGACTGCCGGTGACAAACCGGAGGAAG GTGGGGATGACGTCAAATCATCATGCCCCTTATGATTTGGGCTACACACGTGCTACAATGGACAATACAAAGGGCAGCGAAACCGCGAGGTC AAGCAAATCCCATAAAGTTGTTCTCAGTTCGGATTGTAGTCTGCAACTCGACTACATGAAGCTGGAATCGCTAGTAATCGTAGATCAGCATGC TACGGTGAATACGTTCCCGGGTCTTGTACACACCGCCCGTCACACCACGAGAGTTTGTAACACCCGAAGCCGGTGGAGTAACCTTTTAGGAG CTAGCCGTCGAAGGTGGGACAAATGATTGGGGTGAAGTCGTAACAAGGTAGCCGTATCGGAAGGTGCGGCTGGATCACCTCCTTTCT
	***Enterococcus faecium* strain ATCC 700221, complete genome (GenBank Accession No.: CP014449.1)** **16S rRNA gene: region 430703 – 432271, 1569 bp (5', 3' termini in bold, red font)** Note: VRE chromosome contains 6 copies of 16S rRNA gene (≥ 99% identity). Here shows the 1st one as the example. Amplicon Lengths: 142, 547, 733, 1067, and 1521 bp. TTTTTATGAGAGTTTGATCCTGGCTCAGGACGAACGCTGGCGGCGTGCCTAATACATGCAAGTCGAACGCTTCTTTTTCCACCGGAGCTTGC TCCACCGGAAAAAGAGGAGTGGCGAACGGGTGAGTAACACGTGGGTAACCTGCCCATCAGAAGGGGATAACACTTGGAAACAGGTGCTAAT ACCGTATAACAATCGAAACCGCATGGTTTTGATTTGAAAGGCGCTTTCGGGTGTCGCTGATGGATGGACCCGCGGTGCATTAGCTAGTTGGTG AGGTAACGGCTCACCAAGGCCACGATGCATAGCCGACCTGAGAGGGTGATCGGCCACATTGGGACTGAGACACGGCCCAAACTCCTACGGG AGGCAGCAGTAGGGAATCTTCGGCAATGGACGAAAGTCTGACCGAGCAACGCCGCGTGAGTGAAGAAGGTTTTCGGATCGTAAAACTCTGT TGTTAGAGAAGAACAAGGATGAGAGTAACTGTTCATCCCTTGACGGTATCTAACCAGAAAGCCACGGCTAACTACGTGCCAGCAGCCGCGGT AATACGTAGGTGGCAAGCGTTGTCCGGATTTATTGGGCGTAAAGCGAGCGCAGGCGGTTTCTTAAGTCTGATGTGAAAGCCCCCGGCTCAAC CGGGGAGGGTCATTGGAAACTGGGAGACTTGAGTGCAGAAGAGGAGAGTGGAATTCCATGTGTAGCGGTGAAATGCGTAGATATATGGAGG AACACCAGTGGCGAAGGCGGCTCTCTGGTCTGTAACTGACGCTGAGGCTCGAAAGCGTGGGGAGCAAACAGGATTAGATACCCTGGTAGTC CACGCCGTAAACGATGAGTGCTAAGTGTTGGAGGGTTTCCGCCCTTCAGTGCTGCAGCTAACGCATTAAGCACTCCGCCTGGGGAGTACGAC CGCAAGGTTGAAACTCAAAGGAATTGACGGGGGCCCGCACAAGCGGTGGAGCATGTGGTTTAATTCGAAGCAACGCGAAGAACCTTACCAG GTCTTGACATCCTTTGACCACTCTAGAGATAGAGCTTCCCCTTCGGGGGCAAAGTGACAGGTGGTGCATGGTTGTCGTCAGCTCGTGTCGTGA GATGTTGGGTTAAGTCCCGCAACGAGCGCAACCCTTATTGTTAGTTGCCATCATTCAGTTGGGCACTCTAGCAAGACTGCCGGTGACAAACCG

	GAGGAAGGTGGGGATGACGTCAAATCATCATGCCCCTTATGACCTGGGCTACACACGTGCTACAATGGGAAGTACAACGAGTTGCGAAGTC GCGAGGCTAAGCTAATCTCTTAAAGCTTCTCTCAGTTCGGATTGCAGGCTGCAACTCGCCTGCATGAAGCCGGAATCGCTAGTAATCGCGGAT CAGCACGCCGCGGTGAATACGTTCCCGGGCCTTGTACACACCGCCCGTCACACCACGAGAGTTTGTAACACCCGAAGTCGGTGAGGTAACCT TTTGGAGCCAGTCGCCTAAGGTGGGATAGATGATTGGGGTGAAGTCGTAACAAGGTAGCCGTATCGGAAGGTGCGGCTGGATCACCTCCTT TCTAAGGAA
	***Escherichia coli* SMS-3-5, complete genome (GenBank Accession No.: CP000970.1)** **16S rRNA gene: region 232907 – 234448, 1542 bp (5', 3' termini in bold, red font)** Note*: E. coli* SMS-3-5 chromosome contains 7 copies of 16S rRNA gene (≥ 99% identity). Here shows the 1st one as the example. Amplicon Lengths: 142, 529, 733, 1067, and 1503 bp. AAATTGAAGAGTTTGATCATGGCTCAGATTGAACGCTGGCGGCAGGCCTAACACATGCAAGTCGAACGGTAACAGGAAGAAGCTTGCTTC TTTGCTGACGAGTGGCGGACGGGTGAGTAATGTCTGGGAAACTGCCTGATGGAGGGGGATAACTACTGGAAACGGTAGCTAATACCGCATA ATGTCGCAAGACCAAAGAGGGGGACCTTCGGGCCTCTTGCCATCGGATGTGCCCAGATGGGATTAGCTAGTAGGTGGGGTAACGGCTCACCT AGGCGACGATCCCTAGCTGGTCTGAGAGGATGACCAGCCACACTGGAACTGAGACACGGTCCAGACTCCTACGGGAGGCAGCAGTGGGGAA TATTGCACAATGGGCGCAAGCCTGATGCAGCCATGCCGCGTGTATGAAGAAGGCCTTCGGGTTGTAAAGTACTTTCAGCGGGGAGGAAGGG AGTAAAGTTAATACCTTTACTCATTGACGTTACCCGCAGAAGAAGCACCGGCTAACTCCGTGCCAGCAGCCGCGGTAATACGGAGGGTGCAA GCGTTAATCGGAATTACTGGGCGTAAAGCGCACGCAGGCGGTTTGTTAAGTCAGATGTGAAATCCCCGGGCTCAACCTGGGAACTGCATCTG ATACTGGCAAGCTTGAGTCTCGTAGAGGGGGGTAGAATTCCAGGTGTAGCGGTGAAATGCGTAGAGATCTGGAGGAATACCGGTGGCGAAG GCGGCCCCCTGGACGAAGACTGACGCTCAGGTGCGAAAGCGTGGGGAGCAAACAGGATTAGATACCCTGGTAGTCCACGCCGTAAACGATG TCGACTTGGAGGTTGTGCCCTTGAGGCGTGGCTTCCGGAGCTAACGCGTTAAGTCGACCGCCTGGGGAGTACGGCCGCAAGGTTAAAACTCA AATGAATTGACGGGGGCCCGCACAAGCGGTGGAGCATGTGGTTTAATTCGATGCAACGCGAAGAACCTTACCTGGTCTTGACATCCACGGAA GTTTTCAGAGATGAGAATGTGCCTTCGGGAACCGTGAGACAGGTGCTGCATGGCTGTCGTCAGCTCGTGTTGTGAAATGTTGGGTTAAGTCCC GCAACGAGCGCAACCCTTATCCTTTGTTGCCAGCGGTCCGGCCGGGAACTCAAAGGAGACTGCCAGTGATAAACTGGAGGAAGGTGGGGAT GACGTCAAGTCATCATGGCCCTTACGACCAGGGCTACACACGTGCTACAATGGCGCATACAAAGAGAAGCGACCTCGCGAGAGCAAGCGGA CCTCATAAAGTGCGTCGTAGTCCGGATTGGAGTCTGCAACTCGACTCCATGAAGTCGGAATCGCTAGTAATCGTGGATCAGAATGCCACGGT GAATACGTTCCCGGGCCTTGTACACACCGCCCGTCACACCATGGGAGTGGGTTGCAAAAGAAGTAGGTAGCTTAACCTTCGGGAGGGCGCTT ACCACTTTGTGATTCATGACTGGGGTGAAGTCGTAACAAGGTAACCGTAGGGGAACCTGCGGTTGGATCACCTCCTTA
	Pseudomonas aeruginosa PAO1, complete genome (GenBank Accession No.: AE004091.2) **16S rRNA gene: region 722096 – 723631, 1536 bp (5', 3' termini in bold, red font)** Note*:* PAO1 chromosome contains 4 copies of 16S rRNA gene (≥ 99% identity). Here shows the 1st one as the example. Amplicon Lengths: 142, 523, 733, 1067, 1497 bp. GAACTGAAGAGTTTGATCATGGCTCAGATTGAACGCTGGCGGCAGGCCTAACACATGCAAGTCGAGCGGATGAAGGGAGCTTGCTCCTGG ATTCAGCGGCGGACGGGTGAGTAATGCCTAGGAATCTGCCTGGTAGTGGGGGATAACGTCCGGAAACGGGCGCTAATACCGCATACGTCCTG AGGGAGAAAGTGGGGGATCTTCGGACCTCACGCTATCAGATGAGCCTAGGTCGGATTAGCTAGTTGGTGGGGTAAAGGCCTACCAAGGCGA CGATCCGTAACTGGTCTGAGAGGATGATCAGTCACACTGGAACTGAGACACGGTCCAGACTCCTACGGGAGGCAGCAGTGGGGAATATTGG ACAATGGGCGAAAGCCTGATCCAGCCATGCCGCGTGTGTGAAGAAGGTCTTCGGATTGTAAAGCACTTTAAGTTGGGAGGAAGGGCAGTAA GTTAATACCTTGCTGTTTTGACGTTACCAACAGAATAAGCACCGGCTAACTTCGTGCCAGCAGCCGCGGTAATACGAAGGGTGCAAGCGTTA ATCGGAATTACTGGGCGTAAAGCGCGCGTAGGTGGTTCAGCAAGTTGGATGTGAAATCCCCGGGCTCAACCTGGGAACTGCATCCAAAACTA CTGAGCTAGAGTACGGTAGAGGGTGGTGGAATTTCCTGTGTAGCGGTGAAATGCGTAGATATAGGAAGGAACACCAGTGGCGAAGGCGACC ACCTGGACTGATACTGACACTGAGGTGCGAAAGCGTGGGGAGCAAACAGGATTAGATACCCTGGTAGTCCACGCCGTAAACGATGTCGACT AGCCGTTGGGATCCTTGAGATCTTAGTGGCGCAGCTAACGCGATAAGTCGACCGCCTGGGGAGTACGGCCGCAAGGTTAAAACTCAAATGAA TTGACGGGGGCCCGCACAAGCGGTGGAGCATGTGGTTTAATTCGAAGCAACGCGAAGAACCTTACCTGGCCTTGACATGCTGAGAACTTTCC AGAGATGGATTGGTGCCTTCGGGAACTCAGACACAGGTGCTGCATGGCTGTCGTCAGCTCGTGTCGTGAGATGTTGGGTTAAGTCCCGTAAC

	GAGCGCAACCCTTGTCCTTAGTTACCAGCACCTCGGGTGGGCACTCTAAGGAGACTGCCGGTGACAAACCGGAGGAAGGTGGGGATGACGT CAAGTCATCATGGCCCTTACGGCCAGGGCTACACACGTGCTACAATGGTCGGTACAAAGGGTTGCCAAGCCGCGAGGTGGAGCTAATCCCAT AAAACCGATCGTAGTCCGGATCGCAGTCTGCAACTCGACTGCGTGAAGTCGGAATCGCTAGTAATCGTGAATCAGAATGTCACGGTGAATAC GTTCCCGGGCCTTGTACACACCGCCCGTCACACCATGGGAGTGGGTTGCTCCAGAAGTAGCTAGTCTAACCGCAAGGGGGACGGTTACCACG GAGTGATTCATGACTGGGGTGAAGTCGTAACAAGGTAGCCGTAGGGGAACCTGCGGCTGGATCACCTCCTTA		
***pCFPamy* 663 bp**	FP: 5'- TGCTGAAACGGCGAACAAATC-3' RP: 5'-GCCATAACATTGAGGACGGAAG-3' => CTTCCGTCCTCAATGTTATGGC	60.5 °C	This study
	Cloning vector pCFPamy, complete sequence (GenBank Accession No.: HM204939.1) ***amyE*(front)–*cfp* segment: region 115 – 1377, 1263 bp** ***amyE* gene (front): region 115 – 651 (5', 3' termini in bold, green font)** ***cfp* gene: region 658 – 1377 (5', 3' termini in bold, orange font)** ATGTTTGCAAAACGATTCAAAACCTCTTTACTGCCGTTATTCGCTGGATTTTTATTGCTGTTTCATTTGGTTCTGGCAGGACCGGCGGCTGCGA GTGCTGAAACGGCGAACAAATCGAATGAGCTTACAGCACCGTCGATCAAAAGCGGAACCATTCTTCATGCATGGAATTGGTCGTTCAATACG TTAAAACACAATATGAAGGATATTCATGATGCAGGATATACAGCCATTCAGACATCTCCGATTAACCAAGTAAAGGAAGGGAATCAAGGAG ATAAAAGCATGTCGAACTGGTACTGGCTGTATCAGCCGACATCGTATCAAATTGGCAACCGTTACTTAGGTACTGAACAAGAATTTAAAGAA ATGTGTGCAGCCGCTGAAGAATATGGCATAAAGGTCATTGTTGACGCGGTCATCAATCATACCACCAGTGATTATGCCGCGATTTCCAATGA GGTTAAGAGTATTCCAAACTGGACACATGGAAACACACAAATTAAAAACTGGTCTGATCGAAATAGTACATAATGGGAATTCTTACTTATAA AGTTCGTCCATGCCAAGTGTAATGCCCGCAGCTGTGACAAACTCTAACAGAACCATGTGATCGCGCTTTTCGTTAGGGTCTTTTGACAGCTTA GATTGCGTGCTTAAGTAATGGTTGTCAGGAAGAAGAACCGGTCCATCTCCAATCGGTGTATTCTGCTGGTAATGATCTGCTAATTGAACGCTT CCGTCCTCAATGTTATGGCGGATTTTGAAATTAGCCTTGATTCCGTTTTTTTGCTTATCTGCTGTGATATAAACATTGTGAGAGATGTAATTAT ATTCCAGTTTGTGTCCTAAGATGTTGCCATCCTCCTTAAAGTCAATTCCTTTCAGTTCGATTCTATTGACAAGCGTGTCGCCTTCAAATTTGAC TTCCGCGCGTGTTTTATAATTTCCGTCGTCCTTGAAAAAAATCGTGCGTTCTTGCACATAGCCTTCCGGCATGGCTGATTTGAAGAAATCGTGC TGTTTCATGTGATCCGGGTATCTGCTGAAGCACTGTACTCCCCACGTAAGTGTCGTGACTAATGTAGGCCATGGGACAGGTAACTTTCCTGTT GTGCAGATGAACTTAAGCGTCAGTTTGCCGTACGTAGCATCTCCTTCTCCCTCGCCTGAGACAGAAAATTTATGGCCATTGACATCGCCATCT AATTCGACCAGAATCGGCACTACTCCCGTAAACAGTTCTTCGCCTTTTGAAACCAT		

[a] For primers of the 16S rRNA gene segments, primer numbering relates to *E. coli* 16S rRNA position complementary to the 5' end of the primer. Last letter denotes direction: Forward (F) and Reverse (R). FASTA code: K = G and T; M = A and C; R = G and A; S = C and G; W = A and T; Y = C and T; N = C, A, T and G; positions where the synthesized primer contains equimolar amounts of more than one nucleotide.

Table S3.3. Specific nucleotide contents for the qPCR amplicons of ARGs and 16S rRNA gene. Nucleotide contents were counted using the on-line tool of Wageningen University Bioinformatics group (http://www.bioinformatics.nl/cgi-bin/emboss/wordcount#forms::wordcount).

qPCR amplicon	Number of specific nucleotide base pairs or doublet per amplicon and their relative contents (% of total bps or bases, respectively)						
	AT bp	GC bp	AT+GC bp	5'-TT-3'	5'-TC-3'	5'-CT-3'	5'-CC-3'
blt 266 bp	152 (57.14%)	114 (42.86%)	266	52 (9.77%)	25 (4.70%)	25 (4.70%)	37 (6.95%)
blt 832 bp	503 (60.46%)	329 (39.54%)	832	188 (11.30%)	93 (5.59%)	86 (5.17%)	74 (4.45%)
blt 870 bp	572 (65.75%)	298 (34.25%)	870	237 (13.62%)	109 (6.26%)	95 (5.46%)	56 (3.22%)
blt 1017 bp	666 (65.49%)	351 (34.51%)	1017	270 (13.27%)	123 (6.05%)	113 (5.56%)	69 (3.39%)
*mec*A 1018 bp	685 (67.29%)	333 (32.71%)	1018	263 (12.92%)	114 (5.60%)	100 (4.91%)	59 (2.90%)
*van*A 1030 bp	569 (55.24%)	461 (44.76%)	1030	190 (9.22%)	115 (5.58%)	106 (5.15%)	102 (4.95%)
tet(A) 1054 bp	383 (36.34%)	671 (63.66%)	1054	81 (3.84%)	135 (6.40%)	104 (4.93%)	185 (8.78%)
*amp*C 1006 bp	309 (30.72%)	697 (69.28%)	1006	40 (1.99%)	106 (5.27%)	129 (6.41%)	206 (10.24%)
16S rRNA gene 142 bp (*B. subtilis* 1A189)	62 (43.36%)	81 (56.64%)	143	16 (5.59%)	15 (5.24%)	14 (4.90%)	27 (9.44%)
16S rRNA gene 142 bp (MRSA)	65 (45.45%)	78 (54.55%)	143	18 (6.29%)	15 (5.24%)	14 (4.90%)	25 (8.74%)
16S rRNA gene 142 bp (VRE)	63 (44.37%)	79 (55.63%)	142	16 (5.63%)	14 (4.93%)	14 (4.93%)	27 (9.51%)
16S rRNA gene 142 bp (*E. coli* SMS-3-5)	66 (46.48%)	76 (53.52%)	142	19 (6.69%)	12 (4.23%)	14 (4.93%)	26 (9.15%)
16S rRNA gene 142 bp (PAO1)	61 (42.96%)	81 (57.04%)	142	12 (4.23%)	14 (4.93%)	15 (5.28%)	28 (9.86%)
16S rRNA gene 142 bp (average of 5 ARB)	63 (44.52%)	79 (55.48%)	142	16 (5.69%)	14 (4.92%)	14 (4.99%)	27 (9.34%)
16S rRNA gene 536 bp (*B. subtilis* 1A189)	236 (44.03%)	300 (55.97%)	536	55 (5.13%)	61 (5.69%)	68 (6.34%)	84 (7.84%)
16S rRNA gene 734 bp (*B. subtilis* 1A189)	334 (45.50%)	400 (54.50%)	734	83 (5.65%)	90 (6.13%)	89 (6.06%)	110 (7.49%)
16S rRNA gene 1068 bp (*B. subtilis* 1A189)	483 (45.22%)	585 (54.78%)	1068	124 (5.81%)	134 (6.27%)	137 (6.41%)	158 (7.40%)
16S rRNA gene 1509 bp (*B. subtilis* 1A189)	677 (44.80%)	834 (55.20%)	1511	167 (5.53%)	185 (6.12%)	192 (6.35%)	233 (7.71%)
16S rRNA gene 1509 bp (MRSA)	740 (48.91%)	773 (51.09%)	1513	200 (6.61%)	180 (5.95%)	188 (6.21%)	195 (6.44%)
16S rRNA gene 1509 bp (VRE)	708 (46.55%)	813 (53.45%)	1521	191 (6.28%)	186 (6.11%)	196 (6.44%)	218 (7.17%)
16S rRNA gene 1509 bp	685	818	1503	171	183	193	232

(*E. coli* SMS-3-5)	(45.58%)	(54.42%)		(5.69%)	(6.09%)	(6.42%)	(7.72%)
16S rRNA gene 1509 bp (PAO1)	687 (45.89%)	810 (54.11%)	1497	160 (5.34%)	184 (6.15%)	192 (6.41%)	229 (7.65%)
16S rRNA gene 1509 bp (average of 5 ARB)	699 (46.35%)	810 (53.65%)	1509	178 (5.89%)	184 (6.08%)	192 (6.37%)	221 (7.34%)

[a] Contents of 5'-TT-3', 5'-TC-3', 5'-CT-3', 5'-CC-3' doublets (i.e., # of doublets per amplicon) represent the total doublet contents of both of the two complementary strands of DNA comprising a given amplicon region. For example, the total number of 5'-TT-3' doublets within an amplicon was taken to equal the sum of 5'-TT-3' doublets plus 5'-AA-3' doublets in the sequence (Table S3.3) within one strand of the dsDNA comprising the amplicon region. 5'-TT-3' doublet contents comprise those within 5'-TTT-3' and 5'-TTTT-3' sequences, which were counted as containing two and three 5'-TT-3' doublets, respectively.

Table S3.4. Water quality parameters of pre-disinfection secondary effluents collected from two local WWTPs in Seattle area, WA.

	pH	DOC (mg C/L)	Abs_{254} (cm^{-1})	Alkalinity (mg $CaCO_3$/L)	Turbidity	NH_3-N (mg N/L)	Total N (mg N/L)	Br^- (mg/L)
WWTP 1	7.31	6.63	0.161	198	N.A.	0.03	1.93	6.43
WWTP 2	7.03	6.52	N.A.	132	4.575	27.4	N.A.	77.1

Table S3.5. DNA recovery yields for the pre- and post-disinfection samples collected from two local WWTPs in Seattle area, WA.

Full-scale samples	WWTP 1 (UV)			WWTP 2 (chlorination)		
	η_{dsDNA}	$\eta_{blt1017\text{bp}}$	$\eta_{cfpamy663\text{bp}}$	η_{dsDNA}	$\eta_{blt1017\text{bp}}$	$\eta_{cfpamy663\text{bp}}$
Pre-disinfection effluent	46.1%	16.6%	47.0%	94.2%	147.2%	97.5%
Post-disinfection effluent	52.0%	44.2%	41.0%	86.6%	161.8%	85.8%

Table S3.6. Summary of alternative kinetics parameters (as mean ± standard error) for degradation of ARG/16S rRNA gene amplicons toward UV, FAC, and NH_2Cl [a]

qPCR amplicons of ARGs or 16S rRNA gene segments	Host ARB strain for eDNA isolation	Alternaive rate constants for the complex-kinetics UV via non-linear regression for the 21 amplicon individually (see Text S3.5)			Alternaive rate constants for NH_2Cl by using the previously-measured $k_{NH_2Cl,N\text{-}Cl\ bp}$ value (obained from *blt* 266 bp data)	
		$k_{UV,Amp\text{-}CPD}$ (cm^2/mJ) (eq 3.3 forward)	$k_{UV,PR\text{-}singleCPD}$ (cm^2/mJ) (eq 3.3 reverse)	$k_{UV,single6,4\text{-}P}$ (cm^2/mJ) (eq 3.4)	$k_{NH_2Cl,Amp}$ [b] ($M^{-1}s^{-1}$) (eq 3.5)	$k_{NH_2Cl,N\text{-}Cl\ bp}$ ($M^{-1}s^{-1}$) (eq 3.6)
***blt* 266 bp**	*B. subtilis* 1A189	$2.2(\pm0.1)\times10^{-2}$	$5.9(\pm0.2)\times10^{-3}$		1.7(±0.1)	
***blt* 832 bp**		$7.7(\pm0.1)\times10^{-2}$	$2.0(\pm0.2)\times10^{-2}$		3.6(±0.1)	
***blt* 870 bp**		$1.2(\pm0.1)\times10^{-1}$	$9.2(\pm0.2)\times10^{-3}$		3.8(±0.2)	
***blt* 1017 bp**		$1.3(\pm0.1)\times10^{-1}$	$1.1(\pm0.1)\times10^{-2}$		4.4(±0.2)	
***mec*A 1018 bp**	MRSA	$1.0(\pm0.1)\times10^{-1}$	$1.1(\pm0.1)\times10^{-2}$		4.9(±0.2)	
***van*A 1030 bp**	VRE	$8.7(\pm0.1)\times10^{-2}$	$1.2(\pm0.1)\times10^{-2}$		5.6(±0.2)	
***tet*(A) 1054 bp**	*E. coli* SMS-3-5	$4.6(\pm0.1)\times10^{-2}$	$3.5(\pm1.0)\times10^{-2}$		5.3(±0.2)	
***amp*C 1006 bp**	PAO1	$2.9(\pm0.1)\times10^{-2}$	$1.9(\pm0.5)\times10^{-2}$		2.7(±0.1)	
16S rRNA gene 142 bp	*B. subtilis* 1A189	$8.2(\pm0.2)\times10^{-3}$	$6.2(\pm0.3)\times10^{-3}$	$1.2(\pm0.1)\times10^{-4}$	1.7(±0.2)	$1.6(\pm0.1)\times10^{-4}$
	MRSA	$1.0(\pm0.1)\times10^{-2}$	$8.1(\pm0.4)\times10^{-3}$		3.1(±0.6)	
	VRE	$1.1(\pm0.1)\times10^{-2}$	$1.1(\pm0.1)\times10^{-2}$		2.0(±0.2)	
	E. coli SMS-3-5	$8.5(\pm0.1)\times10^{-3}$	$4.6(\pm0.2)\times10^{-3}$		2.3(±0.2)	
	PAO1	$5.0(\pm0.2)\times10^{-3}$	$7.9(\pm0.7)\times10^{-3}$		1.4(±0.1)	
16S rRNA gene 536 bp	*B. subtilis* 1A189	$3.2(\pm0.1)\times10^{-2}$	$1.9(\pm0.2)\times10^{-2}$		4.3(±0.2)	
16S rRNA gene 734 bp	*B. subtilis* 1A189	$4.3(\pm0.1)\times10^{-2}$	$9.5(\pm0.7)\times10^{-3}$		5.5(±0.3)	
16S rRNA gene 1068 bp	*B. subtilis* 1A189	$7.2(\pm0.1)\times10^{-2}$	$1.7(\pm0.2)\times10^{-2}$		6.8(±0.3)	
16S rRNA gene 1509 bp	*B. subtilis* 1A189	$1.1(\pm0.1)\times10^{-1}$	$2.2(\pm0.2)\times10^{-2}$		$1.1(\pm0.1)\times10^{1}$	
	MRSA	$1.3(\pm0.1)\times10^{-1}$	$2.0(\pm0.1)\times10^{-2}$		$1.2(\pm0.1)\times10^{1}$	
	VRE	$1.4(\pm0.1)\times10^{-1}$	$2.1(\pm0.1)\times10^{-2}$		$1.2(\pm0.1)\times10^{1}$	
	E. coli SMS-3-5	$1.2(\pm0.1)\times10^{-1}$	$2.1(\pm0.2)\times10^{-2}$		8.4(±0.3)	
	PAO1	$1.1(\pm0.1)\times10^{-1}$	$2.4(\pm0.3)\times10^{-2}$		3.5(±0.1)	
	$k_{Disinfectant,Specific}$ [d]	$6.2(\pm0.3)\times10^{-4}$ (M 5'-TT-3'/M amplicon)$^{-1}$ (cm^2/mJ)	N.A.	N.A.	$3.0(\pm0.7)\times10^{-3}$ (M AT+GC)$^{-1}s^{-1}$	N.A.
	$k_{Disinfectant,0}$ [d]	$-0.6(\pm1.9)\times10^{-3}$ (cm^2/mJ)	N.A.	N.A	1.2(±0.6) $M^{-1}s^{-1}$	N.A.

[a] All data were obtained by treatment of extracellular DNA of *B. subtilis* 1A189, MRSA, VRE, *E. coli* SMS-3-5, and PAO1 in 10 mM PB at pH 7 (UV and FAC) or 8 (NH_2Cl). Significands of standard errors of $k_{Disinfectant,\ Amp}$ were rounded up to 0.1 if below 0.1. [b] For each disinfectant, $k_{Disinfectant,\ Specific}$ and $k_{Disinfectant,\ 0}$ are, respectively, the slope and intercept of the correlations obtained by weighted linear regression of the rate constants, $k_{Disinfectant,\ Amp}$, for the 21 amplicons versus corresponding specific nucleotide contents (Figure 3.1), with data points of *amp*C 1006 bp and 16S rRNA gene 1509 bp excluded for NH_2Cl. $k_{Disinfectant,\ Specific}$ represents the sequence-independent, bp- or doublet-specific rate constant for each disinfectant, and $k_{Disinfectant,\ 0}$ is attributed to factors influencing DNA reactivity (e.g., secondary targets, specific sequence elements) that are not fully accounted for by eq 3.7.

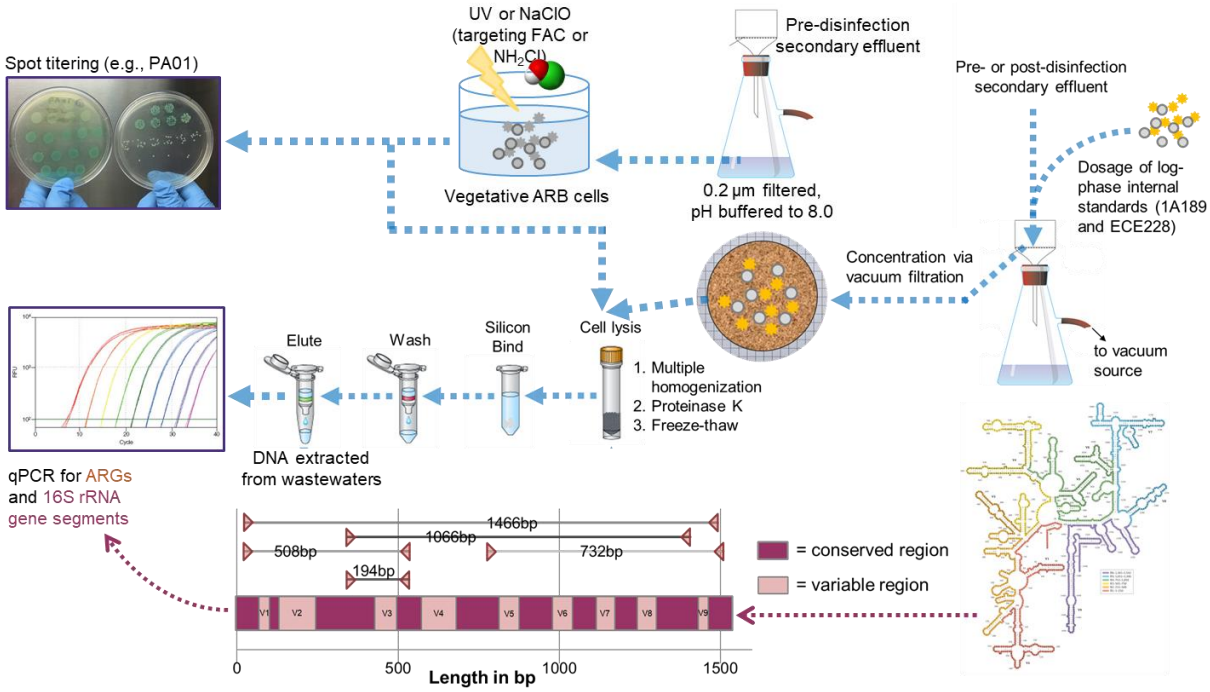

Scheme S3.1. Procedures for wastewater sampling from local WWTPs, bench-scale wastewater disinfection experiments, and the subsequent steps of DNA extraction and analyses.

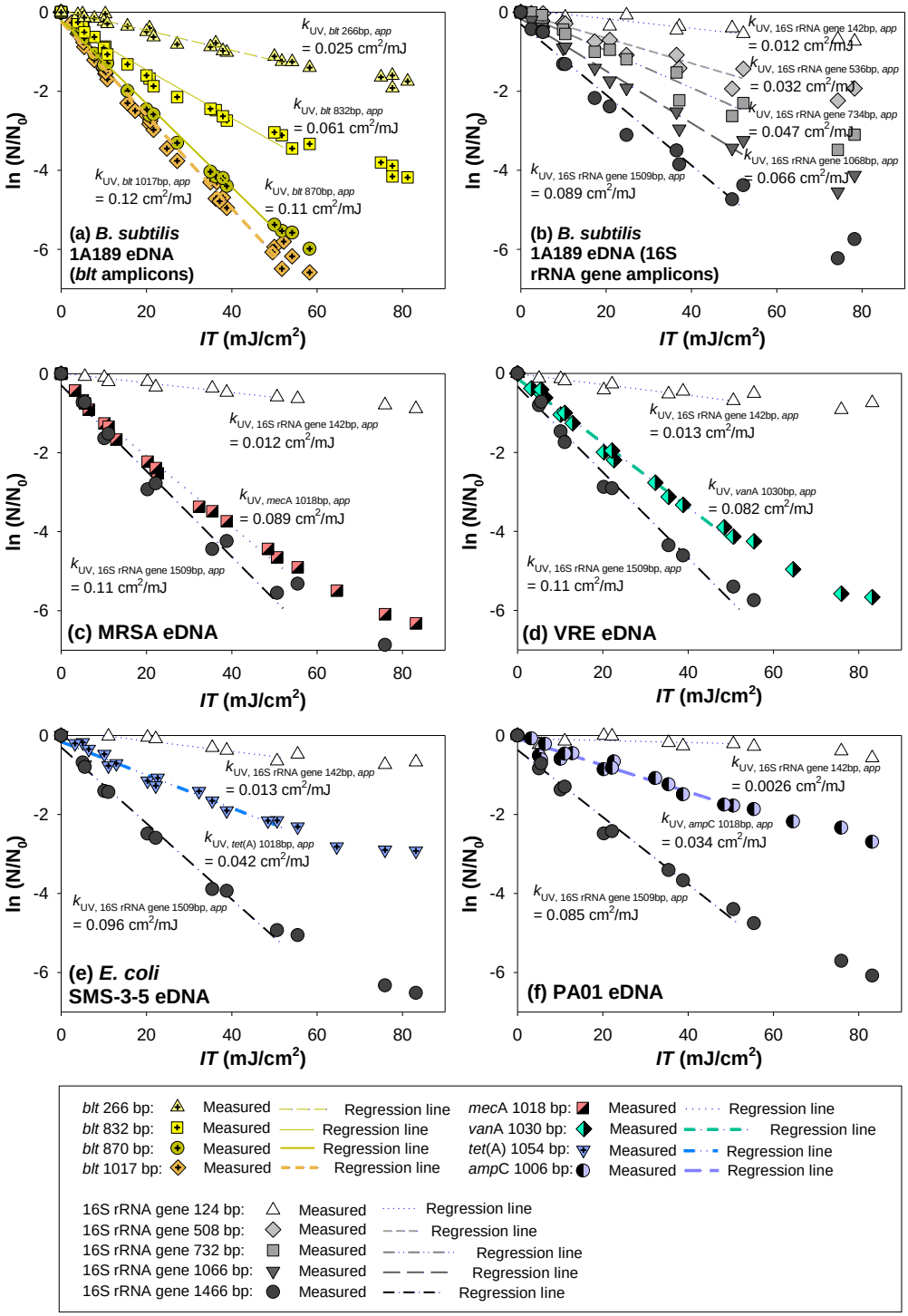

Figure S3.1. Degradation of various ARG amplicons (*blt* 266-1017 bp, *mec*A 1018 bp, *van*A 1030 bp, *tet*(A) 1054 bp, or *amp*C 1006 bp) and varying-lengths of 16S rRNA gene segments (142-1509 bp) during treatment of 1mg/L (as dsDNA) extracellular DNA pre-isolated from vegetative cells of **(a)** and **(b)** *B. subtilis* 1A189, **(c)** MRSA, **(d)** VRE, **(e)** *E. coli* SMS-3-5, or **(f)** PAO1 with 254 nm UV light in 10-mM phosphate buffer at pH 7. Data were pooled from at least duplicate experiments. Apparent fluence-based first-order rate constants ($k_{UV,\ Amp,\ app}$) were determined by linear regressions of $\ln(N/N_0)$ versus *IT* over *IT* values below ~50 mJ/cm^2 to exclude tailing effects (primarily arising from CPD photoreversal at higher exposures).

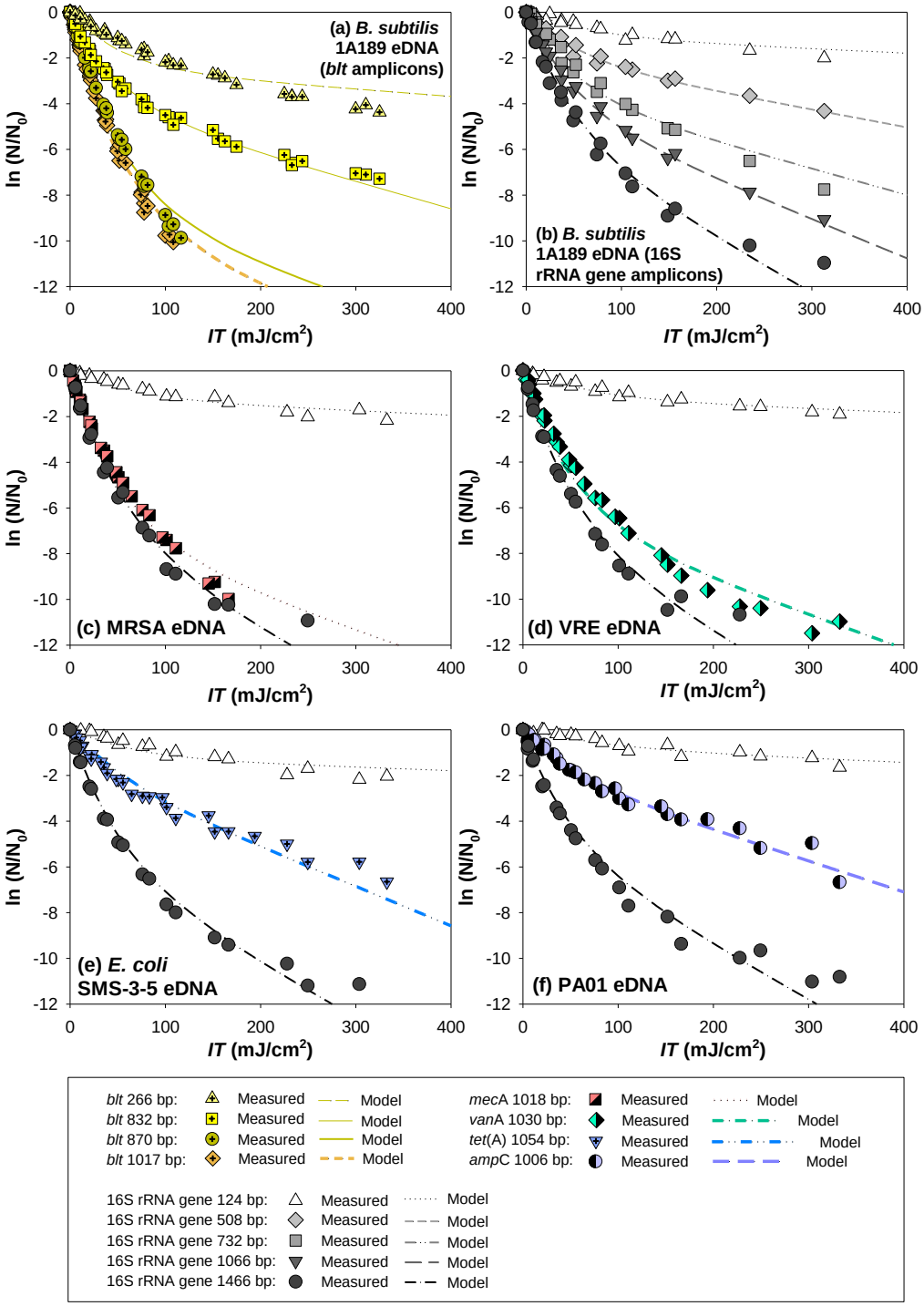

Figure S3.2-Group I. Degradation of various ARG amplicons (*blt* 266-1017 bp, *mec*A 1018 bp, *van*A 1030 bp, *tet*(A) 1054 bp, or *amp*C 1006 bp) and varying-lengths of 16S rRNA gene segments (142-1509 bp) during treatment of 1mg/L (as dsDNA) extracellular DNA pre-isolated from vegetative cells of **(a)** and **(b)** *B. subtilis* 1A189, **(c)** MRSA, **(d)** VRE, **(e)** *E. coli* SMS-3-5, or **(f)** PAO1 with 254 nm UV light in 10-mM phosphate buffer at pH 7. Data were pooled from at least duplicate experiments. Non-linear regression curves are depicted as lines in **Groups I** for the complex-kinetics UV model assuming the rate constant $k_{UV,\ singleCPD,\ r}$ (for photoreversal reaction) is an amplicon-independent constant (see Table S3.5).

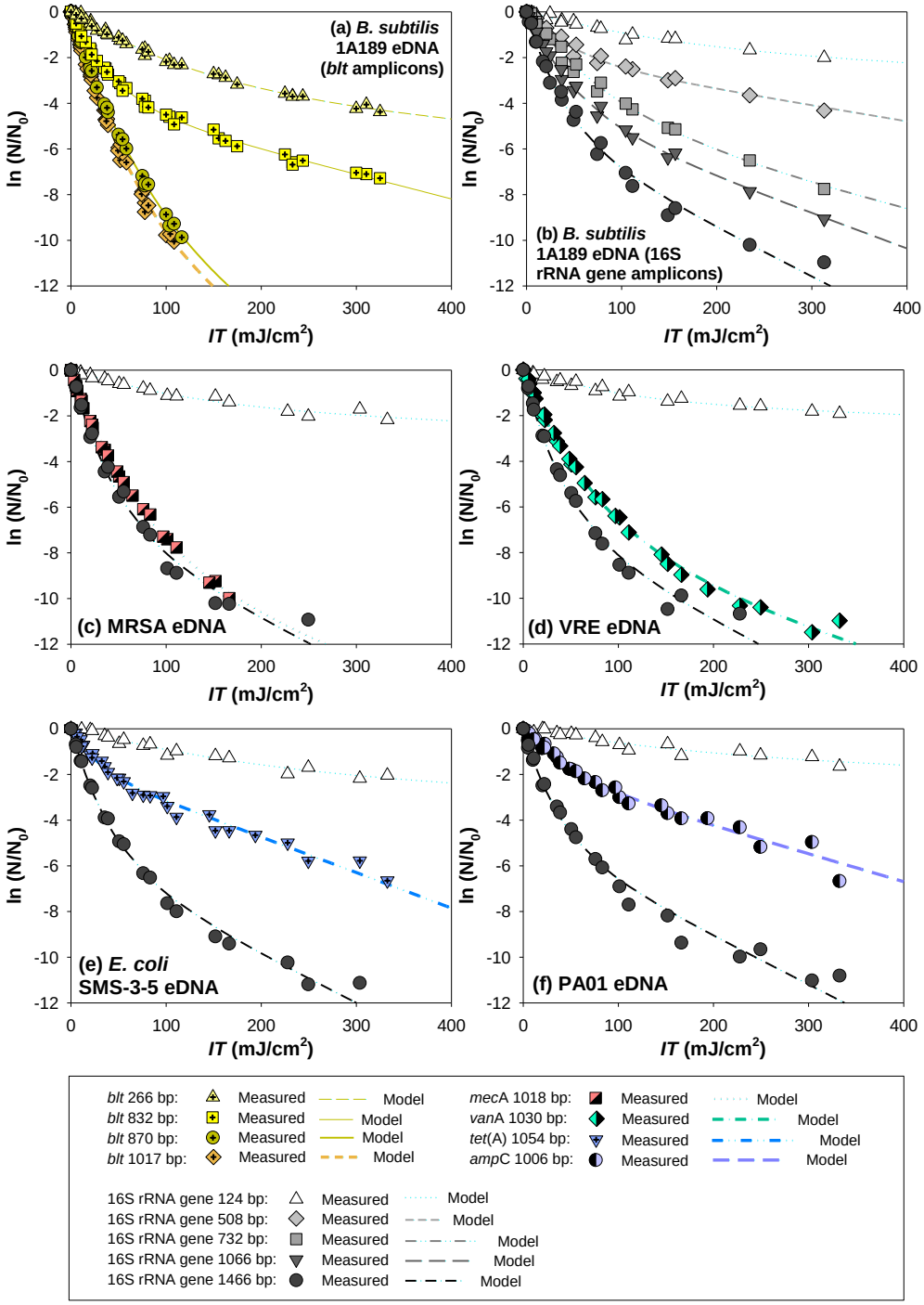

Figure S3.2-Group II. Degradation of various ARG amplicons (*blt* 266-1017 bp, *mec*A 1018 bp, *van*A 1030 bp, *tet*(A) 1054 bp, or *amp*C 1006 bp) and varying-lengths of 16S rRNA gene segments (142-1509 bp) during treatment of 1mg/L (as dsDNA) extracellular DNA pre-isolated from vegetative cells of **(a)** and **(b)** *B. subtilis* 1A189, **(c)** MRSA, **(d)** VRE, **(e)** *E. coli* SMS-3-5, or **(f)** PAO1 with 254 nm UV light in 10-mM phosphate buffer at pH 7. Data were pooled from at least duplicate experiments. Non-linear regression curves are depicted as lines in **Groups II** for the complex-kinetics UV model assuming the rate constant $k_{UV,\ singleCPD,\ r}$ (for photoreversal reaction) is an amplicon-dependent variable (see Table S3.5).

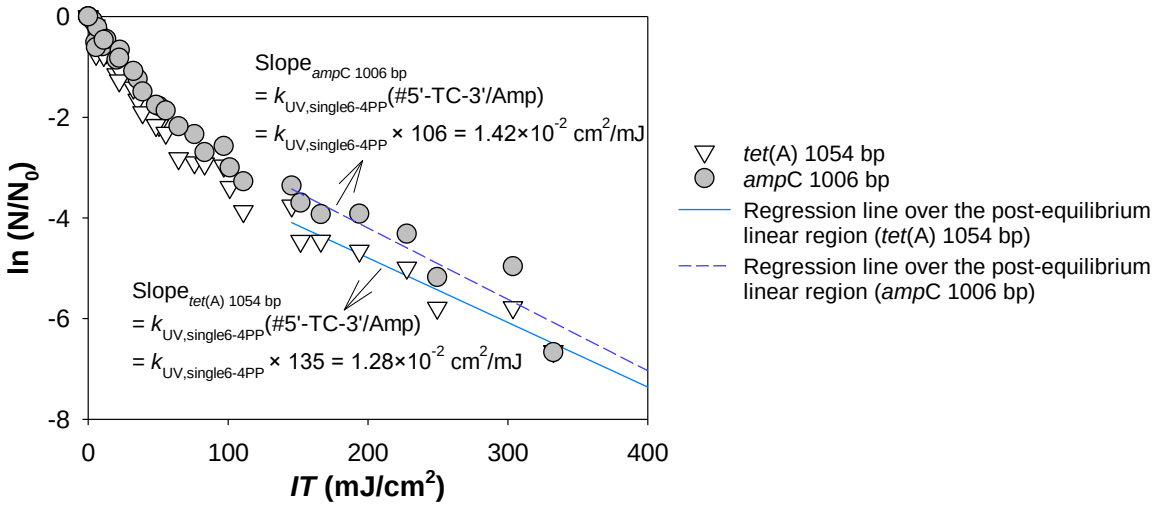

Figure S3.3. Degradation of *tet*(A) 1054 bp and *amp*C 1006 bp during treatment of 1mg/L (as dsDNA) extracellular DNA pre-isolated from vegetative cells of *E. coli* SMS-3-5 and PAO1, respectively, with 254 nm UV light in 10-mM phosphate buffer at pH 7. Data were pooled from at least duplicate experiments. Linear regressions of $\ln(N/N_0)$ versus *IT* were performed over the post-equilibrium linear region (*IT* values ≥ ~150 mJ/cm^2) to derive fluence-based first-order rate constant $k_{UV,\ single6\text{-}4PP}$ (for formation of 6-4 photoproducts at each single 5'-TC-3 site), as described in Text S3.5.

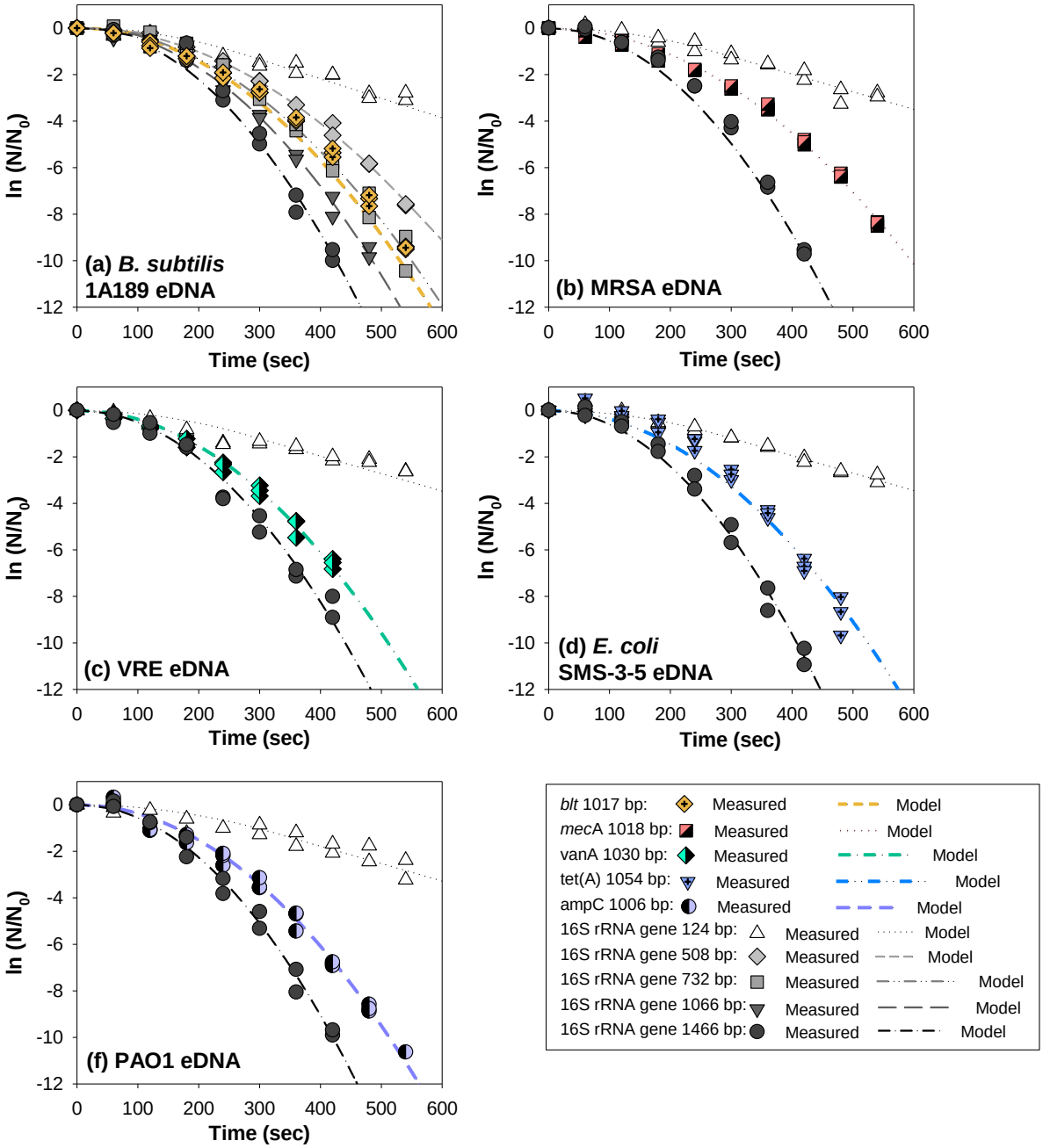

Figure S3.4. Degradation kinetics of various ARGs (*blt* 266-1017 bp, *mec*A 1018 bp, *van*A 1030 bp, *tet*(A) 1054 bp, and *amp*C 1006 bp) and varying-lengths of 16S rRNA gene segments (142-1509 bp) during treatment of 1mg/L (as dsDNA) extracellular DNA pre-isolated from vegetative cells of **(a)** *B. subtilis* 1A189, **(b)** MRSA, **(c)** VRE, **(d)** *E. coli* SMS-3-5, and **(e)** PAO1 with FAC at initial concentrations of 140 μM in 10-mM phosphate buffer at pH 7. The data were plotted as $\ln(N/N_0)$ versus time (in pseudo first-order) since residual FAC concentrations were confirmed to be constant (< 5 % loss) over the treatment periods. Data were pooled from at least duplicate experiments. Model lines were generated using ***measured*** $k_{\text{Amp, FAC}}$ (previously determined for *blt* 1017bp,[2] and in this study for the other amplicons) and $k_{\text{N-Cl bp, FAC}}$ (previously determined)[2].

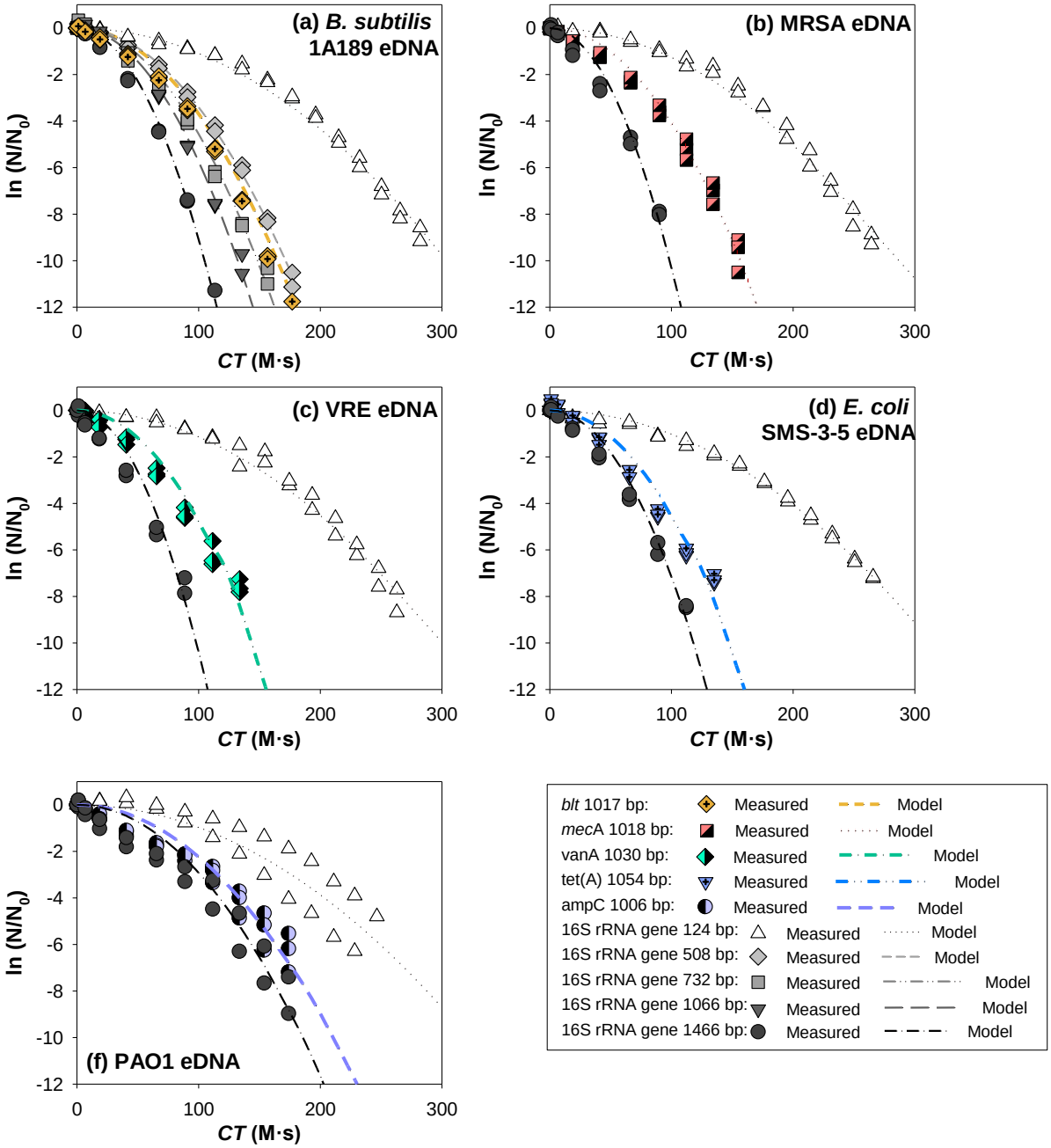

Figure S3.5. Degradation kinetics of various ARGs (*blt* 266-1017 bp, *mec*A 1018 bp, *van*A 1030 bp, *tet*(A) 1054 bp, and *amp*C 1006 bp) and varying-lengths of 16S rRNA gene segments (142-1509 bp) during treatment of 1mg/L (as dsDNA) extracellular DNA pre-isolated from vegetative cells of **(a)** *B. subtilis* 1A189, **(b)** MRSA, **(c)** VRE, **(d)** *E. coli* SMS-3-5, and **(e)** PAO1 with NH_2Cl at initial concentrations of 600 µM in 10-mM phosphate buffer at pH 8. The data were plotted as ln(N/N0) versus *CT* of NH_2Cl instead of time because residual NH_2Cl concentrations could not be assumed constant (> 10% loss) over the treatment periods. Data were pooled from at least duplicate experiments. Model lines were generated using $k_{NH2Cl,\ Amp}$ and $k_{NH2Cl,\ N\text{-}Cl\ bp}$ measured in this study ($k_{NH2Cl,\ N\text{-}Cl\ bp}$ was remeasured using 16S rRNA gene 142 bp, and found to be much higher than the previous value obtained using *blt* 266 bp).

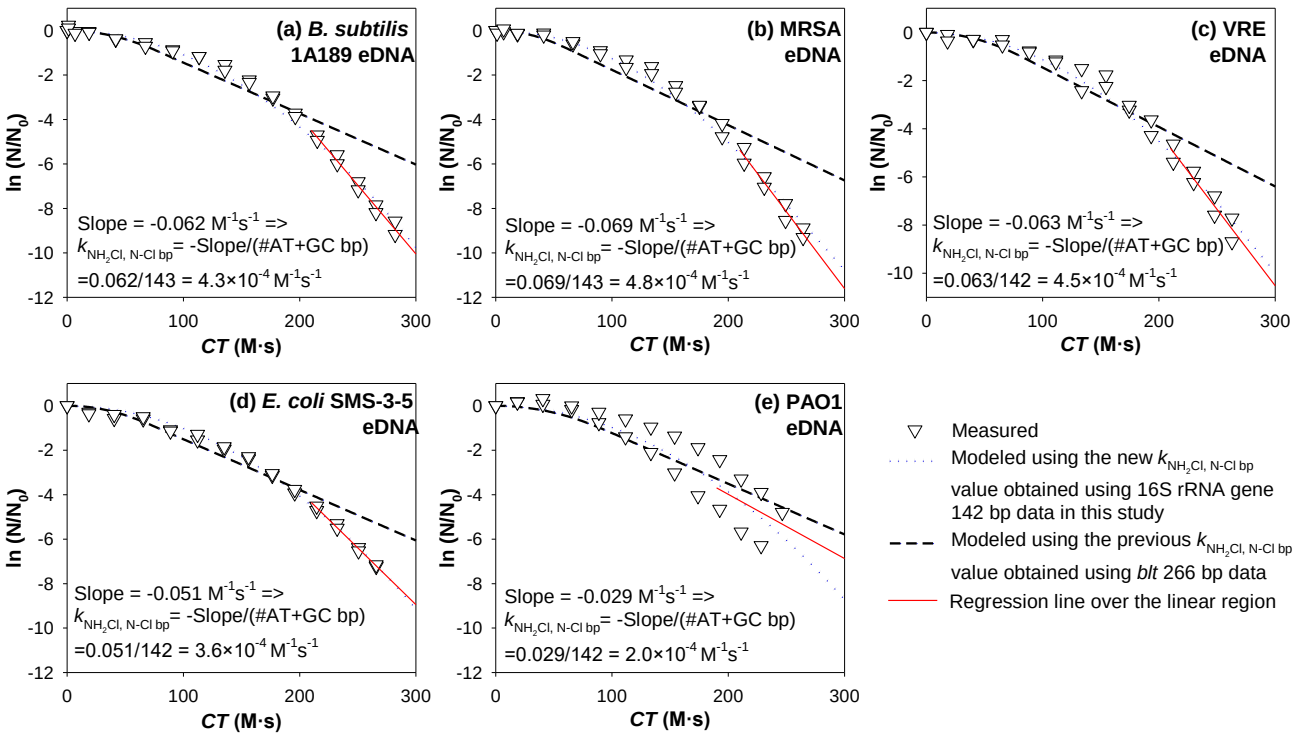

Figure S3.6. Degradation kinetics of 16S rRNA gene 142 bp amplicon during treatment of 1mg/L (as dsDNA) extracellular DNA pre-isolated from vegetative cells of **(a)** *B. subtilis* 1A189, **(b)** MRSA, **(c)** VRE, **(d)** *E. coli* SMS-3-5, and **(e)** PAO1 with NH_2Cl at initial concentrations of 600 μM in 10-mM phosphate buffer at pH 8. The data were plotted as ln(N/N0) versus *CT* instead of time because residual NH_2Cl concentrations could not be assumed constant (> 10% loss) over the treatment periods. $k_{NH2Cl,\ N\text{-}Cl\ bp}$ was remeasured through linear regression over the *CT* range of the maximum slope.

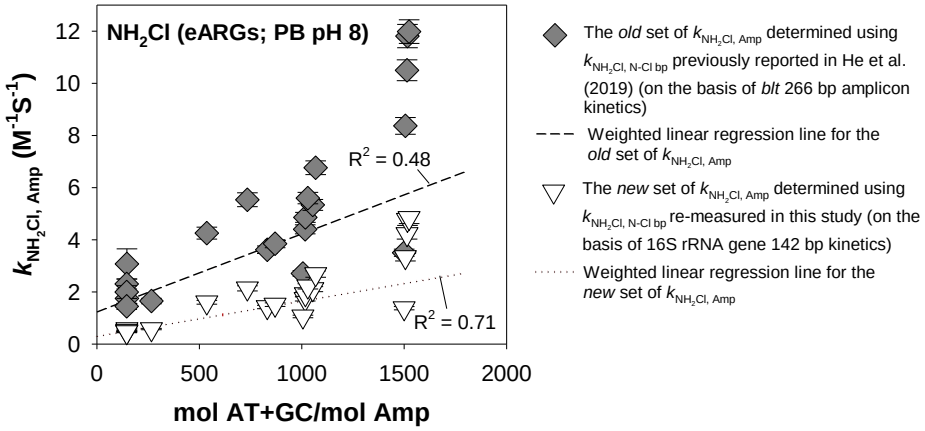

Figure S3.7. Comparison of the old and new sets of $k_{NH2Cl,\ Amp}$ generated using $k_{NH2Cl,\ N\text{-}Cl\ bp}$ previously reported in He et al. (2019) (obtained from *blt* 266 bp kinetics data)[2] and re-determined in this study (obtained from 16S rRNA gene 142 bp kinetics data) in plots of $k_{NH2Cl,\ Amp}$ versus AT+GC bp content for the 21 amplicons. All the data were obtained during treatment of 1mg/L (as dsDNA) extracellular DNA pre-isolated from vegetative cells of *B. subtilis* 1A189, MRSA, VRE, *E. coli* SMS-3-5, and PAO1 with NH_2Cl at initial concentrations of 600 μM in 10-mM phosphate buffer at pH 8.

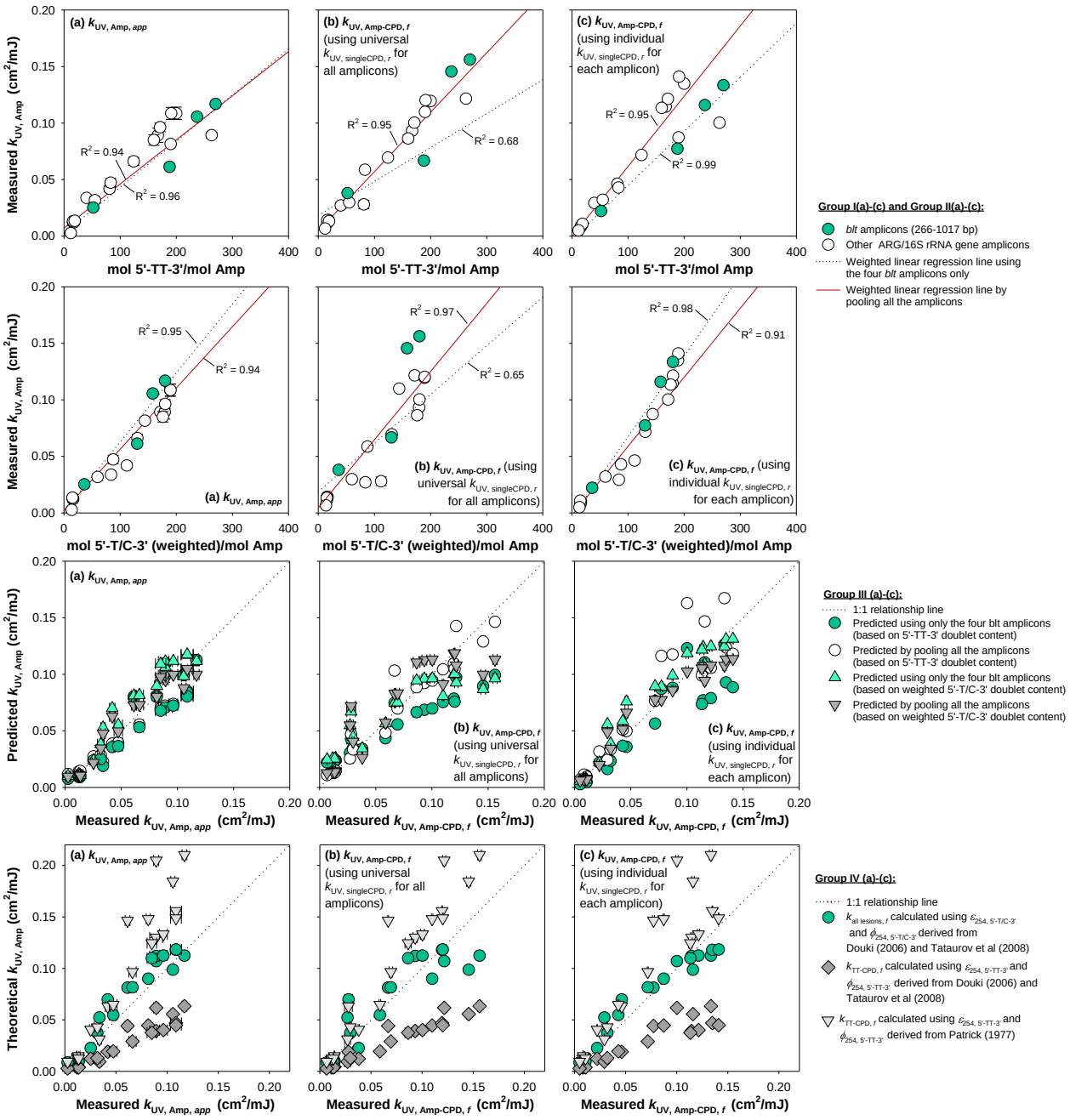

Figure S3.8. Plots of fluence-based first-order rate constants ($k_{UV, Amp}$) versus **(Group I)** 5'-TT-3' doublet contents or **(Group II)** weighted 5'-T/C-3' doublet contents, and **(Group III)** predicted or **(Group IV)** theoretical $k_{UV, Amp}$ versus the measured values. Each group includes three panels using measured rate constants of **(a)** $k_{UV, Amp, app}$, **(b)** $k_{UV, Amp-CPD, f}$ (determined using the universal $k_{UV, singleCPD, r}$ for all the amplicons) and **(c)** $k_{UV, Amp-CPD, f}$ (determined using individual $k_{UV, singleCPD, r}$ value for each amplicon).

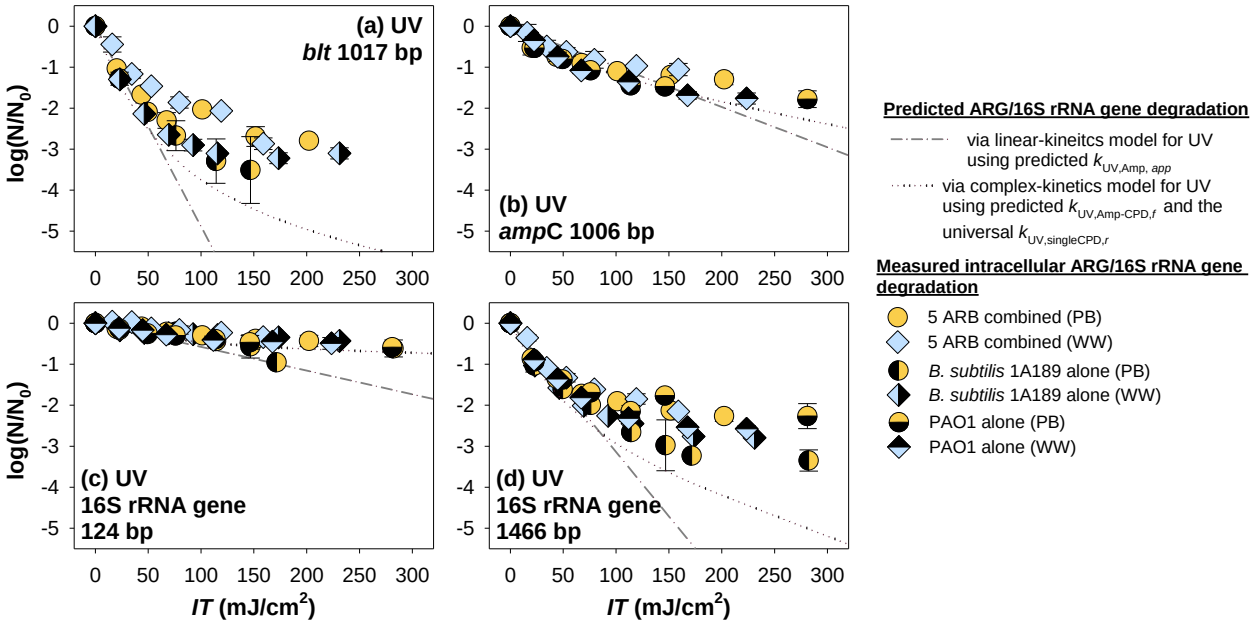

Figure S3.9. Degradation kinetics of **(a)** *blt* 1017 bp, **(b)** *amp*C 1006 bp, **(c)** 16S rRNA gene 142 bp, and **(d)** 16S rRNA gene 1509 bp during UV irradiation of vegetative cells of (i) *B. subtilis* 1A189, MRSA, VRE, *E. coli* SMS-3-5, and PAO1 combined together, (ii) *B. subtilis* 1A189 alone, or (iii) PAO1 alone, in 10 mM phosphate buffers or 0.2 μm filtered pre-UV effluent samples from WWTP 1 at pH 7.

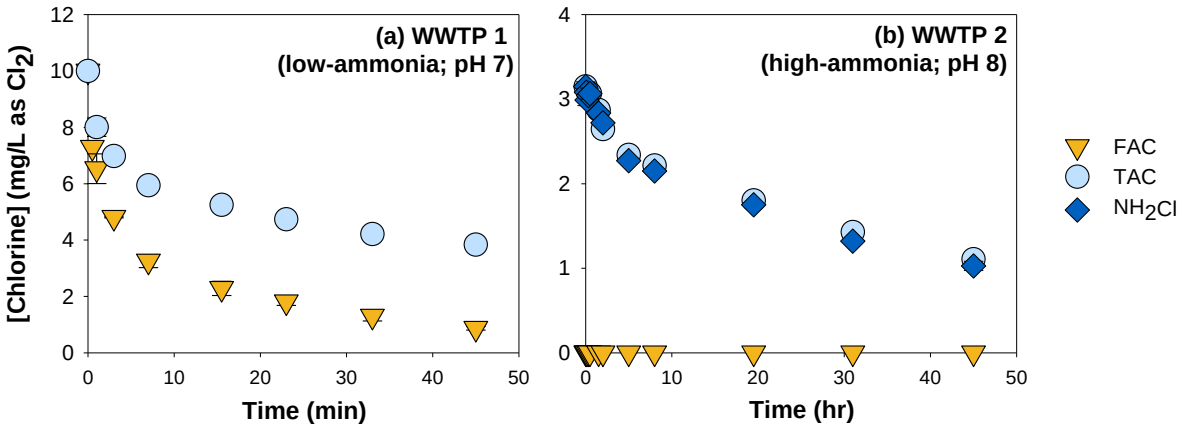

Figure S3.10. Example chlorine consumption curves for bench-scale wastewater chlorination experiments: residual concentrations of chlorine species (including FAC, NH_2Cl, and/or TAC) versus time during chlorination treatment of intact ARB cells (including *B. subtilis* 1A189, MRSA, VRE, *E. coli* SMS-3-5, and PAO1, combined or individually) in pre-disinfection secondary effluents (0.2 μm filtered, pH buffered in 10 mM PB) collected from **(a)** WWTP 1 (at pH 7, dominated by FAC) and **(b)** WWTP 2 (at pH 7, dominated by NH_2Cl) at 20±1 °C. Error bars represent standard deviations obtained from independent experiments in duplicate.

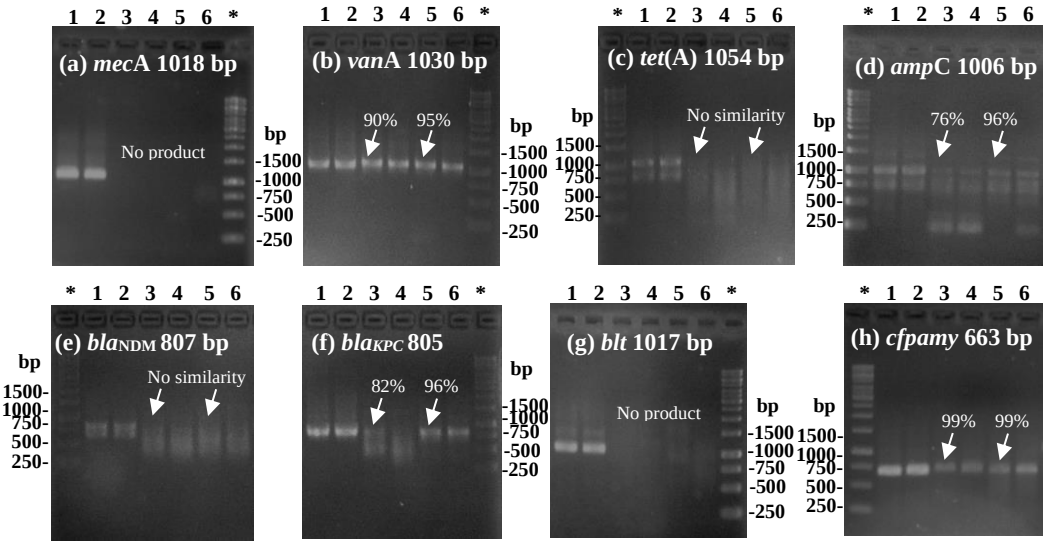

Figure S3.11. Agarose gel images (1.5% agarose, 100 V, 60 min, 1× TAE buffer) for qPCR products targeting various clinically-relevant ARGs (including **(a)** *mec*A 1018bp, **(b)** *van*A 1030 bp, **(c)** *tet*(A) 1054 bp, **(d)** *amp*C 1006 bp, **(e)** bla_{NDM} 807 bp, **(f)** bla_{KPC} 805 bp) and two internal standard genes (including **(g)** *blt* 1017 bp and **(h)** *cfpamy* 663 bp), which were amplified using DNA samples extracted from pre- and post-disinfection effluents of WWTP 1 and 2 in Seattle area, WA. In each panel of (a)-(h), the lanes are **(*)** DNA ladder (on the very left or right), **(1) (2)** positive controls, **(3)** pre-UV and **(4)** post-UV effluents from WWTP 1, **(5)** pre-chlorination and **(6)** post-chlorination effluents from WWTP 2. Sanger sequencing results of qPCR products amplified from DNA extracts of pre-disinfection effluent samples were compared with the sequence of positive controls (Table S3.2) through BLAST, with their identities (in %) reported at the corresponding lanes.

References

1. Saito, H.; Miura, K., Preparation of transforming deoxyribonucleic acid by phenol treatment. *Biochim. Biophys. Acta.* **1963,** *72*, (4), 619-629.
2. He, H.; Zhou, P.; Shimabuku, K. K.; Fang, X.; Li, S.; Lee, Y.; Dodd, M. C., Degradation and deactivation of bacterial antibiotic resistance genes during exposure to free chlorine, monochloramine, chlorine dioxide, ozone, ultraviolet light, and hydroxyl radical. *Environ. Sci. Technol.* **2019,** *53*, (4), 2013-2026.
3. Lanza, V. F.; de Toro, M.; Garcillán-Barcia, M. P.; Mora, A.; Blanco, J.; Coque, T. M.; de la Cruz, F., Plasmid flux in Escherichia coli ST131 sublineages, analyzed by plasmid constellation network (PLACNET), a new method for plasmid reconstruction from whole genome sequences. *PLoS genetics* **2014,** *10*, (12), e1004766.
4. McKinney, C. W.; Pruden, A., Ultraviolet disinfection of antibiotic resistant bacteria and their antibiotic resistance genes in water and wastewater. *Environ. Sci. Technol.* **2012,** *46*, (24), 13393-13400.
5. Czekalski, N.; Imminger, S.; Salhi, E.; Veljkovic, M.; Kleffel, K.; Drissner, D.; Hammes, F.; Bürgmann, H.; Von Gunten, U., Inactivation of antibiotic resistant bacteria and resistance genes by ozone: from laboratory experiments to full-scale wastewater treatment. *Environ. Sci. Technol.* **2016,** *50*, (21), 11862-11871.

6. Benjamin, M. M.; Lawler, D. F., *Water quality engineering: Physical/chemical treatment processes*. John Wiley & Sons: 2013.
7. Choi, Y.; Dodd, M. C.; Lee, Y., Degradation kinetics of antibiotic resistance gene (mecA) of methicillin-resistant Staphylococcus aureus (MRSA) during water disinfection with chlorine, ozone, and ultraviolet light. *In preparation* **2020**.
8. Pecson, B. M.; Ackermann, M.; Kohn, T., Framework for Using Quantitative PCR as a Nonculture Based Method To Estimate Virus Infectivity. *Environ. Sci. Technol.* **2011,** *45*, (6), 2257-2263.
9. Law, Y. K.; Forties, R. A.; Liu, X.; Poirier, M. G.; Kohler, B., Sequence-dependent thymine dimer formation and photoreversal rates in double-stranded DNA. *Photoch. Photobio. Sci.* **2013,** *12*, (8), 1431-1439.
10. Tataurov, A. V.; You, Y.; Owczarzy, R., Predicting ultraviolet spectrum of single stranded and double stranded deoxyribonucleic acids. *Biophys. Chem.* **2008,** *133*, (1-3), 66-70.
11. Douki, T., Low ionic strength reduces cytosine photoreactivity in UVC-irradiated isolated DNA. *Photoch. Photobio. Sci.* **2006,** *5*, (11), 1045-1051.
12. Yoon, Y.; Dodd, M. C.; Lee, Y., Elimination of transforming activity and gene degradation during UV and UV/H2O2 treatment of plasmid-encoded antibiotic resistance genes. *Environ. Sci.: Wat. Res. Technol.* **2018,** *4*, 1239-1251.
13. Rahn, R. O., Potassium iodide as a chemical actinometer for 254 nm radiation: Use of iodate as an electron scavenger. *Photochem. Photobiol.* **1997,** *66*, (4), 450-455.
14. Matallana-Surget, S.; Meador, J. A.; Joux, F.; Douki, T., Effect of the GC content of DNA on the distribution of UVB-induced bipyrimidine photoproducts. *Photoch. Photobio. Sci.* **2008,** *7*, (7), 794-801.
15. Patrick, M. H., Studies on Thymine-derived UV photoproducts in DNA —I. Formation and Biological Role of Pyrimidine Adducts in DNA. *Photochem. Photobiol.* **1977,** *25*, (4), 357-372.
16. Lascols, C.; Hackel, M.; Marshall, S. H.; Hujer, A. M.; Bouchillon, S.; Badal, R.; Hoban, D.; Bonomo, R. A., Increasing prevalence and dissemination of NDM-1 metallo- β -lactamase in India: data from the SMART study (2009). *J. Antimicrob. Chemother.* **2011,** *66*, (9), 1992-1997.
17. Ramirez, M. S.; Xie, G.; Marshall, S. H.; Hujer, K. M.; Chain, P. S.; Bonomo, R. A.; Tolmasky, M. E., Multidrug-resistant (MDR) Klebsiella pneumoniae clinical isolates: a zone of high heterogeneity (HHZ) as a tool for epidemiological studies. *Clinical Microbiology and Infection* **2012,** *18*, (7), E254-E258.
18. Broberg, C. A.; Palacios, M.; Miller, V. L., Whole-genome draft sequences of three multidrug-resistant Klebsiella pneumoniae strains available from the American Type Culture Collection. *Genome Announc.* **2013,** *1*, (3), e00312-13.
19. Volkmann, H.; Schwartz, T.; Bischoff, P.; Kirchen, S.; Obst, U., Detection of clinically relevant antibiotic-resistance genes in municipal wastewater using real-time PCR (TaqMan). *Journal of microbiological methods* **2004,** *56*, (2), 277-286.
20. Oliveira, D. C.; de Lencastre, H., Multiplex PCR strategy for rapid identification of structural types and variants of the mec element in methicillin-resistant Staphylococcus aureus. *Antimicrobial agents and chemotherapy* **2002,** *46*, (7), 2155-2161.
21. Clark, N.; Cooksey, R.; Hill, B.; Swenson, J.; Tenover, F., Characterization of glycopeptide-resistant enterococci from US hospitals. *Antimicrobial Agents and Chemotherapy* **1993,** *37*, (11), 2311-2317.

22. Dalsgaard, A.; Forslund, A.; Sandvang, D.; Arntzen, L.; Keddy, K., Vibrio cholerae O1 outbreak isolates in Mozambique and South Africa in 1998 are multiple-drug resistant, contain the SXT element and the aadA2 gene located on class 1 integrons. *J. Antimicrob. Chemother.* **2001,** *48*, (6), 827-838.
23. Ng, L.-K.; Martin, I.; Alfa, M.; Mulvey, M., Multiplex PCR for the detection of tetracycline resistant genes. *Molecular and cellular probes* **2001,** *15*, (4), 209-215.
24. Dumas, J.-L.; Van Delden, C.; Perron, K.; Köhler, T., Analysis of antibiotic resistance gene expression in Pseudomonas aeruginosa by quantitative real-time-PCR. *FEMS microbiology letters* **2006,** *254*, (2), 217-225.
25. Tam, V.; Schilling, A.; LaRocco, M.; Gentry, L.; Lolans, K.; Quinn, J.; Garey, K., Prevalence of AmpC over‐expression in bloodstream isolates of Pseudomonas aeruginosa. *Clinical microbiology and infection* **2007,** *13*, (4), 413-418.
26. Luo, Y.; Yang, F.; Mathieu, J.; Mao, D.; Wang, Q.; Alvarez, P. J. J., Proliferation of Multidrug-Resistant New Delhi Metallo-β-lactamase Genes in Municipal Wastewater Treatment Plants in Northern China. *Environ. Sci. Technol. Lett* **2013,** *1*, (1), 26-30.
27. Suzuki, M. T.; Taylor, L. T.; DeLong, E. F., Quantitative analysis of small-subunit rRNA genes in mixed microbial populations via 5′-nuclease assays. *Applied environmental microbiology* **2000,** *66*, (11), 4605-4614.
28. Devereux, R.; Willis, S. G., Amplification of ribosomal RNA sequences. In *Molecular microbial ecology manual*, Springer: 1995; pp 277-287.
29. Baker, G.; Smith, J. J.; Cowan, D. A., Review and re-analysis of domain-specific 16S primers. *Journal of microbiological methods* **2003,** *55*, (3), 541-555.

Chapter 4. Efficacies of the Healthcare Disinfectants Glutaraldehyde, Chlorhexidine, Ethanol, Povidone-Iodine, Benzalkonium Chloride, Phenol, Free Chlorine, and Hydrogen Peroxide in Degrading or Deactivating Antibiotic Resistance Genes on Inanimate Surfaces or in Aqueous Phase

ABSTRACT

This work investigated efficacies of commonly-used healthcare disinfectants – including glutaraldehyde, chlorhexidine, ethanol, povidone-iodine, benzalkonium chloride, phenol, free chlorine, and hydrogen peroxide (H_2O_2) – in eliminating antibiotic resistance genes (ARGs) on inanimate surface or in aqueous phase, using a chromosomal ARG (*blt*) of multidrug-resistant *Bacillus subtilis* 1A189. Surface disinfection experiments were conducted by treating vegetative *B. subtilis* 1A189 cells, inoculated on PTFE-coated carriers, with 2% glutaraldehyde, 2% chlorhexidine, 70% ethanol, 10% povidone-iodine, 0.5% benzalkonium chloride, 5% phenol, and 0.05% free chlorine (as NaOCl). Results showed that exposure to each disinfectant for 2 min and 20 min yielded non-significant or minimal (< 1-$\log_{10}$) elimination of *blt* 1017 bp amplicon copy numbers, although 2–5-$\log_{10}$ ARB inactivation was achieved. Treatment of vegetative *B. subtilis* 1A189 cells with H_2O_2 was conducted in aqueous phase (10 mM phosphate buffer at pH 7). H_2O_2 exposure of up to ~3×10^5 mg/L•min provided ~2 $\log_{10}$ ARG deactivation (transforming activity loss) while no significant ARG degradation (qPCR signal loss of *blt* 266, 832, 870, and 1017 bp amplicons), both lagging far behind viability loss of *B. subtilis* 1A189 cells. The behavior of intracellular ARG deactivation in the presence of H_2O_2 is likely due to the consumption of available iron present within cells that catalyzes H_2O_2 decomposition to form $^{\bullet}OH$, leading to DNA strand fragmentation without base alteration.

4.1 INTRODUCTION

Antibiotic resistance, in relation with antibiotic resistant bacteria and resistance genes (ARB and ARGs), has become severe concern in public health, particularly in hospitals and other healthcare settings.[1-3] Inappropriate prescription of antibiotics and lack of infection controls in healthcare practices have made significant contribution to emergence of ARB/ARGs.[4, 5] Further, the infectious ARB and their associated ARGs can spread amongst patients and healthcare providers, as well as inside/across healthcare facilities, leading to resistance dissemination and increasing cases of hospital acquired infections that might be untreatable.[5] In addition, healthcare facilities are intimately involved in ARB/ARG transport pathways through the entire municipal water cycling, by constantly generating wastewater and discharging effluents containing a variety of ARB/ARGs and substances such as antimicrobials.[6-8]

Disinfection and sterilization are essential in healthcare practices in controlling hospital acquired infections, including those caused by antibiotic resistant pathogens. By providing effective inactivation of ARB cells, healthcare disinfections could potentially compose critical barriers in preventing antibiotic resistance dissemination. However, little information is available on whether healthcare disinfections are also capable of destroying ARGs, which might maintain biological activity even after cell death and result in resistance dissemination via horizontal gene transfers (e.g., natural transformation) in downstream environments.

In the above context, this work was undertaken to investigate a suite of disinfectants commonly applied in healthcare practices, including glutaraldehyde, chlorhexidine, ethanol, povidone-iodine, benzalkonium chloride, phenol, free chlorine, and hydrogen peroxide (H_2O_2), and assessed their capabilities in eliminating ARGs on inanimate surface or in aqueous suspension (if the former test condition does not apply to a certain disinfectant). Here surface test

was adopted in priority because compared with suspension test, it provides more clinically-relevant conditions, as well as more conservative evaluation on disinfection efficacies (as disinfectants are usually less effective on surfaces than in suspensions).[9] A chromosomal ARG *blt* and its host strain multidrug-resistant *Bacillus subtilis* 1A189 were adopted as disinfection targets, and exposed to each disinfectant at typical conditions according to guidance provided by Centers for Disease Control (CDC)[10] or found in literature.[11-13]

4.2 MATERIALS AND METHODS

4.2.1 *Chemicals and Materials.*

All chemical reagents and growth media were purchased from commercial suppliers, of molecular biology grade purity, or at least reagent grade purity if the former was not available, and prepared with Milli-Q water (≥ 18.2 MΩ cm). Working solutions of disinfectants were prepared by diluting commercially-available aqueous stocks of glutaraldehyde (70% w/w in H_2O; Sigma-Aldrich), chlorhexidine (as chlorhexidine digluconate (CHG) solution, 20% w/w in H_2O; Sigma-Aldrich), ethanol (200 Proof, anhydrous, ≥99.5%; Decon), free chlorine (as sodium hypochlorite (NaOCl), 5% w/w in H_2O; Sigma-Aldrich), and hydrogen peroxide (H2O2, 30% w/w in H_2O; J.T. Baker or ACROS Organics™), or by dissolving solids of povidone-iodine (PVDI, as poly(vinylpyrrolidone)–iodine complex; Sigma-Aldrich), benzalkonium chloride (Sigma-Aldrich), and phenol (Clontech).

Antibiotic Medium #3 broth (BD Difco™) and Tryptose Blood agar (TBA; BD Difco™) were pre-dissolved and autoclaved at 121 °C. Dey-Engley (D/E) neutralizing broth (BD Difco™), yeast extract (Fisher BioReagents™), bovine serum albumin (BSA; Fisher BioReagents™), bovine mucin (Alfa Aesar™), and other reagents non-amenable to autoclaving

(e.g., acriflavine) were pre-dissolved and sterilized by filtration with 0.45-μm polyethersulfone (PES) membranes (Millipore). Pre-sterilized biological reagents and disinfectants were used without sterilization.

4.2.2 *Bacterial Strains.*

A multidrug-resistant *Bacillus subtilis* strain 1A189 and its chromosomal gene *blt* (carrying a point mutation *acfA* leading to efflux-pump resistance to fluoroquinolones, chloramphenicol, doxorubicin, and acriflavine)[14] were adopted as disinfection target ARB/ARG in this study, while the wild-type, non-resistant *B. subtilis* strain 1A1 was used as recipient of 1A189 DNA in transformation assays, according to He et al. (2019).[15] Both strains were purchased from the Bacillus Genetic Stock Center (BGSC; Ohio State University), revived, and cultured according to BGSC instructions.

4.2.3 *DNA Extraction.*

A FastDNA Spin Kit (MP Biomedicals) was used to perform DNA extractions in all disinfection experiments (unless otherwise specified) according to the manufacturer's protocol, with modifications as described previously (see Chapter 3). Alternatively, a modified phenol-chloroform-isoamyl alcohol extraction method[15, 16] was applied to obtain DNA used in cases of extracellular experiments or transformation assays following intracellular experiments, which require high purity or high molecular weight of DNA, respectively.

4.2.4 *Analytical methods.*

Natural transformation assay. Transforming activity of *B. subtilis* 1A189 DNA was quantified by culture-based natural transformation, using *B. subtilis* 1A1 as the recipient,[17, 18]

with protocols provided previously.[15] Transformation *frequency* was calculated as transformant cell density (CFU/mL) measured on TBA with 4-mg/L acriflavine over total recipient cell density (CFU/mL) on TBA only.[15] ***Quantitative polymerase chain reaction (qPCR).*** qPCR assays were performed with SsoFast™ EvaGreen® Supermix (Bio-Rad, Hercules, CA) using an Eppendorf RealPlex4 Mastercycler (Hauppauge, NY) or a Roche LightCycler® 96 Instrument (Pleasanton, CA), to quantify copy numbers of *blt* amplicons, targeting varying lengths and regions of *blt* gene, as previously described.[15] Primers were purchased from Eurofins (Huntsville, AL). ***Other analyses.*** DNA fragment sizes were analyzed by pulsed-field gel electrophoresis (PFGE).[15] Double-stranded DNA (dsDNA) concentrations were measured by Hoechst 33258 fluorescence assay with a DNA Quantitation Kit (Bio-Rad or Sigma-Aldrich). Concentrations of monomeric deoxyribonucleoside 5'-monophosphate (dNMP, or nucleotide), including deoxyadenosine 5'-monophosphate (dAMP), deoxyguanosine 5'-monophosphate (dGMP), deoxycytidine 5'-monophosphate (dCMP), and deoxythymidine 5'-monophosphate (TMP), were quantified via nuclease P1 (Sigma) digestion followed by high performance liquid chromatography.[19] Residual viabilities of *B. subtilis* 1A189 cells treated in disinfection experiments were measured by spot-titering[20] on TBA plates containing with 4-mg/L acriflavine.

4.2.5 *Disinfection treatment on inanimate surface.*

Disinfection experiments on inanimate surface were conducted using a modified version of the *quantitative method for evaluating bactericidal activity of microbicides used on hard non-porous surfaces* published in Organisation for Economic Co-operation and Development (OECD) guidance document (series on Biocides No. 6).[21] In brief, vegetative cells of *B. subtilis* 1A189 were harvested from overnight cultures, washed, pelleted by centrifugation, and resuspended in solution of phosphate buffer saline (PBS; 0.625 mM phosphate and 0.15 M NaCl,

pH 7.2) containing soil load (including 3.5 mg/mL yeast extract, 2.5 mg/mL BSA, and 0.8 mg/mL mucin). The cell concentrations in the resulted suspensions were within the range of ~5×10^9 – 1×10^{10} CFU/mL. Here the polytetrafluoroethylene (PTFE)-coated side of silicone septa (24 mm in diameter; Fisher) were used as carriers to represent hard, non-porous environmental surfaces. Three 50-μL droplets of the cell suspension were deposited onto the PTFE surface of one septum. Three to four of such inoculated septa were placed in one Petri dish (with lid open), and dried in biosafety hood for ~2.5 hours. Within 0.5–1 hour after dried, each dried droplet of inocula was treated with 2% glutaraldehyde, 2% chlorhexidine, 70% ethanol, 10% povidone-iodine, 0.5% benzalkonium chloride, 5% phenol, 0.05% free chlorine (as NaOCl), or 3% H_2O_2, by depositing 100 μL of each disinfectant to completely cover the whole droplet. After a pre-defined contact period, each septum was immediately transferred using a sterile polypropylene tweezer into 10 mL D/E neutralizing broth contained in a 50 mL centrifuge tube, which was vigorously vortexed for at least 1 min to terminate the reaction, as well as to elute cells off the PTFE surface. The septum was then removed out of the centrifuge tube with the tweezer, and the treated cells were pelleted by centrifugation and processed through DNA extraction as specified above. DNA recovery was determined by measuring dsDNA concentration of the resulting extracts. Prior to cell recovery, residual viabilities of the treated cells were measured by spot-titering[20] as described above.

Drying controls were conducted by exposing the dried inoculum droplets to the same volume of PBS instead of disinfectant for the same contact period. The viability of recovered cells from the drying controls were compared with that of cell suspensions without drying, to assess viability loss (typically ~1-2 $\log_{10}$) during the drying procedure on PTFE surface. In addition, a separate quenching control was set up for each disinfectant by premixing 300 μL

disinfectant solution with 10 mL D/E neutralizing broth and then immediately dosing 150 μL cell suspension into the mixture, to validate the disinfectant was immediately and completely quenched/neutralized by the neutralizing medium. For each pre-defined contact time (2 min or 20 min), at least triplicate septa were set up for treatment with each disinfectant, and at least four replicates of drying controls were conducted and used for all the disinfectants in one batch of experiments. All surface disinfection experiments were performed at room temperature (20±1 °C). Normalized ARB cell viability (C/C_0) or normalized ARG copy numbers (N/N_0) were calculated by dividing cell viability or ARG copy number of a given sample over the average of the corresponding drying control replicates, respectively.[22]

4.2.6 *Disinfection treatment in aqueous phase (for H_2O_2 only)*

For H_2O_2, disinfection experiments were conducted in aqueous phase instead of on inanimate surface, since the latter condition was unable to provide effective disinfection, i.e., no cell viability loss at all over the whole contact period of 20 min (data not shown). Here the failure of H_2O_2 in surface disinfection might result from rapid decomposition of H_2O_2 triggered by *B. subtilis* catalase,[23] which is supported by the observations of bubbling on application of H_2O_2 to the cells (indicative of O_2 production). Here the defense by the high-density cells inoculated on the surface (150 μL of ~5×10^9 – 1×10^{10} CFU/mL cell suspension) could not be overwhelmed by the amount of H_2O_2 applied in this case (only 300 μL of 3% H_2O_2).

Intracellular ARG treatment with H_2O_2. Vegetative cells of *B. subtilis* 1A189, cultured overnight and washed, were dosed into batch reactors (covered with aluminum foil) containing 1-L autoclaved 10-mM phosphate buffer (PB) solutions at pH 7 to reach a final concentration of ~10^6 CFU/mL. Stock solution of H_2O_2 was dosed to the cell suspensions under stirring to yield

final concentration of 30 mM (~ 0.1% w/w). At pre-defined times, the whole 1-L reaction solution was quenched with bovine liver catalase (Sigma; ≥10-units/μmole H_2O_2) and vacuum filtered through 0.2 μm track-etched polycarbonate membranes (Whatman, NJ) to harvest treated cells. The cells recovered on the membrane filters were then processed through DNA extraction as specified above. ***Extracellular ARG treatment with H_2O_2.*** Pre-isolated *B. subtilis* 1A189 DNA stock was diluted to 1 mg/L in solution of 10-mM PB (pH 7) contained in 25 mL amber bottles. Disinfection reaction was initiated by adding H_2O_2 stock to 1-mg/L DNA solutions with continuously stirring. At pre-defined times, 1-mL reaction solution was taken and quenched with bovine liver catalase (as above).

H_2O_2 stock was standardized spectrophotometrically at 240 nm (ε = 40 $M^{-1}cm^{-1}$),[24] and H_2O_2 concentration of the reaction solutions was monitored during the experiments using Allen's reagent at λ = 350 nm.[24] Cumulative integrated exposure (or *CT* values, in mg/L•min) of H_2O_2 was calculated as $\int_0^t [\text{Disinfectant}]\,dt$. Selected experiments were performed in the presence of 50-mM *tert*-Butanol (*t*-BuOH), a scavenger of hydroxyl radical (•OH), to evaluate potential contributions of •OH to intra- or extracellular ARG degradation/deactivation during exposure to H_2O_2. DNA samples obtained from either intra- or extracellular experiments were subjected to qPCR and transformation assays to quantify residual ARG copy number and transformation frequency, respectively. For intracellular H_2O_2 experiments, residual viability of the treated cells were also measured by spot-titering[20] prior to vacuum filtration of the quenched reaction solution; in addition, DNA recovery was determined by measuring dsDNA concentration of the resulting extracts. All the H_2O_2 experiments were performed in at least duplicate at room temperature (20±1 °C). Normalized ARB cell viability (C/C_0), normalized ARG copy numbers (N/N_0), and normalized transformation frequency (f/f_0) were calculated by dividing cell viability,

ARG copy number, and transformation frequency of a given sample over that of an untreated control, respectively.

4.2.7 *Statistical Analysis.*

Mean values of paired datasets, such as normalized cell viability and normalized ARG copy number for replicate samples treated by the same disinfectant for specific contact time, were compared using two-tailed *t*-tests with $p < 0.05$ and a null hypothesis of no significant difference existing between means of the two datasets. One-tailed *t*-test ($p < 0.05$) was used to analyze whether disinfection treatment resulted in significant ARB inactivation or ARG elimination, where the null hypothesis was no loss in cell viability or qPCR amplicon copy number after treatment (i.e., $\log_{10}$ loss = 0), respectively.

4.3 RESULTS AND DISCUSSION

4.3.1 *ARB inactivation versus ARG elimination during exposure to various healthcare disinfectants on inanimate surface.*

Effects of ARB inactivation and ARG copy number elimination by treatment of various healthcare disinfectants, including glutaraldehyde, chlorhexidine, ethanol, povidone-iodine, benzalkonium chloride, phenol, and chlorine, at typical conditions of healthcare practices are illustrated in Figure 4.1. As shown below, 2% glutaraldehyde (Figure 4.1a) and 5% phenol (Figure 4.1f) are highly effective in inactivating *B. subtilis* 1A189 cells on PTFE surface, each yielding 4–5-$\log_{10}$-loss of cell viability at both contact periods of 2 min and 20 min. Note here for 2% glutaraldehyde (Figure 4.1a), one-tailed *t*-test yielded insignificant loss of cell viability (labeled as n.s.) for 2-min contact time, while not applicable (labeled as n.a.) for 20-min contact time, both of which were due to limited sample numbers (N=2 and N=1, respectively), since the

other replicate(s) were below detection limit, i.e., > 5.5-$\log_{10}$ loss. In comparison, the other five disinfectants (2% chlorhexidine, 70% ethanol, 10% povidone-iodine, 0.5% benzalkonium chloride, and 0.05% free chlorine) exhibited lower efficacies (Figure 4.1b, c, d, e, and g, respectively), leading to no more than 1-$\log_{10}$ inactivation at 2 min, and moderate to high extents of inactivation (~2–4-$\log_{10}$ loss) at 20 min, which declines in the order of 70% ethanol > 10% povidone-iodine ≥ 0.5% benzalkonium chloride > 2% chlorhexidine > 0.05% free chlorine.

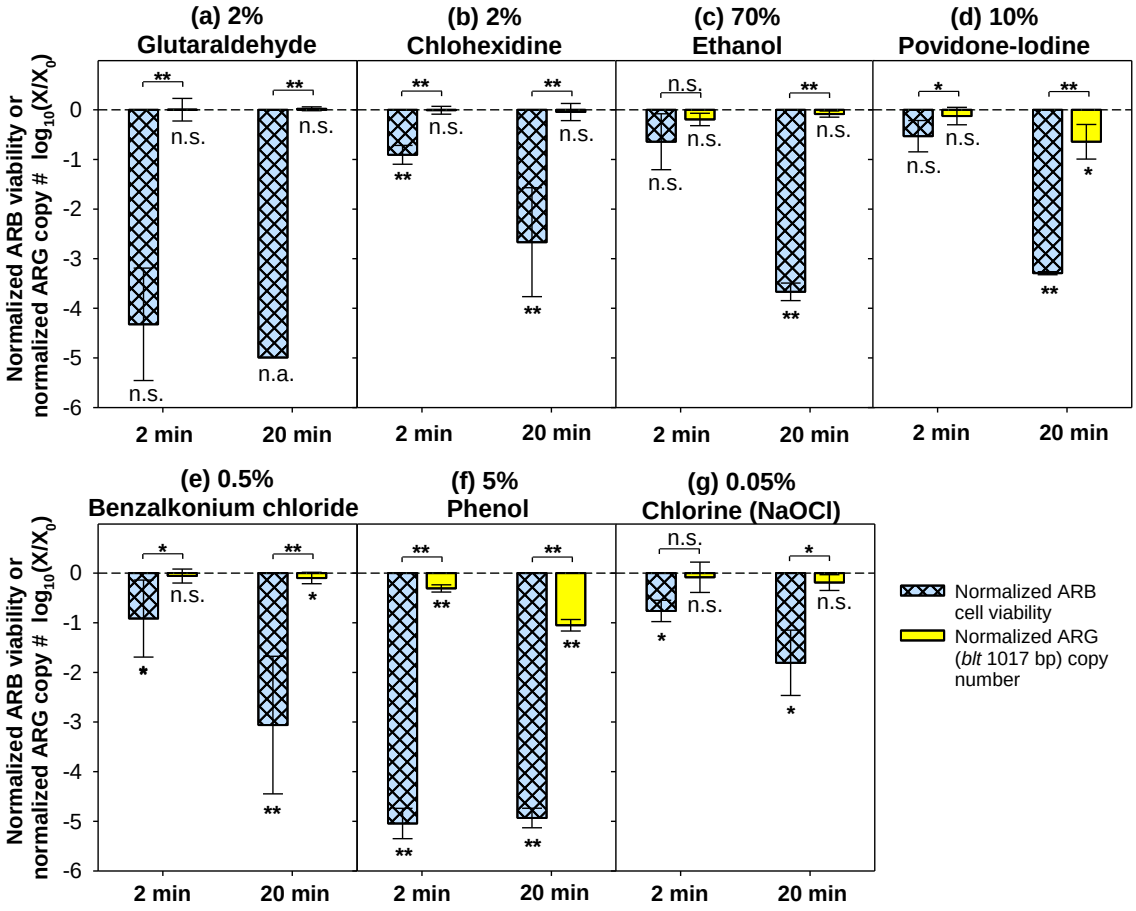

Figure 4.1. Normalized ($\log_{10}$-scale) ARB cell viabilities and normalized ARG copy numbers after treatment of *B. subtilis* 1A189 vegetative cells (as dried inoculum droplets) with **(a)** 2% glutaraldehyde, **(b)** 2% chlorhexidine, **(c)** 70% ethanol, **(d)** 10% povidone-iodine, **(e)** 0.5% benzalkonium chloride, **(f)** 5% phenol, and **(g)** 0.05% chlorine (as NaOCl) for contact periods of 2 min and 20 min on PTFE surface at room temperature (20±1 °C). Two-tailed *t*-tests were performed to analyze whether the means of normalized ARB cell viability and normalized ARG copy number of the same replicate samples significant difference ($p < 0.05$), as well as to analyze whether each of the means were significantly different from zero (i.e., no significant change after treatment), with results labeled across or below bars, respectively (n.s. = no significance; * represents $p < 0.05$; ** represents $p < 0.01$; n.a. = not available, for sample with only one replicate above detection limit).

Despite varying efficacies in ARB inactivation, all the seven disinfectants achieved non-significant or minimal ($\leq$ ~1-$\log_{10}$) elimination in copy number of *blt* 1017 bp amplicon even at 20-min contact time, lagging far behind ARB inactivation. These observations agree well with the fact that several of the investigated disinfectants, including chlorhexidine, ethanol, benzalkonium chloride, and phenol, exhibit cellular inactivation mechanisms such as membrane disruption, enzyme degradation (via protein denaturation/alteration) not directly corresponding to DNA modification.[12, 25] Even for the other disinfectants, glutaraldehyde, povidone-iodine (with free iodine as the active ingredient), and free chlorine, which are reactive toward DNA through nucleotide alteration (e.g., alkylation, halogenation) and/or cross-linking formation,[11, 12] they would interact with other biomolecules (e.g., surface proteins, membrane fatty acids) and disrupts vital cellular processes, prior to reaching DNA and destroying its molecular structure and biological activity.

Here the limited effect of free chlorine in ARG degradation (and moderate effect in ARB inactivation) might also be explained by that: (1) the working solution of NaOCl was diluted from its stock using Milli-Q water without pH buffering, thus highly basic (pH > 9) with OCl^- being the dominant chlorine species, which is typically less reactive than HOCl by two orders of magnitude toward biomolecules;[26] and (2) the high-density cell suspension (~5×10^9 – 1×10^{10} CFU/mL) containing soil load (a mixture of yeast extract, BSA, and mucin) inoculated onto the surface required high chlorine demand, leading to lower chlorine exposure than targeted.

4.3.2 *ARG degradation and deactivation kinetics and mechanisms during exposure to H2O2 in aqueous phase*

Results of ARG degradation (qPCR signal loss) and deactivation (transforming activity loss) kinetics, as well as ARB inactivation kinetics, during exposure to H_2O_2 in aqueous phase

are provided in Figure 4.2a. Typical H_2O_2 *CT* ranges applied in healthcare settings provided over 3-$\log_{10}$ ARB inactivation within *CT* of 5×10^4 mg/L•min, while less than 2-$\log_{10}$ loss of ARG transforming activity and no significant degradation of qPCR amplicons over the entire exposure range (up to ~3×10^5 mg/L•min).

H_2O_2 is not directly reactive toward DNA (as confirmed by treatment of extracellular *B. subtilis* 1A189 DNA with and without *t*-BuOH; Figure 4.3), thus the behavior of intracellular ARG deactivation in the presence of H_2O_2 is likely due to the consumption of available iron present within cells that catalyzes H_2O_2 decomposition to form $^{\bullet}OH$,[27, 28] which is highly reactive toward DNA ($k = 2.3(\pm0.1)\times10^8\ M^{-1}s^{-1}$ per bp; see Chapter 2)[15] and damages DNA predominantly by strand fragmentation (via phosphate backbone cleavage).[29] Natural transformation in *B. subtilis* (driven by homologous recombination) requires not only ~800-1000 bps of homologous sequence flanking the heterologous region to be transformed (in this case a point mutation *acf*A),[30, 31] but also long-enough DNA fragments to ensure attachment and/or donor-acceptor complexation efficiencies.[32] Therefore, $^{\bullet}OH$ induced in intracellular environments could result in reduction of DNA strand length and thus decrease in transformation frequency, without modifying the sequence amplified by qPCR, which could explain the discrepancy between elimination rates of qPCR signals and ARG transforming activity during intracellular H_2O_2 treatment.

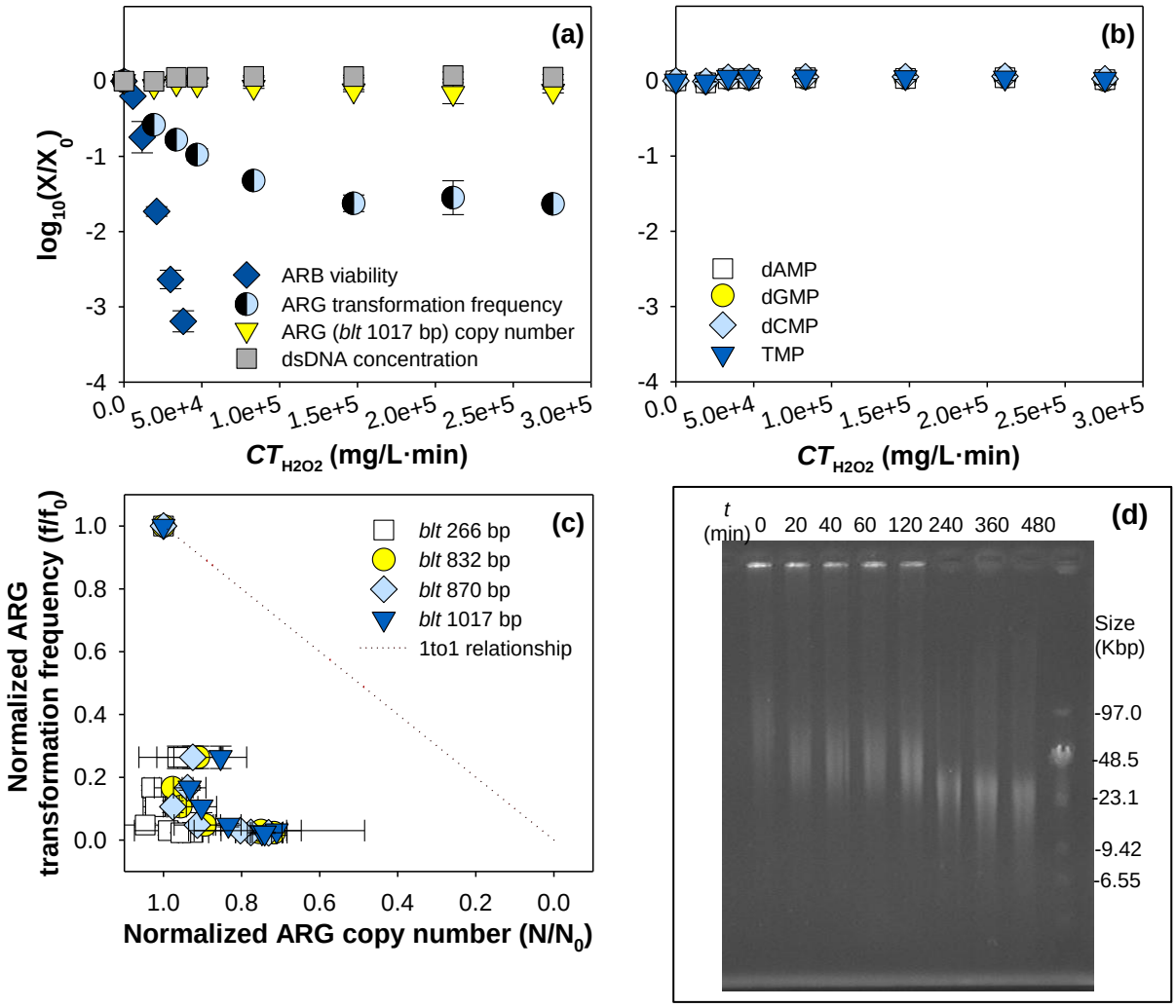

Figure 4.2. Normalized (log_{10}-scale) **(a)** ARB cell viability, ARG transformation frequency, ARG copy number (for *blt* 1017 bp), dsDNA concentration, and **(b)** concentration of individual nucleotides (including dAMP, dGMP, dCMP, and TMP) versus H_2O_2 exposure; **(c)** Normalized transformation frequency versus normalized copy numbers of *blt* 266 bp, 832 bp, 870 bp and 1017 bp amplicons. All data were obtained by treatment of *B. subtilis* 1A189 vegetative cells with 30 mM H_2O_2 in 10 mM PB at pH 7 in presence of 50 mM *t*-BuOH. PFGE image of the DNA extracts obtained during the above treatment is shown in panel **(d)**, with NEB LowRange PFG Marker as reference.

The tendency that ARG transforming activity loss outpaced ARG degradation was emphasized by plotting normalized transformation frequency versus normalized copy numbers of the four *blt* amplicons in Figure 4.2c, where all the data points deviated far away from the 1to1 relationship line. The pattern of the 1to1 ratio plot is highly consistent with that obtained from treatment with hydroxyl radical (•OH) in prior work[15] (or see Figure 2.3f), supporting similar

DNA damage mechanisms existing in the two systems. Concentrations of dsDNA and individual nucleotides (dNMPs) were monitored over H_2O_2 exposures, with normalized results shown in Figure 4.2a and b, respectively. In addition, DNA fragment size distributions of the samples obtained from intracellular H_2O_2 treatment were also analyzed by PFGE, with image provided in Figure 4.2d. Compiling the results in the above panels, it can be found that intracellular H_2O_2 treatment resulted in DNA strand fragmentation but no base alterations, further supporting intracellular generation of •OH in this system, as explained above.

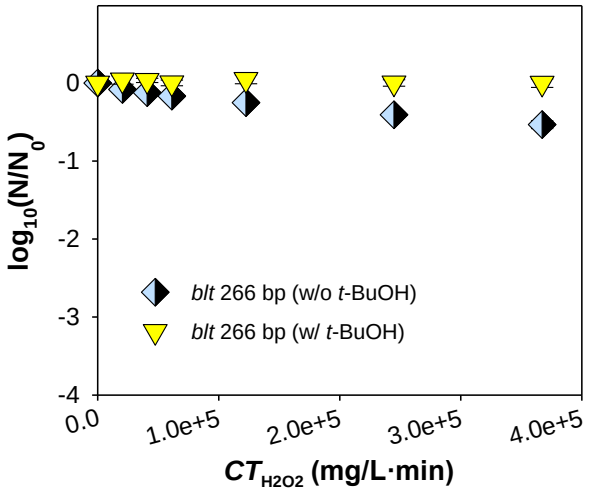

Figure 4.3. Normalized (in $\log_{10}$-scale) copy number of *blt* 266 bp amplicon versus H_2O_2 exposure during treatment of extracellular *B. subtilis* 1A189 (1 mg/L as dsDNA) with 30 mM H_2O_2 in 10 mM PB at pH 7 with and without 50 mM *t*-BuOH.

4.3.3 *Practical implication and future works.*

Results in this study have clearly demonstrated that ARGs could survive (and remain biologically active) after treatment of common healthcare disinfectants, which would potentially lead to antibiotic resistance dissemination through horizontal gene transfer events on inanimate surfaces and/or across other interfaces in healthcare facilities afterwards. Further studies should be focused on investigating elimination of ARG transforming activity during surface disinfection treatment with glutaraldehyde, chlorhexidine, ethanol, povidone-iodine, benzalkonium chloride,

phenol, and free chlorine to complete the dataset and further validate the findings here. In addition, it is worthwhile to extend the study to other (clinically-relevant) model ARB/ARG targets to analyze effect of disinfectants on ARG elimination in different host cells.

ACKNOWLEDGEMENTS

This material is based upon work supported by the National Science Foundation under Grant Number CBET-1254929. Dr. J. Scott Meschke is greatly acknowledged for valuable advice on surface disinfection experiments and technical support on PFGE system. Dr. Dan Zeigler (Bacillus Genetic Stock Center) is gratefully acknowledged for access to *B. subtilis* strains. Dr. Mari Winkler and Bao Nguyen Quoc are greatly thanked for access to qPCR instrumentation.

REFERENCES

1. Davies, J.; Davies, D., Origins and Evolution of Antibiotic Resistance. *Microbiol. Mol. Biol. Rev.* **2010,** *74*, (3), 417-433.
2. *Antibiotic Resistance Theats in the United States, 2013*; U.S. Department of Health and Human Services Centers for Disease Control and Prevention: 2013.
3. Roberts, R. R.; Hota, B.; Ahmad, I.; Scott, R. D.; Foster, S. D.; Abbasi, F.; Schabowski, S.; Kampe, L. M.; Ciavarella, G. G.; Supino, M.; Naples, J.; Cordell, R.; Levy, S. B.; Weinstein, R. A., Hospital and Societal Costs of Antimicrobial-Resistant Infections in a Chicago Teaching Hospital: Implications for Antibiotic Stewardship. *Clin. Infect. Dis.* **2009,** *49*, (8), 1175-1184.
4. Schwartz, B.; Bell, D. M.; Hughes, J. M., Preventing the emergence of antimicrobial resistance: a call for action by clinicians, public health officials, and patients. *Jama* **1997,** *278*, (11), 944-945.
5. Mulvey, M. R.; Simor, A. E., Antimicrobial resistance in hospitals: how concerned should we be? *Cmaj* **2009,** *180*, (4), 408-415.
6. Bäumlisberger, M.; Youssar, L.; Schilhabel, M. B.; Jonas, D., Influence of a non-hospital medical care facility on antimicrobial resistance in wastewater. *PloS one* **2015,** *10*, (3).
7. Wang, Q.; Wang, P.; Yang, Q., Occurrence and diversity of antibiotic resistance in untreated hospital wastewater. *Science of the Total Environment* **2018,** *621*, 990-999.
8. Rodriguez-Mozaz, S.; Chamorro, S.; Marti, E.; Huerta, B.; Gros, M.; Sànchez-Melsió, A.; Borrego, C. M.; Barceló, D.; Balcázar, J. L., Occurrence of antibiotics and antibiotic

resistance genes in hospital and urban wastewaters and their impact on the receiving river. *Water Res.* **2015,** *69*, 234-242.
9. Van Klingeren, B., Disinfectant testing on surfaces. *Journal of hospital infection* **1995,** *30*, 397-408.
10. Rutala, W. A.; Weber, D. J., Guideline for disinfection and sterilization in healthcare facilities, 2008. **2008**.
11. Block, S. S., *Disinfection, sterilization, and preservation*. Lippincott Williams & Wilkins: 2001.
12. Fraise, A. P.; Lambert, P. A.; Maillard, J.-Y., *Russell, Hugo & Ayliffe's principles and practice of disinfection, preservation and sterilization*. John Wiley & Sons: 2008.
13. Wendt, C.; Frei, R.; Widmer, A. F., Decontamination, Disinfection, and Sterilization. In *Manual of Clinical Microbiology, Eleventh Edition*, American Society of Microbiology: 2015; pp 183-216.
14. Ahmed, M.; Lyass, L.; Markham, P. N.; Taylor, S. S.; Vazquezlaslop, N.; Neyfakh, A. A., Two highly similar multidrug transporters of *Bacillus subtilis* whose expression is differentially regulated. *J. Bacteriol.* **1995,** *177*, (14), 3904-3910.
15. He, H.; Zhou, P.; Shimabuku, K. K.; Fang, X.; Li, S.; Lee, Y.; Dodd, M. C., Degradation and deactivation of bacterial antibiotic resistance genes during exposure to free chlorine, monochloramine, chlorine dioxide, ozone, ultraviolet light, and hydroxyl radical. *Environ. Sci. Technol.* **2019,** *53*, (4), 2013-2026.
16. Saito, H.; Miura, K., Preparation of transforming deoxyribonucleic acid by phenol treatment. *Biochim. Biophys. Acta.* **1963,** *72*, (4), 619-629.
17. Bott, K. F.; Wilson, G. A., Development of competence in *Bacillus subtilis* transformation system. *J. Bacteriol.* **1967,** *94*, (3), 562-570.
18. Anagnostopoulos, C.; Spizizen, J., Requirements for transformation in *Bacillus subtilis*. *J. Bacteriol.* **1961,** *81*, (5), 741.
19. Shimelis, O.; Giese, R. W., Nuclease P1 digestion/high-performance liquid chromatography, a practical method for DNA quantitation. *J. Chromatogr. A* **2006,** *1117*, (2), 132-136.
20. Beck, N.; Callahan, K.; Nappier, S.; Kim, H.; Sobsey, M.; Meschke, J., Development of a spot‐titer culture assay for quantifying bacteria and viral indicators. *J. Rapid Methods Autom. Microbiol.* **2009,** *17*, (4), 455-464.
21. *Quantitative method for evaluating bactericidal activity of microbicides used on hard non-porous surfaces*; OECD: Paris, 2013.
22. De Vries, T. A.; Hamilton, M. A., Estimating the antimicrobial Log reduction: Part 1. Quantitative assays. *Quantitative Microbiology* **1999,** *1*, (1), 29-45.
23. Loewen, P. C.; Switala, J., Multiple catalases in Bacillus subtilis. *J. Bacteriol.* **1987,** *169*, (8), 3601-3607.
24. Allen, A. O.; Hochanadel, C.; Ghormley, J.; Davis, T., Decomposition of water and Aqueous solutions under mixed fast neutron and γ-radiation. *J. Phys. Chem.* **1952,** *56*, (5), 575-586.
25. McDonnell, G.; Russell, A. D., Antiseptics and disinfectants: activity, action, and resistance. *Clinical microbiology reviews* **1999,** *12*, (1), 147-179.
26. Operations, U. S. E. P. A. O. o. W. P., *Alternative disinfectants and oxidants guidance manual*. US Environmental Protection Agency, Office of Water: 1999.

27. Brandi, G.; Cattabeni, F.; Albano, A.; Cantoni, O., Role of hydroxyl radicals in escherzchza colz killing induced by hydrogen peroxide. *Free radical research communications* **1989,** *6*, (1), 47-55.
28. Imlay, J. A., Pathways of oxidative damage. *Ann. Rev. Microb.* **2003,** *57*, (1), 395-418.
29. Balasubramanian, B.; Pogozelski, W. K.; Tullius, T. D., DNA strand breaking by the hydroxyl radical is governed by the accessible surface areas of the hydrogen atoms of the DNA backbone. *Proc. Natl. Acad. Sci. U.S.A.* **1998,** *95*, (17), 9738-9743.
30. Contente, S.; Dubnau, D., Marker rescue transformation by linear plasmid DNA in Bacillus subtilis. *Plasmid* **1979,** *2*, (4), 555-571.
31. Dubnau, D., Genetic exchange and homologous recombination. In *Bacillus subtilis and other gram-positive bacteria: biochemistry, physiology, and molecular genetics.*, Sonenshein, A. L.; Hoch, J. A.; Losick, R., Eds. American Society for Microbiology: Washington D.C, 1993; pp 555-584.
32. Morrison, D. A.; Guild, W. R., Activity of Deoxyribonucleic Acid Fragments of Defined Size in *Bacillus subtilis* Transformation. *J. Bacteriol.* **1972,** *112*, (1), 220-223.

Chapter 5. General Conclusions

This dissertation conducted a comprehensive investigation on antibiotic resistance gene (ARG) degradation/deactivation kinetics, mechanisms, and/or efficiencies during disinfection processes in (waste)water treatment and health-care practice, to fill in blanks of understanding whether and how disinfection practices could provide barriers to prevent or mitigate antibiotic resistance dissemination through elimination of ARGs and their biological activity in horizontal gene transfers such as natural transformation. The overarching goals of this work include,

(1) to determine fundamental kinetic parameters and mechanisms governing ARG *degradation* (chemical modification captured by qPCR) and *deactivation* (transforming activity loss) during exposure to common (waste)water disinfectants/oxidants;

(2) to develop a kinetics-based model to predict ARG *degradation* and/or *deactivation* kinetics during exposure to these disinfectants, and apply the model to (selected) bench- and/or full-scale (waste)water disinfection processes;

(3) to assess the efficacies of common healthcare disinfectants/antiseptics in eliminating ARGs and their biological activities, at typical clinical-relevant conditions.

The key outcomes, conclusions, and implications from this work are summarized below following the order of the objectives.

For ***objective (1)***, ARG degradation/deactivation kinetics were characterized by treating a model ARG *blt*, carried on chromosome of multidrug-resistant *Bacillus subtilis* strain 1A189, with (waste)water disinfectants, including free available chlorine (FAC), monochloramine (NH_2Cl), ozone (O_3), chlorine dioxide (ClO_2), ultraviolet (UV) light, and hydroxyl radical ($^{\bullet}OH$). Kinetics measurements found that DNA segment degradation (as measured by qPCR) by FAC and NH_2Cl followed accelerating kinetics with increasing disinfectant exposures (or *CTs*), which likely involve a two-step sequential reactions of **(i)** reversible N-chlorination of nucleobases,

followed by **(ii)** irreversible C-chlorination of the N-chlorinated nucleobase(-pair)s, each following second-order kinetics. ARG degradation was linearly related to *CTs* for O_3 and ClO_2, or to degradation of probing compound for $^{\bullet}OH$, indicating second-order kinetics. For UV irradiation, ARG degradation followed fluence-based first-order kinetics at UV fluences (or *ITs*) up to ~50 mJ/cm^2, while exhibited tailing at higher fluences, which can be addressed by a complex-kinetics model, involving two parallel pathways of **(i)** formation of photo-reversible cyclobutane pyrimidine dimers (CPDs), **(ii)** formation of irreversible lesions primarily as (6-4) photo-products (6-4PPs), with each reaction following fluence-based first-order kinetics.

Second-order or fluence-based first-order rate constants were determined for each of the above elementary reactions for four amplicons of the *blt* gene, ranging from 266-1017 bp, adjacent to or encompassing the *acfA* mutation enabling *blt* overexpression. Results demonstrated that ARG susceptibilities toward different chemical disinfectants varied widely, and the reactivity of a given DNA segment toward each chemical disinfectant declines in the order $^{\bullet}OH$ (2.3×10^{8} $M^{-1}s^{-1}$ per bp) >> O_3 (6.5×10^{1} $M^{-1}s^{-1}$ per bp) > FAC (7.2 $M^{-1}s^{-1}$ per bp) >> ClO_2 (1.1×10^{-2} $M^{-1}s^{-1}$ per bp) > NH_2Cl (3.6×10^{-3} $M^{-1}s^{-1}$ per bp).

For a given disinfectant, second-order or fluence-based first order rate constants (for N-chlorination step of FAC or NH_2Cl reactions, and forward reaction of CPD formation for the complex UV model) increased linearly with amplicon contents of AT+GC base pairs (bps, or amplicon lengths, for FAC, NH_2Cl, O_3, and $^{\bullet}OH$) or intrastrand 5'-TT-3' or 5'-GG-3' doublets (for UV and ClO_2, respectively). These strong correlations ($R^2 \geq 0.98$) not only elucidated the preferential sites of DNA damage induced by each disinfectant, but also highlighted that reactivity of DNA segments toward each disinfectant varied in a predictable manner.

For FAC, NH_2Cl, O_3, ClO_2, and UV, which damage DNA primarily through nucleotide modification (non-preferentially attacking both AT and GC bps, or preferentially targeting 5'-TT-3' or 5'-GG-3' doublets, as elucidated above), *blt* gene transforming activity was eliminated at similar rates as degradation of amplicons approximating a ~800-1000 bp *acfA*-flanking sequence responsible for homologous DNA recombination, the critical step of natural transformation in *B. subtili*s. In contrast, deactivation of *blt* gene outpaced qPCR amplicon degradation for •OH, which can be explained by its distinctive DNA damage mechanisms. Unlike other disinfectants inducing DNA lesions via base alteration, •OH damages DNA primarily through strand fragmentation by cleaving phosphate backbone, as confirmed by analyses of pulsed-field gel electrophoresis. Therefore, any damage by •OH outside the requisite homologous flanking sequence would cleave DNA strand into smaller pieces, which lead to reduction in attachment/complexation efficiencies of donor DNA toward recipient cells, thus decrease in transformation frequency, while not necessarily in qPCR signals.

The above findings allow establishment of a kinetics-based modeling framework to achieve ***objective (2)***, by **(i)** predicting rate constants of ARG/DNA segments toward each (waste)water disinfectant according the DNA sequences' lengths and/or specific nucleotide contents; then **(ii)** predicting ARG *degradation* kinetics by taking the theoretical rate constants into corresponding elementary reactions; and **(iii)** predicting ARG *deactivation* kinetics if the DNA sequence responsible for ARG biological activity is known.

This kinetics-based model was first validated by the *blt* gene itself, which successfully predicted degradation kinetics of the four 266-1017 bp *blt* amplicons, as well as *blt deactivation* kinetics, for both its extracellular from and intracellular form (as vegetative *B. subtilis* 1A189 cells) during exposures to each disinfectant (except •OH) in clean buffers. Then the model was

expanded to a wider array of ARG amplicons (including *blt*, *mec*A, *van*A, *tet*(A), *amp*C, bla_{NDM}, and bla_{KPC}, each around ~800-1000 bp) and varying-length 16S rRNA gene segments (142-1509 bp), each harbored by *Bacillus subtilis*, methicillin-resistant *Staphylococcus aureus* (MRSA), vancomycin-resistant *Enterococcus faecium* (VRE), *Escherichia coli* SMS-3-5, *Pseudomonas aeruginosa* O1 (PAO1), and *Klebsiella pneumoniae Klebsiella pneumoniae* 1.53 and ATCC BAA-1705, respectively. The expanded model, focusing on UV, FAC, and NH_2Cl, was utilized to predict degradation/deactivation profiles (or removal efficiencies) of the above ARGs/16S rRNA gene during bench/full-scale UV- and chlorine-based wastewater disinfection processes. Important findings include:

(i) At practical disinfectant exposures, extra- and intracellular of various ARGs and 16S rRNA gene were 90%-99.9% degraded/deactivated by FAC, O_3, and UV, but recalcitrant to NH_2Cl and ClO_2, which can be adequately predicted by the kinetics-based model under certain circumstances with exceptions as clarified below.

(ii) Intracellular ARG degradation/deactivation always lagged behind host ARB inactivation in cases of all the disinfectants in either clean buffers or wastewater matrixes.

(iii) The complex-kinetics UV model considering CPD photoreversal largely improved model prediction at high fluence range (> 50 mJ/cm^2) compared with traditional linear-kinetics UV model, although cautions should be paid to intracellular gene degradation, which exhibited stronger tailing than that of extracellular genes, potentially due to photo- or dark-repair of vegetative host cells, and could be overestimated by the model at high fluences.

(iv) UV irradiation performed stably on intracellular gene degradation with minimal impacts from different aqueous matrixes (*wastewaters versus clean buffers*), the presence of

suspended solids (*filtered versus unfiltered wastewaters*), or different DNA sources (*from various spiked ARB or native biomass in wastewater*).

(v) Intracellular ARG degradation/deactivation kinetics exhibited tailing at high exposures of O_3 (> 0.1 mg/L•min), potentially resulted from accelerated disinfectant consumption due to solubilization of reactive biomolecules within the cell matrix. Various extents of tailings, related with host strain types, were also found in cases of FAC for similar reasons; and specifically, the significant tailing in intracellular *amp*C degradation kinetics (and in PAO1 viability loss) was likely due to rapid consumption of FAC by extracellular polymeric substances generated by PAO1.

(vi) Bench-scale experimental and modeling results supported observations at two local wastewater treatment plants that UV provided ~1 $\log_{10}$ ARG elimination, while chlorination of high-ammonia (non-nitrified) wastewater yielded no significant ARG removal, due to rapid conversion of FAC into NH_2Cl in excess ammonia, which indicates that chlorination of non-nitrified effluent is unlikely to prevent ARG release into downstream waterbodies.

Last for ***objective (3)***, this work provided a screening investigation on commonly-used healthcare disinfectants, including glutaraldehyde, chlorhexidine, ethanol, povidone-iodine, benzalkonium chloride, phenol, free chlorine, and hydrogen peroxide, which assessed their efficacies in eliminating ARGs (and their biological activities) on inanimate surface (to mimic clinically-relevant conditions) or in aqueous suspensions. Results highlighted that exposure to each of these disinfectants at typical healthcare conditions only achieved limited ARG degradation/deactivation levels (< 2-$\log_{10}$ for H_2O_2 in aqueous phase and < 1-$\log_{10}$ for the others on surface), all lagging behind ARB inactivation. H_2O_2 damages intracellular DNA likely

through strand fragmentation by $^{\bullet}OH$, which was generated from H_2O_2 decomposition catalyzed by intracellular iron, leading to ARG deactivation outpacing degradation.

In summary, findings of this work have uncovered fundamental knowledge on kinetics and/or mechanisms of ARG elimination during exposures to common (waste)water treatment and healthcare disinfectants. Here it has been clearly demonstrated that ARGs could persist (and remain biologically active) after host ARB inactivation provided by disinfection practices in either (waste)water treatment or healthcare scenarios, which would potentially lead to antibiotic resistance dissemination through horizontal gene transfers in downstream aquatic environments or clinical contact surfaces. A quantitative framework has been developed for predicting ARG fate during (waste)water disinfection/oxidation. qPCR is a promising tool in tracking biological activity loss of ARGs and other genetic traits (such as virulence genes and plasmid origins) under carefully selected circumstances. These findings provided significant implications for selection, design, operation, monitoring, and improvement of disinfection practices in such contexts. Future studies are recommended to further extend the modeling framework to diverse nucleic acid sequences harbored by various types of microorganisms to allow establishment of a universal model to predict fate of microbial nucleic acids and genes during disinfection/oxidation processes in both engineered and natural systems.

APPENDIX A

Table A.1. Definitions of important acronyms and symbols

Acronyms	Full-term definition and/or explanation
ABTS	2,2'-azino-bis(3-ethylbenzthiazoline)-6-sulphonic acid-diammonium salt
ARG(s)	Antibiotic resistance gene(s)
AMP	Adenosine 5’-monophosphate
Amp	Amplicon
$Amp_{N\text{-}Cl}$	N-chlorinated amplicon (activated toward C-chlorination)
Amp_{CPD}	CPD-containing amplicons
bp(s)	Nucleotide base pair(s)
CMP	Cytidine 5’-monophosphate
CPDs	Cyclobutane pyrimidine dimers
dAMP	Deoxyadenosine 5’-monophosphate
dCMP	Deoxycytidine 5’-monophosphate
dGMP	Deoxyguanosine 5’-monophosphate
dNMP	Monomeric deoxyribonucleoside 5’-monophosphate, or nucleotide, including dAMP, dCMP, dGMP, and TMP
DPD	*N*,*N*-diethyl-*p*-phenylenediamine
dsDNA	Double-stranded DNA
eARG	Extracellular antibiotic resistance gene
FAC	Free available chlorine
GMP	Guanosine 5’-monophosphate
HGT	Horizontal gene transfer
iARG	Intracellular antibiotic resistance gene
LOD(s)	Limit(s) of detection
LOQ(s)	Limit(s) of quantification
MeOH	Methanol
N-Cl bp(s)	N-chlorinated nucleotide base pair(s)
*p*CBA	*para*-Chlorobenzoic acid
PFGE	Pulsed-field gel electrophoresis
qPCR	Quantitative polymerase chain reaction
ssDNA	Single-stranded DNA

t-BuOH	*tert*-Butanol
TMB	1,3,5-Trimethoxybenzene
TMP	Thymidine 5'-monophosphate (or deoxythymidine 5'-monophosphate)
TT-CPD(s)	5'-TT-3' cyclobutane pyrimidine dimer(s)
UV light	Ultraviolet light at λ = 254 nm
Near-UV light	Ultraviolet light from 290 < λ < 400 nm
5'-*ij*-3'	Intrastrand nucleotide doublet, where *i*, *j* = A, T, G, or C
5'-bipyrimidine-3' or 5'-T/C-3'	Intrastrand bipyrimidine doublet, where bipyrimidine or T/C= TT, TC, CT, or CC
(6-4)PPs	(6-4) Photoproducts
8-oxoA	8-Oxo-7,8-dihydro-2'-deoxyadenosine
8-oxoG	8-Oxo-7,8-dihydro-2'-deoxyguanosine

Symbols	**Dimensions**	**Parameters**
CT	mg/L•min	Cumulative integrated exposures (for chemical disinfectants), calculated as $\int_0^t [\text{Disinfectant}]dt$
C/C_0	Dimensionless	Normalized cell viability
f/f_0	Dimensionless	Normalized transformation frequency
I	mW/cm^2	Fluence rates (for UV)
IT	mJ/cm^2	Fluences (for UV), calculated as $I \times t$
$k_{\text{Disinfectant,Amp}}$	$M^{-1}s^{-1}$ (for chemical disinfectants) cm^2/mJ (for UV)	Second-order or fluence-based first-order rate constants for ARG degradation by each disinfectant, dependent on amplicon length and nucleotide content; $k_{\text{FAC,Amp}}$ and $k_{\text{NH}_2\text{Cl,Amp}}$ represent the rate constant for the first step (i.e., reversible N-chlorination) in the sequential reaction of ARG amplicons with FAC and NH_2Cl, respectively.
$k_{\text{Disinfectant,Specific}}$	$(M\ X)^{-1}s^{-1}$ (for chemical disinfectants); $(M\ 5'\text{-TT-}3'/M\ \text{amplicon})^{-1}$ (cm^2/mJ) (for UV)	*Sequence-independent*, bp- or doublet-specific rate constants for each disinfectant, i.e., the slopes obtained from weighted linear regressions of $k_{\text{Disinfectant,Amp}}$ versus amplicon nucleotide content, where X = AT+GC bps, 5'-GG-3', or 5'-TT-3'.
$k_{\text{Disinfectant,0}}$	$M^{-1}s^{-1}$ (for chemical disinfectants); (cm^2/mJ) (for UV)	Intercepts obtained from weighted linear regressions of $k_{\text{Disinfectant,Amp}}$ versus amplicon nucleotide content

$k_{FAC,Amp_{N\text{-}Cl}}$ $k_{NH_2Cl,Amp_{N\text{-}Cl}}$	$M^{-1}s^{-1}$	Rate constants for the second step in the sequential reaction of ARG amplicons with FAC and NH_2Cl, respectively (i.e., irreversible C-chlorination of N-chlorinated amplicons); $k_{FAC,Amp_{N\text{-}Cl}}$ and $k_{NH_2Cl,Amp_{N\text{-}Cl}}$ are variable terms proportional to the amplicon's *extent* of N-chlorination.
$k_{FAC,N\text{-}Cl\ bp}$ $k_{NH_2Cl,N\text{-}Cl\ bp}$	$M^{-1}s^{-1}$	N-Cl bp-normalized rate constants for the second step in the sequential reaction of ARG amplicons with FAC and NH_2Cl, respectively (i.e., irreversible C-chlorination of N-chlorinated amplicons); $k_{FAC,N\text{-}Cl\ bp}$ and $k_{NH_2Cl,N\text{-}Cl\ bp}$ are constants.
$k_{UV,Amp,\ app}$	cm^2/mJ	Apparent rate constants (fluence-based first-order) characterizing amplicon degradation upon UV irradiation for fluences within ~50 mJ/cm^2 (for the linear UV model)
$k_{UV,Amp\text{-}CPD,f}$	cm^2/mJ	Fluence-based first-order rate constants characterizing formation of CPDs on a given DNA segment (for the complex UV model)
$k_{UV,singleCPD,r}$	cm^2/mJ	Fluence-based first-order rate constants characterizing photoreversal of each single CPD lesion (for the complex UV model)
$k_{UV,single6,4\text{-}PP}$	cm^2/mJ	Fluence-based first-order rate constants characterizing irreversible formation of each single 6-4PP lesion (for the complex UV model)
$k_{TT\text{-}CPD,\ f}$	cm^2/mJ	Predicted rate constants for TT-CPD formation in ARG amplicons during UV irradiation
mol X/mol Amp	Dimensionless	Specific contents of nucleotide bps or doublets within the investigated amplicons, where X = AT+GC bps, 5'-GG-3', or 5'-TT-3'
N/N_0	Dimensionless	Normalized ARG amplicon copy number
# N-Cl bp	Dimensionless	The cumulative number of N-chlorinated base pairs on an N-chlorinated amplicon
$\frac{\#N\text{-}Cl\ bp}{Amp_{N\text{-}Cl}}$	Dimensionless	The average number of N-chlorinated bases pairs per N-chlorinated amplicon within a population of N-chlorinated amplicons
X/X_0	Dimensionless	Normalized cell viability, ARG transformation frequency, or ARG amplicon copy number (i.e., including C/C_0, f/f_0, and N/N_0)

VITA

born in Chongqing, People's Republic of China

2007-2011 **B.S.E.,** Water Supply and Wastewater Engineering
Tongji University; Shanghai, China

2011-2014 **M.S.E.,** Municipal Engineering
Tongji University; Shanghai, China
Thesis: "Removal Characteristics of Assimilable Organic Carbon by the Advanced Process of Ozone - Biological Activated Carbon"

2014-2020 **Ph.D. Student**, Environmental Engineering
University of Washington; Seattle, WA (USA)
Dissertation: "Degradation and Deactivation of Bacterial Antibiotic Resistance Genes during Exposure to (Waste)water Treatment and Healthcare Disinfectants"